PALACKÝ UNIVERSITY OLOMOUC

FACULTY OF SCIENCE

Department of Organic Chemistry

Development of novel antituberculosis agents

Habilitation Thesis

RNDr. Lucie Brulíková, Ph.D.

2022

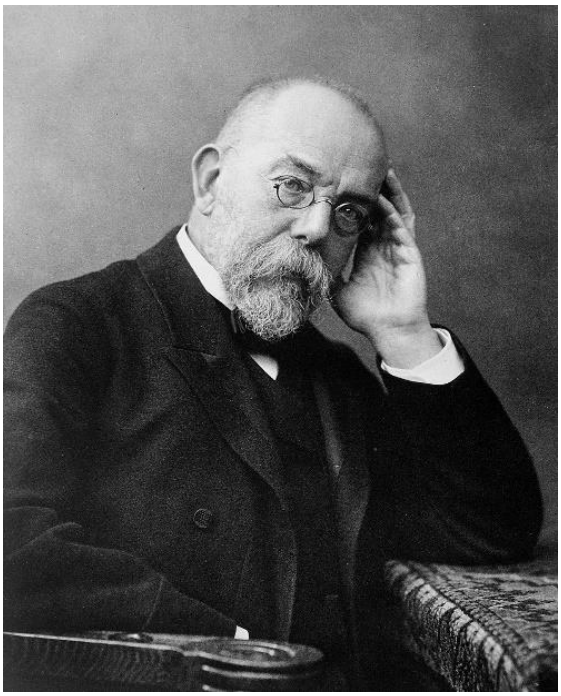

"If my efforts have led to greater success than usual, this is due, I believe, to the fact that during my wanderings in the field of medicine, I have strayed onto paths where the gold was still lying by the wayside. It takes a little luck to be able to distinguish gold from dross, but that is all."

Robert Koch

Acknowledgement:

I would like to express my thanks to many people, and it is hard to select whom first. From the bottom of my heart, I thank the long-time head of the Department of Organic Chemistry, Prof. Jan Hlaváč, for his trust and endless support throughout my study and work in the department. Additionally, I would like to express my thanks to all members of my research group for forming a friendly and cheerful atmosphere in our lab. Their enthusiasm for science encouraged me not to give up the often strenuous way I have chosen. Special thanks go to Milan Dak, Jan Chasák and Veronika Šlachtová.

I would like to thank all colleagues participating in my projects, especially Dr. Davie Cappoen, for the biological background and testing of our compounds against *Mycobacterium tuberculosis*. I also thank colleagues from the Palacký University to Prof. Marek Šebela, doc. Karel Berka, Dr. Václav Bazgier.

I am also grateful for the analytical support in the Department, especially to Dr. Adam Přibylka, for the technical assistant with NMR and HRMS.

I sincerely thank my family, husband, and dear son for their support, encouragement, and love throughout the past years.

I have to thank for financial support (grants no. JG_2019_002, IGA_PrF_2019_027, IGA_PrF_2020_012, IGA_PrF_2021_024) from Palacký University in Olomouc, Czech Republic.

Declaration of originality:

I hereby declare that I am the sole author of the submitted thesis, which, to the best of my knowledge and belief, contains no material previously published by another person, except where due acknowledgement has been made.

The author grants permission to Palacký University in Olomouc to store and display this thesis and its electronic version in the university library and on the official website.

In Olomouc 13. 4. 2022 ……

Lucie BRULÍKOVÁ

Foreword

In 2018, I got the opportunity to establish my research group. In light of the growing problem of drug resistance in *Mycobacterium tuberculosis* and the considerable number of people who die from tuberculosis each year, I decided to choose this topic as the main research interest. The presented thesis aims to provide a summary of the most significant results achieved within the last four years.

In the beginning, my group consisted of one PhD and five Bachelor students. Later on, two Master students joined us. Presently, my research group comprises one PhD, two Master and three Bachelor students. We quickly learned that an efficient approach to tackling tuberculosis disease requires concerted collaboration with experienced partners. In this regard, I am proud of establishing extensive cooperation with different institutions and researchers, which allowed systematic multidisciplinary research involving the design of new compounds, the synthesis of chemical libraries, the screening of antimycobacterial activity, and advanced enzymatic assays. At this point, I would like to emphasize the international cooperation with Dr. Davie Cappoen from the University of Antwerp (Laboratory for Microbiology, Parasitology and Hygiene) and the internal cooperation with Prof. Marek Šebela, doc. Karel Berka and Dr. Václav Bazgier from Palacký University.

Abstract

Tuberculosis (TB) remains a challenging global health concern. TB claims more than a million lives every year and is the world's leading cause of death from a single infectious agent, the leading killer of people with HIV, and a leading cause of deaths related to antimicrobial resistance. On that account, this work is devoted to developing new drugs highly active against drug-resistant TB strains. It highlights our research aimed at identifying new small-molecule leads and associated targets against TB.

The first part of the habilitation thesis is composed of a brief introduction to the current state of antituberculosis research and emphasizes the main achievements in this field. A substantial part of this work belongs to our research mainly aimed at (i) the development of novel mycobacterial ATP synthase inhibitors and (ii) the development of novel mycobacterial Zmp1 inhibitors. The last part of the thesis is dedicated to chemical libraries prepared as a part of phenotypic whole-cell screening. Although this thesis contains some unpublished results, a significant part was already published in peer-reviewed journals.

Keywords:

Mycobacterium tuberculosis, synthesis, inhibitors, mycobacterial ATP synthase, virulence factor Zmp1, phenotypic screening.

Contents

1 Introduction

The habilitation thesis summarizes the results achieved in the field of the development of new antituberculosis drugs. It highlights our research aimed at identifying new small-molecule leads and associated targets against TB. To gain insight into this problem, the introduction is dedicated to the current state of antituberculosis research, discusses the possibilities of tuberculosis treatment, and presents information on the development of tuberculosis drugs and vaccines.

1.1 Tuberculosis

Tuberculosis (TB) is an infectious disease caused by pathogenic bacteria from the *Mycobacteriaceae* family, *Mycobacterium tuberculosis (M. tuberculosis)*. According to the 2021 World Health Organization (WHO) report, tuberculosis is currently the 13th leading cause of death worldwide and the second leading cause of death from a single infectious agent after COVID-19.[1] In 2020, an estimated 10 million people fell ill with tuberculosis worldwide, and a total of 1.5 million people died from tuberculosis in 2020 (1.3 million died among HIV negative people and an additional 214 000 among HIV positive people).[1] Tuberculosis is also a major cause of death related to antimicrobial resistance. The highest reported TB mortality occurs in Africa and South-East Asia.

The disease usually affects the lungs (pulmonary TB); however, extrapulmonary TB affecting other sites also exists. Primary infection by *M. tuberculosis* can progress to active disease. In the ideal case, it can be defeated by the host immune system. However, *M. tuberculosis* has the ability to adapt to the human immune system and survive latently under low-energy conditions in a nonreplicating or dormancy-like state.[2] It is estimated that this latent TB infects approximately one-third of the world´s population (about two billion people).[3] Latent TB infection (LTBI) can develop into active disease, especially in immunosuppressed patients, such as people coinfected with HIV/AIDS or people undergoing anticancer chemotherapy. Indeed, most new TB cases involve the reactivation of dormant *M. tuberculosis* that resides in LTBI hosts.[2] Targeted LTBI treatment is, therefore, a key part of the End TB Strategy.[3]

Although TB is preventable and curable, the alarming increase in drug-resistant tuberculosis cases dramatically complicates the treatment. Until today, multidrug-resistant (MDR) and extensively drug-resistant (XDR) TB strains are a significant problem for current antituberculosis therapy.[1] It is obvious that a considerable research breakthrough is needed to rapidly reduce the incidence of TB worldwide, mainly in terms of new strategies to reduce the duration of treatment regimens, as well as the development of TB drugs that would be highly effective against drug-resistant strains of *M. tuberculosis.*

1.2 Drug resistance

M. tuberculosis has the ability to quickly develop resistance to antimicrobial drugs, which significantly complicates treatment. Consequently, drug-resistant tuberculosis strains represent a significant public health concern worldwide.[1] There is an alarming increase in the new cases of TB strains resistant to rifampicin, the most potent first-line anti-TB agent. Globally in 2020, 71 % of people diagnosed with bacteriologically confirmed pulmonary TB were tested for rifampicin resistance, up from 61 % in 2019 and 50 % in 2018.[1]

The development of resistance to *M. tuberculosis* is a very complex problem. Much has been written about this issue, e.g. by Singh, V. *et al.*[4] and Castro R. A. D. *et al.* in recent reviews.[5] Drug resistance in *M. tuberculosis* can develop mainly due to spontaneous mutations on the bacterial chromosome. As a consequence of these mutations, the structure of the biomolecular target within the bacteria may change and stop responding to the antimycobacterial drug effective until now. In addition, prodrug activation can be affected, drug permeability can be reduced, or effective intracellular antimicrobial concentration by efflux can be decreased.[4,5] Besides, inadequate dosing and incomplete treatment regimens contribute significantly to the increase in drug-resistant TB cases.

The latest WHO report[1] describes the classification of drug-resistant TB into five categories: (1) isoniazid-resistant TB, (2) rifampicin-resistant TB (RR-TB), (3) multidrug-resistant TB (MDR-TB), (4) pre-extensively drug-resistant TB (pre-XDR-TB), and (5) extensively drug-resistant TB (XDR-TB). The definition of the first two is obvious. MDR-TB is defined as resistance to the two most effective first-line anti-TB drugs, rifampicin and isoniazid. Pre-XDR TB is TB caused by *M. tuberculosis* strains that

fulfil the definition of MDR/RR-TB and are also resistant to fluoroquinolones (a class of second-line anti-TB drugs). Finally, XDR-TB is TB caused by *M. tuberculosis* strains that fulfil the definition of MDR/RR-TB and are also resistant to fluoroquinolones and at least one additional drug, bedaquiline or linezolid.

1.3 Current treatment of tuberculosis

Effective treatment of tuberculosis was first developed in the 1940s, when the antibiotic Streptomycin was discovered. Currently, the standard treatment of drug-susceptible TB relies on the combination of four antibiotics (isoniazid, ethambutol, rifampicin and pyrazinamide) administered for two months in an intensive phase, followed by the administration of two drugs (isoniazid and rifampicin) for an additional four months (Table 1).[6]

In contrast, the duration of the treatment of drug-resistant TB strains can extend up to 20 months and has to be supported with careful monitoring for adverse events. Usually, the treatment requires a course of second-line drugs for at least nine months. In 2020, WHO published a detailed overview of recommendations on the treatment of MDR/RR-TB[3] that comprises recommended regimen for: (1) rifampicin-susceptible and isoniazid-resistant TB; (2) shorter all-oral bedaquiline-containing regimen for MDR/RR-TB; (3) longer regimens for MDR/RR TB; and (4) the bedaquiline, pretomanid and linezolid (BPaL) regimen for MDR-TB with additional fluoroquinolone resistance.

According to the WHO consolidated guidelines on tuberculosis - drug-resistant tuberculosis treatment,[3] medicines recommended for use in longer MDR-TB regimens were classified into three groups (Table 1). Group A comprises highly efficient fluoroquinolones levofloxacin and moxifloxacin, bedaquiline and linezolid recommended for all regimens. Group B covers agents of the second choice. Furthermore, Group C includes other drugs that can complete the regimen when compounds from the first two groups cannot be used. It should be noted that the last group of compounds is considered the least safe from those described above.

WHO also mentioned other medicines not included in Group A, B or C.[3] For example, earlier used aminoglycosides kanamycin and capreomycin that are no longer recommended for treatment due to serious side effects. On the other hand, β-lactam drug clavulanic acid can be included in MDR/RR TB regimens; however, only as a companion agent to the carbapenems.

Table 1: Sorting of drugs recommended for the treatment of drug-susceptible and drug-resistant TB (adopted from WHO).[7]

Groups and steps	Medicine	Abbreviation
First-line	isoniazid	INH (H)
	ethambutol	EMB (E)
	rifampicin	RIF (R)
	pyrazinamide	PZA (Z)
Group A Include all three medicines	levofloxacin or moxifloxacin	LFX MFX
	bedaquiline	BDQ
	linezolid	LZD
Group B Add one or both medicines	clofazimine	CFZ
	cycloserine or terizidone	CS TRD
Group C Add to complete the regimen, and when medicines from Groups A and B cannot be used	ethambutol	EMB
	delamanid	DLM
	pyrazinamide	PZA
	imipenem-cilastatin or meropenem	IPM-CLN MPM
	amikacin (or streptomycin)	AMK (STM (S))
	ethionamide or prothionamide	ETO PTO
	p-aminosalicylic acid	PAS

1.4 New TB drugs and vaccines development

1.4.1 New TB drugs

The current situation requires new TB drugs that would act more effectively without serious side effects and significantly shorten the duration of therapy, especially in the case of drug-resistant TB strains. The ideal antituberculosis drug must display high activity with a low MIC value, especially against MDR and XDR strains and latent TB infections. In addition, an ideal new drug should possess low toxicity and adequate safety profile, optimized pharmacokinetic and pharmacodynamic properties, allow to shorten the duration of therapy, have limited interactions with other drugs to allow combination

therapy, particularly with antiretroviral agents. The main goals in successfully treating tuberculosis are shortening the duration of therapy and the complexity of drug regimens.

In general, research of new drugs or new chemical entities comprises preclinical and clinical development. The Working Group on New TB Drugs (WGND) carefully track the progress of new candidates during the whole process, from lead optimization to clinical trials and regularly update the database. The last update was presented in March 2022 and is depicted in Table 2.[8] Nowadays, we can find 25 drugs, several combination regimens, and 14 vaccine candidates in clinical trials (August 2021).[1] Groups of drugs undergoing clinical development comprise new chemical entities as well as repurposed drugs. Structures of the representative examples are demonstrated in Fig. 1.

Moreover, there are four drugs under investigation as host-directed therapy for individuals with latent TB infection or the treatment of pulmonary TB (imatinib, pravastatin, auranofin and metformin).

Table 2: Global new TB drug pipeline (adopted from WGND).[8]

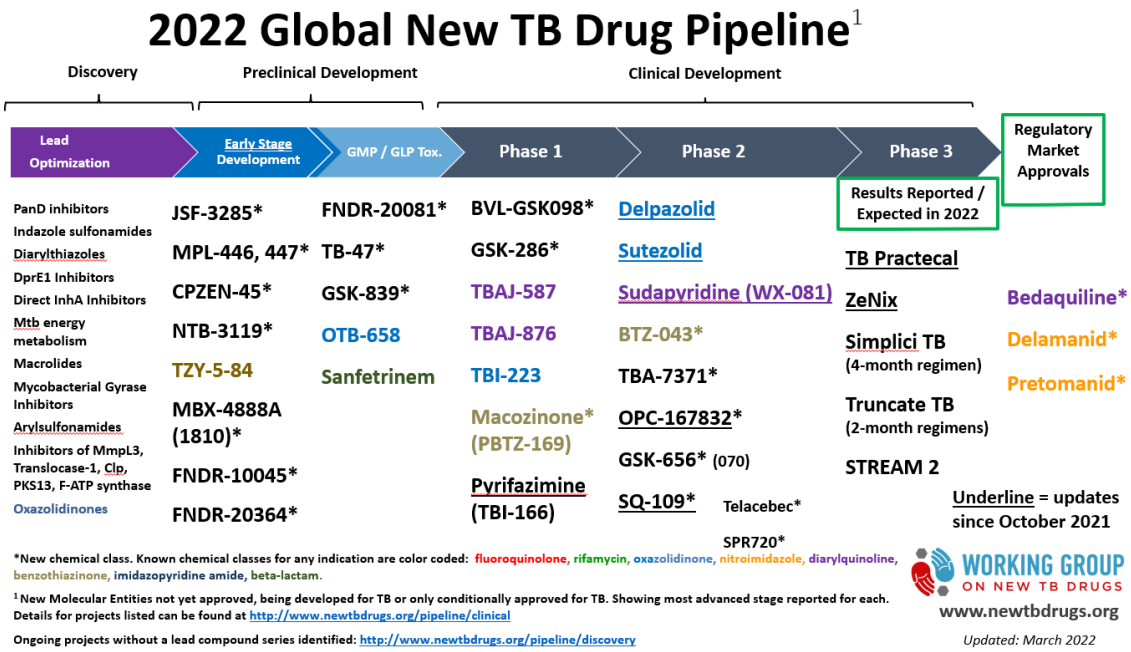

The most exciting drug with a unique mechanism of action is bedaquiline (Fig. 1). This compound was approved for MDR-TB treatment by the FDA in 2012 and was the first new medicine for TB treatment in more than forty years. Bedaquiline is a member of the diarylquinoline class targeting mycobacterial adenosine triphosphate (ATP) synthase. It is also the part of novel TB regimens currently in development (BEAT-TB;

bedaquiline – pretomanid – moxifloxacin – pyrazinamide; bedaquiline – pretomanid – linezolid – moxifloxacin; bedaquiline – pretomanid – linezolid).[8] To date, bedaquiline is the only approved drug targeting mycobacterial ATP synthase.

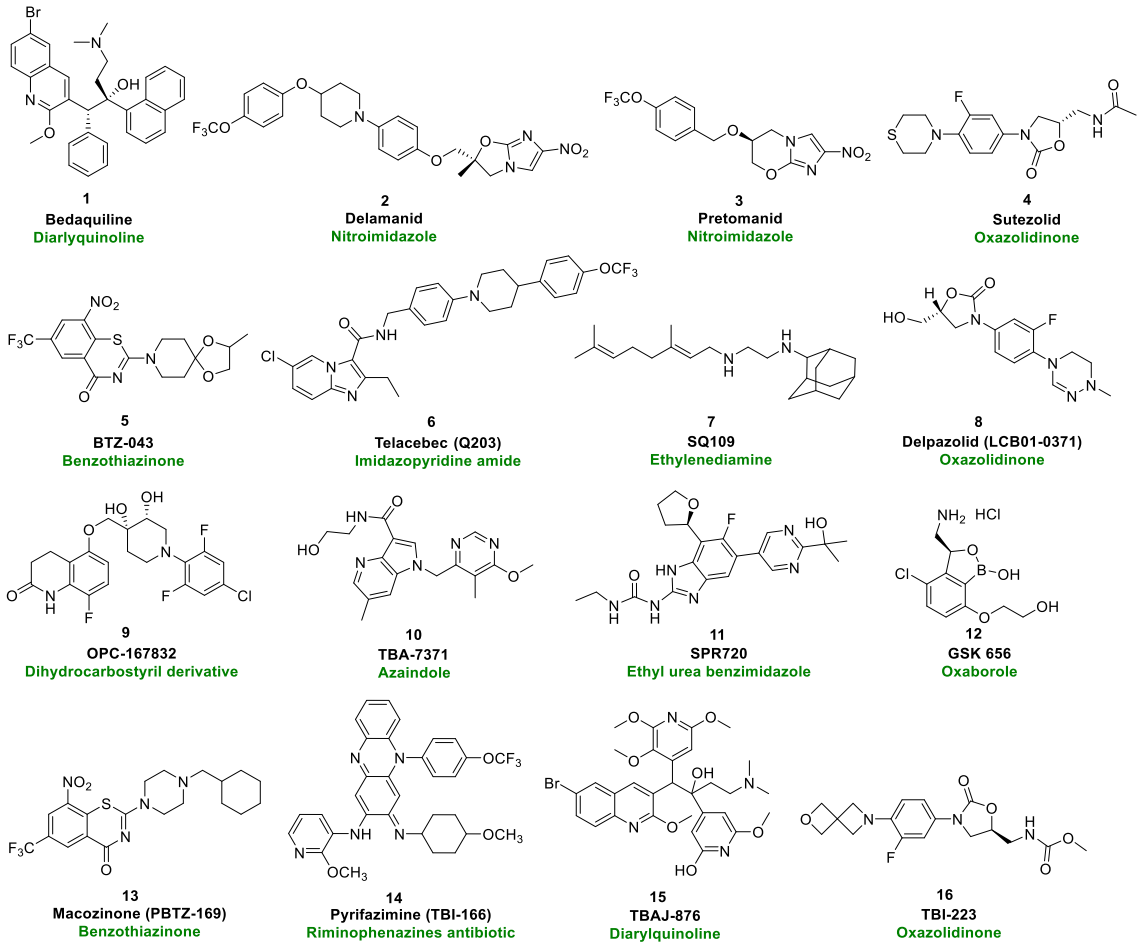

Fig. 1: Structures of representative examples of drugs in different stages of clinical development.

Another compound approved for medication used to treat multidrug-resistant TB is delamanid (Fig. 1). Delamanid was approved in 2014 for use in the EU and Japan.[9] This compound belonging to the nitroimidazoles interferes with mycolic acid biosynthesis by inhibiting the synthesis of ketomycolic and methoxymycolic acids. This inhibition leads to the disruption of the mycobacterial cell wall and better drug penetration into bacteria.

The third tuberculosis drug to receive FDA approval is pretomanid (Fig. 1). Pretomanid is the next nitroimidazole approved by FDA for medical use in August 2019. Pretomanid has been developed by TB Alliance for the treatment of drug-resistant TB infections in combination with bedaquiline and linezolid as part of the bedaquiline – pretomanid – linezolid (BPaL) regimen. As well as the delamanid mentioned above,

pretomanid acts as an inhibitor of mycolic acid biosynthesis and kills actively replicating mycobacteria. Moreover, pretomanid acts as a respiratory poison under anaerobic conditions against non-replicating bacteria.

1.4.2 Vaccines development

A hundred years ago, Albert Calmette and Camille Guérin developed the most effective vaccine to prevent TB disease to date.[10] The bacilli Calmette-Guérin (BCG) vaccine, based on attenuation of bacteria, remains the only licensed vaccine that effectively prevents severe forms of tuberculosis in children. Nevertheless, vaccine efficacy is much lower in adults. However, there are 14 vaccine candidates in clinical trials: three in Phase I, nine in Phase II and two in Phase III (Table 3).[3]

Table 3: The global clinical development pipeline for new TB vaccines (adopted from WHO report).[3]

Phase I	Phase IIa	Phase IIb	Phase III
AEC/BC02 Anhui Zhifei Longcom	MTBVAC Biofabri, TBVI, University of Zaragoza	DAR-901 booster Dartmouth, GHIT	VPM1002 SIIPL, VPM
Ad5 Ag85A McMaster, CanSino	ID93 + GLA-SE IDRI, Wellcome Trust	H56: IC31 SSI, Valneva, IAVI	MIP/Immuvac ICMR, Cadila Pharmaceuticals
ChAdOx185A-MVA85A (ID/IM/Aerosol) University of Oxford	TB/FLU-04L RIBSP	M72/AS01E GSK, Gates MRI	
	GamTBvac Ministry of Health, Russian Federation	BCG revaccination Gates MRI	
		RUTI® Archivel Farma, S.L.	

Viral vector
Protein/adjuvant
Mycobacterial – whole cell or extract
Mycobacterial – live

1.4.3 Two strategies in the development of the new drugs

Two different strategies in developing the new drugs are widely used - a target-based approach and a phenotypic whole-cell screening approach.[e.g.11–15] Target-based approaches proceed from knowledge of a specific target, e.g. enzyme or receptor. This

rational approach requires identifying and validating the target and looking for a candidate that efficiently binds to and modulates the target.

However, high-throughput phenotypic screening strategies are highly desired to enhance TB drug discovery and development efficiency, especially in connection with resistant TB strains. Phenotypic whole-cell based assays screen for compounds inhibiting pathogen growth by identifying hits for further optimization and deconvolution of the mode of action (MoA). Phenotypic whole-cell screens have historically provided the best successes from hit to pre-clinical or clinical candidate.

1.5 Mycobacterial drug targets and host-directed therapies

In 1998, Cole *et al.* determined the complete genome sequence of the best-characterized strain of *Mycobacterium tuberculosis*, H37Rv.[16] This significant discovery opened up a new era of target-based designing of antituberculosis drugs. To date, we know many targets at the level of *M. tuberculosis* and the level of the host.[17] The brief overview of mycobacterial targets and host-directed therapies is depicted in Fig. 2.

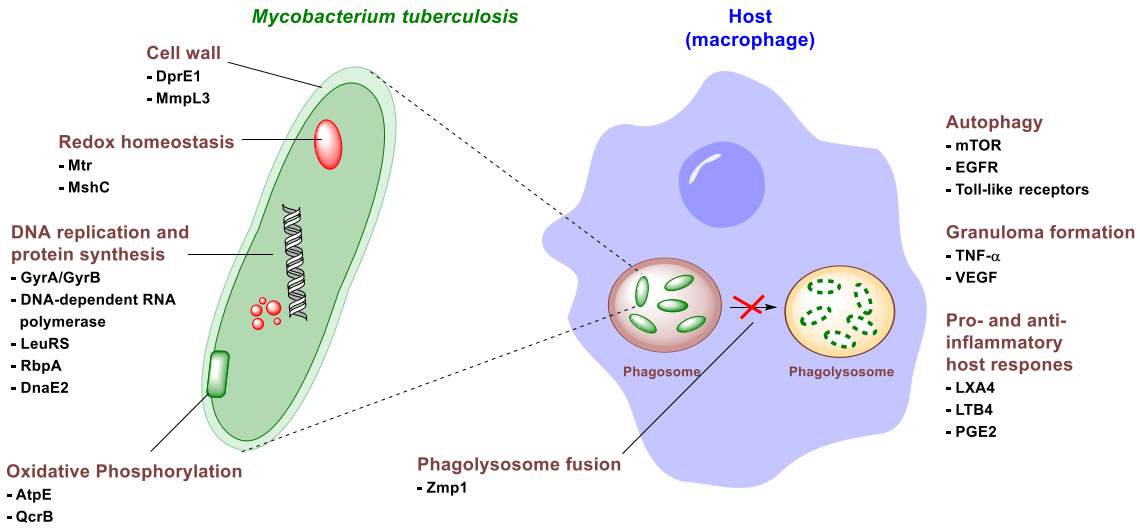

Fig. 2: Overview of the mycobacterial drug targets and targeting essential processes at the level of the host (this picture was drawn according to Torfs *et al.*).[17]

At the level of bacteria itself, the attention of many researchers is focused on the targeting of vitally important pathways such as oxidative phosphorylation, cell wall biosynthesis, DNA replication and protein synthesis, etc. Furthermore, targeting mycobacterial virulence factors (molecules produced by bacteria that can block the

immune response) is an attractive approach for developing potential anti-TB adjuvants. This approach can be represented by targeting Zmp1, which interferes with the immune system (this will be described in more detail in Chapter 3).

A detailed overview of mycobacterial drug targets is also described by WGND on their web page.[8] From the adopted data shown in Table 4, it is apparent that the most explored are those targets associated with mycobacterial cell wall biosynthesis.

Table 4: Overview of mycobacterial drug targets (adopted from WGND).[8]

	Peptidoglycan Layer	Arabinogalactan Layer	Mycolic Acid Layer
Cell Wall Synthesis	• Lipid II • D,D-transpeptidase • L,D-transpeptidase • Mur ligases • D-alanine:D-alanine Ligase (DDL) • Translocase 1 (MurX or Mra Y)	• Arabinosyl transferase • WecA inhibitor • DprE1 Covalent Inhibitors • DPRE1 Noncovalent Inhibitors	• MmpL3 Inhibitor • InhA Inhibitor • KasA Inhibitors • Unknown Target Mycolic Acid Inhibitors
DNA Replication	• DNA gyrase		
DNA Transcription	• RNA Polymerase		
RNA Translation	• rRNA / Ribosome		
Energy Metabolism	• ATP-Synthase • Cytochrome bc1-aa3 • NADH Dehydrogenase Type II • MenG Inhibitor		
Proteolysis & Proteostasis	• ClpP1P2 • ClpC		
Cellular Metabolism	• Unknown Target Cholesterol Metabolism • Tryptophan Synthase (TrpAB) • Aspartate decarboxylase (PanD) • Efflux transport of antibiotics (efpA)		

The last decade has witnessed an increase in the research approach, the so-called Host-Directed Therapy (HDT).[eg.18–21] This strategy is based on the modification of the host response related to the activity and pathogenicity of *M. tuberculosis* infection. The crucial fact is that HDT drugs, unlike classical antibiotics, act by modulating host cell functions; therefore, the development of drug-resistance by infecting *M. tuberculosis* is avoided. Key HDT mechanisms include autophagy induction, modulation of host epigenetics, and modulation of the cytokine and lymphocyte-mediated response.[21] It is a relatively new concept in the treatment of TB and a promising strategy for treating drug-resistant TB cases.

Obviously, the TB pandemic requires the identification of novel drugs with a novel mechanism of action that would be highly efficient against resistant strains and latent TB infection. A combined effort of academic research and industrial partners, new trends, and approaches could lead to the eradication of this infectious disease in the future.

2 Mycobacterial ATP synthase inhibitors

Mycobacterial adenosine triphosphate (ATP) synthase is a key enzyme in the energy metabolism of bacteria that has been found to be essential for the growth and survival of bacteria in both replicating and non-replicating states.[22] Mycobacterial ATP synthase is a validated clinical target in the treatment of drug-resistant tuberculosis.[23–25] Due to the significant structural differences between bacterial and mammalian ATP synthases, inhibition of mycobacterial ATP synthase is considered a relatively safe approach in the treatment of multidrug-resistant (MDR) and extensively drug-resistant (XDR) *M. tuberculosis* infections.

Mycobacterium tuberculosis is an obligate aerobic bacterium highly dependent on oxidative phosphorylation that produces ATP for growth and survival. Furthermore, the production of ATP is also essential in the dormant state, as ATP synthase carries specific characteristics that facilitate survival under non-replicating conditions, including oxygen insufficiency, nutrient limitation, and acidic pH.[26]

Oxidative phosphorylation (Fig. 3) is the source of energy that drives ATP synthase to convert the electrochemical potential energy into chemical energy in the form of ATP by the reaction of ADP with inorganic phosphate (Pi).[22]

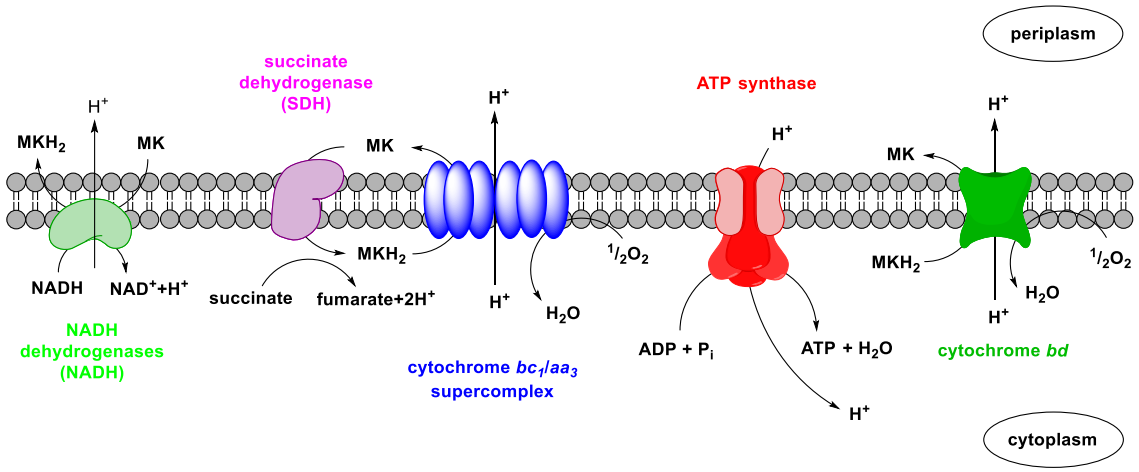

Fig. 3: Oxidative phosphorylation in *M. tuberculosis* (this figure was drawn according to Bald *et al.*).[25]

Mycobacteria are endowed with dehydrogenases that fuel the electron transport chain (ETC). Furthermore, the reduction of dioxygen coupled with the generation of a proton motive force (PMF) is arranged with two respiratory oxidases. In 2021, we reviewed in detail known inhibitors targeting the most important enzymes included in oxidative phosphorylation.[22]

2.1 Structure of mycobacterial ATP synthase

The mycobacterial F_1F_0-ATP synthase (F-ATP synthase) is a membrane protein complex consisting of two domains (F_1 and F_0) and nine subunits (α_3:β_3:γ:δ:ε:*e*:*a*:*b*:*b´*:c_9) encoded by the *atp* operon (Fig. 4).[eg.27–29] The hydrophilic stator domain F_1 is formed with subunits α_3:β_3:γ:ε, where α_3:β_3-hexamer forms the catalytic centre. The proton-translocation domain F_0 includes a structurally conserved *a* subunit and a ring of nine *c* subunits. Both domains are connected through a central stalk containing γ and ε subunits reversibly coupling proton flow to either ATP synthesis or hydrolysis. The prevention of α_3:β_3-subcomplex rotation is ensured by a peripheral stalk formed with *b*-δ fused part and subunit *b´*.

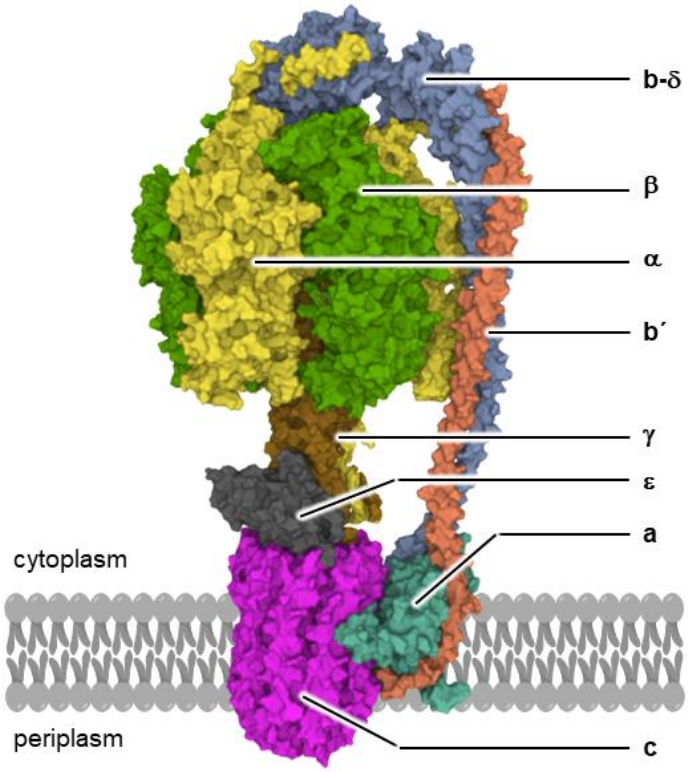

Fig. 4: Structure of mycobacterial ATP synthase from *Mycobacterium smegmatis* (figure created using Mol* Viewer and PDB: 7NJP).

The transmembrane proton motive force drives the proton translocation throughout the F_0 rotor domain, causing the rotation of the γ-ε-c_9 complex and subsequent conformational changes in the catalytic α_3:β_3-subcomplex. As a consequence, the synthesis of ATP occurs. Importantly, the specific structure of mycobacterial F-ATP synthase results in suppression of proton motive force formation during ATP hydrolysis and its low or latent ATPase activity in the fast- or slow-growing form.

2.2 Mycobacterial ATP synthase inhibitors

The first highly effective ATP synthase inhibitor, bedaquiline, was described in 2005[30] and approved for MDR-TB treatment by the FDA in 2012. This compound represented a new class of antimycobacterial drugs with a novel mode of action. Interestingly, it was the first new medicine for treating tuberculosis in more than forty years. Bedaquiline exhibits excellent anti-TB activity against both dormant and actively replicating mycobacteria.

To date, bedaquiline is the only approved drug targeting mycobacterial ATP synthase. Recently, Guo and co-workers revealed by cryo-electron microscopy that bedaquiline binds to the highly conserved subunit *c* of ATP synthase in *Mycobacterium smegmatis*, closely related to *M. tuberculosis*.[28] This binding induces significant conformational changes in mycobacterial ATP synthase, creating distinct contacts between bedaquiline and subunit *a*. Importantly, mycobacterial subunits *c* and *a* differ from human ATP synthase, which explains the specificity of bedaquiline for mycobacteria mentioned above.

Later, new scaffolds such as thiazolidinediones, pyrazolopyrazinones, diaminopyrimidines, diaminoquinazolines, chloroquinolines, or squaramides appeared, as we recently reviewed.[22] For brief illustration, only a few examples will be depicted below.

2.2.1 Bedaquiline analogues

The discovery of bedaquiline by a Janssen Pharmaceutica research team has triggered a broad interest of medicinal chemists.[e.g.31,32,41–44,33–40] Despite its significant efficiency and promising antitubercular profile, bedaquiline has several drawbacks, such as high lipophilicity (contributing to its long terminal half-life and toxicity) and low solubility.

Therefore, several research groups have focused on developing analogues with better safety profiles.

For example, the Palmer group made an intensive effort in this field.[36,38–40,43] They reported several bedaquiline analogues, including derivatives **20** and **21** (Scheme 1), with reduced cardiovascular toxicity compared to bedaquiline.[43] The synthesis of these analogues proceeded by the standard synthetic pathway outlined in Scheme 1 from 6-bromo-2-methoxyquinoline **17** and the appropriate aldehydes. LDA-mediated coupling of benzylquinolines **19** with selected ketones provided final analogues **20**. The 6-cyano compounds **21** were prepared from the corresponding 6-bromo analogues by direct cyanation. The desired diastereomers were isolated by supercritical fluid (SFC) HPLC.

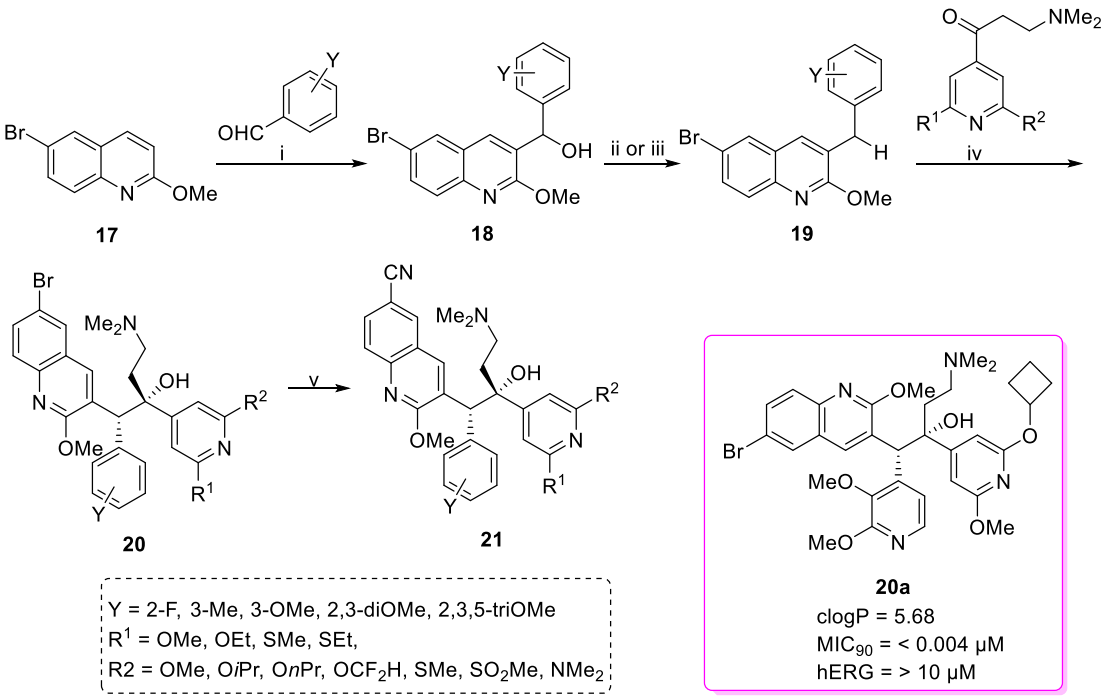

Scheme 1. Synthesis of bedaquiline analogues **20** and **21**.[43] Reagent and conditions: (i) LiTMP, THF, −75 °C, 1.5 h then the appropriate aldehyde, −75 °C, 4 h; (ii) Et_3SiH, TFA, DCM; (iii) MsCl, Et_3N, DMF, then $NaBH_4$; (iv) LDA, THF, −75 °C, 1.5 h then the appropriate ketone, then HOAc, 24-87 %; (v) $Zn/Zn(CN)_2$, $Pd_2(dba)_3/P(o\text{-}tol)_3$, DMF, 50 +°C, then separation of the diastereomers by SFC HPLC, 51-88 %.

2.2.2 Inhibitors based on pyrazolopyrazinone scaffold

The screening of chemically diverse compounds using the *Mycobacterium smegmatis* ATP synthase enzyme pointed out a non-diaryl quinoline scaffold pyrazolopyrazinone as

an attractive structure (Scheme 2).[37] Synthesis of these scaffolds started with trimethylaluminium mediated monoamidation of commercially available pyrazole-3,5-dicarboxylate **22**. Subsequent treatment with *p*-TSA afforded the cyclized product **24**. Dehydration using methanesulfonic acid followed by reaction with trimethylaluminum and piperidine gave piperidinyl amide **26**. The final reaction of intermediate **26** with substituted benzyl bromides furnished the final compounds **27**.

Compounds **27a** (Scheme 2) showed the most promising results from the extensive SAR study exhibiting IC_{50} = 0.28 μM. Interestingly, compounds **27** do not inhibit any CYP450 enzymes and could be a starting point for further research in the field of anti-TB drug discovery. However, the authors of this publication did not mention any specific binding to ATP synthase.

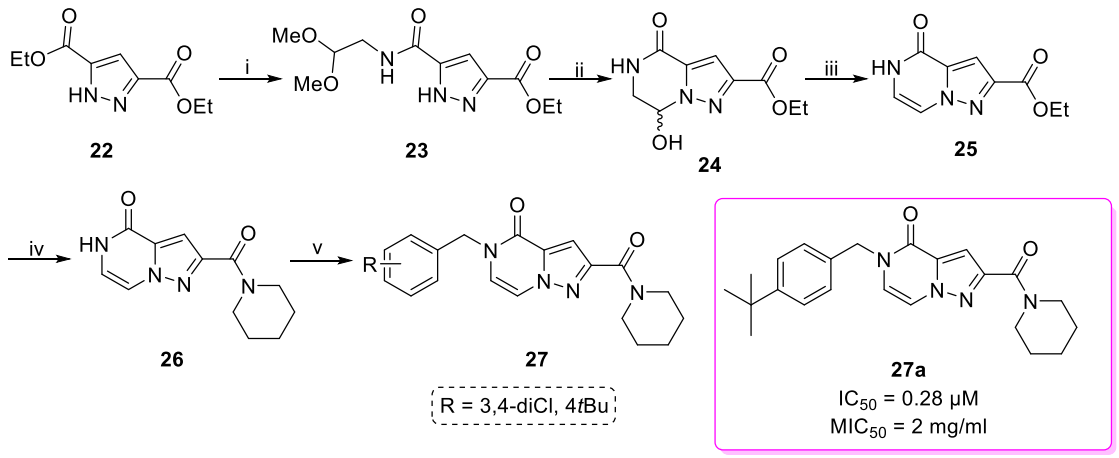

Scheme 2. Synthesis of pyrazolopyrazinones **27**.[37] Reagent and conditions: (i) aminoacetaldehyde dimethyl acetal, $(AlMe_3)_2$, THF, reflux, 50 %; (ii) *p*-TSA, acetone-H_2O, reflux, 67 %; (iii) methanesulfonic acid, rt, 72 h, 41 %; (iv) piperidine, $(AlMe_3)_2$, THF, rt, 2 h, 79 %; (v) NaH, $RBnCH_2Br$, DMF, rt, 78-80 %.

2.2.3 Inhibitors based on diaminopyrimidine scaffold

One of the latest promising results was published by Hotra *et al.*, who reported a novel antimycobacterial drug **34** targeting the γ subunit of ATP synthase (Scheme 3).[42] A synthetic protocol for compound **34** (GaMF1) started with the preparation of precursor **30** (Scheme 3). 2,4-Dichloro-6-methyl pyrimidine **28** was reacted with ethylamine in hot ethanol, giving a mixture of the two regioisomers separated chromatographically.

Acylation of 4-nitroaniline with 3-bromobenzoyl chloride, reduction of the nitro group and reaction with intermediate **30** gave the final compound **34**.

Compound **34**, termed GaMF1, inhibits specific mycobacterial ATP synthase through the binding to the γ subunit. Furthermore, GaMF1 was found to increase the potency of bedaquiline, which makes this compound potent for an efficient multidrug combination.

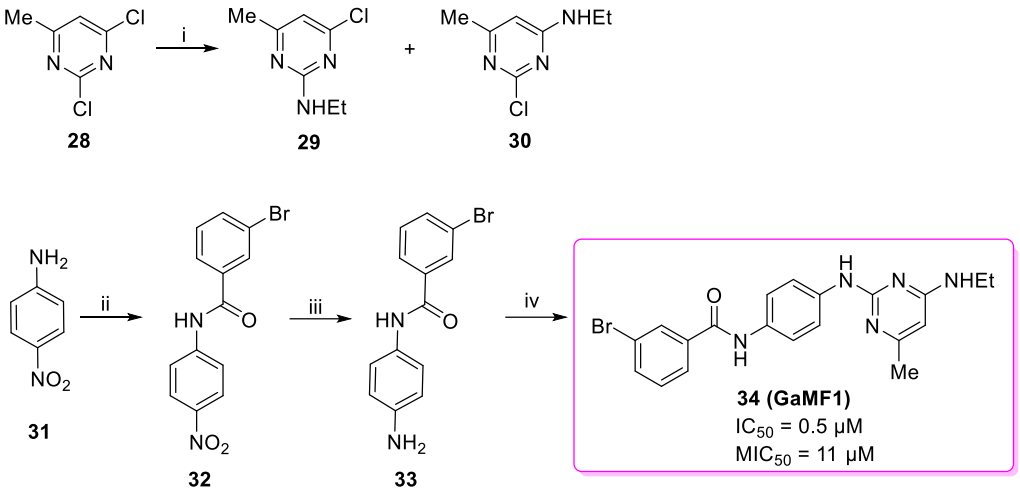

Scheme 3. Synthesis of GaMF1.[42] Reagents and conditions: (i) $EtNH_2$, DIPEA, EtOH, 50 °C, 24 h, 33 %; (ii) 3-BrPhCOCl, K_2CO_3, THF, rt, 16 h, 98 %; (iii) Pt/C/S, H_2, 100 psi, 100 °C, 99 %; (iv) **30**, DIPEA, dioxane, reflux, 2 days, 80 %.

2.2.4 Inhibitors based on the squaramide scaffold

The most exciting compounds related to our research are squaramides, firstly published as antimycobacterial agents by Tantry *et al.* in 2017 (Scheme 4).[35] They described morpholine squaramide derivative **38a** as a novel mycobacterial ATP synthase inhibitor with nanomolar antituberculosis activity.

Synthesis of squaramides depicted in Scheme 4 proceeded from commercially available squaric acid **35** *in situ* converted to dichloro intermediate **36**. Subsequent arylation of **36** and reaction with pyridin-2-ylmethanamine in the presence of the base afforded squaramides **38**.

Compound **38a** displayed efficiency in a mouse TB infection model. Studies on a membrane-based biochemical assay (Myc_ATPS IC_{50} 0.03 μM) measuring ATP synthesis through oxidative phosphorylation suggested mycobacterial ATP synthase as a molecular target. Furthermore, compound **38a** showed sensitivity against a bedaquiline-

resistant mutant, which indicated that this compound might occupy a different binding site of the ATP synthase compared to that of bedaquiline.

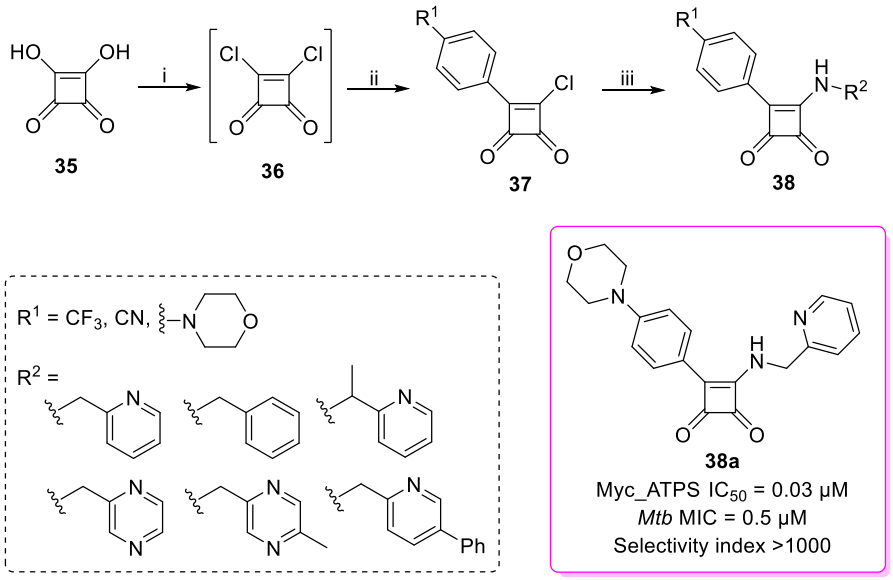

Scheme 4. Synthesis of squaramide **38**.[35] Reagents and conditions: (i) $SOCl_2$, 80 °C, 3 h; (ii) R^1-Ph, $AlCl_3$, DCM, 0 °C, 2 h, 16 %; (iii) R^2NH_2, TEA, 1,4-dioxan, 0-2 °C, 30 min, 16 %.

Subsequently, Li *et al.* enriched the library of squaramides with diamino substituted compounds **42** (Fig. 5).[41] Moreover, they synthesized other series, including furan-2(5*H*)-ketone and maleimide (Fig. 5, compounds **39**-**41**). However, none of the studied squaramides exhibited higher potential than those published earlier by Tantry *et al.*[35]

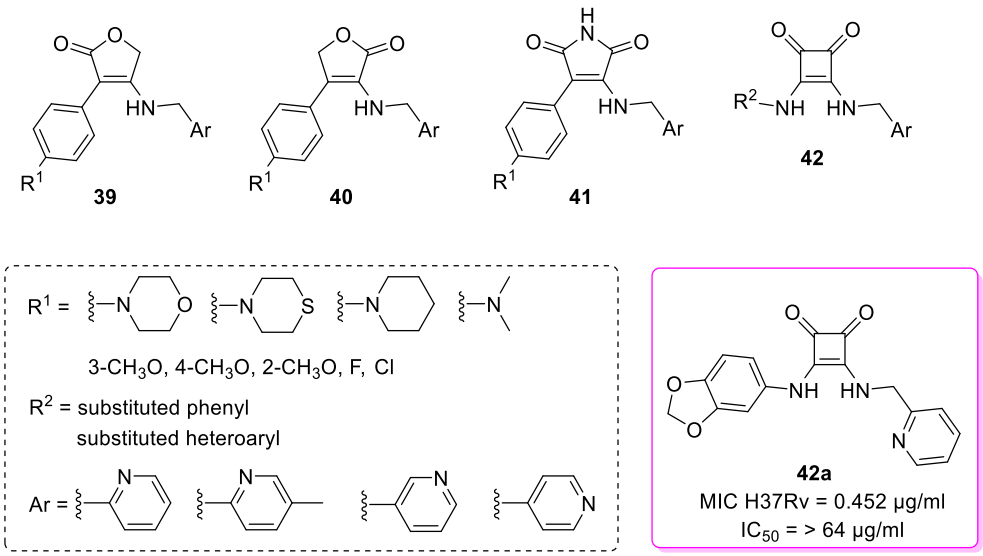

Fig. 5: Overview of ATP synthase inhibitors published by Li *et al.*[41]

2.2.5 Squaramides developed by our group

SAR studies on squaramides performed by Tantry *et al.* (Scheme 4) suggested that 2-pyridylmethyl substitution on the right-hand side (RHS) of the squaric acid scaffold (Fig. 6) is crucial for reaching the desired potency. On the other hand, the left-hand side (LHS) of molecule **38** is incomparably less explored. Tantry *et al.* studied only three different modifications on the LHS, where a morpholinophenyl moiety was found to be the best. For this reason, we decided to explore further possibilities and broaden the SAR study of squaramides. Based on this knowledge, we initially designed and synthesized two series of modified squaramides **38** and **43** (Fig. 6).

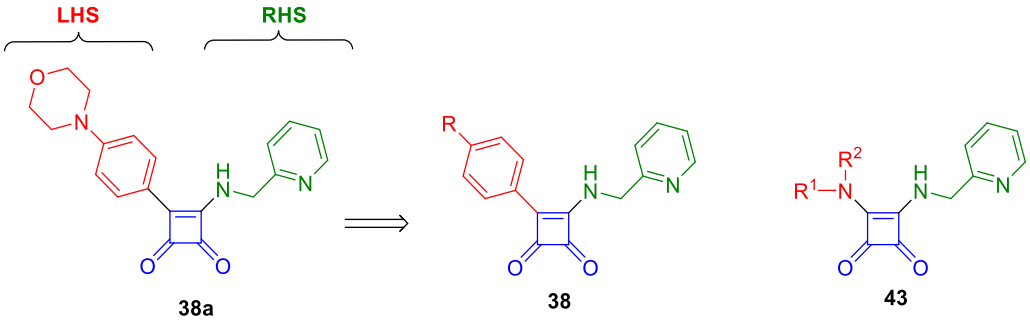

Fig. 6: Design of new squaramides **38** and **43**.

Our first synthetic effort leading to the target compounds **38** proceeded from the work published by Tantry *et al.*[35] (Scheme 5). Based on their experiences, we used commercially available squaric acid **35** and converted it to the corresponding dichloro derivative **36**. Subsequently, crude **36** was subjected to arylation with various aromatic compounds in the presence of 0.25 equiv $AlCl_3$ as Lewis acid giving precursors **37**. Since the yields of this reaction were very low (1-23 %), compound **36** was purified prior to the next step and obtained in a 55% yield. Further, we increased the amount of $AlCl_3$ to 2 equiv. Finally, crude intermediates **37** were directly reacted with pyridin-2-ylmethanamine in the presence of the base giving products **38a-f** in moderate to good yields (14-73 % yield over two steps).

To properly compare the biological activity of the published compound **38a** with our analogues, the squaramide **38a** was also synthesised for this purpose. Synthesis of squaramides **38** depicted in Scheme 5 was the part of the Bachelor and Master thesis of Jan Chasák.[45,46]

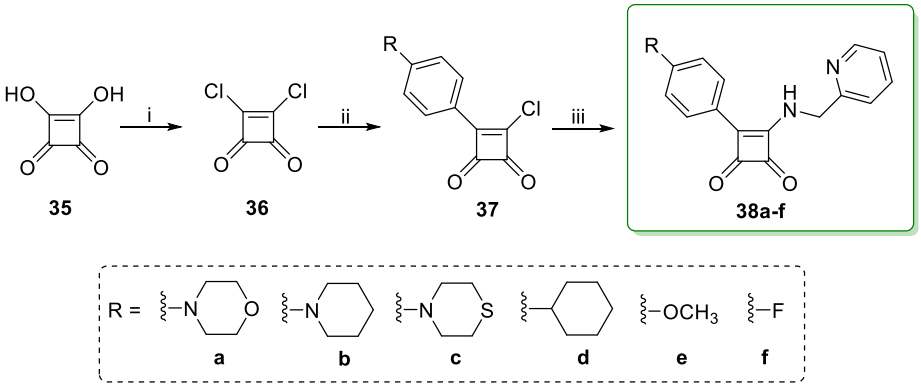

Scheme 5. Synthesis of target compounds **38a-f**. Reagents and conditions: (i) $SOCl_2$, DMF, 80 °C, 1 h, 55 %; (ii) R-Ph, $AlCl_3$, DCM, 0 °C - rt, 2 h; (iii) pyridin-2-ylmethanamine, 1,4-dioxane, TEA, 0 °C, 30 min, 14-73 %.

Since the method described above failed during our efforts to introduce 1-phenylpiperazine or 4-phenylpiperidine moiety into the final structure **38**, we were forced to completely modify this synthetic route (Scheme 6).

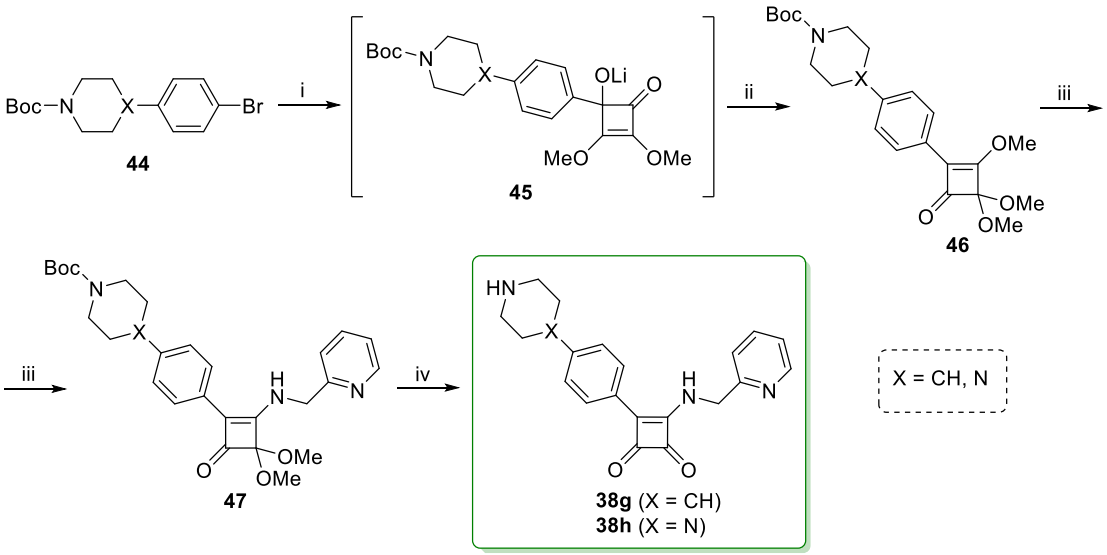

Scheme 6. Synthesis of target compounds **38g-h**. Reagents and conditions: (i) 3,4-dimethoxycyclobut-3-ene-1,2-dione, 1.7M *t*-BuLi, dry THF, -78 °C, 1-1.5 h; (ii) TFAA, MeOH, -78 °C - rt, 20 min, 24-51 %; (iii) pyridin-2-ylmethanamine, MeCN, rt, 16 h, 74-95 %; (iv) for **38g**: 10% HCl, DCM, rt, 15 min, 73 %; for **38h**: 10% HCl, rt, 15 min; then TFA, DCM, rt, 2 h, 28 %.

3,4-Dimethoxycyclobut-3-ene-1,2-dione was treated with the *in situ* prepared lithium salt of **44**. The addition of trifluoroacetic anhydride to the reaction solution with subsequent

reaction termination with MeOH yielded monoketals **46**. Then, intermediates **46** were reacted with pyridin-2-ylmethanamine. Finally, the ketal and Boc protecting groups were removed using 10% HCl solution to afford the target compound **38g** in a 73% yield. TFA in DCM had to be added to remove protecting groups in the case of compound **38h** thoroughly. This synthetic procedure was developed by my PhD student Milan Dak.

To further modify the central scaffold and implement an additional NH group to increase the possibility of hydrogen-bond interaction between the compound and ATP synthase, we designed and synthesized diamine analogues **43** (Scheme 7).

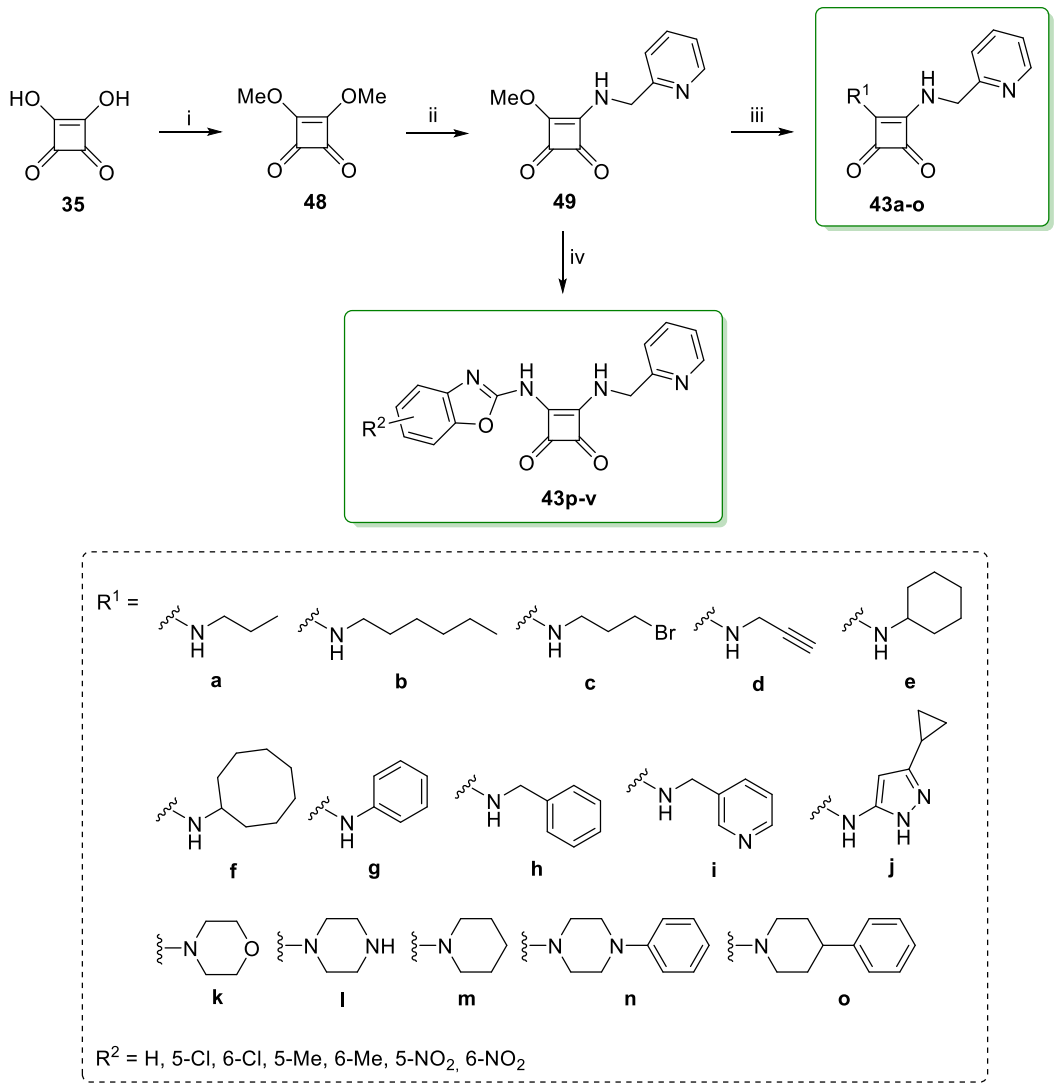

Scheme 7. Synthesis of target compounds **43**. Reagents and conditions: (i) trimethylorthoformate, dry MeOH, 65 °C, 24 h, 89 %; (ii) pyridin-2-ylmethanamine, MeCN, rt, 40 min, 80 %; (iii) amines, MeCN, rt or 50°C, 16 h, 33-87 %; (iv) 2-aminobenzoxazoles, DBU, MeCN, 50 °C, 16 h, 8-50 %.

Firstly, dimethoxy analogue **48** prepared from squaric acid **35** was reacted with pyridin-2-ylmethanamine to give precursor **49**. Target compounds **43a-o** were synthesized by reacting **49** with various aliphatic, alicyclic or aromatic amines at room temperature or 50 °C in moderate to high yield (33 – 87 %). On the other hand, the reaction of **49** with various 2-aminobenzoxazoles (prepared according to the protocol we developed)[47] required a higher reaction temperature (50 °C) and the presence of the base. Final compounds **43p-v** were obtained in low to moderate yield (8 - 50 %) influenced by the lower solubility of target compounds. Synthesis of squaramides **43** depicted in Scheme 7 was the part of the Bachelor and Master thesis of Jan Chasák.[45,46]

Subsequently, squaramides **38** and **43** were tested for their antimycobacterial activity. All these experiments were performed by Dr. Davie Cappoen from the University of Antwerp (Belgium). The libraries of squaramides **38** and **43** were initially screened in a single shot assay against *Mycobacterium tuberculosis* H37Ra. From the total library of investigated compounds **38** and **43**, only members belonging to the phenyl substituted sub-library **38** were identified as primary hits with a detection cut off > 60% at 10 μM after 7 days of incubation. The phenyl substituted analogues **38** were submitted for a MIC determination. We identified two compounds, **38b** and **38c** (Fig. 7), with submicromolar (0.6 - 0.7 μM) activity against *M. tuberculosis* H37Ra. For none of these derivatives, we detected acute cytotoxicity against the MRC-5 lung fibroblast, HepG2 metabolic active hepatocytes or Raw264.7 macrophage-like monocytes at concentrations up to 128 μM.

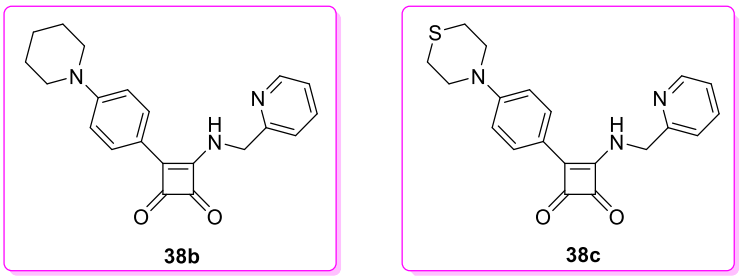

Fig. 7: Structures of the most potent compounds.

Following the broad-spectrum screening, the compounds were further screened against a panel of pathogenic bacteria and parasites. The only activity detected in the broad screening was reported for compound **38b**, which showed minor activity against *Leishmania donovani*.

To access the activity against intracellular replicating *M. tuberculosis*, a macrophage infection was performed with the compound series **38**. Briefly, Raw264.7 macrophage-like monocytes were infected at a multiplicity of infection of 10 with *M. tuberculosis* H37Ra and subsequently treated with the compounds. Both compounds **38b** and **38c** showed superior activity in the macrophage infection assay by achieving a 90% reduction of intracellular bacillary load after 4 days of treatment within the macrophage monolayer.

In order to identify the exact molecular target, the spontaneous resistant mutants were raised against 10x the MIC concentration of the tested compound **38b**. Genotyping of the AtpA-G units in the mutants showed the Lys (AAG) → Asn (AAT) transition at position 179 to be dominant and causing resistance to the phenyl substituted analogues (Fig 8). This mutation was mapped to subunit *a* of ATP synthase encoded by *atpB*.

Fig. 8: Single nucleotide polymorphism in squaramide **38b** resistant mutants.

Next, the compounds were tested against a bedaquiline (BDQ) resistant mutant confirming the susceptibility of the BDQ resistant mutant for the test compounds at a concentration (0.6 - 0.7 μM).

To further study the toxicity, the possibility for genotoxicity was excluded with a vitotox assay, closely correlated to an Ames test. No genotoxicity was detected for the compound series **38** for concentrations tested up to 128 μM.

To evaluate the drugability of the compounds, we tested their metabolic stability. All compounds showed extreme susceptibility for metabolic destruction by phase I murine CP450 enzymes but less extended to the phase II UGT enzymes. However, when repeating the assay with human CP450 and UGT enzymes, the overall stability improved, with a remainder of 85 and 95 % of the parental compound after enzymatic exposure.

Our squaramides were also docked into a model of ATP synthase, which was performed by our colleagues Karel Berka and Václav Bazgier from the Department of Physical Chemistry UP. Since no experimental structure was available for *M. tuberculosis*, we have used a homology model built using the SwissModel server over *M. smegmatis* structures. Since both mycobacteria share similar sequences with more than 75% identity, we have first docked squaramides using Autodock Vina into structures from *M. smegmatis* in various states. We have identified that squaramides bind specifically into the cavity between rotating *c* subunits (*atpE*) and static *a* subunit (*atpB*), but only to state 2. Squaramides bound with RHS directly interact with this residue (Fig. 9). LHS containing nitrogen as a hydrogen bond acceptor interacts with *M. smegmatis atpB* N174 (*M. tuberculosis* eq N172). Most contacts to *atpE* subunits are provided by nonpolar interactions - e.g. *M. smegmatis* I59 (*M. tuberculosis* I55). Squaramides thus fit the interface between subunits, effectively blocking the movement of the rotating subunits by binding to E177 residue.

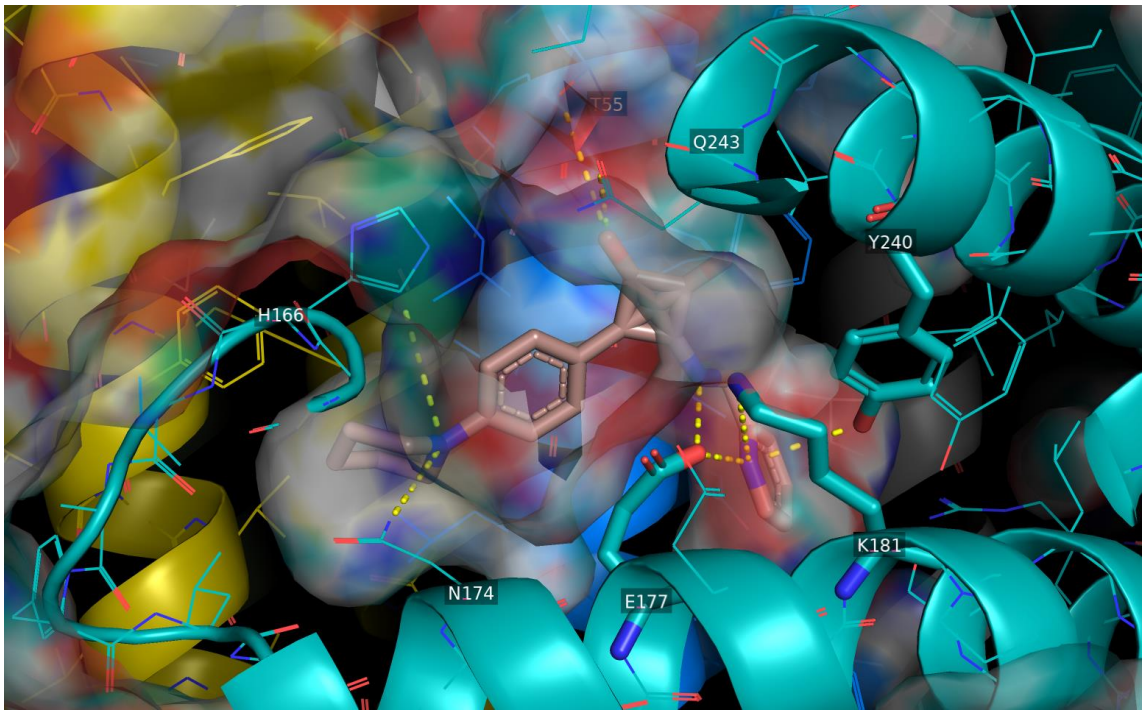

Fig. 9: Binding pose for compound **38b** into *Msm* ATP synthase in state 2 – pdbid:7njp. AtpB subunit is shown with cyan cartoon, AtpE subunits are shown in yellow and green colours in the background.

All results mentioned above in this chapter have been summarized in the manuscript and are prepared for publication. This multidisciplinary work comprises the design of

new analogues, their synthesis and characterization, and biological evaluation. Two undergraduate students and one PhD student were involved in synthesising new derivatives.

2.2.6 New synthetic pathways leading to various squaramides

The binding pose for compound **38b** into *Msm* ATP synthase illustrates a vast space for further modification of structure **38** (Fig. 10). We realized that the squaric acid skeleton is a unique feature, and its structural modification does not seem to be rational. On the other hand, there are many possibilities to optimize the LHS and RHS part of the squaramide structure.

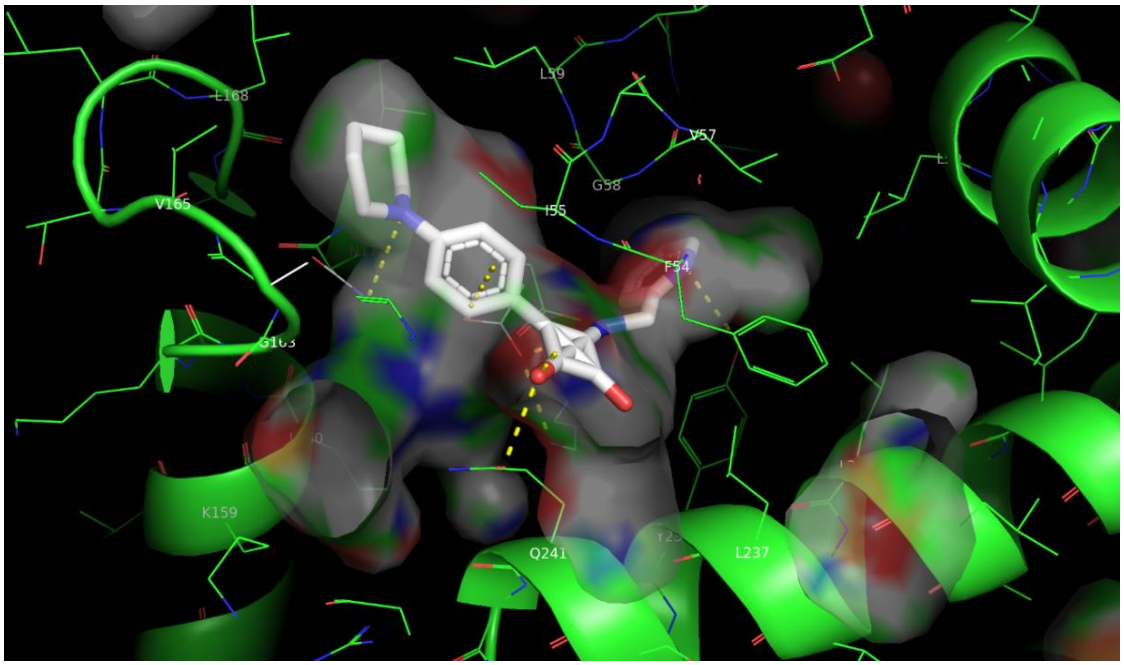

Fig. 10: Binding pose for compound **38b** into *Msm* ATP synthase, illustrating further possibilities for modification of parent structure.

For this reason, we aimed to develop novel and highly universal synthetic pathways that would enable us to prepare a wide range of squaramide analogues from available precursors. For our initial work in this area, we selected the Liebeskind-Srogl coupling as a universal method for C-C coupling using the number of commercially available boronic acids (Scheme 8). Synthesis utilized dichloro derivative **36** that was *in situ* converted to monochlor analogue **50**. The reaction of intermediate **50** with *p*-methoyxythiofenol followed by Liebeskind-Srogl cross-coupling reaction gave products **52**. Final

squaramides **53** were obtained upon the reaction of **52** with pyridin-2-ylmethanamine. I would like to point out that my student Jan Chasák carried out described synthetic work within his Master thesis.[46]

To develop a universal synthetic methodology, we used several boronic acids without a specific selection of substrates. However, consecutively, we will select appropriate analogues based on molecular docking and simultaneous biological tests.

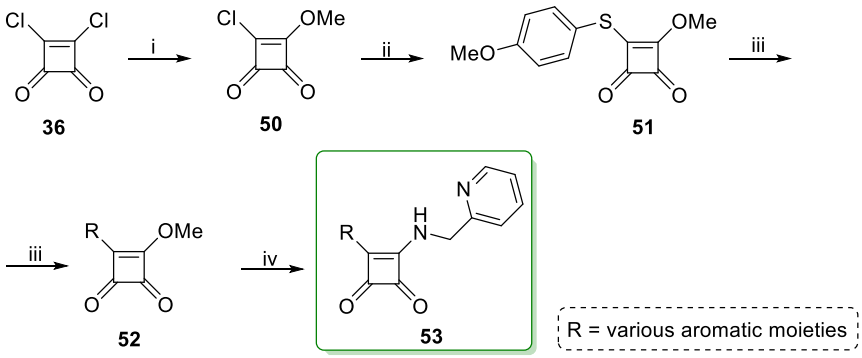

Scheme 8. Synthesis of new squaramide anlogues **53** based on the Liebeskind-Srogl coupling. Reagents and conditions: (i) dry MeOH, dry DCM, rt, 16 h; (ii) *p*-methoyxythiofenol, TEA, dry THF, rt, 30 min, 42-64 % over two steps; (iii) boronic acid/pinacol, CuTC, TFP, $Pd(dba)_3$, dry dioxan, 100 °C, 20 h, 12-89 %; (iv) pyridin-2-ylmethanamine, MeCN, rt, 30 min, 65-85 %.

We suggested new analogues **56** differing from previous compounds in amide bonds based on molecular docking. For suggested compounds, an efficient synthetic approach was developed (Scheme 9). Firstly, intermediate **54** was successfully prepared in high yield and converted to amides **55**. The final reaction with pyridin-2-ylmethanamine yielded compounds **56**. All amides **56** were synthesized by my PhD student Milan Dak.

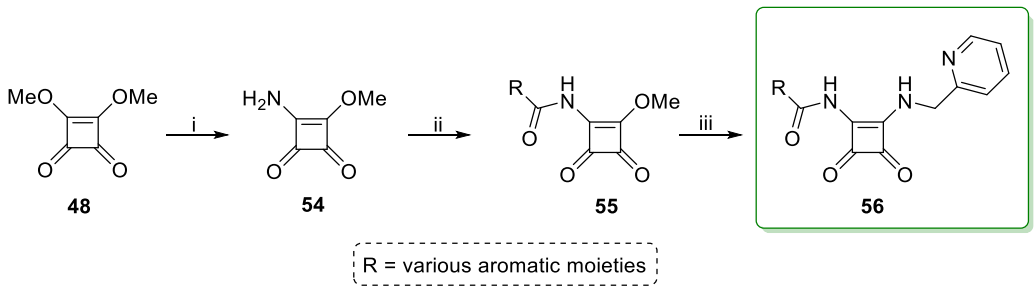

Scheme 9. Synthesis of squaramides **56**. Reagents and conditions: (i) NH_3 (g), Et_2O, 0 °C, 30 min, 89 %; (ii) R-COOH, EDC.HCl, DMAP, DMF, rt, 2h, 26-60 %; (iii) pyridin-2-ylmethanamine, MeCN, rt, 1 h, 60-90 %.

Analogues **56** are currently undergoing initial biological screening for their activity against *M. tuberculosis* H37Ra.

Obviously, the squaric acid scaffold is a particular feature with the potential to be further developed into drug candidates for tuberculosis. Our systematic investigation of squaric acid analogues revealed some specific modifications, demonstrating the significant potential for structure-based design in developing next-generation antituberculosis drugs.

3 Mycobacterial Zmp1 inhibitors

Zinc metalloprotease 1 (Zmp1) is a *Mycobacterium tuberculosis* 75 kDa secreted enzyme found to be essential for intracellular survival and *M. tuberculosis* pathogenicity.[48,49] In 2008, Master *et al.* described that mycobacterial Zmp1 interferes with the macrophage phagosome maturation by inhibiting caspase-1 activation and thereby reduction of IL-1β secretion (Fig. 11).[48] This disruption of the signalling pathway for inflammasome activation prevents the early inflammatory response necessary for the complete clearance of the invalid pathogen.[50] However, the molecular mechanism of caspase-1 inhibition by Zmp1 has not been fully elucidated to date. Zmp1 and its inhibition leading to attenuation of virulence may represent a potentially useful drug target and is worthy of further investigation.

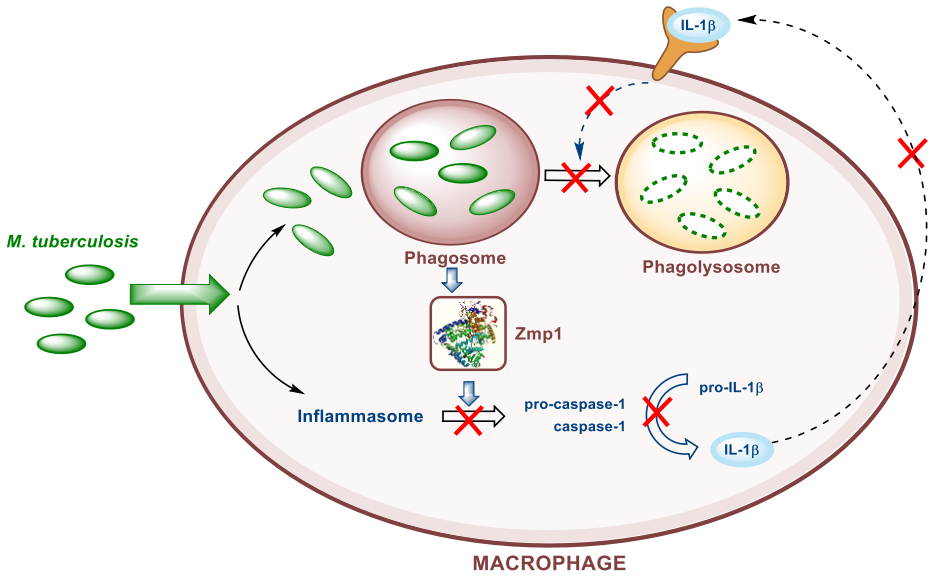

Fig. 11: Inhibition of the phagosome maturation process by mycobacterial Zmp1 (this figure was drawn according to Ferraris and Rizzi).[51]

3.1 Structure of mycobacterial Zmp1

The first structural characterization of Zmp1 was published in 2011 by Ferraris *et al.* (Fig. 12).[52] They recombinantly expressed Zmp1 in *Escherichia coli*, purified and co-crystalized with the known broad-spectrum inhibitor of Zn-dependent metalloproteases

phosphoramidone. Experiments carried out showed that Zmp1 is composed of two mainly α-helical lobes interconnected by several loops distributed over the protein equatorial line (Fig. 12). The active site of Zmp1 is located between two lobes with the catalytic zinc ion coordinated in a tetrahedral geometry by the conversed residues His497 and His493.

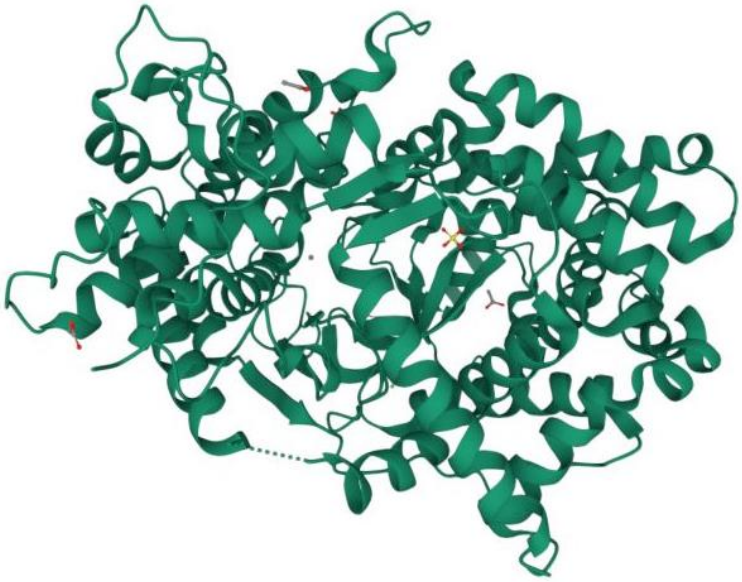

Fig. 12: Crystal structure of *Mycobacterium tuberculosis* zinc metalloprotease Zmp1 in complex with inhibitor (PDB: 3ZUK; figure created using Mol* Viewer).[52]

The exciting study describing two open-state cryo-EM (cryo-electron microscopy) structures of Zmp1 was published recently by Liang *et al.* (Fig. 13).[53] Their structural analysis highlighted the key conformational states for structural enzymology studies.

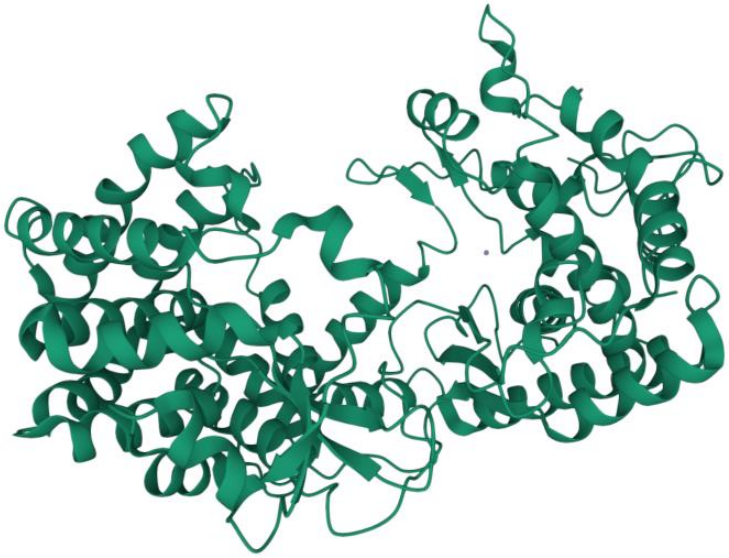

Fig. 13: Cryo-Em structure of *M. tuberculosis* Zmp1 in the open state (PDB: 6XLY; figure created using Mol* Viewer).[53]

3.2 Zmp1 inhibitors

The initial study on effective mycobacterial Zmp1 inhibitors was published by Peterea *et al.* in 2012, who investigated the interaction of this metalloprotease with phosphormadion and chelators such as 1,10-phenanthroline and EDTA.[50] A relatively limited number of additional studies on this topic followed.[54–59] All published substances contain the rhodanine skeleton,[54–57] hydroxamate moiety[58] or thiazolidinedione heterocycle.[59] They are characterized by a chemical entity with an affinity towards Zn^{2+} ion called zinc-binding group (ZBG).

The most potent inhibitors are depicted in Fig. 14, along with the relevant available data. However, it is hard to compare the functionality of these inhibitors as some of them were studied merely theoretically in terms of Zmp1 inhibition using molecular docking studies (Fig. 14, compounds **59** and **60**).[55,56] Regarding the mycobacterial Zmp1 inhibition, compound **61**[58] exhibited the best experimental results to date. All structures will be discussed in more detail below.

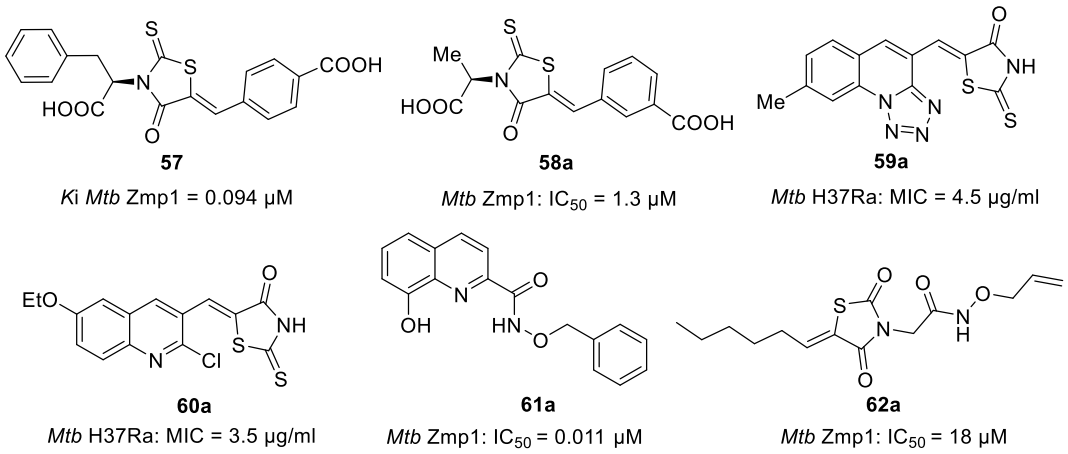

Fig. 14: Structures of known Zmp1 inhbitors.[54–59]

3.2.1 Inhibitors containing rhodanine heterocycle

The first inhibitors containing rhodanine skeleton were described by Mori *et al.* in 2014.[54] The combination of *in silico* design and biochemical studies led to the identification of the small molecule inhibitor **57** reaching the nanomolar K_i of 94 nM (Scheme 10). Synthesis of this compound started from optically pure phenylalanine **63**, which was reacted with carbon disulfide, giving intermediate **64**. Subsequent reaction with sodium

chloroacetate, acidic cyclization, and final Knoevenagel condensation (Verley modification) gave the desired inhibitor **57**.

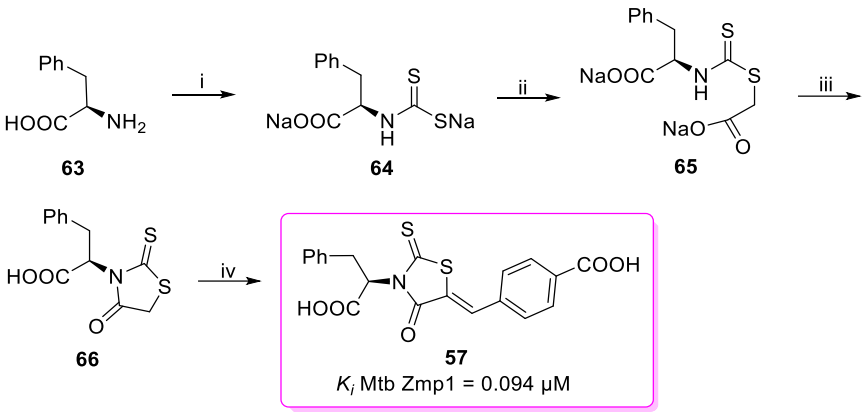

Scheme 10. Synthesis of title compound **57**.[54] Reagent and conditions: (i): CS_2, NaOH, H_2O, rt, on; (ii) sodium chloroacetate, H_2O, rt, 2 h; (iii) 6 M HCl, $POCl_3$, 75 °C, 4 h, 66 %; (iv) *p*-carboxybenzaldehyde, *β*-alanine, CH_3COOH, reflux, 6 h, 83 %.

Mori and co-workers enriched the library of rhodanines with inhibitors **58** (Scheme 11).[57] Synthesis proceeded analogously as in the case of previous inhibitor **57** with the application of appropriate precursors.

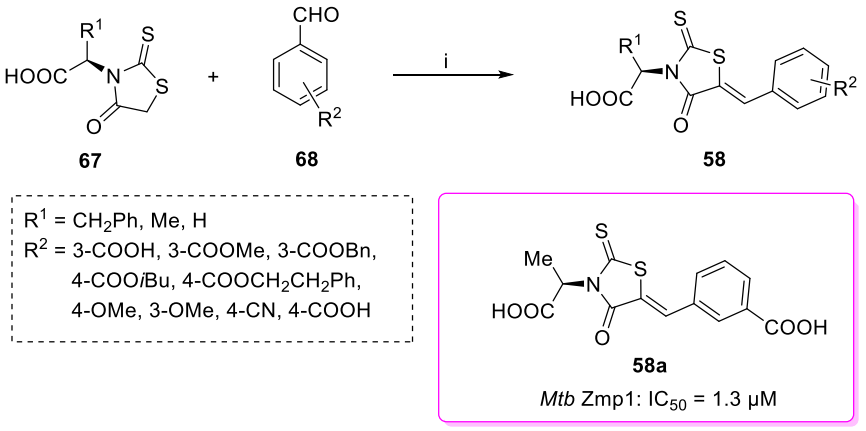

Scheme 11. Synthesis of the title compounds **58**.[57] Reagent and conditions: (i): *β*-alanine, CH_3COOH, reflux, 6 h, 50-94 %.

Furthermore, Mori *et al.* synthesized aminothiazoles **72** and **73** as possible rhodanine-mimetics (Scheme 12).[57] Synthesis of aminothiazole analogues started with methylation of commercially available D-phenylalanine **63**, giving methyl ester **69**. Subsequently, this ester was reacted with methoxycarbonyl isothiocyanate and

hydrolyzed with sodium hydroxide to obtain thiourea **71**. The Hantzsch synthesis of thiazole consisting of the condensation of α-bromoacetophenones with thiourea **71** yielded the final compounds **72**. The saponification of methyl esters **72** gave the corresponding dicarboxylic acids **73**.

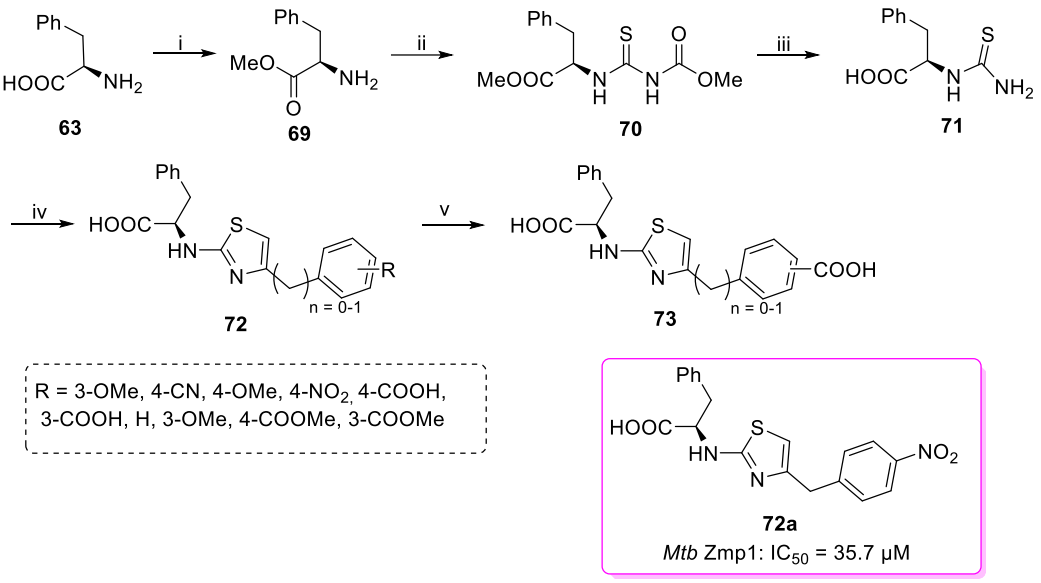

Scheme 12. Synthesis of thiazole conjugates **72** and **73**.[57] Reagent and conditions: (i) $SOCl_2$, dry MeOH, 0 °C to rt, 1 h, 99 %; (ii) methoxycarbonyl isothiocyanate, DIPEA, DCM, 0 °C to rt, 1 h, 94 %; (iii) 3 N NaOH, MeOH, reflux, 1 h, 74 %; (iv) DMF, rt, 1-3 h, 72-91 %; (v) NaOH/MeOH/THF, reflux, 3 h, 83-87 %.

Evaluation of the inhibitory activity of rhodanines **58** and thiazoles **72** and **73** against recombinant Zmp1 of *M. tuberculosis* revealed that all tested rhodanines exhibited activity in the range IC_{50} = 1.3 – 43.9 μM. On the other hand, only two thiazoles showed modest inhibition. The most active thiazole **72a** is depicted in Scheme 12.

Further rhodanine-based compounds were studied by Subhedar *et al.* in 2016 (Scheme 13).[55] Collective of authors synthesized various conjugates **59** using [HDBU] $[HSO_4]$ acidic ionic liquid as a catalyst for the key step of synthesis – Knoevenagel condensation. Authors studied all synthesized compounds **59** for their biological activity against several pathogens. However, the research point consists of assessing antimycobacterial activity against *M. tuberculosis* and the molecular docking studies against mycobacterial Zmp1. The most active analogue **59a** exhibited MIC = 4.5 μg/ml.

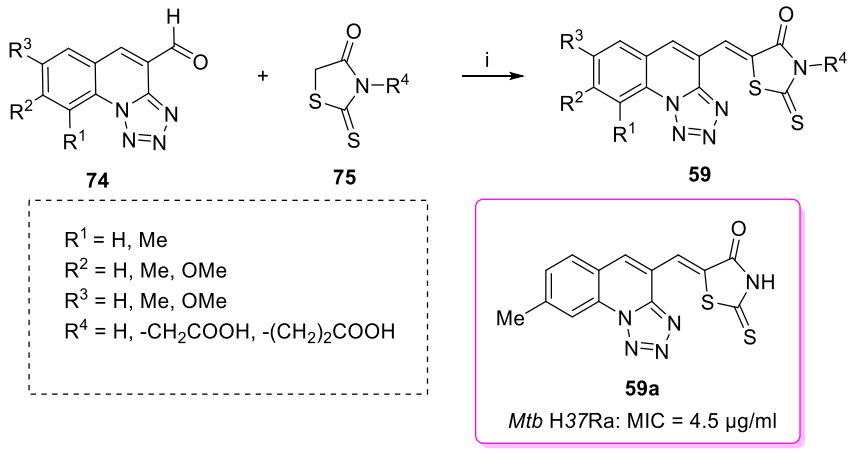

Scheme 13. Synthesis of rhodanine-tetrazoloquinoline conjugates **59**.[55] Reagents and conditions: (i) [HDBU][HSO_4], solvent-free, 80 °C, 30 min, 82-90 %.

A year later, the same group published a study on rhodanine-quinolidine conjugates (Scheme 14).[56] Authors prepared aldehydes **78** that were further subjected to DBU acetate catalyzed Knoevenagel condensation with various rhodanines giving final substrates **60** in high yields. A series of conjugates were evaluated for their *in vitro* antimycobacterial properties against *Mycobacterium tuberculosis* H37Ra and *Mycobacterium bovis* BCG. Several compounds exhibited antimycobacterial activity with MIC ranging from 3.5 to 19.9 µg/ml against *M. tuberculosis* H37Ra. The most active analogue **60a** is depicted in Scheme 14. Follow-up molecular docking studies indicated the binding modes of concerned molecules in the active site of mycobacterial Zmp1. Nevertheless, no experimental study in this respect was provided.

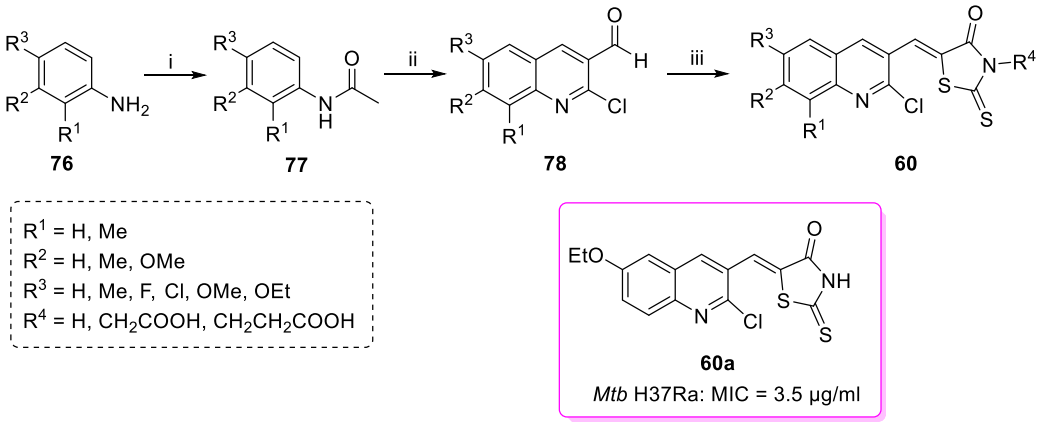

Scheme 14. Synthesis of rhodanine-quinolidine conjugates **60**.[56] Reagents and conditions: (i) acetanhydride, reflux, 3-4 h; (ii) DMF, $POCl_3$, 100 °C, 16 h; (iii) rhodanines, [DBUH][OAc], solvent-free, 80 °C, 30 min, 80-91 %.

3.2.2 Inhibitors containing hydroxamates

In 2018, Paolino *et al.* published the most active Zmp1 inhibitors to date based on the hydroxyquinoline-hydroxamate skeleton.[58] Authors synthesized a small set of 8-hydroxyquinoline-2-hydroxamates **61** through a straightforward synthetic approach depicted in Scheme 15. Using a fluorimetric assay, all final compounds were studied for their *in vitro* inhibitory properties against Zmp1. Moreover, the binding mode was further analyzed by molecular docking studies. Interestingly, five compounds from the evaluated library exhibited nanomolar potencies. The best candidate, **61a**, is depicted in Scheme 15.

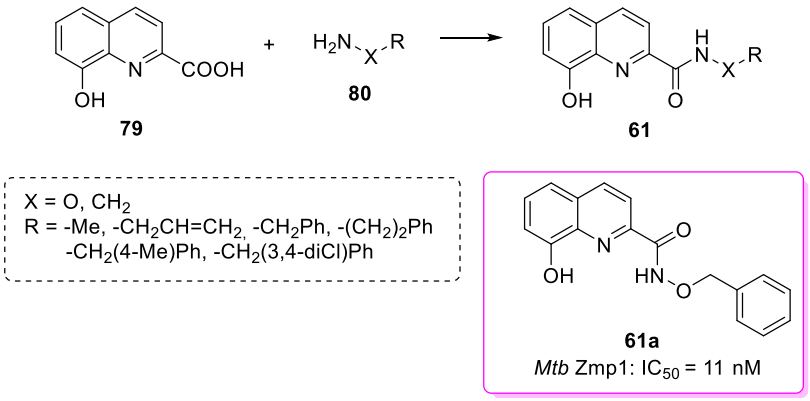

Scheme 15. Synthesis of hydroxyquinoline-hydroxamates **61**.[58] Reagents and conditions: HOBt, EDC, NMM, DMF, rt, 2 h, 35-77 %.

3.2.3 Inhibitors containing thiazolidinediones

The last described inhibitors to date were published by our group in 2020.[59] We have developed an efficient and straightforward synthetic protocol to prepare a series of thiazolidinedione-hydroxamates **84** and **62** (Scheme 16). Synthesis of both series started with thiazolidinedione **81**. Firstly, the starting material was converted to esters **82** by reacting with bromoacetate or methyl 2-bromopropionate. Subsequent acid-catalyzed hydrolysis and coupling reaction with *O*-allylhydroxylamine hydrochloride or *O*-benzylhydroxylamine hydrochloride gave products **84**. Synthesis of inhibitors **62** was initiated with Knoevenagel condensation of thiazolidinedione **81** with various aldehydes yielding precursors **85**. The rest of the reaction sequence proceeded similarly to the previous synthesis of products **84**.

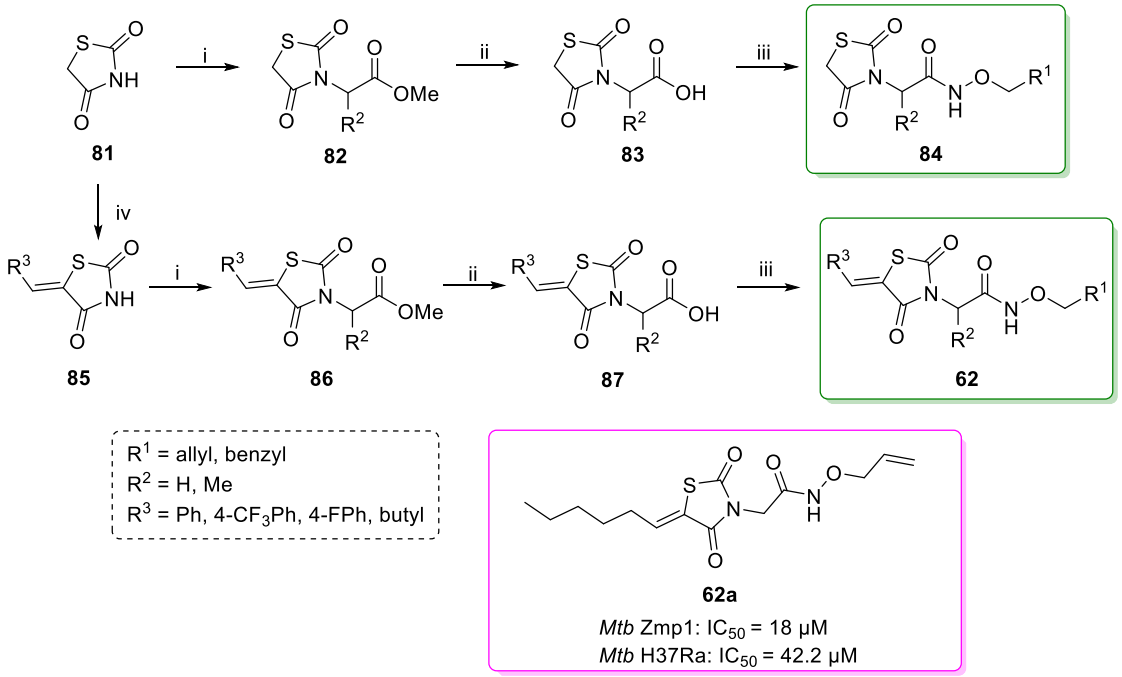

Scheme 16. Synthesis of thiazolidinediones **84** and **62**.[59] Reagents and conditions: (i) methyl bromoacetate or methyl 2-bromopropionate, NaH, DMF dry, rt, 16 h; (ii) HBr (40%), reflux, 5 h; (iii) *O*-allylhydroxylamine hydrochloride or *O*-benzylhydroxylamine hydrochloride, EDC.HCl, H_2O, rt, 2 h, 31-75 %; (iv) aldehyde, piperidine, EtOH, reflux, 5 h.

Further, the inhibitory properties of prepared compounds towards a recombinant Zmp1 from *Mycobacterium tuberculosis* were assessed by prof. Marek Šebela (Department of Biochemistry, UP Olomouc) by MALDI-TOF MS. This characterization was completed by the evaluation of their antimycobacterial activity and acute cytotoxicity using whole-cell assays performed by Dr. Davie Cappoen (University of Antwerp, Belgium).

As expected, the extracellular antimycobacterial activity was rather limited, whereas antimycobacterial activity against intracellular residing bacteria was present for most tested compounds. Moreover, our results showed that none of the synthesised thiazolidinedione-hydroxamates possessed acute cytotoxic effects against RAW264.7 macrophages. The existing structural differences were reflected in the variability of the *in silico* predicted parameters and biologically determined responses. Our results indicate a significant potency of the suggested thiazolidinedione-hydroxamates, where compound **62a** (Scheme 16) was considered the best candidate from the first generation library.

3.2.4 Other inhibitors prepared by our group

Molecular docking of the first generation of thiazolidinediones[59] showed us that the studied compounds would rather occupy the entrance into the central cavity than the zinc catalytic site.[59] Therefore, we designed novel derivatives **88** with a longer peptide chain containing a terminal zinc-binding group COOH or COOMe (Fig. 15) that was proven to interact with the zinc ion at the active site according to molecular docking studies.

Furthermore, thiazolidinediones are presented as PAINS (pan-assay interfering compounds) and might be problematic for developing drug-like molecules.[60] Careful biophysical tests will have to be performed to verify the target engagement of the hit compounds. For this reason, we designed novel classes **89** and **90** of compounds (Fig. 15) with the modified central heterocyclic scaffold. Based on molecular docking, these compounds appear to bind with a similar or higher affinity toward Zmp1 than those from the first generation.

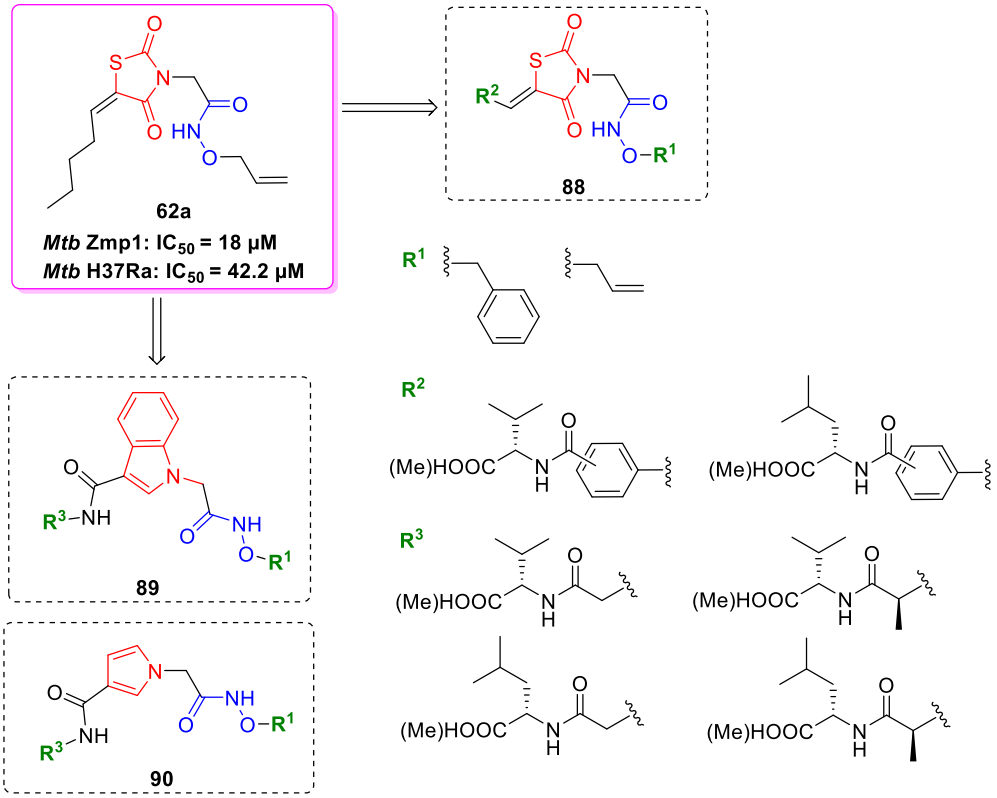

Fig. 15: Design of novel Zmp1 inhibitors.

Synthesis of inhibitors **88** was performed by my PhD student Milan Dak (Scheme 17). The first step of the reaction sequence was an aldol condensation between thiazolidine-2,4-dione **80** and the corresponding aldehydes to form esters that were

hydrolyzed, giving acids **91**. The subsequent reaction between the corresponding carboxylic acids **91** and the suitably modified amino acids gave thiazolidinediones **92**. These modified thiazolidinedione derivatives **92** were subsequently alkylated using *tert*-butyl bromoacetate. The removal of the *tert*-butyl group using a mixture of trifluoroacetic acid and dichloromethane gave the corresponding carboxylic acids **93**, which were further subjected in the final step to reaction with the corresponding hydroxylamines using EDC.HCl.

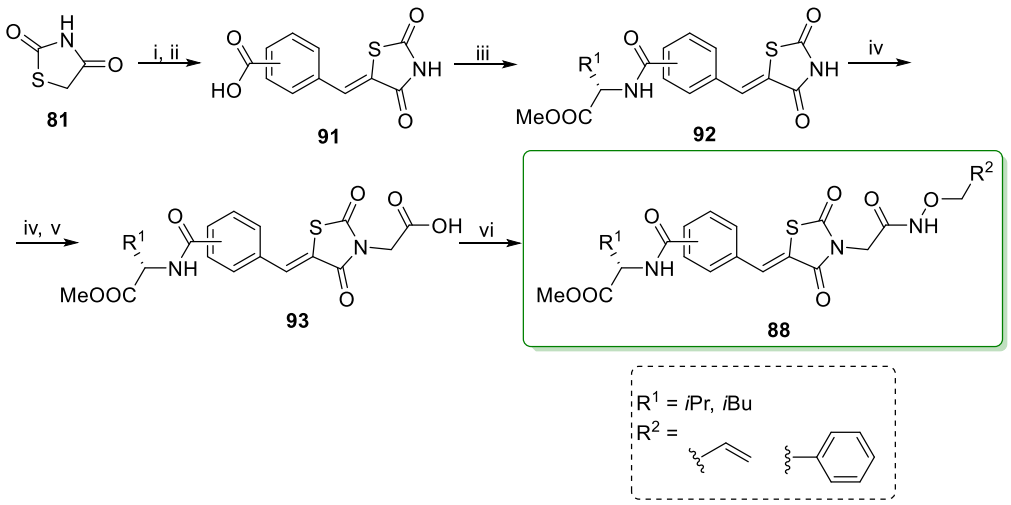

Scheme 17. Synthesis of thiazolidinediones **88**. Reagents and conditions: (i) methyl 4/3-formylbenzoate, piperidine, EtOH, reflux, 20 h, 73-74 %; (ii) 6M HCl, reflux, 4 h, 84-94 %; (iii) L-leucine / L-valine methyl ester.HCl, DIPEA, HOBt, EDC.HCl, DMF, rt, 19 h, 50-64 %; (iv) *tert*-butyl bromoacetate, K_2CO_3, TBAI, acetone, 40 °C, 18 h, 70-93 %; (v) TFA, DCM, rt, 2 h, 82-95 %; (vi) allyl/benzyl hydroxylamine.HCl, EDC.HCl, H_2O:THF, rt, 2 h, 59-86 %.

To avoid unwanted interactions of TZDs as pan-assay interfering compounds (PAINS),[60] we utilized scaffold hopping to substitute the central TZD for an indole or pyrrole moiety proposing hydroxamates **89** or **90**, respectively (Fig. 15). Despite some structural similarity with previous TZD-hydroxamates, a notably different synthetic pathway toward indole/pyrrole hydroxamates was needed and carried out by my PhD student Veronika Šlachtová.[61]

All the synthetic effort started with constructing the dipeptide side chains, which is described in the PhD thesis of Veronika Šlachtová in more detail.[61] The synthesis of indole/pyrrole final compounds proceeded according to the protocol depicted in

Scheme 18. Commercially available methyl indole or pyrrole-3-carboxylates **94** were chosen as starting materials. The reaction sequence started with *N*-alkylation utilizing *tert*-butyl bromoacetate. Selective removal of *tert*-butyl from diesters provided intermediates **95**. The desired heterocyclic hydroxamates **96** resulted from the coupling of intermediate acids **95** with *O*-alkyl hydroxylamine hydrochlorides. Subsequent basic hydrolysis of the methyl ester produced the free acids **97** conjugated with various dipeptides giving intermediates **98**. Base-mediated methyl ester cleavage accomplished the formation of the target indole / pyrrole-hydroxamates **89** and **90**. Our synthetic protocol yielded two series of heterocyclic hydroxamates **89** and **90** isolated in lower yields ranging from 2 to 60 % in two steps.

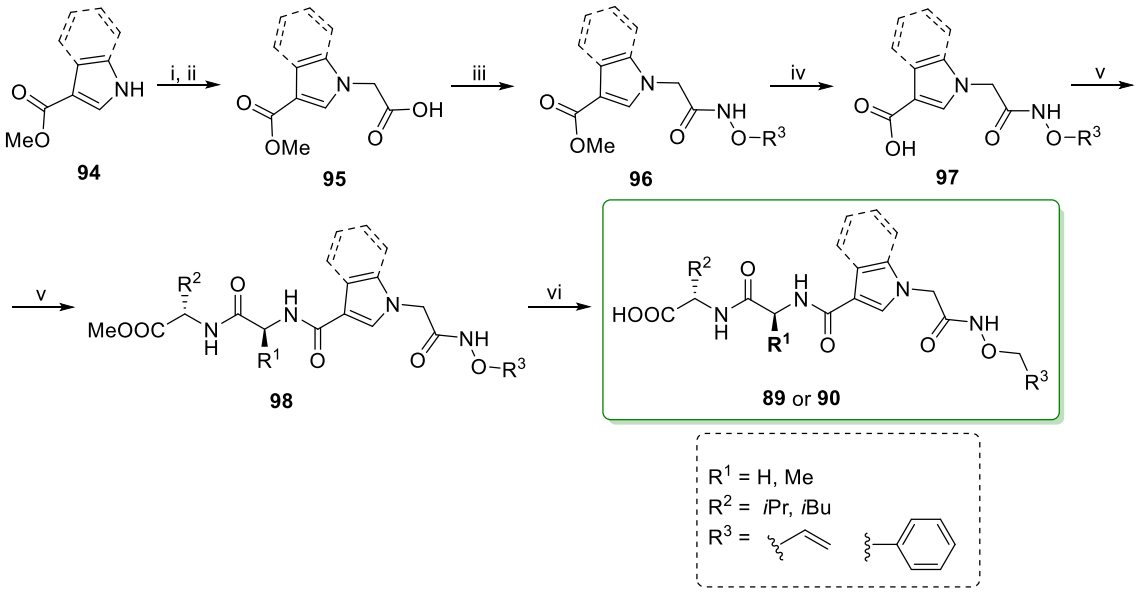

Scheme 18. Synthesis of pyrrole/indole-hydroxamates **89** and **90**. Reagents and conditions: (i) K_2CO_3, *tert*-butyl bromoacetate, MeCN, reflux, 16 h 83-90 %; (ii) TFA, DCM, rt, 2 h, 95-98 %; (iii) *O*-allylhydroxylamine.HCl/*O*-benzylhydroxylamine.HCl, EDC.HCl, H_2O, rt, 2 h, 73-92 %; (iv) 2 M aq. LiOH, THF, 60 °C, 2 h, 56-98 %; (v) dipeptides, EDC.HCl, HOBt, DIPEA, DMF, rt, 16 h; (vi) LiOH, H_2O, MeOH, rt, 2 h, 2-60 %.

No direct activity of synthesized heterocyclic hydroxamates **88-90** was observed in the whole-cell assay against *Mycobacterium tuberculosis* and *Mycobacterium bovis*. However, the thiazolidinediones **88** showed dose-dependent inhibition of intracellular survival of *Mycobacterium tuberculosis* H37Ra. Furthermore, the inhibition was structure-dependent, with the most active derivative **88a** (Fig. 16) inducing an 83.2%

reduction of bacterial survival within the macrophage host cell. The promising biological activity confirmed thiazolidinediones **88** as potent Zmp1 inhibitors that can be used as tool compounds for further exploration of the role of Zmp1 for *in vivo* pathogenicity.

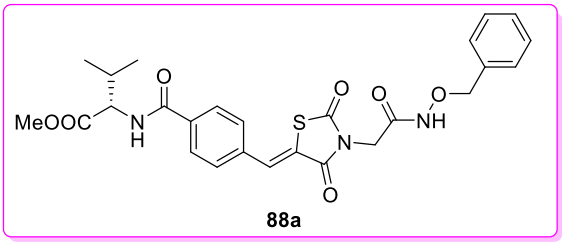

Fig. 16: The most active analogue from tested heterocyclic hydroxamates **88-90** in a macrophage infection assay.

Further, interesting inhibitory properties of analogues **88-90** towards a recombinant Zmp1 were analyzed by MALDI-TOF MS by our colleague prof. Marek Šebela (Department of Biochemistry, UP Olomouc). Followed a previously developed procedure[59] based on monitoring the peptidolytic conversion of angiotensin II (DRVY↓IHPF) in the reaction mixture, we assessed the inhibitory properties of all derivatives **88-90**. Most compounds provided only a weak inhibition at 40 µM concentration. However, a few exceptions are depicted in Fig. 17.

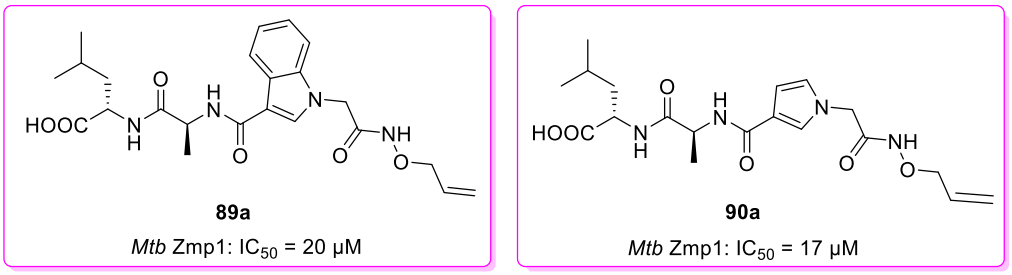

Fig. 17: Structures of the most potent inhibitors from libraries of analogues **88-90** analyzed by MALDI-TOF MS.

IC_{50} values were 20 and 17, respectively, narrowing the best candidates to **89a** and **90a** (Fig. 17). A possible interpretation suggests the superiority of the pyrrole and indole central moiety over that of thiazolidinedione. The most favourable substitutions R^1, R^2 and R^3 at the pyrrole/indole-based scaffold seem to be Me, *i*Bu, and allyl, respectively, or, with lower efficiency, H, *i*Pr and benzyl, respectively.

To sum up our achievements in the new mycobacterial Zmp1 inhibitors development, we designed and synthesized collections of new compounds and evaluated their inhibitory properties. Our first generation of thiazolidinedione-hydroxamates comprising the most active inhibitor **87a** reaching the IC_{50} = 18 μM (*M. tuberculosis* Zmp1) was published in *Eur. J. Med. Chem.* in 2020.[59] Following the first generation of thiazolidinedione-hydroxamate analogues, we designed and synthesized next-generation libraries **88**-**90**. While these compounds did not exhibit significant antimycobacterial potency, few analogues proved to be as active as previous analogue **87a**. The presented study results clearly indicate the potency of our inhibitors towards zinc-dependent metalloprotease Zmp1 and provide a platform for future structure-based optimization.

4 Phenotypic screening

Phenotypic screening is one of two strategies in new drug development, as discussed in Chapter 1.4.3. Phenotypic whole-cell-based assays screen for compounds inhibiting pathogen growth to identify hits for further optimization and deconvolution of the mode of action (MoA). Importantly, this approach has a high potential to open the path for discovering compounds that could inhibit completely new targets or new pathways, leading to the identification of a new compound highly active against MDR or XDR TB strains.

The efficient use of this approach is fueled by progress in combinatorial chemistry comprising synthetic methods used to prepare a large number of compounds in a single process. Consequently, high-throughput screening (HTS) is established as a tool for the fast screening of the biological activity of the compound library. HTS can identify candidates for further optimization and rapidly exclude compounds with a poor or no effect.

Without any particular mycobacterial target, we suggested several libraries to be synthesized and evaluated for their biological activity using a phenotypic screening approach (Fig. 18).

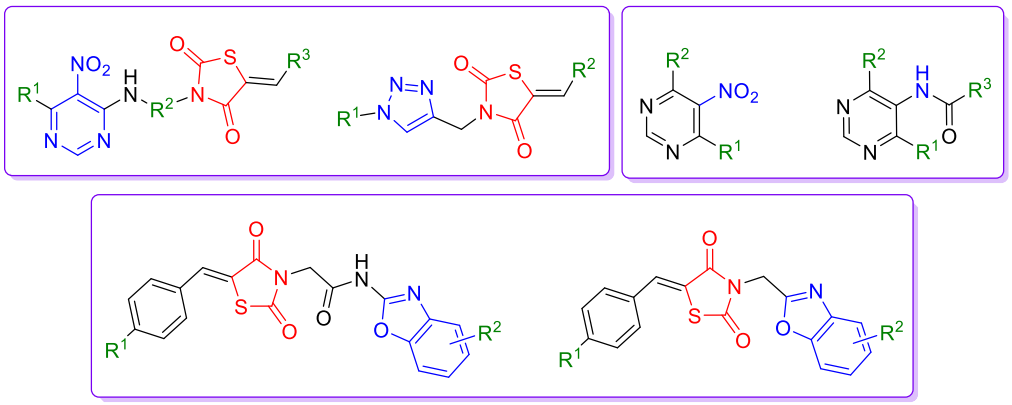

Fig. 18: Compounds designed for phenotypic screening (note: substituents R^1-R^3 will be explained further).

All these structures were designed as a follow-up to analogies in the literature. All chemical libraries were parts of the Bachelor, Master, or PhD thesis of my students and

will be discussed separately below. It should also be mentioned that these students´ projects were mainly devoted to developing synthetic procedures leading to designed compounds.

4.1 Thiazolidinedione-based conjugates

When we studied the thiazolidinedione heterocycle described above as a scaffold for Zmp1 inhibitors, we realized many biologically active compounds comprising this structural motive. Since the combination of two pharmacophores is a well-established approach for designing more potent drugs with a significant increase in biological activity, we decided to combine thiazolidinedione with other pharmacophores.

4.1.1 Thiazolidinedione-pyrimidine conjugates

Our first conjugates published in 2019 were based on the combination of a thiazolidinedione and pyrimidine heterocycles (Scheme 19).[62] First of all, we decided to employ the solid-phase synthetic approach based on easily accessible building blocks and very simple chemical operations, enabling the effective development of potent experimental therapeutics of this type in a combinatorial manner. The target conjugates were synthesized on Wang resin *via* immobilization of lipophilic amino acids to optimize the overall drug-likeness of final hybrids.[63] Both heterocycles were connected by an appropriate linker. Herein, ethylenediamine and propylenediamine were selected for primary screening. Modification of thiazolidinedione core included a typical benzylidene or alkylidene substitution pattern.[64]

The solid-phase synthesis started with amino acid immobilization on Wang resin (Scheme 19). Resin **100** underwent Fmoc deprotection, substitution with 4,6-dichloro-5-nitropyrimidine and treatment with aminoethanol or aminopropanol, resulting in resins **101**. Subsequent Fukuyama-Mitsunobu transformation then yielded the key polymer-supported intermediate **102**. Knoevenagel condensation of resins **102** with various aldehydes resulted in conjugates **104**. The desired thiazolidinedione-pyrimidine conjugates **103** and **105** were finally isolated by standard acidic cleavage and subsequent HPLC purification. Notably, after Knoevenagel condensation, the formation of two geometrical isomers *E* or *Z* is possible. These two isomers can be easily distinguished by the ^{1}H NMR spectral characteristics. The NMR elucidation confirmed the formation of *Z* isomers for all our products. The reaction proceeded smoothly with aromatic aldehydes

bearing electron-withdrawing or electron-donating groups as well as aliphatic aldehydes, giving the target products in crude purity between 58 and 91 %. Overall yields ranged from 29 to 63 %. All synthetic procedures were performed by my student Veronika Šlachtová within her PhD thesis, in which all detailed information can be found[61] besides the published paper.[62]

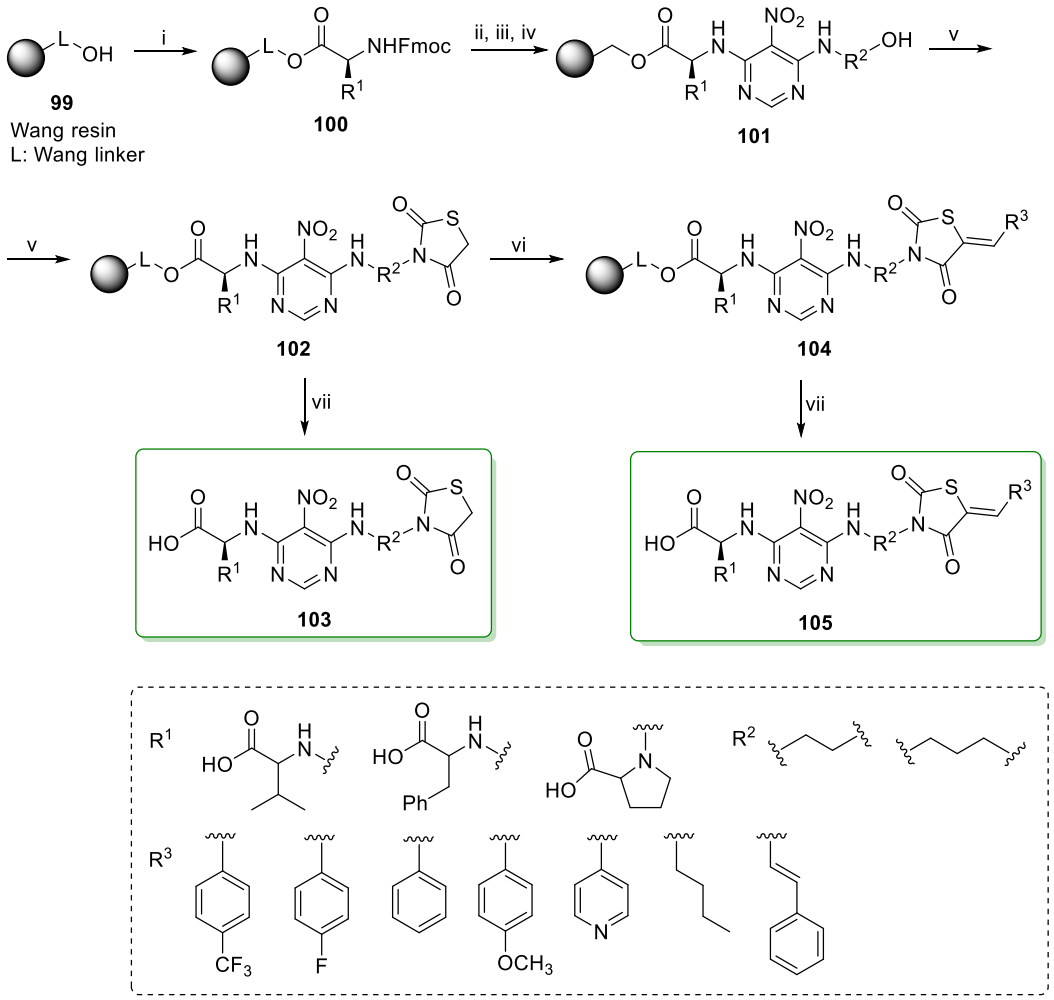

Scheme 19. Solid-phase synthesis of thiazolidinedione-pyrimidines **103** and **105**. Reagents and conditions: (i) Fmoc-amino acid, HOBt, DMAP, DIC, DMF/DCM (1:1), rt, 16 h; (ii) 50% piperidine, DMF, rt, 15 min; (iii) 4,6-dichloro-5-nitropyrimidine, DIPEA, DMF, rt, 2 h; (iv) amino alcohol, DIPEA, DMF, rt, 2 h; (v) thiazolidine-2,4-dione, PPh_3, DIAD, THF, rt, 1 h; (vi) aldehyde, piperidine, DMF, 70 °C, 16 h; (vii) 50% TFA in DCM, rt, 1 h.

Afterwards, all final compounds were evaluated for their antimycobacterial and antibacterial properties. All these assays were performed by Dr. Lucie Janovská from the

Department of Microbiology, Faculty of Medicine and Dentistry, UP. We assessed their properties against several gram-positive and gram-negative bacterial strains (*S. aureus*, *P. aeruginosa*, *E. coli*, *E. faecalis*) and two fungal strains (*C. albicans*, *A. niger*). Thiazolidinedione-pyrimidines **103** turned out completely inactive. On the contrary, conjugates **105** were a little bit more potent. However, none of the compounds was considered acceptable for further optimization (Fig. 19).

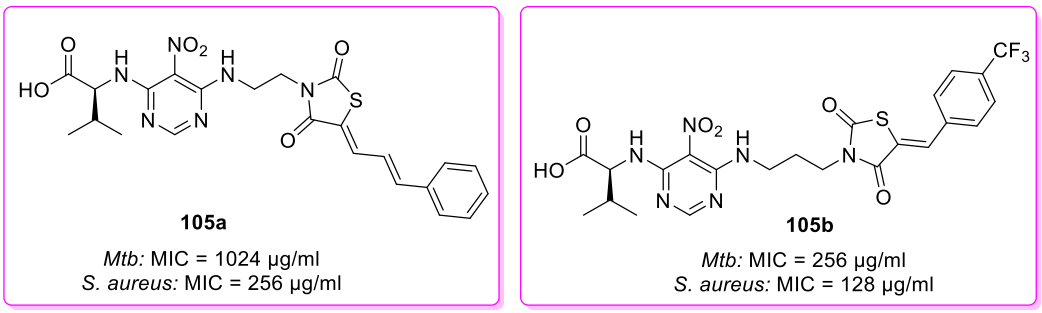

Fig. 19: The most active analogues from the series **103** and **105**.

It is worthy of notice that we implemented a rather controversial nitro group to our structures. The nitro group is often considered a toxic moiety leading to mutagenicity and genotoxicity. However, it was proved that mycobacteria have an ability to deal with this problem, as is demonstrated by two FDA approved drugs (Delamanid and Pretomanid) comprising the nitro group in their structures.

4.1.2 Thiazolidinedione-triazole conjugates

We decided to continue with the thiazolidinedione-based combinatorial approach to extend the possibilities for phenotypic screening. In this case, we focused on the triazole moiety with unique antimycobacterial potential[65] and constructed conjugates of thiazolidinedione with 1,2,3-triazole (Scheme 20). Our interest in such a combination was further enhanced by the reported promising pharmacological properties of the thiazolidinedione-triazole hybrids.[66,67]

Synthesis of designed hybrids relied on Cu^{I} catalyzed azide-alkyne cycloaddition (Scheme 20).[68] For this reason, we selected three simple azide-substituted residues R^1 for the initial investigation to reveal any possible consequences of the triazole ring modification. Moreover, thiazolidinedione heterocycle was further diversified by various benzylidenes or alkylidenes according to the prevalent literature.[64]

A straightforward synthetic protocol (Scheme 20) performed by my PhD student Veronika Šlachtová[61] started with *N*-alkylation of thiazolidinedione **80** with propargyl bromide under standard conditions using K_2CO_3 in refluxing acetone[69] giving derivative **106**. Subsequently, alkyne derivative **106** underwent Cu^I catalyzed azide-alkyne cycloaddition resulting in the desired hybrids **107** in low to moderate isolated yields of 13-58 %. Synthesis of thiazolidinedione-triazole conjugates **110** (Scheme 20) was initiated with Knoevenagel condensation and followed with *N*-alkylation providing alkynes **109** in excellent 50-97% isolated yields. Final compounds **110** were obtained after Huisgen cycloaddition of **109** with various azides.

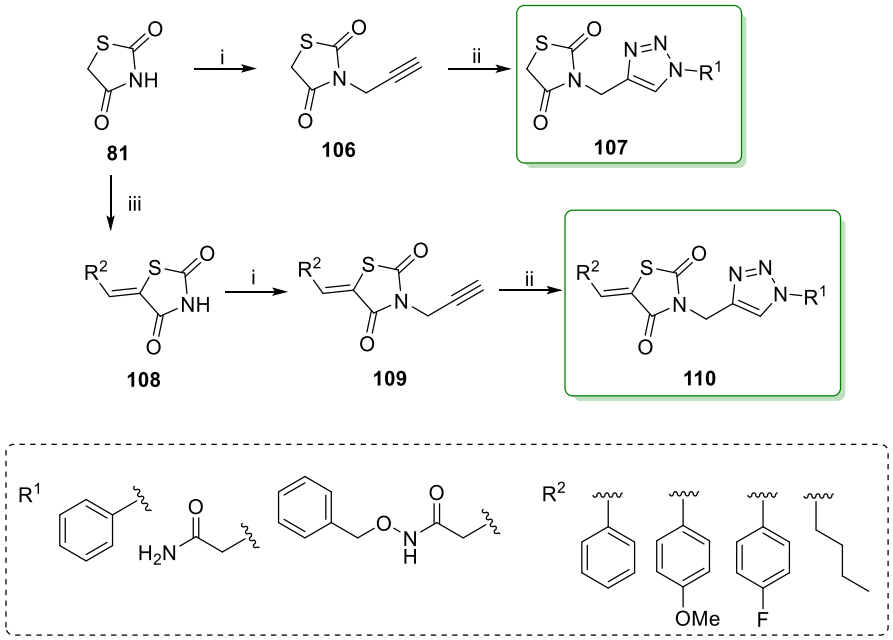

Scheme 20. Synthesis of thiazolidinedione-triazoles **107** and **110**. Reagents and conditions: (i) propargyl bromide, K_2CO_3, acetone, reflux, 16 h, 48 %; (ii) azide, sodium ascorbate, $CuSO_4 \cdot 5H_2O$, DMF, rt, 5 h; (iii) aldehyde, piperidine, EtOH, reflux, 16-20 h.

We tested the antimycobacterial potency of the thiazolidinedione-triazole library against *M. tuberculosis* H37Ra in cooperation with Dr. Davie Cappoen. None tested conjugates showed significant antimycobacterial activity with IC_{50} and MIC values > 64 μM. Further, acute cytotoxicity against human lung fibroblast MRC-5 cells (ATCC® CCL-171) was assessed. Three compounds, all harbouring a pentilidene group, showed a cytotoxic effect with CC_{50} values of 31.29, 28.47 and 35.49 μM (Fig. 20). Though, these effects do not exceed the cytotoxic effect of the reference drug tamoxifen (CC_{50} = 11.06 μM).

Apart from the antimycobacterial activity, the compounds were tested for their activity against the Gram-negative bacterium *Escherichia coli* (ATCC® 8739TM), the Gram-positive bacterium *Staphylococcus aureus* (ATCC® 6538TM) and the yeast *Candida albicans* (SC5314). None of the compounds showed activity against these species with IC_{50} > 64 μM.

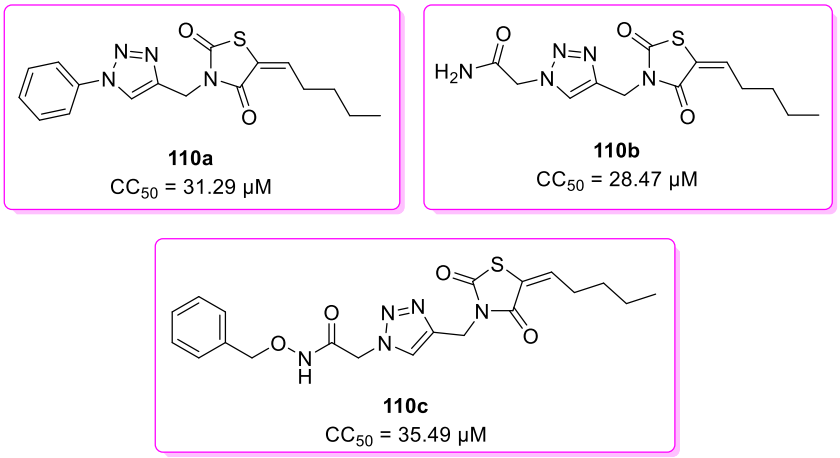

Fig. 20: Compounds exhibiting acute cytotoxicity against human lung fibroblast MRC-5 cells.

4.1.3 Thiazolidinedione-benzoxazole conjugates

Further conjugates synthesized by Michal Kolařík as a part of his Bachelor thesis[70] comprised thiazolidinedione and benzoxazole heterocycle. The synthetic pathway leading to designed compounds is depicted in Scheme 21.

Firstly, thiazolidinedione **81** was subjected to Knoevenagel condensation followed by alkylation and hydrolysis, giving acid **113**. Condensation of **113** with 2-aminobenzoxazoles prepared according to our published protocol[47] afforded final compounds **114**. Derivatives **116** with a simple methylene bridge were synthesized from acids **113** upon condensation with various aminophenoles and subsequent intramolecular Mitsunobu reactions.

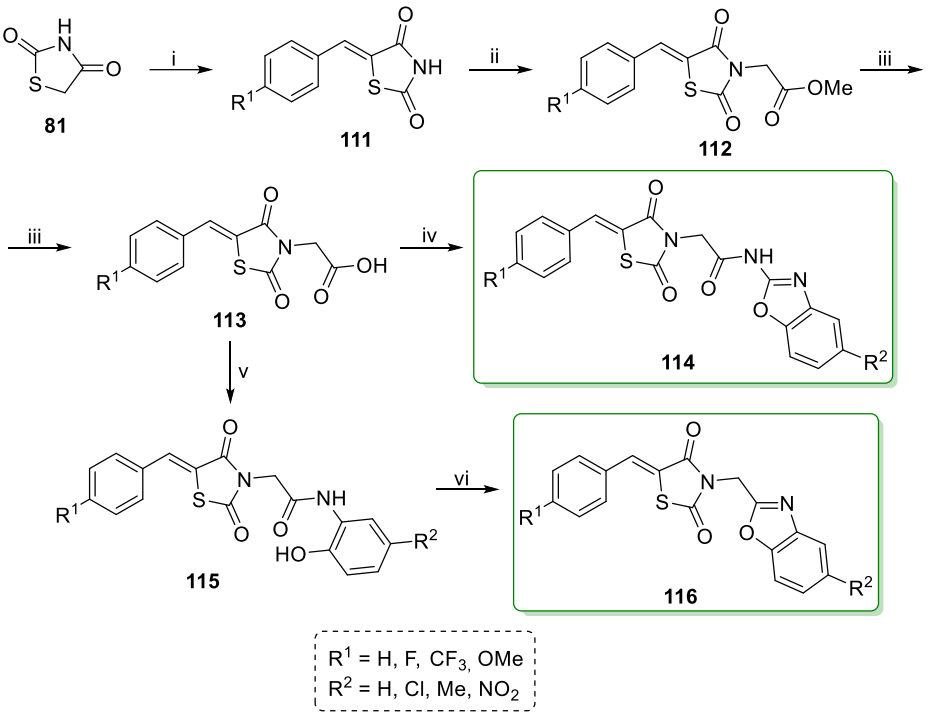

Scheme 21. Synthesis of thiazolidinedione-benzoxazole conjugates **114** and **116**. Reagents and conditions: (i) aldehydes, piperidine, EtOH, 89 °C, 16 h; (ii) methyl bromoacetate, NaH, DMF dry, rt, 16 h; (iii) HBr (40%), reflux, 5 h; (iv) 2-aminobenzoxazoles, DIC, HOBt, DCM dry, rt, 16 h; (v) aminophenoles, DIC, HOBt, DCM dry, rt, 16 h; (vi) PPh_3, DIAD, THF dry, 16 h.

Final thiazolidinedione-benzoxazole conjugates **114** and **116** were evaluated for their antimycobacterial and antibacterial properties. None of the tested analogues exhibited activity against *M. tuberculosis*. However, analogue **114a** proved significant activity against *Mycobacterium vaccae* and *Pseudomonas aeruginosa* (Fig. 21).

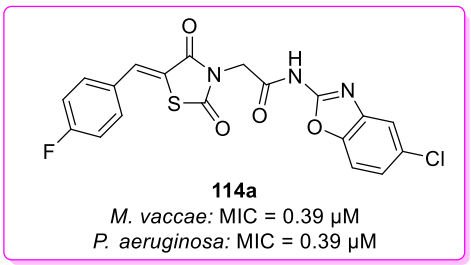

Fig. 21: Structure of the most active analogue from the library of conjugates **114** and **116**.

Three chemical libraries of thiazolidinedione conjugates were reported in this chapter: (i) thiazolidinedione-pyrimidines, (ii) thiazolidinedione-triazoles, and (iii) thiazolidinedione-benzoxazoles. We implemented the wide structural diversity needed for phenotypic screening using various pharmacophores. Despite the low antimycobacterial potential of studied compounds, we came up with structures that showed interesting antibacterial activity and can be further optimized and studied. Moreover, compounds **110a** and **110b** (Fig. 20) exhibited promising antileishmanial properties undergoing an extensive biological study.

4.2 Pyrimidines for phenotypic screening

In 2020, we reported the solid-phase synthesis of new pyrimidine derivatives.[71] Inspired by the literature, we suggested two different types of scaffolds, consisting of the central pyrimidine heterocycle (Scheme 22 and 23).[71] First derivatives comprised a 5-nitropyrimidine scaffold and two positions on the pyrimidine central core that differs from the used amino acid and amine. Moreover, the second scaffold was modified with various carboxylic acids. Synthesis of designed compounds was carried out by my student Romana Machníková within her Master thesis.[72]

Target compounds **120** were synthesized from the resin-bound precursors **117** (Scheme 22). Firstly, Wang resin was acylated with five different Fmoc-protected amino acids (Fmoc-*β*-Ala-OH, Fmoc-Phe-OH, Fmoc-Pro-OH, Fmoc-Met-OH, and Fmoc-Val-OH). The Fmoc protecting group was then removed through exposure to 50% piperidine, and the free amino group reacted with commercially available 4,6-dichloro-5-nitropyrimidine. Subsequently, the nucleophilic substitution of the resulting chloride **118** afforded resin-bound pyrimidines **119**. Standard cleavage with 50% TFA in DCM and subsequent high-performance liquid chromatography (HPLC) purification afforded the first library of pyrimidines **120**. All final compounds **120** were obtained in excellent crude purity ranging from 74 to 92 % as measured by LC-UV traces at 210–500 nm.

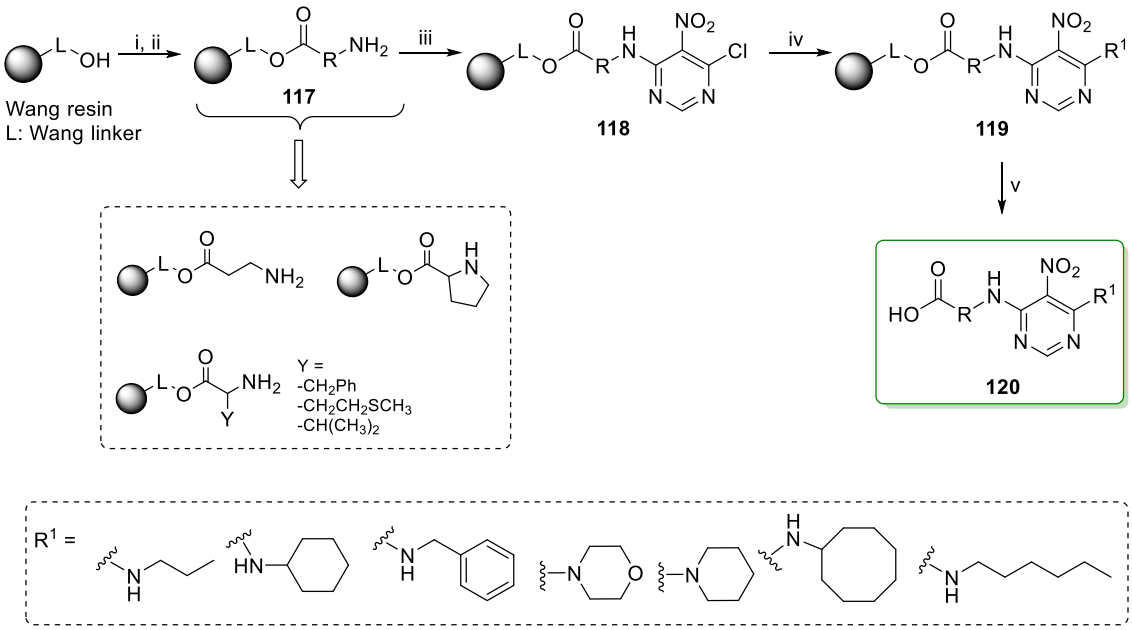

Scheme 22. Solid-phase synthesis of pyrimidines **120**.[71] Reagents and conditions: (i) Fmoc-amino acid, HOBt, DMAP, DIC, DMF/DCM (1:1), rt, 16 h; (ii) 50% piperidine, DMF, rt, 15 min; (iii) 4,6-dichloro-5-nitropyrimidine, DIPEA, dry DMF, rt, 2 h; (iv) amine, DIPEA, DMF, rt, 16 h; (v) 50% TFA in DCM, rt, 1 h.

Synthesis of the second type of pyrimidine scaffold proceeded according to the solid-phase synthetic pathway depicted in Scheme 23. Valine and cyclohexylamine substitutions were chosen considering the initial antibacterial activity. After immobilizing Fmoc-Val-OH on Wang resin and cleavage of the Fmoc protecting group, the resulting intermediate **121** was reacted with 4,6-dichloro-5-nitropyrimidine. Nucleophilic substitution of chloride **121** with cyclohexylamine delivered 5-nitropyrimidine **123**. Further, nitro group **123** was reduced using sodium dithionite. The third core was introduced to the resin-bound amine **124** *via* acylation, for which ten different carboxylic acids were selected. Finally, acid-mediated cleavage from the resin with TFA in DCM and subsequent HPLC purification yielded a series of compounds **126** for biological activity testing.

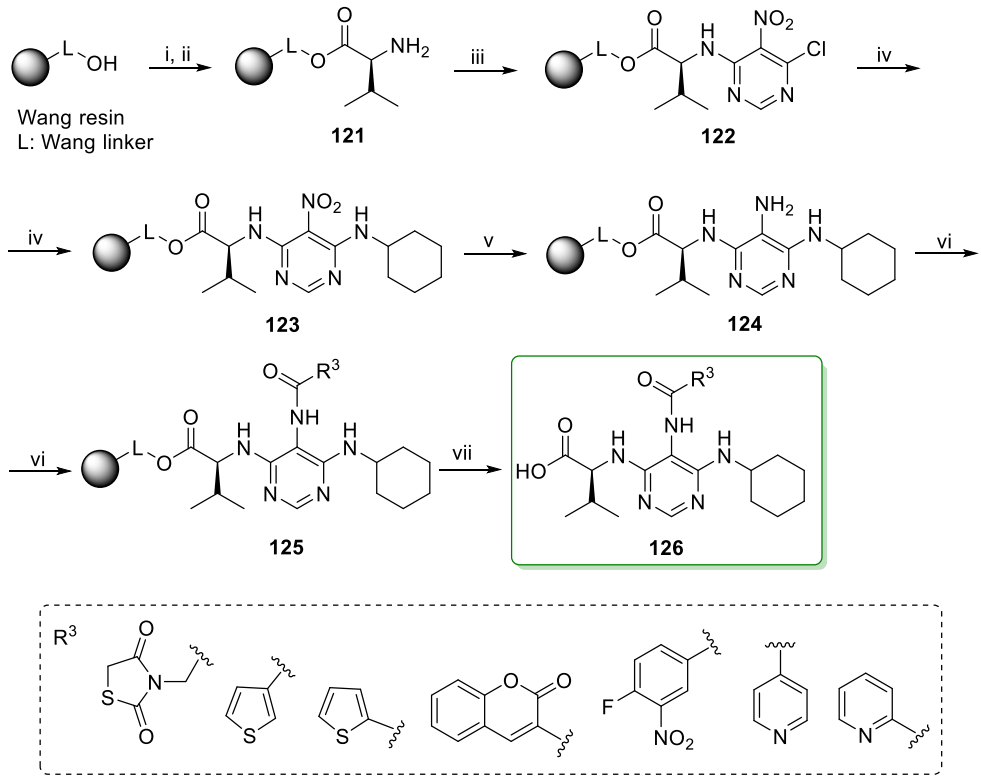

Scheme 23. Solid-phase synthesis of final compounds **126**. Reagents and the conditions: (i) Fmoc-valine, *N*-hydroxybenzotriazole (HOBt), DMAP, DIC, DMF/DCM (1 : 1), rt, 16 h; (ii) 50% piperidine, DMF, rt, 15 min; (iii) 4,6-dichloro-5-nitropyrimidine, DIPEA, dry DMF, rt, 2 h; (iv) amine, DIPEA, DMF, rt, 16 h; (v) $Na_2S_2O_4$, K_2CO_3, ethyl viologen diiodide, H_2O/DCM, rt, 16 h; (vi) carboxylic acid, HOBt, DMAP, DIC, DMF/DCM (1 : 1) or DMF, rt, 16 h; (vii) 50% TFA in DCM, rt, 1 h.

All final pyrimidines were screened for their *in vitro* antibacterial activity against *M. tuberculosis* H37Rv and several Gram-positive and Gram-negative strains such as *S. aureus, P. aeruginosa*, *E. coli*, and *E. faecalis* in the concentration range of 1024 – 0.0312 μg/ml. Additionally, their antifungal activity against *C. albicans* and *A. niger* was also investigated. None of the tested compounds **120** and **126** exhibited any activity against fungal strains, *E. coli*, *S. aureus*, and *E. faecalis*. On the other hand, compound **120a** (Fig. 22) showed considerable activity against *P. aeruginosa* (the bactericidal activity was observed in the range of concentrations 2-8 μg/ml) and was found to be as active as the standard (gentamicin). Further, compound **126a** (Fig. 22) with the 4-pyridinyl moiety exhibited moderate antimycobacterial activity with a MIC value of 32 μg/ml.

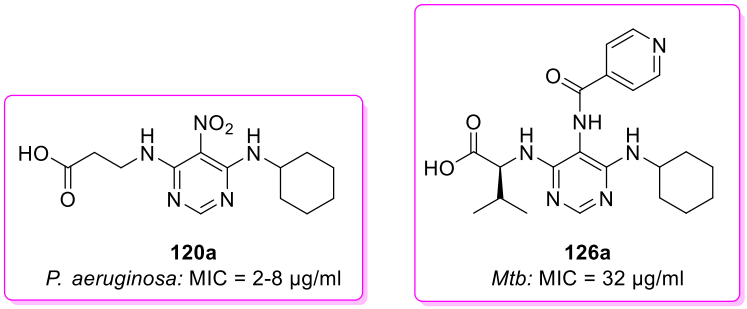

Fig. 22: The most active analogues from the pyrimidine libraries **120** and **126**.[71]

5 Conclusions and future perspectives

Prior to the Covid-19 pandemic, tuberculosis was the leading cause of death from a single infectious agent worldwide. Even though TB is treatable in almost all cases, many drug-resistant strains emerge. WHO estimates that half a million people annually have disease resistance to the most effective antimicrobials used to treat it. For this reason, I decided to establish my research group aimed at the development of new antimycobacterial agents.

During the last four years, my research group has reached significant results in antituberculosis drugs development. We mainly focused on the specific target at the level of bacteria. However, some rather synthetic projects were involved in phenotypic whole-cell screening.

From my point of view, the most exciting results were achieved in the projects comprising the development of new mycobacterial ATP synthase inhibitors. Inspired by the literature, we designed and synthesized several libraries of squaramide analogues. Notably, few analogues exhibited nanomolar antimycobacterial activity, and for this reason, Dr. Davie Cappoen (University of Antwerp) comprised these analogues in the advanced biological test. They were able to generate spontaneous resistant mutants and exactly proved the molecular target of our squaramides, subunit *a* of mycobacterial ATP synthase. Moreover, our compounds showed sensitivity to bedaquiline-resistant strains. These results will be submitted for publication in a short time.

Another promising direction in this work is targeting mycobacterial virulence factor Zmp1. Employing this approach, we can help the immune system fight against bacteria more efficiently. Focusing on this non-lethal pathway could result in efficient adjunctive treatment options that have the potential to increase the antibiotic susceptibility of *M. tuberculosis*. We prepared two generations of analogues based on the thiazolidinedione-hydroxamate scaffold. Although we did not reach more active inhibitors compared to those published in the literature, we originated several analogues that could be further optimized in other to improve pharmacological properties.

Many of my students (Bachelor, Master, PhD) were involved in the research that resulted in the successful synthesis of several libraries for phenotypic screening.

However, we did not accomplish significant results related to antimycobacterial drugs development in this field. On the other hand, we discovered an exciting hit compound showing high activity against bacteria like *Pseudomonas aeruginosa*.

We published seven papers related to our research in peer-reviewed impact journals, and two additional are currently prepared for publication. Our multidisciplinary work comprises the design of new analogues, their synthesis and characterization, and biological evaluation. Regarding the latest, we established international cooperation with the team of biologists from the University of Antwerp (Laboratory for Microbiology, Parasitology and Hygiene), led by Dr. Davie Cappoen.

During the last years, we have been immersed in the exciting issue of antituberculosis research and discovered valuable structures. However, many outstanding questions for future research remain. We will continue our effort to target some of the vital processes of bacteria or target non-lethal pathways.

6 Abbreviations

AIDS	acquired immunodeficiency syndrome
AMK	amikacin
ATP	adenosin triphosphate
BCG	bacillus Calmette–Guérin
BDQ	bedaquiline
CC_{50}	50% cytotoxic concentration
CFZ	clofazimine
CS	cycloserine
CuTC	copper(I)-thiophene-2-carboxylate
DCM	dichloromethane
DIC	*N*,*N'*-diisopropycarbodiimide
DIPEA	*N*,*N*-diisopropylethylamine
DLM	delamanid
DMAP	(4-dimethylamino)pyridine
DMF	*N*,*N*-dimethylformamide
DOTS	directly observed treatment, short course
DR-TB	drug-resistant tuberculosis
EDTA	ethylenediaminetetraacetic acid
EMB	ethambutol
Et	ethyl
ETO	ethionamide
FDA	food drug administration
Fmoc	9-fluorenylmethoxycyrbonyl
[HDBU][HSO_4]	1,8-diazabicyclo[5.4.0]-undec-7-ene-8-ium hydrogensulfate
HDT	host-directed therapy
HIV	human immunodeficiency virus
HOBt	1-hydroxybenzotriazole
HPLC	high performance liquid chromatography
IC_{50}	half maximal inhibitory concentration

INH	isoniazid
IPM-CLN	imipenem-cilastatin
LDA	lithium diisopropylamide
LFX	levofloxacin
LTBI	latent TB infection
LZD	linezolid
M. tuberculosis	*Mycobacterium tuberculosis*
MALDI-TOF MS	matrix-assisted laser desorption/ionization-time of flight mass spectrometry
MDR/RR-TB	multidrug-resistant or rifampicin-resistant tuberculosis
MDR-TB	multidrug-resistant tuberculosis
Me	methyl
MFX	moxifloxacin
MIC	minimum inhibitory concentration
MIC	minimum inhibitory concentration
MPM	meropenem
NMM	*N*-methylmorpholine
PAS	*p*-aminosalicylic acid
PTO	prothionamide
PZA	pyrazinamide
RIF	rifampicin
RR-TB	rifampicin-resistant tuberculosis
rt	room temperature
SAR	structure-activity relationship
SFC	supercritical fluid chromatography
STM	streptomycin
TB	tuberculosis
TFA	trifluoroacetic acid
TFP	tri(2-furyl)phosphine
THF	tetrahydrofuran
TRD	terizidone
WGND	working group on new TB drugs
WHO	world health organization
XDR-TB	extensively drug-resistant tuberculosis

ZBG	zinc-binding group
Zmp1	zinc-dependent metalloprotease 1

7 References

(1) World Health Organization. *Global Tuberculosis report* **2021**.

(2) Gengenbacher, M.; Kaufmann, S. H. E. Mycobacterium Tuberculosis: Success through Dormancy. *FEMS Microbiol. Rev.* **2012**, *36* (3), 514–532.

(3) World Health Organization. *Global Tuberculosis report* **2020**.

(4) Singh, V.; Chibale, K. Strategies to Combat Multi-Drug Resistance in Tuberculosis. *Acc. Chem. Res.* **2021**, *54* (10), 2361–2376.

(5) Castro, R. A. D.; Borrell, S.; Gagneux, S. The Within-Host Evolution of Antimicrobial Resistance in Mycobacterium Tuberculosis. *FEMS Microbiol. Rev.* **2021**, *45* (4).

(6) World Health Organization. *Global Tuberculosis report* **2017**.

(7) World Health Organization. *WHO consolidated guidelines on tuberculosis. Module 4 treatment - drug-resistant tuberculosis treatment_2020* **2020**.

(8) *https://www.newtbdrugs.org/*.

(9) Blair, H. A.; Scott, L. J. Delamanid: A Review of Its Use in Patients with Multidrug-Resistant Tuberculosis. *Drugs* **2015**, *75* (1), 91–100.

(10) Lange, C.; Aaby, P.; Behr, M. A.; Donald, P. R.; Kaufmann, S. H. E.; Netea, M. G.; Mandalakas, A. M. 100 Years of Mycobacterium Bovis Bacille Calmette-Gueŕin. *Lancet Infect. Dis.* **2022**, *22* (1), e2.

(11) Ballell, L.; Bates, R. H.; Young, R. J.; Alvarez-Gomez, D.; Alvarez-Ruiz, E.; Barroso, V.; Blanco, D.; Crespo, B.; Escribano, J.; Gonzalez, R.; Lozano, S.; Huss, S.; Santos-Villarejo, A.; Martin-Plaza, J. J.; Mendoza, A.; Rebollo-Lopez, M. J.; Remuinan-Blanco, M.; Lavandera, J. L.; Perez-Herran, E.; Gamo-Benito, F. J.; Garcia-Bustos, J. F.; Barros, D.; Castro, J. P.; Cammack, N. Fueling Open-Source Drug Discovery: 177 Small-Molecule Leads against Tuberculosis. *ChemMedChem* **2013**, *8* (2), 313–321.

(12) Baptista, R.; Bhowmick, S.; Nash, R. J.; Baillie, L.; Mur, L. A. J. Target Discovery Focused Approaches to Overcome Bottlenecks in the Exploitation of Antimycobacterial Natural Products. *Future Med. Chem.* **2018**, *10* (7), 811–822.

(13) Grzelak, E. M.; Choules, M. P.; Gao, W.; Cai, G.; Wan, B.; Wang, Y.; McAlpine,

J. B.; Cheng, J.; Jin, Y.; Lee, H.; Suh, J.-W.; Pauli, G. F.; Franzblau, S. G.; Jaki, B. U.; Cho, S. Strategies in Anti-Mycobacterium Tuberculosis Drug Discovery Based on Phenotypic Screening. *J. Antibiot. (Tokyo).* **2019**, *72* (10), 719–728.

(14) Oh, S.; Trifonov, L.; Yadav, V. D.; Barryiii, C. E.; Boshoff, H. I. Tuberculosis Drug Discovery: A Decade of Hit Assessment for Defined Targets. *Front. Cell. Infect. Microbiol.* **2021**, *11*, 611304.

(15) Han, J.; Liu, X.; Zhang, L.; Quinn, R. J.; Feng, Y. Anti-Mycobacterial Natural Products and Mechanisms of Action. *Nat. Prod. Rep.* **2022**, *39* (1), 77–89.

(16) Cole, S. T.; Brosch, R.; Parkhill, J.; Garnier, T.; Churcher, C.; Harris, D.; Gordon, S. V; Eiglmeier, K.; Gas, S.; Barry, C. E. I. I. I.; Tekaia, F.; Badcock, K.; Basham, D.; Brown, D.; Chillingworth, T.; Connor, R.; Davies, R.; Devlin, K.; Feltwell, T.; Gentles, S.; Hamlin, N.; Holroyd, S.; Hornsby, T.; Jagels, K.; Krogh, A.; McLean, J.; Moule, S.; Murphy, L.; Oliver, K.; Osborne, J.; Quail, M. A.; Rajandream, M.-A.; Rogers, J.; Rutter, S.; Seeger, K.; Skelton, J.; Squares, R.; Squares, S.; Sulston, J. E.; Taylor, K.; Whitehead, S.; Barrell, B. G. Deciphering the Biology of Mycobacterium Tuberculosis from the Complete Genome Sequence. *Nat.* **1998**, *393* (6685), 537–544.

(17) Torfs, E.; Piller, T.; Cos, P.; Cappoen, D. Opportunities for Overcoming Mycobacterium Tuberculosis Drug Resistance: Emerging Mycobacterial Targets and Host-Directed Therapy. *Int. J. Mol. Sci.* **2019**, *20* (12), 2868.

(18) Krug, S.; Parveen, S.; Bishai, W. R. Host-Directed Therapies: Modulating Inflammation to Treat Tuberculosis. *Front. Immunol.* **2021**, *12*, 660916.

(19) Perveen, S.; Kumari, D.; Singh, K.; Sharma, R. Tuberculosis Drug Discovery: Progression and Future Interventions in the Wake of Emerging Resistance. *Eur. J. Med. Chem.* **2022**, *229*, 114066.

(20) Yang, L.; Hu, X.; Chai, X.; Ye, Q.; Pang, J.; Li, D.; Hou, T. Opportunities for Overcoming Tuberculosis: Emerging Targets and Their Inhibitors. *Drug Discov. Today* **2022**, *27* (1), 326–336.

(21) Mehta, K.; Spaink, H. P.; Ottenhoff, T. H. M.; van der Graaf, P. H.; van Hasselt, J. G. C. Host-Directed Therapies for Tuberculosis: Quantitative Systems Pharmacology Approaches. *Trends Pharmacol. Sci.* **2022**, *43* (4), 293–304.

(22) Urban, M.; Šlachtová, V.; Brulíková, L. Small Organic Molecules Targeting the Energy Metabolism of Mycobacterium Tuberculosis. *Eur. J. Med. Chem.* **2021**, *212*, 113139.

(23) Koul, A.; Dendouga, N.; Vergauwen, K.; Molenberghs, B.; Vranckx, L.; Willebrords, R.; Ristic, Z.; Lill, H.; Dorange, I.; Guillemont, J.; Bald, D.; Andries, K. Diarylquinolines Target Subunit c of Mycobacterial ATP Synthase. *Nat. Chem. Biol.* **2007**, *3* (6), 323–324.

(24) Lu, P.; Lill, H.; Bald, D. ATP Synthase in Mycobacteria: Special Features and Implications for a Function as Drug Target. *Biochim. Biophys. Acta, Bioenerg.* **2014**, *1837* (7), 1208–1218.

(25) Bald, D.; Villellas, C.; Lu, P.; Koul, A. Targeting Energy Metabolism in Mycobacterium Tuberculosis, a New Paradigm in Antimycobacterial Drug Discovery. *MBio* **2017**, *8* (2), e00272-17/1-e00272-17/11.

(26) Koul, A.; Vranckx, L.; Dendouga, N.; Balemans, W.; Van den Wyngaert, I.; Vergauwen, K.; Goehlmann, H. W. H.; Willebrords, R.; Poncelet, A.; Guillemont, J.; Bald, D.; Andries, K. Diarylquinolines Are Bactericidal for Dormant Mycobacteria as a Result of Disturbed ATP Homeostasis. *J. Biol. Chem.* **2008**, *283* (37), 25273–25280.

(27) Zhang, A. T.; Montgomery, M. G.; Leslie, A. G. W.; Cook, G. M.; Walker, J. E. The Structure of the Catalytic Domain of the ATP Synthase from Mycobacterium Smegmatis Is a Target for Developing Antitubercular Drugs. *Proc. Natl. Acad. Sci. U. S. A.* **2019**, *116* (10), 4206–4211.

(28) Guo, H.; Courbon, G. M.; Bueler, S. A.; Mai, J.; Liu, J.; Rubinstein, J. L. Structure of Mycobacterial ATP Synthase Bound to the Tuberculosis Drug Bedaquiline. *Nat. (London, United Kingdom)* **2021**, *589* (7840), 143–147.

(29) Harikishore, A.; Saw, W.-G.; Ragunathan, P.; Litty, D.; Dick, T.; Muller, V.; Gruber, G. Mutational Analysis of Mycobacterial F-ATP Synthase Subunit δ Leads to a Potent δ Enzyme Inhibitor. *ACS Chem. Biol.* **2022**, *17* (3), 529–535.

(30) Andries, K.; Verhasselt, P.; Guillemont, J.; Goehlmann, H. W. H.; Neefs, J. M.; Winkler, H.; Van Gestel, J.; Timmerman, P.; Zhu, M.; Lee, E.; Williams, P.; de Chaffoy, D.; Huitric, E.; Hoffner, S.; Cambau, E.; Truffot-Pernot, C.; Lounis, N.; Jarlier, V. A Diarylquinoline Drug Active on the ATP Synthase of Mycobacterium Tuberculosis. *Sci. (Washington, DC, United States)* **2005**, *307* (5707), 223–227.

(31) Qiao, C.-J.; Li, S.; Qiao, C.-J.; Wang, X.-K.; Xie, F.; Zhong, W.; Li, S. Asymmetric Synthesis and Absolute Configuration Assignment of a New Type of Bedaquiline Analogue. *Molecules* **2015**, *20* (12), 22272–22285.

(32) Singh, S.; Roy, K. K.; Khan, S. R.; Kashyap, V. K.; Sharma, A.; Jaiswal, S.; Sharma, S. K.; Krishnan, M. Y.; Chaturvedi, V.; Lal, J.; Sinha, S.; Dasgupta, A.; Srivastava, R.; Saxena, A. K. Novel, Potent, Orally Bioavailable and Selective Mycobacterial ATP Synthase Inhibitors That Demonstrated Activity against Both Replicating and Non-Replicating M. Tuberculosis. *Bioorg. Med. Chem.* **2015**, *23* (4), 742–752.

(33) Rombouts, J. A.; Veenboer, R. M. P.; Villellas, C.; Lu, P.; Ehlers, A. W.; Andries, K.; Koul, A.; Lill, H.; Ruijter, E.; Orru, R. V. A.; Lammertsma, K.; Bald, D.; Slootweg, J. C. Synthesis, Characterization and Biological Activity of Fluorescently Labeled Bedaquiline Analogues. *RSC Adv.* **2016**, *6* (110), 108708–108716.

(34) Tantry, S. J.; Shinde, V.; Balakrishnan, G.; Markad, S. D.; Gupta, A. K.; Bhat, J.; Narayan, A.; Raichurkar, A.; Jena, L. K.; Sharma, S.; Kumar, N.; Nanduri, R.; Bharath, S.; Reddy, J.; Panduga, V.; Prabhakar, K. R.; Kandaswamy, K.; Kaur, P.; Dinesh, N.; Guptha, S.; Saralaya, R.; Panda, M.; Rudrapatna, S.; Mallya, M.; Rubin, H.; Yano, T.; Mdluili, K.; Cooper, C. B.; Balasubramanian, V.; Sambandamurthy, V. K.; Ramachandran, V.; Shandil, R.; Kavanagh, S.; Narayanan, S.; Iyer, P.; Mukherjee, K.; Hosagrahara, V. P.; Solapure, S.; Hameed P, S.; Ravishankar, S. Scaffold Morphing Leading to Evolution of 2,4-Diaminoquinolines and Aminopyrazolopyrimidines as Inhibitors of the ATP Synthesis Pathway. *Medchemcomm* **2016**, *7* (5), 1022–1032.

(35) Tantry, S. J.; Markad, S. D.; Shinde, V.; Bhat, J.; Balakrishnan, G.; Gupta, A. K.; Ambady, A.; Raichurkar, A.; Kedari, C.; Sharma, S.; Mudugal, N. V; Narayan, A.; Naveen Kumar, C. N.; Nanduri, R.; Bharath, S.; Reddy, J.; Panduga, V.; Prabhakar, K. R.; Kandaswamy, K.; Saralaya, R.; Kaur, P.; Dinesh, N.; Guptha, S.; Rich, K.; Murray, D.; Plant, H.; Preston, M.; Ashton, H.; Plant, D.; Walsh, J.; Alcock, P.; Naylor, K.; Collier, M.; Whiteaker, J.; McLaughlin, R. E.; Mallya, M.; Panda, M.; Rudrapatna, S.; Ramachandran, V.; Shandil, R.; Sambandamurthy, V. K.; Mdluli, K.; Cooper, C. B.; Rubin, H.; Yano, T.; Iyer, P.; Narayanan, S.; Kavanagh, S.; Mukherjee, K.; Balasubramanian, V.; Hosagrahara, V. P.; Solapure, S.; Ravishankar, S.; Hameed, P. Discovery of Imidazo[1,2-a]Pyridine Ethers and Squaramides as Selective and Potent Inhibitors of Mycobacterial Adenosine Triphosphate (ATP) Synthesis. *J. Med. Chem.* **2017**, *60* (4), 1379–1399.

(36) Choi, P. J.; Sutherland, H. S.; Tong, A. S. T.; Blaser, A.; Franzblau, S. G.; Cooper, C. B.; Lotlikar, M. U.; Upton, A. M.; Guillemont, J.; Motte, M.; Queguiner, L.; Andries, K.; Van, den B. W.; Denny, W. A.; Palmer, B. D. Synthesis and Evaluation of Analogues of the Tuberculosis Drug Bedaquiline Containing Heterocyclic B-Ring Units. *Bioorg. Med. Chem. Lett.* **2017**, *27* (23), 5190–5196.

(37) Surase, Y. B.; Samby, K.; Amale, S. R.; Sood, R.; Purnapatre, K. P.; Pareek, P. K.; Das, B.; Nanda, K.; Kumar, S.; Verma, A. K. Identification and Synthesis of Novel Inhibitors of Mycobacterium ATP Synthase. *Bioorg.Med.Chem.Lett.* **2017**, *27* (15), 3454–3459.

(38) Tong, A. S. T.; Choi, P. J.; Blaser, A.; Sutherland, H. S.; Tsang, S. K. Y.; Guillemont, J.; Motte, M.; Cooper, C. B.; Andries, K.; Van den Broeck, W.; Franzblau, S. G.; Upton, A. M.; Denny, W. A.; Palmer, B. D.; Conole, D. 6-Cyano Analogues of Bedaquiline as Less Lipophilic and Potentially Safer Diarylquinolines for Tuberculosis. *ACS Med. Chem. Lett.* **2017**, *8* (10), 1019–1024.

(39) Blaser, A.; Sutherland, H. S.; Tong, A. S. T.; Choi, P. J.; Conole, D.; Franzblau, S. G.; Cooper, C. B.; Upton, A. M.; Lotlikar, M.; Denny, W. A.; Palmer, B. D. Structure-Activity Relationships for Unit C Pyridyl Analogues of the Tuberculosis Drug Bedaquiline. *Bioorg. Med. Chem.* **2019**, *27* (7), 1283–1291.

(40) Sutherland, H. S.; Tong, A. S. T.; Choi, P. J.; Blaser, A.; Conole, D.; Franzblau, S. G.; Lotlikar, M. U.; Cooper, C. B.; Upton, A. M.; Denny, W. A.; Palmer, B. D. 3,5-Dialkoxypyridine Analogues of Bedaquiline Are Potent Antituberculosis Agents with Minimal Inhibition of the HERG Channel. *Bioorg. Med. Chem.* **2019**, *27* (7), 1292–1307.

(41) Li, P.; Wang, B.; Li, G.; Fu, L.; Zhang, D.; Lin, Z.; Huang, H.; Lu, Y. Design, Synthesis and Biological Evaluation of Diamino Substituted Cyclobut-3-Ene-1,2-Dione Derivatives for the Treatment of Drug-Resistant Tuberculosis. *Eur. J. Med. Chem.* **2020**, *206*, 112538.

(42) Hotra, A.; Ragunathan, P.; Ng, P. S.; Seankongsuk, P.; Harikishore, A.; Sarathy, J. P.; Saw, W.-G.; Lakshmanan, U.; Sae-Lao, P.; Kalia, N. P.; Shin, J.; Kalyanasundaram, R.; Anbarasu, S.; Parthasarathy, K.; Pradeep, C. N.; Makhija, H.; Droege, P.; Poulsen, A.; Tan, J. H. L.; Pethe, K.; Dick, T.; Bates, R. W.; Grueber, G. Discovery of a Novel Mycobacterial F-ATP Synthase Inhibitor and

Its Potency in Combination with Diarylquinolines. *Angew. Chemie, Int. Ed.* **2020**, *59* (32), 13295–13304.

(43) Sutherland, H. S.; Tong, A. S. T.; Choi, P. J.; Blaser, A.; Franzblau, S. G.; Cooper, C. B.; Upton, A. M.; Lotlikar, M.; Denny, W. A.; Palmer, B. D. Variations in the C-Unit of Bedaquiline Provides Analogues with Improved Biology and Pharmacology. *Bioorg. Med. Chem.* **2020**, *28* (1), 115213.

(44) Barbaro, L.; Nagalingam, G.; Triccas, J. A.; Tan, L.; West, N. P.; Baell, J. B.; Priebbenow, D. L. Synthesis and Evaluation of Pyridine-Derived Bedaquiline Analogues Containing Modifications at the A-Ring Subunit. *RSC Med. Chem.* **2021**, *12* (6), 943–959.

(45) Chasák, J. Synthesis of Novel Squaramides as Potent Mycobacterial ATP Synthase Inhibitors, *Bachelor thesis*, **2020**, Palacký University Olomouc.

(46) Chasák, J. Design and Synthesis of Novel Mycobacterial ATP Synthase Inhibitors, *Master thesis*, **2022**, Palacký University Olomouc.

(47) Šlachtová, V.; Chasák, J.; Brulíková, L. Synthesis of Various 2-Aminobenzoxazoles: The Study of Cyclization and Smiles Rearrangement. *ACS Omega* **2019**, *4* (21), 19314–19323.

(48) Master, S. S.; Rampini, S. K.; Davis, A. S.; Keller, C.; Ehlers, S.; Springer, B.; Timmins, G. S.; Sander, P.; Deretic, V. Mycobacterium Tuberculosis Prevents Inflammasome Activation. *Cell Host Microbe* **2008**, *3* (4), 224–232.

(49) Lazarevic, V.; Martinon, F. Linking Inflammasome Activation and Phagosome Maturation. *Cell Host Microbe* **2008**, *3* (4), 199–200.

(50) Petrera, A.; Amstutz, B.; Gioia, M.; Hahnlein, J.; Baici, A.; Selchow, P.; Ferraris, D. M.; Rizzi, M.; Sbardella, D.; Marini, S.; Coletta, M.; Sander, P.; Hähnlein, J.; Baici, A.; Selchow, P.; Ferraris, D. M.; Rizzi, M.; Sbardella, D.; Marini, S.; Coletta, M.; Sander, P. Functional Characterization of the Mycobacterium Tuberculosis Zinc Metallopeptidase Zmp1 and Identification of Potential Substrates. *Biol. Chem.* **2012**, *393* (7), 631–640.

(51) Ferraris, D. M.; Rizzi, M. Zinc-Dependent Metalloprotease-1 (Zmp1). In *Encycl.Inorg.Bioinorg.Chem.*; John Wiley & Sons Ltd., 2013; pp 1–7.

(52) Ferraris, D. M.; Sbardella, D.; Petrera, A.; Marini, S.; Amstutz, B.; Coletta, M.; Sander, P.; Rizzi, M. Crystal Structure of Mycobacterium Tuberculosis Zinc-Dependent Metalloprotease-1 (Zmp1), a Metalloprotease Involved in Pathogenicity. *J. Biol. Chem.* **2011**, *286* (37), 32475–32482, S32475/1.

(53) Liang, W. G.; Mancl, J. M.; Zhao, M.; Tang, W.-J. Structural Analysis of Mycobacterium tuberculosis M13 Metalloprotease Zmp1 Open States. *Struct. (Oxford, United Kingdom)* **2021**, *29* (7), 709-720.e3.

(54) Mori, M.; Moraca, F.; Deodato, D.; Ferraris, D. M.; Selchow, P.; Sander, P.; Rizzi, M.; Botta, M. Discovery of the First Potent and Selective Mycobacterium Tuberculosis Zmp1 Inhibitor. *Bioorg.Med.Chem.Lett.* **2014**, *24* (11), 2508–2511.

(55) Subhedar, D. D.; Shaikh, M. H.; Nawale, L.; Yeware, A.; Sarkar, D.; Khan, F. A. K.; Sangshetti, J. N.; Shingate, B. B. Novel Tetrazoloquinoline-Rhodanine Conjugates: Highly Efficient Synthesis and Biological Evaluation. *Bioorganic Med. Chem. Lett.* **2016**, *26* (9), 2278–2283.

(56) Subhedar, D. D.; Shaikh, M. H.; Shingate, B. B.; Nawale, L.; Sarkar, D.; Khedkar, V. M.; Kalam, K. F.; Sangshetti, J. N. Quinolidene-Rhodanine Conjugates: Facile Synthesis and Biological Evaluation. *Eur J Med Chem* **2017**, *125*, 385–399.

(57) Mori, M.; Deodato, D.; Kasula, M.; Ferraris, D. M.; Sanna, A.; De Logu, A.; Rizzi, M.; Botta, M. Design, Synthesis, SAR and Biological Investigation of 3-(Carboxymethyl)Rhodanine and Aminothiazole Inhibitors of Mycobacterium Tuberculosis Zmp1. *Bioorg.Med.Chem.Lett.* **2018**, *28* (4), 637–641.

(58) Paolino, M.; Brindisi, M.; Vallone, A.; Butini, S.; Campiani, G.; Nannicini, C.; Giuliani, G.; Anzini, M.; Lamponi, S.; Giorgi, G.; Sbardella, D.; Ferraris, D. M.; Marini, S.; Coletta, M.; Palucci, I.; Minerva, M.; Delogu, G.; Pepponi, I.; Goletti, D.; Cappelli, A.; Gemma, S.; Brogi, S. Development of Potent Inhibitors of the Mycobacterium Tuberculosis Virulence Factor Zmp1 and Evaluation of Their Effect on Mycobacterial Survival inside Macrophages. *ChemMedChem* **2018**, *13* (5), 422–430.

(59) Šlachtová, V.; Šebela, M.; Torfs, E.; Oorts, L.; Cappoen, D.; Berka, K.; Bazgier, V.; Brulíková, L. Novel Thiazolidinedione-Hydroxamates as Inhibitors of Mycobacterium Tuberculosis Virulence Factor Zmp1. *Eur. J. Med. Chem.* **2020**, *185*, 111812.

(60) Pouliot, M.; Jeanmart, S. Pan Assay Interference Compounds (PAINS) and Other Promiscuous Compounds in Antifungal Research: Miniperspective. *J. Med. Chem.* **2016**, *59* (2), 497–503.

(61) Šlachtová, V. Synthesis and Biological Activity of New Potent Antituberculotics, 2021.

(62) Šlachtová, V.; Janovská, L.; Brulíková, L. Solid Phase Synthesis of New Thiazolidinedione-Pyrimidine Conjugates and Their Antibacterial Properties. *J. Mol. Struct.* **2019**, *1183*, 182–189.

(63) Krylov, I. S.; Kashemirov, B. A.; Hilfinger, J. M.; McKenna, C. E. Evolution of an Amino Acid Based Prodrug Approach: Stay Tuned. *Mol. Pharm.* **2013**, *10* (2), 445–458.

(64) Ponnuchamy, S.; Kanchithalaivan, S.; Ranjith Kumar, R.; Ashraf Ali, M.; Soo Choon, T. Antimycobacterial Evaluation of Novel Hybrid Arylidene Thiazolidine-2,4-Diones. *Bioorg. Med. Chem. Lett.* **2014**, *24* (4), 1089–1093.

(65) Keri, R. S.; Patil, S. A.; Budagumpi, S.; Nagaraja, B. M. Triazole: A Promising Antitubercular Agent. *Chem. Biol. Drug Des.* **2015**, *86* (4), 410–423.

(66) Yagnam, S.; Trivedi, R.; Krishna, S.; Giribabu, L.; Praveena, G.; Prakasham, R. S. Bioactive Isatin (Oxime)-Triazole-Thiazolidinedione Ferrocene Molecular Conjugates: Design, Synthesis and Antimicrobial Activities. *J. Organomet. Chem.* **2021**, *937*, 121716.

(67) Shinde, D. N.; Trivedi, R.; Vamsi Krishna, N.; Lingamallu, G.; Sridhar, B.; Khursade, P. S.; Reddy Shetty, P. 2, 4-Thiazolidinedione as a Bioactive Linker for Ferrocenyl Sugar–Triazole Conjugates: Synthesis, Characterization and Biological Properties. *Eur. J. Inorg. Chem.* **2018**, *2018* (14), 1571–1580.

(68) Rostovtsev, V. V; Green, L. G.; Fokin, V. V; Sharpless, K. B. A Stepwise Huisgen Cycloaddition Process: Copper (I)-catalyzed Regioselective "Ligation" of Azides and Terminal Alkynes. *Angew. Chemie* **2002**, *114* (14), 2708–2711.

(69) Marson, C. M.; Khan, A.; Porter, R. A. Stereocontrolled Formation of Epoxy Peroxide FunctionalityAppended to a Lactam Ring. *J. Org. Chem.* **2001**, *66* (14), 4771–4775.

(70) Kolařík, M. Synthesis of new benzoxazole-thiazolidinedione derivatives with potent antibacterial activity, *Bachelor thesis*, **2020**, Palacký University Olomouc.

(71) Machníková, R.; Janovská, L.; Brulíková, L. Solid-Phase Synthetic Approach towards New Pyrimidines as Potential Antibacterial Agents. *J. Mol. Struct.* **2020**, *1200*, 127101.

(72) Machníková, R. Synthesis of New Benzoxazole and Pyrimidine Derivatives with Potent Antibacterial Activity, *Master thesis*, **2019**, Palacký University Olomouc.

8 List of included publications

1. Urban, M.; Šlachtová, V.; **Brulíková, L.*** *Eur. J. Med. Chem.* **2021**, *212*, 113139. Small organic molecules targeting the energy metabolism of Mycobacterium tuberculosis. DOI: 10.1016/j.ejmech.2020.113139
2. Chasák, J.; Šlachtová, V.; Urban, M.; **Brulíková, L.*** *Eur. J. Med. Chem.* **2021**, *209*, 112872. Squaric acid analogues in medicinal chemistry. DOI: 10.1016/j.ejmech.2020.112872
3. Šlachtová, V.; Šebela, M.; Torfs, E.; Oorts, L.; Cappoen, D.; Berka, K.; Bazgier, V.; **Brulíková, L.*** *Eur. J. Med. Chem.* **2020**, *185*, 111812. Novel thiazolidinedione-hydroxamates as inhibitors of Mycobacterium tuberculosis virulence factor Zmp1. DOI: 10.1016/j.ejmech.2019.111812
4. Machníková. R.; Janovská L.; **Brulíková, L.*** *J. Mol. Struct.* **2020**, *1200*, 127101. Solid-phase synthetic approach towards new pyrimidines as potential antibacterial agents. DOI: 10.1016/j.molstruc.2019.127101
5. Šlachtová, V.; Chasák, J.; **Brulíková, L.*** *ACS Omega* **2019**, *4*(21), 19314-19323. Synthesis of various 2-aminobenzoxazoles: the study of cyclization and Smiles rearrangement. DOI: 10.1021/acsomega.9b02702
6. Šlachtová, V.; Janovská, L.; **Brulíková, L.*** *J. Mol. Struct.* **2019**, *1183*, 182-189. Solid phase synthesis of new thiazolidinedione-pyrimidine conjugates and their antibacterial properties. DOI: 10.1016/j.molstruc.2019.01.073
7. Šlachtová, V.; **Brulíková, L.*** *ChemistrySelect* **2018**, *3*(17), 4653-4662. Benzoxazole Derivatives as Promising Antitubercular Agents. DOI: 10.1002/slct.201800631

Appendix 1

Small organic molecules targeting the energy metabolism of Mycobacterium tuberculosis

Urban, M.; Šlachtová, V.; **Brulíková, L.***

Eur. J. Med. Chem. **2021**, *212*, 113139.

European Journal of Medicinal Chemistry 212 (2021) 113139

Contents lists available at ScienceDirect

European Journal of Medicinal Chemistry

journal homepage: http://www.elsevier.com/locate/ejmech

Review article

Small organic molecules targeting the energy metabolism of *Mycobacterium tuberculosis*

Milan Urban [a, 1], Veronika Šlachtová [b, 1], Lucie Brulíková [b, *]

[a] Institute of Molecular and Translational Medicine, Medicinal Chemistry, Faculty of Medicine and Dentistry, Palacky University in Olomouc, Hněvotínská 5, 779 00, Olomouc, Czech Republic
[b] Department of Organic Chemistry, Faculty of Science, Palacky University Olomouc, 17. Listopadu 12, 771 46, Olomouc, Czech Republic

ARTICLE INFO

Article history:
Received 11 July 2020
Received in revised form
22 December 2020
Accepted 23 December 2020
Available online 29 December 2020

Keywords:
Mycobacterium tuberculosis
Oxidative phosphorylation
ATP synthase
QcrB
Inhibitors

ABSTRACT

Causing approximately 10 million incident cases and 1.3–1.5 million deaths every year, *Mycobacterium tuberculosis* remains a global health problem. The risk is further exacerbated with latent tuberculosis (TB) infection, the HIV pandemic, and increasing anti-TB drug resistance. Therefore, unexplored chemical scaffolds directed towards new molecular targets are increasingly desired. In this context, mycobacterial energy metabolism, particularly the oxidative phosphorylation (OP) pathway, is gaining importance. Mycobacteria possess primary dehydrogenases to fuel electron transport; aa_3-type cytochrome *c* oxidase and *bd*-type menaquinol oxidase to generate a protonmotive force; and ATP synthase, which is essential for both growing mycobacteria as well as dormant mycobacteria because ATP is produced under both aerobic and hypoxic conditions. Small organic molecules targeting OP are active against latent TB as well as resistant TB strains. FDA approval of the ATP synthase inhibitor bedaquiline and the discovery of clinical candidate Q203, which both interfere with the cytochrome bc_1 complex, have already confirmed mycobacterial energy metabolism to be a valuable anti-TB drug target. This review highlights both preferable molecular targets within mycobacterial OP and promising small organic molecules targeting OP. Progressive research in the area of mycobacterial OP revealed several highly potent anti-TB compounds with nanomolar-range MICs as low as 0.004 μM against *Mtb* H37Rv. Therefore, we are convinced that targeting the OP pathway can combat resistant TB and latent TB, leading to more efficient anti-TB chemotherapy.

Contents

* Corresponding author.
E-mail address: lucie.brulikova@upol.cz (L. Brulíková).
[1] These authors contributed equally.

https://doi.org/10.1016/j.ejmech.2020.113139
0223-5234/

1. Introduction

Tuberculosis (TB) is a communicable disease associated with the bacillus *Mycobacterium tuberculosis* (*Mtb*), and it is the most common cause of death among patients with a single infectious agent [1]. Worldwide, there are approximately 1.3–1.5 million deaths associated with this disease every year, and it is estimated that approximately 10 million people fall ill with TB annually [1]. Moreover, an estimated 1.7 billion people have latent TB infection (LTBI), defined as the state of persistent immune response to stimulation by MT antigens without clinically manifested active TB disease. Considering the very large reactivation risk, LTBI-infected people represent a dangerous reservoir for new, active TB cases. In particular, patients coinfected with HIV are at high risk for the development of active TB from its latent phase [2]. Targeted LTBI treatment is, therefore, a key part of the End TB Strategy. Despite rapid development in the pharmaceutical industry and health care systems in many countries during the past few decades, it seems that treatment options for TB have reached their limits for several reasons. First, at the end of the boom of new antibiotics, it seemed that the library of antibacterial drugs was highly diverse to treat almost all bacterial infections, including the complicated superinfections associated with attacks by multiple bacterial strains. At that time, there was no need for the development of new structures with alternative mechanisms of action, and the development of antibacterial drugs was significantly reduced. At the same time, antibiotics became a prevalent cure for most bacterial infections, and in many cases, these drugs were misused for the treatment of illnesses not associated with bacteria, including improvement in animal husbandry, etc. As a result, most of the antibiotics polluted the environment, influencing the naturally occurring bacteria. Some of the bacterial pathogens have evolved in environments loaded with antibiotics and become resistant. Other routes of resistance development occurred in patients treated by antibiotics who, for one reason or another, did not obey the prescription directions, interrupted treatment sooner than they were supposed to, or took subtherapeutic doses. In all cases, the bacteria encountered antibiotics in low enough concentrations for the development of drug resistance. On the molecular level, the main force driving drug resistance is the acquisition of mutations in genes coding the drug target or drug-activating enzymes. These mutations usually originate in the form of insertion, deletion or single-nucleotide polymorphism [3]. TB drug resistance appears *via* two main mechanisms. The first one is primary or transmitted drug resistance which forms when resistant strains are transmitted to a new host. On the contrary, secondary or acquired drug resistance is mediated by the acquisition of drug resistance mutations to one or more drugs [4–6]. Currently, these resistant bacterial strains represent a major health threat to the world's population, and among them, multidrug resistant (MDR) or extensively resistant (XDR) TB is probably the most serious problem. Their treatment requires the use of several drugs, many of which are toxic and have various side effects. For example, aminoglycosides such as amikacin, kanamycin and streptomycin cause ototoxicity due to effects to the eighth cranial nerve [7]. Secondly, Capreomycin induces tubular neuropathy resulting in renal side effects and alkalosis [8]. Also, isoniazid-mediated hepatotoxicity *via* a choline deficiency is often observed [9]. Linezolid, as a reversible nonselective monoamine oxidase inhibitor, interacts with adrenergic and serotonergic agents increasing the risk of serotonin syndrome [10]. Finally, rifamycins induce CYP3A4 and thus interact with azole compounds leading to subtherapeutic serum concentrations while CYP2D6 isozyme is included in the metabolism of thioridazine resulting in elevated levels and enhanced cardiotoxicity when the compound is administered in combination with CYP2D6 inhibitors such as fluoxetine or propranolol [11,12]. All the side effects make the treatment expensive and, even worse, to take a long time and often fail. For the abovementioned reasons, research on new antitubercular agents has been resurrected, and its main area of focus is new compounds with a new mechanism of action that would allow for the treatment of resistant TB strains and the latent phase of the disease.

There are several mechanisms by which *Mycobacterium tuberculosis* acquires resistance. *Mtb* may develop a thick, waxy, hydrophobic cell envelope that is impenetrable to antibiotics, it may express enzymes that degrade the antibiotic or modify their molecular targets to reduce their affinity to the drug. Commonly, *Mtb* starts the expression of diverse multidrug transporters encoded by their DNA that transport various xenobiotics from the bacteria into their surroundings [13]. The effectiveness of multidrug resistance is often provided by the combination of several mechanisms, and the efflux systems probably serve as a stepping stone for the development of high-level multidrug resistance [13]. These transporters are predominantly dependent on proton motive force or ATP availability [14]. Small compounds that would interfere with the bacterial electron transport chain are therefore promising candidates for the treatment of MDR or XDR TB. Additionally, *Mtb* uses its electron transport chain (ETC) for energy production *via* oxidative phosphorylation during both replicating and latent (dormant) persistence [15–18]. As a result, small molecules inhibiting energy metabolism possess remarkable potential for LTBI, MDR TB, and XDR TB treatment. This review is focused on the description of new antitubercular drugs targeting bacterial energetics in these main areas: 1. NADH, 2. QcrB, and 3. ATP synthase and homeostasis.

2. Druggable molecular targets within the ETC in *Mtb*

In bacteria, the ETC is integrally involved in energy production *via* oxidative phosphorylation. During oxidative phosphorylation, various ETC protein complexes establish a transmembrane proton motive force (PMF). PMF energy is subsequently used for the ATP synthase-mediated production of ATP (Fig. 1) [19]. Energetic metabolism and the ETC in *Mtb* are rather complicated, having multiple side pathways and alternative mechanisms that have been

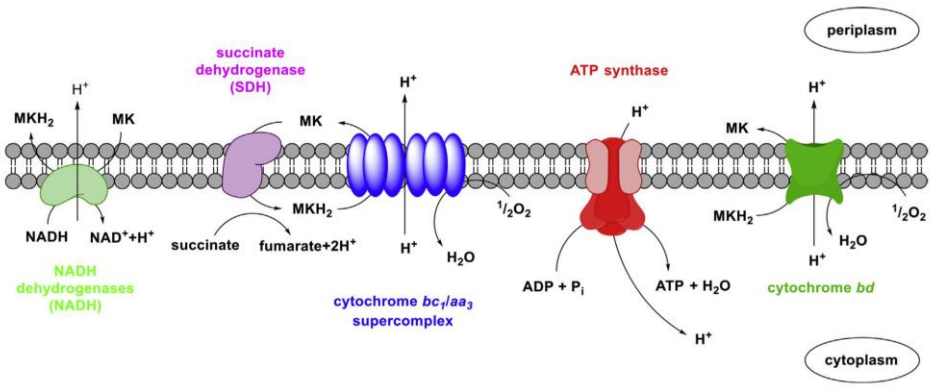

Fig. 1. Oxidative phosphorylation in Mtb (this figure was drawn according to Bald and Koul) [26].

reported multiple times [14,19,20]. To briefly summarize all mycobacterial ETCs, *Mtb* harbors multiple primary dehydrogenases to transport electrons to the lipophilic redox carrier menaquinone. Alternatively, *Mtb* possesses several reducing equivalents (e.g., nitrate reductase and fumarate reductase) to facilitate turnover under anaerobic conditions [21,22]. Depending on oxygen availability, electrons are then passed to terminal oxidases, an aa_3-type cytochrome *c* oxidase and cytochrome *bd-type* menaquinol reductase, for dioxygen reduction [23]. Such a process is coupled to the generation of a PMF, thus powering ATP synthase to synthesize ATP [14,24]. Individual roles of the main components of the ETC are detailed below.

Recently, a very informative review article was published summarizing the proteins and members of the ETC that may serve as potential targets for drug development [25]. The review mostly focuses on the biological aspects of the proteins and includes a table with the eight most promising small molecules targeting these proteins. These derivatives are all at advanced stages of drug development towards resistant *Mtb* [25]. Additionally, there were two more reviews published earlier as a summary of clinical candidates and approved drugs targeting mycobacterial metabolism [14,26]. However, there are no more recent and comprehensive overviews of early-stage research and development of small molecules interacting with mycobacterial energetics published. Therefore, the main scientific contribution and novelty of our review consist of the focus on basic research in medicinal chemistry and early-stage development of small molecules targeting the ETC. Furthermore, the review contains not only the most promising lead compounds but summarizes all of the research.

2.1. Mycobacterial primary dehydrogenases

Mycobacteria harbor multiple primary dehydrogenases to fuel the electron transport chain. The NADH dehydrogenase complex (complex I) accepts electrons from NADH and passes them to the electron carrier menaquinone [27]. NADH I dehydrogenase is preferred under aerobic conditions, while NADH II predominates in an anaerobic environment with menaquinone connecting electron-donating and electron-accepting reactions [28]. Succinate dehydrogenase forms complex II of the respiratory chain and couples oxidative phosphorylation to central carbon metabolism via the tricarboxylic acid cycle (TCA). Mycobacterial type-II NADH dehydrogenase (NDH-2) as a promising target for the treatment of tuberculosis was reviewed in 2017 [29]. The review mostly focused on the biological properties of the enzyme and the methods of its evaluation as a reasonable target. Therefore, in our review, we will be more oriented towards small molecules as inhibitors and on the newest articles on this topic.

2.1.1. NADH dehydrogenases

In prokaryotes, NADH is produced in the cytosol by glycolytic enzymes (glyceraldehyde, 3-phosphate dehydrogenase, pyruvate dehydrogenase) and enzymes in the tricarboxylic acid cycle (isocitrate, α-ketoglutarate, malate dehydrogenases) [30]. X-ray structural determination of the bacterial NADH dehydrogenase complex revealed that it is L-shaped and composed of a hydrophobic membrane arm and a hydrophilic matrix arm (Fig. 1) [27]. Mycobacteria were identified to contain two types of respiratory NADH dehydrogenases. First, proton-pumping NADH I dehydrogenase transfers electrons to menaquinone [31]. Coupled with the downhill electron transfer, there is uphill proton or sodium translocation across the membranes with concomitant generation of a membrane potential enabling ATP synthesis [32]. Electron transfer occurs in the matrix arm *via* iron-sulfur clusters, while transmembrane α-helices form proton pumping modules in the membrane arm. Every two-electron menaquinone reduction causes four protons to be pumped into the crista space, generating approximately half of the total proton motive force in mitochondria [27]. On the other hand, nonproton pumping NADH II dehydrogenase does not conserve energy, and its specific role is still unclear. Since NADH II inhibitors are bactericidal towards nonreplicating *M. tuberculosis*, they are probably essential for the recycling of NADH under hypoxic conditions [33]. A more detailed description of *Mtb* NADH dehydrogenases, their properties, their role in virulence, and their possible use as therapeutic targets may be found in Ref. [34].

2.1.2. Succinate dehydrogenase

Although embedded in the crista membrane, succinate dehydrogenase does not contribute to proton motive force by pumping protons. Therefore, it is not considered an integral part of the respiratory chain. Succinate dehydrogenase transfers two electrons directly to menaquinone, bypassing NADH dehydrogenase [27]. Most mycobacteria possess two succinate dehydrogenases, SDH1 and SDH2 [35]. Observations have indicated that SDH1 could be dedicated to succinate dehydrogenase and that SDH2 catalyzes

fumarate reductase activity, which is important for survival under hypoxia [36]. SDH1 is a key regulator of oxidative phosphorylation, catalyzing the oxidation of succinate to fumarate with a simultaneous interchange of menaquinone to menaquinol, while fumarate reductase catalyzes the reverse reaction vital for proton motive force maintenance [37,38]. However, the structure of both of these mycobacterial enzymes remains experimentally unresolved [25]. Remodeling of the TCA confirmed that the activity of SDH is essential for mycobacterial persistence and therefore represents a potential novel drug target [14].

2.1.3. Inhibitors of mycobacterial primary dehydrogenases

Phenothiazine derivatives (Fig. 2) have been used as therapeutics for a long time. Among them, thioridazine **1**, chlorpromazine **2**, and trifluoperazine **3** are commonly used antipsychotic agents. Promethazine **4**, on the other hand, is used to treat various symptoms of allergies. The possibility of the use of these compounds in antitubercular treatment was reviewed by Singh and coworkers [39]. In addition to their primary use, the compounds were investigated because of their significant anti-TB activity *in vitro*. The review article summarizes all of the results from the antitubercular research of phenothiazine derivatives and concludes that their main target is *Mtb* type II NADH dehydrogenase, a key component of the *Mtb* respiratory chain that helps the bacterium survive under stress conditions [39,40]. Importantly, this protein is not a part of the mammalian genome; therefore, it is a promising target for selective inhibition. Therefore, targeting this component of the ETC seems to be a promising strategy against latent *Mtb*. Thioridazine **1** was one of the most promising derivatives for potential antitubercular drug development, even showing effectiveness against phagocytosed *Mtb*. Compound **1** is not a single target inhibitor since it also inhibits bacterial efflux pumps, thereby helping to increase the efficacy of other drugs [39]. In addition, the fact that all of these compounds are currently used as drugs would simplify their development into commercial drugs and reduce research costs during the late stages of clinical trials.

In 2012, a primary article was published on quinolinyl pyridines with the general formula 5 along with their significant anti-TB activity [41]. Their activity was associated with the inhibition of NADH II. A small SAR study showed that compound **6** had an MIC = 1.91 μM, while the IC_{50} against NADH II = 43 nM.

Additionally, advanced *in silico* experiments were performed [42]. Tethering fragment-based drug discovery revealed disulfide **7** as the most potent NADH II inhibitor. Its aromatic ring was predicted to bind within a hydrophobic clamp formed by GLN317 and ILE379 deep in the quinone binding pocket. Moreover, there are three predicted hydrogen bonds, between the carbonyl oxygen of compound **7** and THR349 as well as between the backbone carbonyl of ILE379 to the nitrogen in the fragment tail responsible for the high binding affinity [42].

Wang and coauthors identified two types (**8** and **9**) of selective NADH II inhibitors using multicomponent high-throughput screening [43]. Altogether, they investigated 800 000 compounds, obtained 7000 primary hits, and after multiple advanced screenings (e.g., removing cytotoxic compounds), they ended up with structures **8** and **9**. These compounds showed the highest potency against both *Msmeg* and *Mtb* NADH II (IC_{50} 10.7 nM and 64.7 nM, respectively). Their activity against *Mtb* NADH A was similarly potent [43].

A series of 2-mercaptoquinozalines was prepared by Boshoff et al. [44]. Whole-cell SARs for this series of identified compounds with the general formula 10 were the most active. The authors screened for pharmacological parameters, toxicity, and other properties of the compounds related to drug development, and compounds **10a** − **10c** were identified as the most potent. They exhibit MIC values = 0.3–0.8 μM against *Mtb*, while microsomal clearance was reasonable in the range of 1.4–4.7 mL/min/g and the kinetic solubility was high enough (83–250 μM). Additionally, **10a**

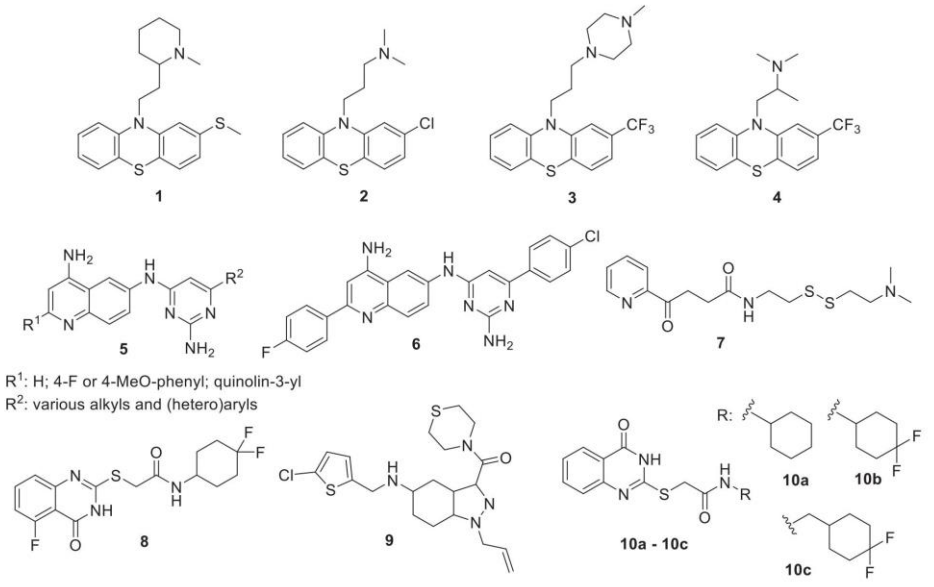

Fig. 2. Structures of antitubercular agents that inhibit NADH reductases.

– **10c** were indicated to inhibit NADH II noncompetitively in an enzyme kinetic study [44].

A series of 7-phenyl benzoxaborole derivatives was prepared and found to be active against *Mtb* with IC_{90} values as low as 5.1 μM by Sacchettini and coworkers [45]. Resistant mutants towards the most active 7-phenyl benzoxaborole were isolated and characterized, and mutations were found in the genes for NADH dehydrogenase (NADH) or the regulatory protein Mce3R, which suggests that Ndh may be the target of this series of compounds [45].

Other molecules that are known to inhibit the growth of *Mtb* are quinoline quinones [46]. Therefore, Cook and coauthors focused on the elucidation of the mechanism of action and found that quinoline quinones target *Mtb* NADH II, which activates NADH oxidation and generates a bactericidal level of ROS in a similar but more efficient manner compared to the anti-*Mtb* drug clofazimine [47]. The most recent work on quinoline quinones was published by Timmer et al. in which a large series of compounds were prepared and evaluated; however, the best derivative, 7-chloro-6-propargylamino-quinoline-5,8-dione, had only a moderate MIC = 8 μM [48].

2.2. Mycobacterial cytochrome oxidases

Mycobacteria display a branched respiratory chain with two terminal oxidases, aa_3-type Cu-heme cytochrome *c* oxidase encoded by *ctaB, ctaC, ctaD* and *ctaF* genes and cytochrome *bd* menaquinol oxidase, which are both present for dioxygen reduction coupled to proton motive force generation (Fig. 3). The cross-membrane potential provides energy for various cellular components, such as ATP synthase. The aa_3-type cytochrome *c* oxidase, which forms a supercomplex with cytochrome bc_1 reductase, is the major respiratory route under aerobic conditions [49,50]. On the other hand, the bioenergetically less efficient cytochrome *bd* branch is synthesized at low oxygen concentrations. Their expression is regulated according to an oxygen supply, but the molecular mechanisms remain unknown [24,51].

2.2.1. The aa_3-type cytochrome c oxidase

The cytochrome *c* route consists of menaquinol-cytochrome *c* oxidoreductase termed the bc_1 complex and an aa_3-type cytochrome *c* oxidase [20]. This pathway represents the main mycobacterial respiratory route under standard aerobic conditions. The bc_1 complex is composed of redox groups, including a 2Fe/2S center located on a Rieske protein (QcrA), a single polypeptide bearing low and high potential *b*-type hemes (QcrB) and cytochrome c_1 heme (QcrC). Cytochrome oxidase *c* functions as a proton pump [52].

2.2.1.1. Structural organization of the bc_1 complex.

The overall structure of *the* bc_1 complex can be divided into three regions: the membrane-spanning, the intermembrane space, and the matrix regions (Fig. 3). The subunit composition of bc_1 complexes varies significantly from 13 transmembrane helices in human mitochondria to 10 or 11 helices in bacteria [53]. Despite such structural diversity, all bc_1 complexes have three redox subunits in common: a cytochrome *b* protein containing two *b*-type hemes with high (b_h) and low (b_l) potential, a *c*-type heme and an iron-sulfur protein (ISP) with a high-potential *2Fe–2S* iron-sulfur cluster. Furthermore, the purified bc_1 complex contains ubiquinone and phospholipids. All additional (supernumerary) subunits do not have a well-established cellular function, and they are believed to contribute to the enhanced overall stability [54,55].

2.2.1.2. Functions of the bc_1 complex.

The cytochrome bc_1 complex is essential in the respiratory chain for electron transport across the membrane from menaquinol to cytochrome *c* [56,57]. The cytochrome *b* protein forms the hydrophobic core, enabling further interactions within the complex [58]. There are two identical *b*-type hemes, b_h and b_l, located on the cytoplasmatic and exterior faces of the membrane, respectively [53]. Subunit b_h contributes to menaquinone reduction (Q_N), whereas b_l engages in menaquinol oxidation (Q_P). The bc_1 complex transfers H^+ to the coupled aa_3 cytochrome *c* oxidase that carries out oxygen reduction [59].

2.2.2. Cytochrome bd-type oxidase

Cytochrome *bd* oxidase has been investigated to a lesser extent, and its function may be complex. Although not required for aerobic growth, cytochrome *bd* plays an important role in the response to antibacterial stress and adaptation to a reduced oxygen environment [60]. The cytochrome *bd* complex generates charge separation *via* electron transport instead of translocating H^+ [61,62]. The mycobacterial cytochrome bc_1 complex has already been validated as a promising drug target. It displays two substrate (quinone/quinol) binding sites that may be able to accommodate a variety of small-molecule inhibitors. Moreover, targeting cytochrome *bd* appears highly efficient, but further structural and functional analysis is needed to explore this enzyme [26].

2.2.3. Inhibitors of mycobacterial cytochrome oxidases

Imidazo[1,2-α]pyridines were synthesized as potent lead anti-TB molecules from a high-throughput screen [63]. The most promising compounds, **14** and **15**, had notable antitubercular potency in various *Mtb* strains with MICs = 0.03 μM–5 μM and acceptable pharmacokinetic profiles. Furthermore, a dose-response

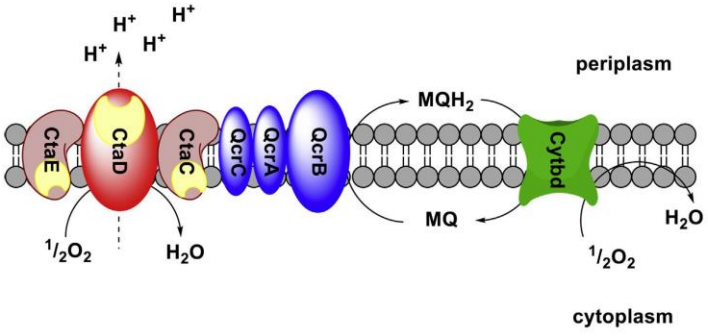

Fig. 3. Mycobacterial cytochrome oxidases.

efficacy study in an acute murine model revealed bacteriostatic behavior *in vivo*, demonstrating a 2 log CFU reduction with respect to nontreated controls. Resistant mutants were generated to find the molecular target of the best derivative (**14**), which was identified as QcrB by genome sequencing [63]. Additional proof of this target was given when the MIC of compound **14** increased significantly (from 0.5 μM to 8 μM) in bacteria with significantly overexpressed QcrB. This is one of the earliest studies showing QcrB as a promising anti-TB target.

A set of five chemically diverse heterocyclic compounds was investigated [64]. Among them, compounds **16**–**18** were the most interesting, with imidazo[1,2-α]pyridine **16** being the most active against *M. tuberculosis* H37Rv, inhibiting its visible growth with MIC >50 μM and more than 90% resazurin reduction under MABA conditions of 0.15 μM. Imidazo[1,2-α]pyridine **16** exhibited an inability to inhibit *Mtb* H37Rv while inhibiting the transfer of electrons followed by resazurin reduction as well as the final ATP production with kinetics similar to BDQ. Such an inability was probably caused by the upregulation of cytochrome *bd* oxidase as an alternative respiratory complex. Indeed, the cytochrome *bd* oxidase mutant (cydKO) was found to be highly susceptible to imidazo[1,2-α]pyridines with an MIC of less than 0.024 μM and MABA less than 0.024 μM [64].

Surprisingly, another imidazopyridine, zolpidem (**19**, used for the treatment of insomnia), was found to have anti-TB activity (*M. tuberculosis* H37Rv, MIC 10–50 μM) [61]. A rationally designed set of zolpidem analogs was subsequently synthesized, and their antitubercular potency was evaluated. Among them, compound **20** had an MIC = 0.004 μM. Since the target was of great interest, screening against a panel of *qcrB*-resistant mutants revealed that all the tested imidazopyridines were bc_1 complex inhibitors, as demonstrated by their loss of potency [61]. Another zolpidem analog was studied in Ref. [65]. The authors rationally designed a large library of the analogs and anagrams with the main scaffold imidazopyridine and tested them against *Mtb*. The most potent derivatives had MICs as low as 0.004 μM and reasonable selectivity, which made them potential therapeutics.

Other imidazo[1,2-α]pyridines were subjected to target elucidation. Compounds **21a** – **21c** showed the best potency against intracellular *Mtb* and were therefore chosen for the next experiments. They exhibited significant inhibition of *M. tuberculosis* R37Rv with an IC_{50} of 0.15–0.39 μM. As the *Mtb* $QcrBT_{313I}$ mutant strain showed resistance to the tested compounds with at least 8-fold shifts in MICs (MIC_{90} 6.5->20 μM), QcrB was proposed to be their molecular target. Disrupted pH homeostasis and depleted ATP levels provided further evidence of an effect on the electron transport chain. Protein Rv1339, a member of the β-lactamase superfamily, was established as the secondary target. This protein could affect cell wall structure, thereby impacting compound permeation. Finally, none of the tested compounds was cytotoxic against THP1 cells, making them potential drug candidates [66].

A set of more than fifty pyrrolo[3,4-c]pyridine-1,3(2*H*)-diones was prepared by Westhuyzen et al. [67], and their HTS identified hit pyrrolopyridine **22** that was active against *Mtb* (*M. tuberculosis* H37RvMa, MIC_{90} 0.132 μM). Unfortunately, pharmacological parameter tests showed that its ester moiety undergoes microsomal hydrolysis (only 35% of **22** remained in solution after 40 min of incubation). Subsequently, bioisosteric replacements of the labile ester were investigated. The 1,2,4-oxadiazole moiety was identified as biologically active and metabolically stable. *In vivo* pharmacokinetic studies of **23** in mice indicated high clearance and low plasma exposure (c_{max} = 0.033 μM), but the metabolic stability was highly improved (97% of **23** remained in solution after 40 min of exposure to microsomes). Codosing **23** with aminobenzotriazole (ABT) improved the unfavorable parameters. To determine the mechanism of action, target identification studies were performed. Hypersensitivity of the cydKO deletion mutant and the cross-resistance of the cydKO/QcrBA317T mutant strongly indicated that these compounds target the QcrB subunit of the *bc1* complex [67].

Novel phenoxyalkylbenzimidazoles were prepared to expand the SAR studies. Observed key determinants for antimycobacterial activity were methyl groups at both the C-6 of the benzimidazole and the C-4 of the terminal phenyl, a three-carbon atom linker, and a nitrogen heteroatom on the alkyl chain. One of the most potent compounds against *Mtb* H37Rv, **24**, had MIC = 0.47 μM, improved derivative **25** had an MIC = 0.061–0.070 μM. First, QcrB targeting was confirmed by testing the MIC. All tested compounds showed a 5-fold lower MIC against the resistant mutant $QcrB_{M342T}$ compared to the parental strain. The benzene ring may be responsible for QcrB targeting since the $QcrB_{M342T}$ mutant was not resistant to the imidazole analogs. Second, ATP depletion together with decreased intracellular pH provided further evidence for QcrB as a target [68].

A phenotypic screen by GSK identified 2-(quinoline-4-yloxy) acetamides as potent *Mtb* growth inhibitors. A preliminary SAR investigation of the antitubercular activity identified five analogs, **26a** – **26b** and **27a** – **27b** (Fig. 4; MIC_{90} *Mtb* H37Rv, 0.3–3.3 μM). Based on the SAR, another set of compounds was prepared with the best compounds, **27c** – **27e**, showing activity of 0.62–0.45 μM against *M. tuberculosis* H37Rv determined by MABA and thus showing improved potency compared with the original hits, with an activity of 1.11 μM under the same conditions. In general, bulky, lipophilic substituents at R improved the potency, while a methoxy at C-6 was critical for activity. In addition, the tested compounds exhibited enhanced MICs of 0.12-<0.063 μM towards the *Mtb* cydKO strain. Based upon the magnitude of MIC enhancement, these compounds were established as cytochrome bc_1 oxidase inhibitors [69].

The next promising antitubercular agents are imidazo[2,1-*b*] thiazole-5-carboxamides, which are endowed with nanomolar potency (*Mtb* H37Rv MIC < 0.05 μM). Moreover, compounds **28a** – **28c** were exceptionally potent against mono-drug resistant strains (MIC_{rRMP} less than 0.04–0.201 μM, MIC_{rINH} less than 0.04–0.506 μM). Antituberculosis assays revealed two unsuitable modifications, namely, a trifluoromethyl group in the ortho position and a biaryl ether aniline compared to the biaryl ether benzylamine. To suggest the molecular target, compounds **28a - 28c** were screened against six QcrB mutants. As a result, their QcrB selectivity was confirmed [70,71].

The synergistic effects between phenoxylakylbenzimidazoles (PABs, e.g., **29**) and other compounds targeting the bacterial respiratory chain, such as clofazimine and bedaquiline, were investigated [72]. It was found that the combination of PABs with clofazimine led to strong synergistic killing of both replicating and nonreplicating *Mtb*. On the other hand, the combination of PABs with bedaquiline showed antagonism, which disappeared within three weeks, and as a result, the PAB-bedaquiline combination became strongly bactericidal.

A new series of antimycobacterial 4-amino-thieno[2,3-d]pyrimidines targeting cytochrome bc_1 oxidoreductase was discovered. From 78 screened small molecule nucleotide mimetics, **30** exhibited the highest growth inhibition with an IC_{50} of 2.7 ± 0.84 μM. Finally, enhanced activity against *qcrB* mutants and depletion of ATP levels confirmed cytochrome bc_1 as a target [73].

Four derivatives, **31**–**34** (Fig. 5), within a larger 2-ethylthio-4-methyaminoquinazoline chemical library showed good activity ranging from 0.02 to 0.09 μg/mL against *Mtb* H37Rv and HepG2 cells, respectively, and low toxicity (TD_{50} > 5 μg/mL) *in vitro*. Quinazoline **32** was the most selective from this series. Considering the SAR, fluorine atoms at positions 6 and 8 and ethyl thioalkyl chains

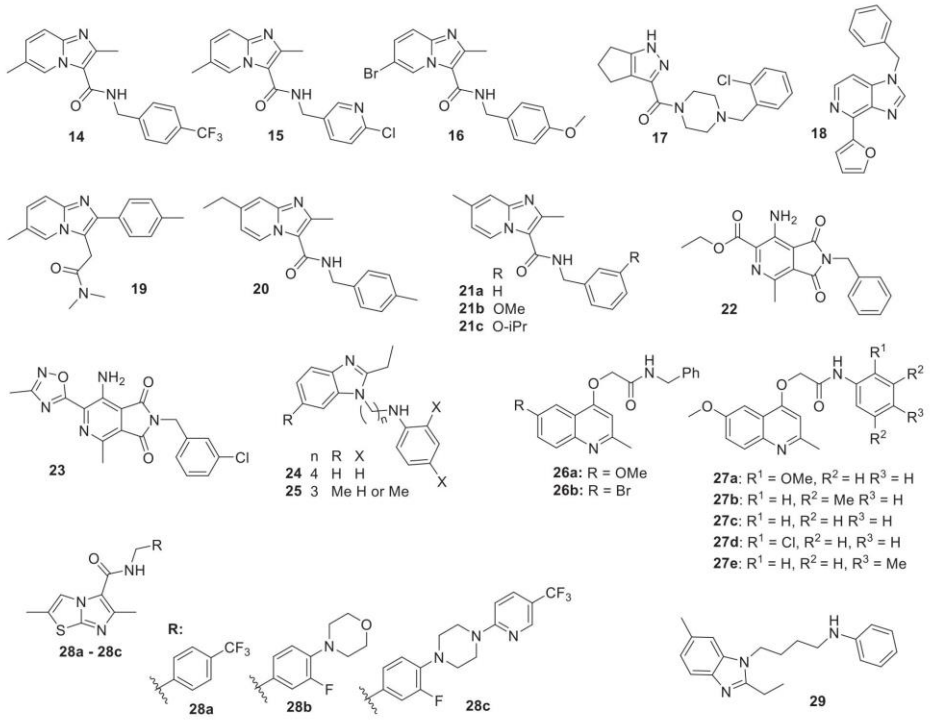

Fig. 4. Inhibitors of mycobacterial cytochrome oxidases.

were found to be preferable. Moreover, the smallest substitution in position 4 was observed to enhance the antitubercular activity. Quinazolines were revealed to target cytochrome bc_1 by whole-genome sequencing [74].

The 2-(quinoline-4-yloxy)acetamides (QOAs) of general formula 35 (Fig. 5) were reported to be promising antitubercular agents. These molecules have intracellular activity similar to INH and RMP (MIC = 0.01–0.08 μg/mL) and great efficacy against resistant *M. tuberculosis* isolates (MIC = 0.01–0.08 μg/mL). Target identification based on genome sequencing and MIC indicated two targets: DNA gyrase and the cytochrome *bc1* complex. Docking experiments revealed that the *b*-subunit of the cytochrome, namely, protein residues THR313, MET342 and LEU167, are responsible for the main interactions. Firstly, the hydroxyl group of the THR313 mediates polar interaction essential to inhibitor stabilization in the protein active site. Secondly, MET342 and LEU167 are involved in hydrophobic interactions with the Q_P quinol oxidation site, which is vital for cell survival [75].

Whole-cell screening identified morpholinothiophene analogs as potential antitubercular scaffolds. Initial hit **36** (Fig. 5) showed good antitubercular activity against *Mtb* H37Rv (MIC = 0.72 μM). Moreover, compound **36** showed acceptable physicochemical and pharmacokinetic properties. Therefore, many more morpholinothiophenes with the general formula 37 (Fig. 5) were synthesized for the SAR study. Since the SAR suggested that the phenethyl linker and the amide carbonyl were critical aspects of the pharmacophore, it appeared that the whole series shared a similar pharmacophore to scaffolds that target QcrB. To confirm the molecular target, ATP and growth were monitored in the same experiment. As a result, ATP depletion occurred in a dose-dependent manner, similar to Q203 (a known QcrB inhibitor) [76].

As potent antitubercular agents *in vitro*, arylvinylpiperazine amides were studied intensively. The investigated arylvinylpiperazine amides demonstrated potent antitubercular activity against *Mtb* H37Rv *in vitro* (MIC 0.05–0.1 μM), and the IC_{50} for *Mtb*-infected TFP-1 macrophages ranging from 0.1 to 0.3 μg/mL reflects the potent *ex vivo* activity of these molecules. In addition, all compounds had low cytotoxicity. Compounds **38a** and **38c** (Fig. 5) proved the *in vivo* activity determined in a mouse model of acute TB. Both compounds significantly reduced the bacterial loads in mouse lungs by 0.4 and 0.6 $\log_{10}$, respectively, compared to the vehicle control. A cross-resistance study revealed different interactions with the quinol binding pocket of the cytochrome *bc1-aa3* oxidase QcrB subunit compared to Q203. Additionally, transcriptomic and bioenergetic flux studies confirmed QcrB as the primary target [77].

Various commercial chemical libraries were screened by Cechetto and coworkers to find diverse anti-tubercular compounds [78]. As a result, imidazopyridine amide derivative **39a** was identified as the best inhibitor. Compound **39a** was synthesized and fully screened *in vitro* to find that its activity against MDR and XDR *Mtb* is in the nanomolar range, and subsequent experiments found

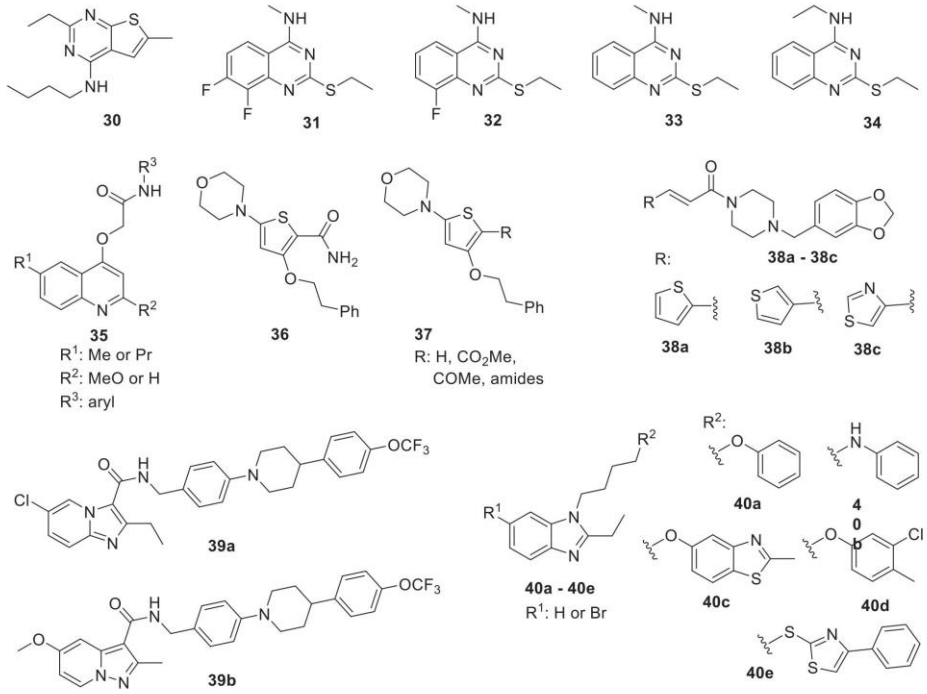

Fig. 5. Inhibitors of mycobacterial cytochrome oxidases.

it to have *in vivo* activity at doses lower than 1 mg per 1 kg body weight. The mechanism of action was elucidated and it was shown that nanomolar concentrations significantly lower the levels of ATP, which led to the suggestion that the compound inhibits cytochrome *bc1* activity [78]. Based on the structure of **39a**, bioisosteric pyrazolo[1,5-*a*]pyridine-3-carboxamide analogs were prepared and identified as potential new antitubercular agents with high activity against *Mtb* H37Rv (MIC_{90} = 0.125 μg/mL) [79]. More importantly, lead compound **39b** (Fig. 5) had remarkable activity against 56 Mtb isolates, including 37 MDR and 2 XDR strains. Moreover, a lack of toxicity combined with high oral bioavailability was reported. Docking studies of **39b** in the Q_p binding site revealed π-π interactions with the aromatic side chains of TYR321 and PHE156, similar to the interactions observed with Q203. Surprisingly, **39b** exhibited a strong synergy with subtherapeutic concentrations of PZA and RMP, causing a 4- and 5-fold reduction in lung CFU [79].

High-throughput screening identified phenoxyalkylbenzimidazoles as very adaptable scaffolds with nanomolar MICs (MIC_{50} = 0.34–5.3 μM) against *Mtb*. They inhibit *Mtb* growth inside macrophages with insignificant cytotoxicity. These compounds likely target QcrB, a component of the cytochrome bc_1 complex. However, *Mtb* is able to reroute its ETC to provide resistance to therapy. Considering these factors, combinations of ETC-targeting compounds with synergistic activity are needed. Such synergistic killing was achieved with compounds **40a**-**40e** (Fig. 5) in combination with CFZ under both replicating and nonreplicating conditions [72].

2.3. Mycobacterial ATP synthase

2.3.1. Characterization and function of mycobacterial ATP synthase

ATP synthase is a ubiquitous enzyme present in mitochondria, chloroplasts, or plasmatic membranes. Resembling a turbine, the structure of ATP synthase consists of two components: a rotor (F_0) and a stator (F_1) connected through a central stalk, reversibly coupling proton flow to either ATP synthesis or hydrolysis [27,80]. Oxidative phosphorylation is the source of energy that drives ATP synthase to convert the electrochemical potential energy into chemical energy in the form of ATP by the reaction of ADP with inorganic phosphate (P_i) [14,81].

Considering the mycobacterial ATP synthase (Fig. 6A), three α and three β subunits alternate to form the hydrophilic stator (F_1), which extends into the cytoplasm. The membrane-embedded rotor (F_0) includes one *a*, two *b*, and a ring of more than ten *c* subunits. Rotor and stator connection *via* the central stalk containing γ, δ and ε subunits has specific fusion between one *b* and one δ subunit [82]. The resulting *b*/δ fusion protein improves the bonding interaction between ATP precursors and the $\alpha_3\beta_3$ hexamer, while the free *b* subunit increases power transmission within the ATP synthase complex. As a result, the presence of two different *b* subunits probably enhances their overall mutual interaction [83].

Compared to mycobacterial ATP synthase, bacterial ATP synthase (Fig. 6B) shows structural differences, such as relaxed junctions between the *b* and δ subunits. Moreover, bacterial ATP synthase usually contains exactly ten *c* subunits with proton-binding sites. A lower number of monomers per subunit of the *c*

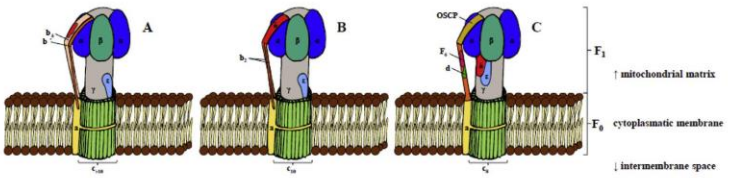

Fig. 6. Mycobacterial (A), bacterial (B), and human (C) ATP synthases (this figure was drawn according to Lu and Bald) [80].

oligomer may decrease the H^+/ATP ratio and thus complicate ATP synthesis under low proton motive force conditions [84]. On the other hand, eukaryotic ATP synthase (Fig. 6C) contains homologous oligomycin sensitivity-conferring protein (OSCP) instead of the δ subunit, with only one *b* subunit accompanied by minor *d* and F_6 subunits and eight monomers in the *c* ring [85,86]. Finally, in ATP synthase in chloroplasts, the *b* homodimer is replaced by two homologous *b* and *b'* subunits [87].

ATP synthase is strongly evolutionarily conserved among prokaryotes and eukaryotes. *M. tuberculosis*, an obligate aerobic bacterium, is dependent on oxidative phosphorylation to produce ATP for growth and survival. Apart from replicating mycobacteria, ATP synthase is also essential in the dormant state, carrying specific features facilitating survival under nonreplicating conditions, including oxygen insufficiency, nutrient limitation, and acidic pH [88].

As such, mycobacterial ATP synthase features several functional adaptations. First, mycobacterial ATP synthase lacks the ATP hydrolysis function to prevent ATP from being wasted. Suppression of the hydrolytic activity may be caused by inhibitory binding of Mg-ADP, subunit ε dysregulation, or by the inhibitory protein subunit ζ [89]. The second specific feature to mention is the ability to synthesize ATP under low proton motive force (−110 mV), which is closely linked to the structure of subunit *c*. A large *c* oligomer causes increased H^+/ATP turnover, resulting in promoted ATP formation. Even an unusual stiffness of the stator stalk or highly lipophilic cytoplasmatic membrane may speed up ATP synthesis [35,90].

All of the aforementioned differences compared to human ATP synthase may be crucial to understand the design and development of selective ATP synthase inhibitors.

2.3.2. Inhibitors of mycobacterial ATP synthase

One of the first compounds found to target *Mtb* ATP synthase, especially its subunit *c*, was bedaquiline **41** (Fig. 7) [91–95]. The compound was efficient even against MDR *Mtb* and developed by Jansen Pharmaceuticals [96]. Despite its high potency, compound **41** has several drawbacks, such as a long half-life, high lipophilicity, and low solubility; therefore, several research groups have focused on analogs with better pharmacological profiles. Palmer and co-authors synthesized 26 analogs with the naphthalene unit replaced with pyridines were to reduce the lipophilicity and half-life [96]. Compounds **42** and **43** (Fig. 7) significantly inhibited bacterial growth of *Mtb* H37Rv under both replicating (MABA) and non-replicating (LORA) conditions. Specifically, derivative **42** had an MIC_{90} of 0.01 μg/mL under MABA conditions and 0.06 μg/mL under LORA conditions, and derivative **43** had an MIC_{90} of 0.02 μg/mL under MABA conditions and 0.02 μg/mL under LORA conditions. Both compounds were also effective *in vivo* (CFU reduction) and noncytotoxic (IC_{50} values > 10 μg/mL in the Vero assay). Both compounds have notably lower hERG potencies than bedaquiline, resulting in reduced cardiovascular toxicity [96].

A luciferin-based ATP assay selected thiazolidinone derivative **44** for further studies. Compound **44** showed excellent anti-TB activity (*Mtb* H37Rv, MIC_{90} = 0.5 μg/mL, and intracellular MIC_{90} in macrophages = 4.0 μg/mL) and low cytotoxicity (therapeutic window 80). Additionally, **44** exhibited a 2-8-fold higher MIC in RMP^R and MDR isolates of *Mtb*. Considering the molecular target, screening against *M. smegmatis* ATP synthase on an inverted membrane was performed (IC_{50} 0.312 μM). Docking analysis showed that residue LEU59 of *Mtb* ATP synthase was involved in H-bond interactions with the phenyl ring of **44**. Finally, π-π interactions between TYR64 and the abovementioned phenyl ring were detected [97].

In silico methods such as homology modeling and virtual screening can find various molecules that effectively inhibit *Mtb* F_1F_0 ATPase. In this quest, four virtual hits, **45**–**48**, were obtained and showed better binding affinity compared to bedaquiline **41**. Molecular docking revealed key interactions with GLU61 and ARG186 [98].

Simplification to the structure of bedaquiline used a fragment-based approach and resulted in 4 series of 3-(4-(*N*,*N*-dimethylaminomethyl)phenyl)quinolines. Among these compounds, **49** and **50** were found to be the most potent candidates against *Mtb* H37Rv with MICs = 0.43 and 0.44 μg/mL and against DR isolates (MIC 0.48–0.94 μg/mL). Therefore, **49** and **50** were assayed for their capacity to inhibit *Mtb* ATP synthase, showing a direct impact with IC_{50} values of 20.3 ± 1.0 and 38.8 ± 1.0 μM, respectively. Compound **49** was the best candidate with an improved log*P* of 5.55, which is beneficial for pharmacokinetic properties [99].

A very large SAR study of squaramides resulted in compounds with nanomolar potencies in an ATP synthesis inhibition assay [100]. The most active was derivative **51**. Complete stasis after two weeks of treatment with a 200 mg/kg dose established the *in vivo* efficacy of **51** in a mouse model of acute TB, and the activity against *Mtb* H37Rv showed an MIC = 0.43 μM. SAR exploration revealed that 2-pyridylmethyl substitution is critical for achieving good potency. On the left-hand side of the molecule, a morpholinophenyl moiety was found to be the best. ATP synthase was suggested as a molecular target based on a membrane-based biochemical assay (Myc_ATPS IC_{50} 0.03 μM) measuring ATP synthesis through oxidative phosphorylation. This result was confirmed by spontaneous resistant mutant characterization. To understand the binding mode, **51** was docked into *Mtb* ATP synthase. The pyridine nitrogen of **51** forms π-π interactions and H-bonds with ARG186 of subunit *a*. Furthermore, the morpholine oxygen interacts with PHE69 of subunit *c* through H-bonding [100].

The novel scaffold 6,7-dihydropyrazolo[1,5-a]pyrazin-4-one was identified by screening using *M. smegmatis* ATP synthase. A scaffold hopping approach revealed compounds **52** with improved activity against *Mtb* H37Rv with MIC 2–4 μM. They do not inhibit any of the CYP450 enzymes and could be a starting point for anti-TB drug discovery [101].

Novel *Mtb* ATP synthase inhibitors derived from neuroleptic phenothiazines were synthesized. Compounds **53a** and **53b** with the strongest *Mtb* H37Rv growth inhibition (MIC = 6.25 μg/mL) were screened for ATP synthesis inhibition using inverted

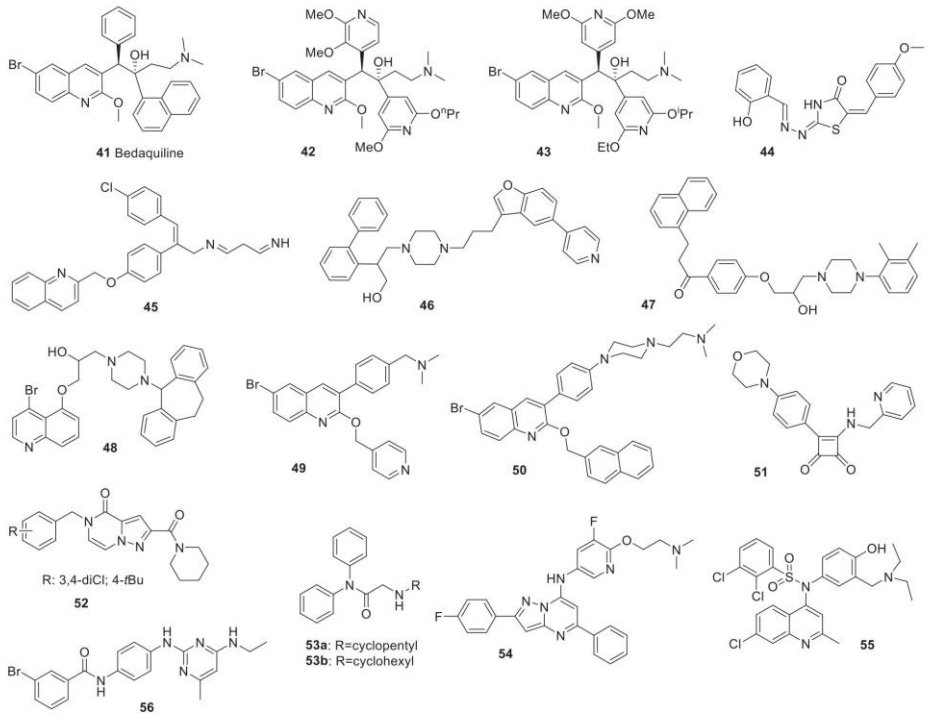

Fig. 7. Inhibitors of mycobacterial ATP synthase.

membrane *M. smegmatis* vesicles (IC_{50} values of 14 and 10.4 μM, respectively). The blood-brain barrier crossing ability (Pe 2.7×10^{-6} and 3.0×10^{-6} cm/s) was reduced compared to chlorpromazine, indicating diminished CNS side effects. Docking studies showed π-π interactions between the phenyl rings of 53 and PHE69. Since PHE69 is absent in human enzymes, compounds **53** tended to be safe and efficacious [102].

First, HTS resulted in the identification of 2,4-diaminoquinazolines as ATP synthase inhibitors. Second, scaffold hopping led to pyrazolopyrimidines with over 100-fold improved selectivity for *Mtb* ATP synthase (Myc_ATPS $IC_{50} = 0.5$ μM; SI = 20). Compound **54** docked into the bedaquiline binding site showed a 4-fluorophenyl group responsible for the blocking capacity between the Atp-a and Atp-c subunits. However, the absence of cross-resistance against bedaquiline-resistant strains suggested that pyrazolopyrimidines interact with ATP synthase differently than bedaquiline despite binding at the same site [103]. Compound **54** had antitubercular activity against *Mtb* H37Rv with an MIC = 6.2 μM.

A large study of potential antitubercular compounds was performed [104]. First, a large virtual library of compounds was screened *in silico*, and then a set of compounds was prepared from the most promising hit. Among them, chloroquinolines of general formula 55 with cytotoxicity above the detection limit (CC_{50} ˃300 μg/mL) and excellent ATPase inhibitory activity and selectivity (IC_{50} 0.51 ± 0.030 μM; SI ˃200) were identified as lead compounds. Compound **55a** was the best compound and exhibited bactericidal effects in the hypoxic *Mtb* culture (more than 2.3 $\log_{10}$ reductions in CFU). In a murine model of chronic TB, compound **55a** showed 2.12 $\log_{10}$ reductions in CFU in both the lung and spleen at a dose of 173 μmol/kg. Pharmacokinetic studies on **55a** indicated quick absorption, high distribution volume (V_{ss} 0.41 L/kg), moderate clearance (0.06 L/h/kg), and a long half-life (4.2 h). These results suggest that **55a** is a promising drug candidate (activity against *Mtb* H37Rv, MIC 3.12 μg/mL) [104]. Another study on six new chloroquinoline derivatives containing the same scaffold **55** was published in Ref. [105], the activity against *Mtb* was MIC_{50} = 3.12–6.25 μg/mL, and the IC_{50} against ATP synthase was 0.36–1.83 μM. Compound **55b** was selected as the best compound with an MIC_{50} of 3.12 μg/mL against *Mtb* and an IC_{50} against ATP synthase of 0.39 μM.

To overcome the clinical resistance and long terminal half-life of BDQ, a new generation of 3,5-dialkoxypyridine analogs is currently under investigation. Among them, compound **56** had remarkable properties and activity against *Mtb* H37Rv with a MIC_{50} = 33 μM. An inverted membrane vesicle (IMV) assay was used to confirm mycobacterial ATP synthase inhibition (IC_{50} of 0.5 ± 0.1 μM against *M. smegmatis* and 5.2 ± 1.1 μM against *M. bovis* BCG). Biochemical and NMR studies showed that **56** inhibits ATP synthase by binding to the γ subunit loop. Preliminary *in vitro* ADME profiling revealed that **56**, with a clogP of 4.37, is less lipophilic than BDQ and metabolically stable in mouse liver microsomes. Finally, *in vitro* ATP synthesis experiments indicated a synergistic effect with BDQ [106].

2.3.3. Small molecules influencing ATP homeostasis

Small molecules interfering with energy metabolism may not be restricted just to ATP synthase inhibitors, but they may influence ATP homeostasis by the activation of latent ATP hydrolytic activity or by rerouting electron flow to reactive electron species. Since the results are similar to those of ATP synthase inhibitors, we are adding them to this chapter (Fig. 8).

New amino lipopeptides named trichoderins were isolated from the marine-derived fungus *Trichoderma* sp. These compounds were tested for their antimycobacterial activities, and among them, trichoderin A (**56**) was the most potent with activity against *Mtb* H37Rv (MIC 0.12 μg/mL). This sparked interest in identifying its molecular target by influencing gene expression. It was found that mycobacteria with the highly overexpressed genes *atpB, atpE, atpF, atpH*, and parts of *atpA* coding mycobacterial ATP synthase became resistant to Trichoderin A (**56**), which is indirect proof that compound **56** targets ATP synthase. In addition, **56** reduced the intracellular ATP concentration in *M. bovis* BCG [107].

The low level of bacterial respiration is an important point of *Mtb* metabolic vulnerability. Therefore, a hypoxic ATP depletion model has been developed to carry out HTS campaigns. Among 60 0000 screened compounds, thiophenes were identified to significantly disrupt ATP homeostasis (hypoxic ATP IC_{50} 3.4 μM, aerobic MIC_{50} 1.7 μM for compound **57**) [108].

A cellular screen and subsequent lead optimization provided various anti-TB pyrimidine-imidazoles (PIs). Mechanism of action studies linked their activity to glycerol metabolism. PIs cause the accumulation of glycerol phosphate coupled with ATP depletion, thereby impairing *Mtb* growth. Compound **58** strongly affected carbon metabolism, leading to the highest anti-TB activity against within a PI series with an MIC = 0.036 μM against *Mtb* H37Rv [109].

3. Author's insight on the topic

Due to the ever-increasing risk of drug-resistant and latent TB, searching for alternative molecular targets is becoming a hot topic. Since energy metabolism represents a fundamental feature in mycobacterial adaptation, targeting various ETC protein complexes is a promising way to generate new anti-TB drugs. Progressive research in the field of mycobacterial energy metabolism has identified several small organic molecule inhibitors with significant anti-TB potency, as summarized in Table 1. Considering the most active scaffolds, some promising QcrB inhibitors, such as imidazopyridine **20** [61], phenoxyalkylbenzimidazoles **25** [68], imidazo [2,1-*b*]thiazole-5-carboxamides **28** [70], and arylvinylpiperazine amides **38** [77], showed nanomolar MICs against *Mtb* H37Rv. Nanomolar MICs against *Mtb* H37Rv were also found among ATP synthase inhibitors, including C-pyridyl analogs **42** and **43** [96] and pyrimidine-imidazole **58** [110].

To highlight the efficacy of targeting OP, there are already various clinical candidates and approved drugs that have been identified among small molecules targeting mycobacterial energy metabolism. Their structures, current status, and targeted protein components of the mycobacterial ETC pathway are summarized in Table 2. Such therapeutic potential reinforces the importance of OP as a promising drug target. Furthermore, these ETC-targeted drugs combined with other drugs acting *via* different mechanisms lead to synergistic killing, enabling more effective treatment of drug-susceptible and drug-resistant TB [19,25].

4. Conclusion

This review summarizes the efforts in the development of a new type of antitubercular drug focused on energetic metabolism inhibitors. Such compounds are very promising for the treatment of MDR, XDR, and latent stage tuberculosis, especially in combination with other drugs. In this review, we focused mostly on inhibitors of NADH dehydrogenase, *Mtb* cytochrome oxidases, and ATP synthase.

NADH dehydrogenase is a promising molecular target for *Mtb* infection since the protein is not a part of the mammalian genome, and thus, its selective inhibition may selectively kill *Mtb*. Since this enzyme is important for bacteria even in the latent stage, compounds targeting *Mtb* NADH dehydrogenase may be advantageous over compounds that are only effective against the active form. However, the amount of literature on this topic is rather limited. This may be because it is rather complicated to find compounds that selectively target just this protein or due to the fact that it is time-consuming and complicated to prove that NADH dehydrogenase is the target since similar effects, such as ATP depletion, may be reached by targeting different proteins. Up to date, compound **8** (Fig. 2) exhibited the highest potency against *Msmeg* as well as *Mtb* NADH II with IC_{50} of 10.7 nM and thus was identified as a primary hit [43]. In our opinion, there is remarkable room for the development of new small molecules targeting this part of the ETC.

A number of articles were published on inhibitors of *Mtb* cytochrome oxidases. Some of them have nanomolar MIC values, which probably makes them the most promising small molecules for the future treatment of tuberculosis. Herein, imidazopyridines tuned out to represent the key heterocyclic cores. Among them, imidazopyridine **20**, derived from zolpidem **19** (Fig. 4), possess

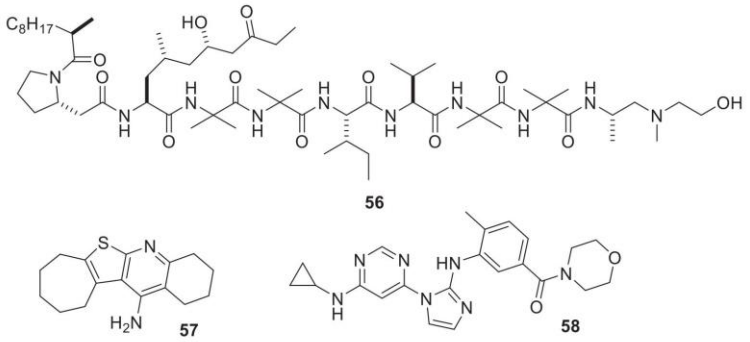

Fig. 8. Compounds disrupting mycobacterial ATP homeostasis.

Table 1
The most potent small organic molecules targeting mycobacterial energy metabolism with nanomolar MICs.

Compound	Target(s)	MIC value(s)
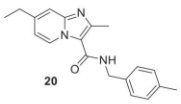 **20**	Cytochrome bc_1 complex	0.004 μM
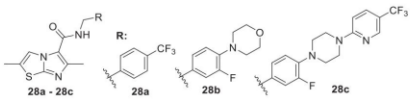 **28a - 28c** **28a** **28b** **28c**	Cytochrome bc_1 complex	0.061–0.070 μM
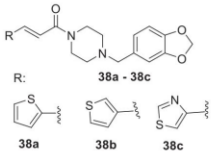 **38a - 38c** **38a** **38b** **38c**	Cytochrome bc_1 complex	<0.05 μM
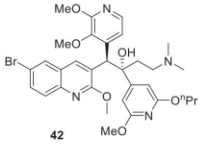 **42**	Cytochrome bc_1 complex	0.05–0.1 μM
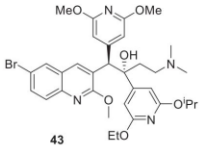 **43**	ATP synthase	0.01 μg/mL
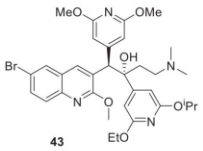 **43**	ATP synthase	0.02 μg/mL
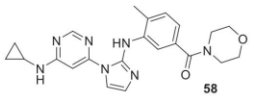 **58**	ATP homeostasis	0.036 μM

outstanding inhibitory potency on the *bc1* complex with MIC as low as 0.004 μM [61]. In addition, several compounds with the highest activity have been used for a long time as treatments for other diseases. Given that, their pharmacological parameters, toxicity, adverse effects, and other important properties are known, which would significantly speed up anti-*Mtb* drug development while reducing the price.

It is well known that mycobacterial ATP synthase carries idiosyncratic features that contribute to efficient ATP production. Therefore, elucidating the exact mechanism of how ATP synthase works can add to the understanding of its general function and reveal specific molecular adaptations. A better insight into all these processes may provide key input for the rational design of new small molecule entities acting as ATP synthase inhibitors. Moreover, mycobacterial ATP synthase exhibits critical differences compared with human ATP synthase and thus reinforces the design and development of selective ATP synthase inhibitors as antitubercular agents. The most promising ATP synthase inhibitors **42** and **43** were derived from bedaquiline **41** (Fig. 7) by Palmer and coworkers [96] by replacing the naphthalene unit with pyridines to achieve reduced cardiotoxicity, lipophilicity and half-life. Both compounds inhibited bacterial growth of *Mtb* H37Rv under MABA with MIC_{90} of 0.01 and 0.02 μg/mL as well as LORA conditions with MIC_{90} of 0.06 and 0.02 μg/mL, respectively.

Table 2
Clinical candidates and approved drugs within small molecules targeting the mycobacterial ETC pathway.

Name	Structure	Target	Current status
Bedaquiline **41**	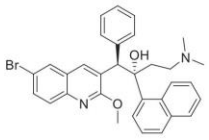	ATP synthase (subunit *c*)	Approved
Squaramide **51**	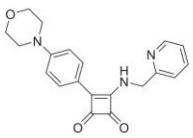	ATP synthase (subunit *a*)	Preclinical
Q203 **39a**	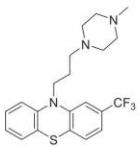	Cytochrome bc_1 complex (Q_P site)	Phase 1
Thioridazine **3**	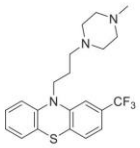	NADH II (ROS-mediated oxidation)[a]	Approved
Clofazimine	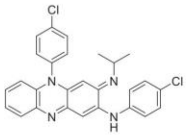	NADH II	Approved
SQ109	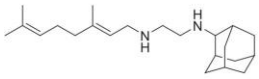	Proton motive force (MmpL3 inhibitor)[b]	Phase 2

[a] Reactive oxygen species.
[b] Mycobacterial membrane protein Large 3.

This review summarizes all literature published about targeting of energy metabolism of *Mtb* in order to find new therapeutics. This article should be useful, especially for medicinal chemists that are focused on the development of compounds with antitubercular activity, since it shows the best structures from the majority of the research articles published on this topic.

5. Future directions

Tuberculosis is one of the most prevalent infectious diseases, and despite the long-term existence of antitubercular drugs, this infection kills millions of people. The major problems are resistance to mycobacterial strains and *Mtb* in the latent stage, which can become reactivated when the immune system of the infected person weakens due to various conditions, such as HIV infection, cancer, or immunosuppressive treatment. Targeting *Mtb* energy metabolism is a recent approach to overcome these problems with old-fashioned antituberculotics. First, resistance is often caused by overexpression of efflux pumps that need energy in the form of ATP to drive xenobiotics (including antituberculotics) out of the bacterial cell. Decreasing the level of cellular ATP by inhibiting bacterial energy metabolism likely impedes drug efflux and makes the bacteria more vulnerable to the drug. It is advisable to use inhibitors of the ETC in combination with other antitubercular drugs to shorten the time of treatment and to treat MDR, XDR, and latent tuberculosis [111].

The previous research of *Mtb* has resulted in several druggable targets and a number of small molecules that are capable of inhibiting *Mtb* growth. The main goal – full eradication of this infectious disease, however, remains unresolved for the future research and it seems that reaching this goal will be very difficult if not impossible. Therefore, several easier goals should be achieved in the meantime. First of all, it is important to use all tools of molecular and chemical biology to identify alternative targets and more molecules that inhibit the infection. These are important for overcoming the bacterial resistance. Especially functional genomic

may be useful in components that are critical for *Mtb* to survive in the human body. Secondly, more focus should be given to the full understanding of the biology of *Mtb* and especially to the mechanism of the development of the latent infection and its transition into active phase. Such knowledge should result in either prevention of this transition or possibility to completely cure the *Mtb* in latent phase. Third, alternative drug regimens should be established that would allow for more efficient usage of existing and new drugs, shortening the duration of the cure, limiting the side effects, reducing costs, and allowing for an effective treatment of immunodeficient patients and patients with co-morbidities. Last not least, new methods for fast and reliable diagnostics are of a high interest, new biochemical assays should be developed that would be compatible with the majority of the *in vivo* microenvironments.

Declaration of competing interest

The authors declare that they have no known competing financial interests or personal relationships that could have appeared to influence the work reported in this paper.

Acknowledgements

This work was supported by grant no. JG_2019_002 from Palacký University in Olomouc. Authors are grateful to Milan Dak, Tereza Šlitrová and Jan Chasák, who contributed to this review with Figures of OP, mycobacterial cytochrome oxidases and ATP synthases.

Abbreviations

TB	tuberculosis
Mtb	*Mycobacterium tuberculosis*
LTBI	latent tuberculosis infection
MDR	multi-drug resistant
XDR	extensively drug-resistant
DNA	deoxyribonucleic acid
ATP	adenosine triphosphate
ETC	electron transport chain
NADH	nicotinamide adenine dinucleotide
QcrB	subunit b of the cytochrome bc_1 complex
PMF	proton motive force
TCA	tricarboxylic acid cycle
SDH	succinate dehydrogenase
MIC	minimal inhibitory concentration
ROS	reactive oxygen species
ISP	iron-sulfur protein
CFU	colony-forming units
MABA	microplate Alamar Blue assay
BDQ	bedaquiline
HTS	high-throughput screening
ABT	aminobenzotriazole
GSK	GlaxoSmithKline
SAR	structure-activity relationship
PAB	phenoxy alkyl benzimidazole
INH	isoniazid
RMP	rifampicin
PZA	pyrazinamide
CFZ	clofazimine
ADP	adenosine diphosphate
OSCP	oligomycin-sensitivity-conferring protein
LORA	Low-oxygen recovery assay
IMV	inverted membrane vesicles
PI	pyrimidine-imidazoles

References

[1] W.H. Organization, Global Tuberculosis Report 2019, World Health Organization; 2019, Geneva (Switzerland), 2019.
[2] S. Kiazyk, T.B. Ball, Tuberculosis (TB): latent tuberculosis infection: an overview, Can. Comm. Dis. Rep. 43 (2017) 62.
[3] N. Dookie, S. Rambaran, N. Padayatchi, S. Mahomed, K. Naidoo, Evolution of drug resistance in Mycobacterium tuberculosis: a review on the molecular determinants of resistance and implications for personalized care, J. Antimicrob. Chemother. 73 (2018) 1138–1151.
[4] S.H. Gillespie, Evolution of drug resistance in Mycobacterium tuberculosis: clinical and molecular perspective, Antimicrob. Agents Chemother. 46 (2002) 267–274.
[5] J.C. Palomino, A. Martin, Drug resistance mechanisms in Mycobacterium tuberculosis, Antibiotics 3 (2014) 317–340.
[6] P.E. Almeida Da Silva, J.C. Palomino, Molecular basis and mechanisms of drug resistance in Mycobacterium tuberculosis: classical and new drugs, J. Antimicrob. Chemother. 66 (2011) 1417–1430.
[7] C.A. Peloquin, S.E. Berning, A.T. Nitta, P.M. Simone, M. Goble, G.A. Huitt, M.D. Iseman, J.L. Cook, D. Curran-Everett, Aminoglycoside toxicity: daily versus thrice-weekly dosing for treatment of mycobacterial diseases, Clin. Infect. Dis. 38 (2004) 1538–1544.
[8] G. Di Perri, S. Bonora, Which agents should we use for the treatment of multidrug-resistant Mycobacterium tuberculosis? J. Antimicrob. Chemother. 54 (2004) 593–602.
[9] W.E. Sanders Jr., C.C. Sanders, Toxicity of antibacterial agents: mechanism of action on mammalian cells, Annu. Rev. Pharmacol. Toxicol. 19 (1979) 53–83.
[10] A.C. Go, L.K. Golightly, G.R. Barber, M.A. Barron, Linezolid interaction with serotonin reuptake inhibitors: report of two cases and incidence assessment, Drug Metab. Pers. Ther. 25 (2010) 41–47.
[11] W.J. Burman, K. Gallicano, C. Peloquin, Comparative pharmacokinetics and pharmacodynamics of the rifamycin antibacterials, Clin. Pharmacokinet. 40 (2001) 327–341.
[12] W.A. Daniel, M. Syrek, A. Haduch, J. Wójcikowski, Pharmacokinetics and metabolism of thioridazine during co-administration of tricyclic antidepressants, Br. J. Pharmacol. 131 (2000) 287–295.
[13] S.M. Gygli, S. Borrell, A. Trauner, S. Gagneux, Antimicrobial resistance in Mycobacterium tuberculosis: mechanistic and evolutionary perspectives, FEMS Microbiol. Rev. 41 (2017) 354–373.
[14] P.A. Black, R.M. Warren, G.E. Louw, P.D. van Helden, T.C. Victor, B.D. Kana, Energy metabolism and drug efflux in Mycobacterium tuberculosis, Antimicrob. Agents Chemother. 58 (2014) 2491–2503, https://doi.org/10.1128/AAC.02293-13, 14 pp.
[15] N. Kamariah, P. Ragunathan, J. Shin, W.-G. Saw, C.-F. Wong, T. Dick, G. Grüber, Unique structural and mechanistic properties of mycobacterial F-ATP synthases: implications for drug design, Prog. Biophys. Mol. Biol. 152 (2020) 64–73.
[16] A. Harikishore, S.S.M. Chong, P. Ragunathan, R.W. Bates, G. Grüber, Targeting the menaquinol binding loop of mycobacterial cytochrome bd oxidase, Mol. Divers. (2020) 1–8.
[17] V. Patil, V. Jain, Insights into the physiology and metabolism of a mycobacterial cell in an energy-compromised state, J. Bacteriol. 201 (2019) e00210–e00219.
[18] G.S. Shetye, S.G. Franzblau, S. Cho, New tuberculosis drug targets, their inhibitors, and potential therapeutic impact, Transl. Res. 220 (2020) 68–97.
[19] D. Bald, A. Koul, Respiratory ATP synthesis: the new generation of mycobacterial drug targets? FEMS Microbiol. Lett. 308 (2010) 1–7.
[20] H.I.M. Boshoff, C.E. Barry III., Tuberculosis: metabolism and respiration in the absence of growth, Nat. Rev. Microbiol. 3 (2005) 70–80, https://doi.org/10.1038/nrmicro1065.
[21] R.K. Dhiman, S. Mahapatra, R.A. Slayden, M.E. Boyne, A. Lenaerts, J.C. Hinshaw, S.K. Angala, D. Chatterjee, K. Biswas, P. Narayanasamy, M. Kurosu, D.C. Crick, Menaquinone synthesis is critical for maintaining mycobacterial viability during exponential growth and recovery from non-replicating persistence, Mol. Microbiol. 72 (2009) 85–97, https://doi.org/10.1111/j.1365-2958.2009.06625.x.
[22] K. Hards, C. Adolph, L.K. Harold, M.B. McNeil, C.-Y. Cheung, A. Jinich, K.Y. Rhee, G.M. Cook, Two for the price of one: attacking the energetic-metabolic hub of mycobacteria to produce new chemotherapeutic agents, Prog. Biophys. Mol. Biol. 152 (2020) 35–44.
[23] B.S. Lee, E. Sviriaeva, K. Pethe, Targeting the cytochrome oxidases for drug development in mycobacteria, Prog. Biophys. Mol. Biol. (2020).
[24] G.M. Cook, K. Hards, C. Vilcheze, T. Hartman, M. Berney, Energetics of respiration and oxidative phosphorylation in mycobacteria, Microbiol. Spectr. 2 (2014) 20, https://doi.org/10.1128/microbiolspec.MGM2-0015-2013. MGM200152013/1-MGM200152013/20.
[25] K.K. Roy, M.A. Wani, Emerging opportunities of exploiting mycobacterial electron transport chain pathway for drug-resistant tuberculosis drug discovery, Expet Opin. Drug Discov. 15 (2020) 231–241, https://doi.org/10.1080/17460441.2020.1696771.
[26] D. Bald, C. Villellas, P. Lu, A. Koul, Targeting energy metabolism in Mycobacterium tuberculosis, a new paradigm in antimycobacterial drug discovery, mBio 8 (2017), https://doi.org/10.1128/mBio.00272-17 e00272-17/1-e00272-17/11.

[27] B. Alberts, J. Alexander, J. Lewis, M. Raff, K. Roberts, P. Walter, Molecular Biology of the Cell, fourth ed., Wiley, 2004.
[28] L. Shi, C.D. Sohaskey, B.D. Kana, S. Dawes, R.J. North, V. Mizrahi, M.L. Gennaro, Changes in energy metabolism of Mycobacterium tuberculosis in mouse lung and under in vitro conditions affecting aerobic respiration, Proc. Natl. Acad. Sci. U.S.A. 102 (2005) 15629–15634, https://doi.org/10.1073/pnas.0507850102.
[29] S. Sellamuthu, M. Singh, A. Kumar, S.K. Singh, Type-II NADH Dehydrogenase (NDH-2): a promising therapeutic target for antitubercular and antibacterial drug discovery, Expert Opin. Ther. Targets 21 (2017) 559–570.
[30] T. Yagi, Bacterial NADH-quinone oxidoreductases, J. Bioenerg. Biomembr. 23 (1991) 211–239, https://doi.org/10.1007/BF00762218.
[31] E.A. Weinstein, T. Yano, L.-S. Li, D. Avarbock, A. Avarbock, D. Helm, A.A. McColm, K. Duncan, J.T. Lonsdale, H. Rubin, Inhibitors of type II NADH: menaquinone oxidoreductase represent a class of antitubercular drugs, Proc. Natl. Acad. Sci. U.S.A. 102 (2005) 4548–4553, https://doi.org/10.1073/pnas.0500469102.
[32] A.M.P. Melo, T.M. Bandeiras, M. Teixeira, New insights into type II NAD(P)H: quinone oxidoreductases, Microbiol. Mol. Biol. Rev. 68 (2004) 603–616, https://doi.org/10.1128/MMBR.68.4.603-616.2004.
[33] S.P.S. Rao, S. Alonso, L. Rand, T. Dick, K. Pethe, The protonmotive force is required for maintaining ATP homeostasis and viability of hypoxic, non-replicating Mycobacterium tuberculosis, Proc. Natl. Acad. Sci. U. S. A. 105 (2008) 11945–11950, https://doi.org/10.1073/pnas.0711697105.
[34] C. Vilchèze, B. Weinrick, L.W. Leung, W.R. Jacobs, Plasticity of Mycobacterium tuberculosis NADH dehydrogenases and their role in virulence, Proc. Natl. Acad. Sci. Unit. States Am. 115 (2018) 1599–1604.
[35] M. Berney, G.M. Cook, Unique flexibility in energy metabolism allows mycobacteria to combat starvation and hypoxia, PloS One 5 (2010), https://doi.org/10.1371/journal.pone.0008614. No pp. given.
[36] J.E. Griffin, J.D. Gawronski, M.A. DeJesus, T.R. Ioerger, B.J. Akerley, C.M. Sassetti, High-resolution phenotypic profiling defines genes essential for mycobacterial growth and cholesterol catabolism, PLoS Pathog. 7 (2011), e1002251, https://doi.org/10.1371/journal.ppat.1002251.
[37] T. Hartman, B. Weinrick, C. Vilcheze, M. Berney, J. Tufariello, G.M. Cook, W.R. Jacobs Jr., Succinate dehydrogenase is the regulator of respiration in Mycobacterium tuberculosis, PLoS Pathog. 10 (2014) 15, https://doi.org/10.1371/journal.ppat.1004510, e1004510/1-e1004510/15.
[38] S. Watanabe, M. Zimmermann, M.B. Goodwin, U. Sauer, C.E. Barry III, H.I. Boshoff, Fumarate reductase activity maintains an energized membrane in anaerobic Mycobacterium tuberculosis, PLoS Pathog. 7 (2011), e1002287, https://doi.org/10.1371/journal.ppat.1002287.
[39] S. Sharma, A. Singh, Phenothiazines as anti-tubercular agents: mechanistic insights and clinical implications, Expet Opin. Invest. Drugs 20 (2011) 1665–1676, https://doi.org/10.1517/13543784.2011.628657.
[40] M.G. Nizi, J. Desantis, Y. Nakatani, S. Massari, M.A. Mazzarella, G. Shetye, S. Sabatini, M.L. Barreca, G. Manfroni, T. Felicetti, Antitubercular polyhalogenated phenothiazines and phenoselenazine with reduced binding to CNS receptors, Eur. J. Med. Chem. (2020) 112420.
[41] P.S. Shirude, B. Paul, N. Roy Choudhury, C. Kedari, B. Bandodkar, B.G. Ugarkar, Quinolinyl pyrimidines: potent inhibitors of NDH-2 as a novel class of anti-TB agents, ACS Med. Chem. Lett. 3 (2012) 736–740, https://doi.org/10.1021/ml300134b.
[42] A. Heikal, Y. Nakatani, W. Jiao, C. Wilson, D. Rennison, M.R. Weimar, E.J. Parker, M.A. Brimble, G.M. Cook, "Tethering" fragment-based drug discovery to identify inhibitors of the essential respiratory membrane protein type II NADH dehydrogenase, Bioorg. Med. Chem. Lett 28 (2018) 2239–2243, https://doi.org/10.1016/j.bmcl.2018.05.048.
[43] M.B. Harbut, B. Yang, R. Liu, T. Yano, C. Vilcheze, B. Cheng, J. Lockner, H. Guo, C. Yu, S.G. Franzblau, H.M. Petrassi, W.R.J. Jacobs, H. Rubin, A.K. Chatterjee, F. Wang, Small molecules targeting Mycobacterium tuberculosis type II NADH dehydrogenase exhibit antimycobacterial activity, Angew. Chem. Int. Ed. 57 (2018) 3478–3482, https://doi.org/10.1002/anie.201800260.
[44] D. Murugesan, P.C. Ray, T. Bayliss, G.A. Prosser, J.R. Harrison, K. Green, C. Soares de Melo, T.-S. Feng, L.J. Street, K. Chibale, D.F. Warner, V. Mizrahi, O. Epemolu, P. Scullion, L. Ellis, J. Riley, Y. Shishikura, L. Ferguson, M. Osuna-Cabello, K.D. Read, S.R. Green, D.A. Lamprecht, P.M. Finin, A.J.C. Steyn, T.R. Ioerger, J. Sacchettini, K.Y. Rhee, K. Arora, C.E. Barry III, P.G. Wyatt, H.I.M. Boshoff, 2-Mercapto-Quinazolinones as inhibitors of type II NADH dehydrogenase and Mycobacterium tuberculosis: structure-activity relationships, mechanism of action and absorption, distribution, metabolism, and excretion characterization, ACS Infect. Dis. 4 (2018) 954–969, https://doi.org/10.1021/acsinfecdis.7b00275.
[45] A. Korkegian, T. O'Malley, Y. Xia, Y. Zhou, D.S. Carter, B. Sunde, L. Flint, D. Thompson, T.R. Ioerger, J. Sacchettini, The 7-phenyl benzoxaborole series is active against Mycobacterium tuberculosis, Tuberculosis 108 (2018) 96–98.
[46] B.J. Mulchin, C.G. Newton, J.W. Baty, C.H. Grasso, W.J. Martin, M.C. Walton, E.M. Dangerfield, C.H. Plunkett, M.V. Berridge, J.L. Harper, The anti-cancer, anti-inflammatory and tuberculostatic activities of a series of 6, 7-substituted-5, 8-quinolinequinones, Bioorg. Med. Chem. 18 (2010) 3238–3251.
[47] A. Heikal, K. Hards, C.-Y. Cheung, A. Menorca, M.S.M. Timmer, B.L. Stocker, G.M. Cook, Activation of type II NADH dehydrogenase by quinolinequinones mediates antitubercular cell death, J. Antimicrob. Chemother. 71 (2016) 2840–2847.
[48] K.T. Santoso, A. Menorca, C.-Y. Cheung, G.M. Cook, B.L. Stocker, M.S.M. Timmer, The synthesis and evaluation of quinolinequinones as anti-mycobacterial agents, Bioorg. Med. Chem. 27 (2019) 3532–3545.
[49] L.G. Matsoso, B.D. Kana, P.K. Crellin, D.J. Lea-Smith, A. Pelosi, D. Powell, S.S. Dawes, H. Rubin, R.L. Coppel, V. Mizrahi, Function of the cytochrome bc1-aa3 branch of the respiratory network in Mycobacteria and network adaptation occurring in response to its disruption, J. Bacteriol. 187 (2005) 6300–6308, https://doi.org/10.1128/JB.187.18.6300-6308.2005.
[50] J.L. Small, S.W. Park, B.D. Kana, T.R. Ioerger, J.C. Sacchettini, S. Ehrt, Perturbation of cytochrome c maturation reveals adaptability of the respiratory chain in Mycobacterium tuberculosis, mBio 4 (2013).
[51] B.D. Kana, E.A. Weinstein, D. Avarbock, S.S. Dawes, H. Rubin, V. Mizrahi, Characterization of the cydAB-encoded cytochrome bd oxidase from Mycobacterium smegmatis, J. Bacteriol. 183 (2001) 7076–7086, https://doi.org/10.1128/JB.183.24.7076-7086.2001.
[52] J.A. Megehee, J.P. Hosler, M.D. Lundrigan, Evidence for a cytochrome bcc-aa3 interaction in the respiratory chain of Mycobacterium smegmatis, Microbiology 152 (2006) 823–829, https://doi.org/10.1099/mic.0.28723-0.
[53] D. Xia, L. Esser, W.-K. Tang, F. Zhou, Y. Zhou, L. Yu, C.-A. Yu, Structural analysis of cytochrome bc1 complexes: implications to the mechanism of function, Biochim. Biophys. Acta Bioenerg. 1827 (2013) 1278–1294, https://doi.org/10.1016/j.bbabio.2012.11.008.
[54] P.O. Ljungdahl, J.D. Pennoyer, D.E. Robertson, B.L. Trumpower, Purification of highly active cytochrome bc1 complexes from phylogenetically diverse species by a single chromatographic procedure, Biochim. Biophys. Acta Bioenerg. 891 (1987) 227–241, https://doi.org/10.1016/0005-2728(87)90218-0.
[55] C.-A. Yu, L. Yu, Structural role of phospholipids in ubiquinol-cytochrome c reductase, Biochemistry 19 (1980) 5715–5720, https://doi.org/10.1021/bi00566a008.
[56] Y. Ko, I. Choi, Putative 3D structure of QcrB from Mycobacterium tuberculosis cytochrome bc1 complex, a novel drug-target for new series of antituberculosis agent Q203, Bull. Kor. Chem. Soc. 37 (2016) 725–731, https://doi.org/10.1002/bkcs.10765.
[57] M. Blaise, L. Kremer, Self-control of vitamin K2 production captured in the crystal, J. Biol. Chem. 295 (2020) 3771–3772.
[58] Z. Pan, Y. Wang, X. Gu, J. Wang, M. Cheng, Refined homology model of cytochrome bcc complex B subunit for virtual screening of potential anti-tuberculosis agents, J. Biomol. Struct. Dyn. 38 (2020) 4733–4745.
[59] B.L. Trumpower, Cytochrome bc1 complexes of microorganisms, Microbiol. Rev. 54 (1990) 101–129, https://doi.org/10.1128/mmbr.54.2.101-129.1990.
[60] S.T. Cole, R. Brosch, J. Parkhill, T. Garnier, C. Churcher, D. Harris, S. V Gordon, K. Eiglmeier, S. Gas, C.E. Barry III, F. Tekaia, K. Badcock, D. Basham, D. Brown, T. Chillingworth, R. Connor, R. Davies, K. Devlin, T. Feltwell, S. Gentles, N. Hamlin, S. Holroyd, T. Hornsby, K. Jagels, A. Krogh, J. McLean, S. Moule, L. Murphy, K. Oliver, J. Osborne, M.A. Quail, M.-A. Rajandream, J. Rogers, S. Rutter, K. Seeger, J. Skelton, R. Squares, S. Squares, J.E. Sulston, K. Taylor, S. Whitehead, B.G. Barrell, Deciphering the biology of Mycobacterium tuberculosis from the complete genome sequence. [Erratum to document cited in CA129:77224], Nature 396 (1998) 190–198, https://doi.org/10.1038/24206.
[61] L. Bown, S.K. Srivastava, B.M. Piercey, C.K. McIsaac, K. Tahlan, Mycobacterial membrane proteins QcrB and AtpE: roles in energetics, antibiotic targets, and associated mechanisms of resistance, J. Membr. Biol. 251 (2018) 105–117, https://doi.org/10.1007/s00232-017-9997-3.
[62] C.V. Holyoake, R.K. Poole, M. Shepherd, The CydDC family of transporters and their roles in oxidase assembly and homeostasis, Adv. Microb. Physiol. 66 (2015) 1–53, https://doi.org/10.1016/bs.ampbs.2015.04.002.
[63] K.A. Abrahams, J.A.G. Cox, V.L. Spivey, N.J. Loman, M.J. Pallen, C. Constantinidou, R. Fernandez, C. Alemparte, M.J. Remuinan, D. Barros, L. Ballell, G.S. Besra, Identification of novel imidazo[1,2-a]pyridine inhibitors targeting M. tuberculosis QcrB, PloS One 7 (2012), e52951, https://doi.org/10.1371/journal.pone.0052951.
[64] K. Arora, B. Ochoa-Montano, P.S. Tsang, T.L. Blundell, S.S. Dawes, V. Mizrahi, T. Bayliss, C.J. MacKenzie, L.A.T. Cleghorn, P.C. Ray, P.G. Wyatt, E. Uh, J. Lee, C.E. Barry, H.I. Boshoff, Respiratory flexibility in response to inhibition of cytochrome c oxidase in Mycobacterium tuberculosis, Antimicrob. Agents Chemother. 58 (2014) 6962–6965, https://doi.org/10.1128/AAC.03486-14, 5 pp.
[65] G.C. Moraski, P.A. Miller, M.A. Bailey, J. Ollinger, T. Parish, H.I. Boshoff, S. Cho, J.R. Anderson, S. Mulugeta, S.G. Franzblau, Putting tuberculosis (TB) to rest: transformation of the sleep aid, Ambien, and "anagrams" generated potent antituberculosis agents, ACS Infect. Dis. 1 (2015) 85–90.
[66] T. O'Malley, T. Alling, J. V Early, H.A. Wescott, A. Kumar, G.C. Moraski, M.J. Miller, T. Masquelin, P.A. Hipskind, T. Parish, Imidazopyridine compounds inhibit mycobacterial growth by depleting ATP levels, Antimicrob. Agents Chemother. 62 (2018), https://doi.org/10.1128/aac.02439-17 e02439-17/1-e02439-17/8.
[67] R. van der Westhuyzen, S. Winks, C.R. Wilson, G.A. Boyle, R.K. Gessner, C. Soares de Melo, D. Taylor, C. de Kock, M. Njoroge, C. Brunschwig, N. Lawrence, S.P.S. Rao, F. Sirgel, P. van Helden, R. Seldon, A. Moosa, D.F. Warner, L. Arista, U.H. Manjunatha, P.W. Smith, L.J. Street, K. Chibale, Pyrrolo[3,4-c]pyridine-1,3(2H)-diones: a novel antimycobacterial class targeting mycobacterial respiration, J. Med. Chem. 58 (2015) 9371–9381,

https://doi.org/10.1021/acs.jmedchem.5b01542.
[68] N.S. Chandrasekera, B.J. Berube, G. Shetye, S. Chettiar, T. OMalley, A. Manning, L. Flint, D. Awasthi, T.R. Ioerger, J. Sacchettini, T. Masquelin, P.A. Hipskind, J. Odingo, T. Parish, Improved phenoxyalkylbenzimidazoles with activity against Mycobacterium tuberculosis appear to target QcrB, ACS Infect. Dis. 3 (2017) 898–916, https://doi.org/10.1021/acsinfecdis.7b00112.
[69] N. Phummarin, H.I. Boshoff, P.S. Tsang, J. Dalton, S. Wiles, C.E. Barry 3rd, B.R. Copp, SAR and identification of 2-(quinolin-4-yloxy)acetamides as Mycobacterium tuberculosis cytochrome bc1 inhibitors, Med. Chem. Comm. 7 (2016) 2122–2127, https://doi.org/10.1039/C6MD00236F.
[70] G.C. Moraski, N. Seeger, P.A. Miller, A.G. Oliver, H.I. Boshoff, S. Cho, S. Mulugeta, J.R. Anderson, S.G. Franzblau, M.J. Miller, Arrival of imidazo[2,1-b]thiazole-5-carboxamides: potent anti-tuberculosis agents that target QcrB, ACS Infect. Dis. 2 (2016) 393–398, https://doi.org/10.1021/acsinfecdis.5b00154.
[71] G.C. Moraski, N. Deboosère, K.L. Marshall, H.A. Weaver, A. Vandeputte, C. Hastings, L. Woolhiser, A.J. Lenaerts, P. Brodin, M.J. Miller, Intracellular and in vivo evaluation of imidazo [2, 1-b] thiazole-5-carboxamide anti-tuberculosis compounds, PloS One 15 (2020), e0227224.
[72] B.J. Berube, T. Parish, Combinations of respiratory chain inhibitors have enhanced bactericidal activity against Mycobacterium tuberculosis, Antimicrob. Agents Chemother. 62 (2018) 1–10, https://doi.org/10.1128/aac.01677-17.
[73] G.A. Harrison, A.E.M. Bridwell, M. Singh, K. Jayaraman, L.A. Weiss, R.L. Kinsella, J.S. Aneke, K. Flentie, M.E. Schene, M. Gaggioli, S.D. Solomon, S.A. Wildman, M.J. Meyers, C.L. Stallings, Identification of 4-Amino-Thieno [2,3-d]Pyrimidines as QcrB inhibitors in Mycobacterium tuberculosis, mSphere 4 (2019), https://doi.org/10.1128/msphere.00606-19 e00606-e00619/1-e00606-19/14.
[74] A. Lupien, C.S.-Y. Foo, S. Savina, A. Vocat, J. Piton, N. Monakhova, A. Benjak, D.A. Lamprecht, A.J.C. Steyn, K. Pethe, V.A. Makarov, S.T. Cole, New 2-ethylthio-4-methylaminoquinazoline derivatives inhibiting two subunits of cytochrome bc1 in Mycobacterium tuberculosis, PLoS Pathog. 16 (2020), https://doi.org/10.1371/journal.ppat.1008270 e1008270/1-e1008270/19.
[75] F.T. Subtil, A.D. Villela, B.L. Abbadi, V.S. Rodrigues-Junior, C.V. Bizarro, L.F.S.M. Timmers, O. Norberto de Souza, K. Pissinate, P. Machado, A. Lopez-Gavin, G. Tudo, J. Gonzalez-Martin, L.A. Basso, D.S. Santos, Activity of 2-(quinolin-4-yloxy)acetamides in Mycobacterium tuberculosis clinical isolates and identification of their molecular target by whole-genome sequencing, Int. J. Antimicrob. Agents 51 (2018) 378–384, https://doi.org/10.1016/j.ijantimicag.2017.08.023.
[76] L.A.T. Cleghorn, P.C. Ray, J. Odingo, A. Kumar, H. Wescott, A. Korkegian, T. Masquelin, A. Lopez Moure, C. Wilson, S. Davis, M. Huggett, P. Turner, A. Smith, O. Epemolu, F. Zuccotto, J. Riley, P. Scullion, Y. Shishikura, L. Ferguson, J. Rullas, L. Guijarro, K.D. Read, S.R. Green, P. Hipskind, T. Parish, P.G. Wyatt, Identification of morpholino thiophenes as novel Mycobacterium tuberculosis inhibitors, targeting QcrB, J. Med. Chem. 61 (2018) 6592–6608, https://doi.org/10.1021/acs.jmedchem.8b00172.
[77] C.S. Foo, A. Lupien, M. Kienle, A. Vocat, A. Benjak, A.R. Sommer, D.A. Lamprecht, A.J.C. Steyn, K. Pethe, J. Piton, K.-H. Altmann, S.T. Colea, Arylvinylpiperazine amides, a new class of potent inhibitors targeting QcrB of Mycobacterium tuberculosis, mBio 9 (2018), https://doi.org/10.1128/mbio.01276-18 e01276-18/1-e01276-18/13.
[78] K. Pethe, P. Bifani, J. Jang, S. Kang, S. Park, S. Ahn, J. Jiricek, J. Jung, H.K. Jeon, J. Cechetto, Discovery of Q203, a potent clinical candidate for the treatment of tuberculosis, Nat. Med. 19 (2013) 1157–1160.
[79] X. Lu, Z. Williams, K. Hards, J. Tang, C.-Y. Cheung, H.L. Aung, B. Wang, Z. Liu, X. Hu, A. Lenaerts, L. Woolhiser, C. Hastings, X. Zhang, Z. Wang, K. Rhee, K. Ding, T. Zhang, G.M. Cook, Pyrazolo[1,5-a]pyridine inhibitor of the respiratory cytochrome bcc complex for the treatment of drug-resistant tuberculosis, ACS Infect. Dis. 5 (2019) 239–249, https://doi.org/10.1021/acsinfecdis.8b00225.
[80] P. Lu, H. Lill, D. Bald, ATP synthase in mycobacteria: special features and implications for a function as drug target, Biochim. Biophys. Acta Bioenerg. 1837 (2014) 1208–1218, https://doi.org/10.1016/j.bbabio.2014.01.022.
[81] M. Berney, G.M. Cook, Respiration and oxidative phosphorylation in mycobacteria, Adv. Photosynth. Respir. 39 (2014) 277–293, https://doi.org/10.1007/978-94-017-8742-0_15.
[82] C.S. Gajadeera, J. Weber, Escherichia coli F1Fo-ATP synthase with a b/δ fusion protein allows analysis of the function of the individual b subunits, J. Biol. Chem. 288 (2013) 26441–26447.
[83] P.A. Del Rizzo, Y. Bi, S.D. Dunn, ATP synthase b subunit dimerization domain: a right-handed coiled coil with offset helices, J. Mol. Biol. 364 (2006) 735–746, https://doi.org/10.1016/j.jmb.2006.09.028.
[84] T. Meier, N. Morgner, D. Matthies, D. Pogoryelov, S. Keis, G.M. Cook, P. Dimroth, B. Brutschy, A tridecameric c ring of the adenosine triphosphate (ATP) synthase from the thermoalkaliphilic Bacillus sp. strain TA2.A1 facilitates ATP synthesis at low electrochemical proton potential, Mol. Microbiol. 65 (2007) 1181–1192, https://doi.org/10.1111/j.1365-2958.2007.05857.x.
[85] I.M. Willis, R.D. Moir, Integration of nutritional and stress signaling pathways by Maf1, Trends Biochem. Sci. 32 (2007) 51–53, https://doi.org/10.1016/j.tibs.2006.12.001.
[86] W. Jiang, J. Hermolin, R.H. Fillingame, The preferred stoichiometry of c subunits in the rotary motor sector of Escherichia coli ATP synthase is 10, Proc. Natl. Acad. Sci. U.S.A. 98 (2001) 4966–4971, https://doi.org/10.1073/pnas.081424898.
[87] A.L. Cozens, J.E. Walker, The organization and sequence of the genes for ATP synthase subunits in the cyanobacterium Synechococcus 6301. Support for an endosymbiotic origin of chloroplasts, J. Mol. Biol. 194 (1987) 359–383, https://doi.org/10.1016/0022-2836(87)90667-X.
[88] A. Koul, L. Vranckx, N. Dendouga, W. Balemans, I. Van den Wyngaert, K. Vergauwen, H.W.H. Goehlmann, R. Willebrords, A. Poncelet, J. Guillemont, D. Bald, K. Andries, Diarylquinolines are bactericidal for dormant mycobacteria as a result of disturbed ATP homeostasis, J. Biol. Chem. 283 (2008) 25273–25280, https://doi.org/10.1074/jbc.M803899200.
[89] A.C. Haagsma, N.N. Driessen, M.-M. Hahn, H. Lill, D. Bald, ATP synthase in slow- and fast-growing mycobacteria is active in ATP synthesis and blocked in ATP hydrolysis direction, FEMS Microbiol. Lett. 313 (2010) 68–74, https://doi.org/10.1111/j.1574-6968.2010.02123.x.
[90] P. Lu, H. Lill, D. Bald, ATP synthase in mycobacteria: special features and implications for a function as drug target, Biochim. Biophys. Acta Bioenerg. 1837 (2014) 1208–1218, https://doi.org/10.1016/j.bbabio.2014.01.022.
[91] A. Koul, N. Dendouga, K. Vergauwen, B. Molenberghs, L. Vranckx, R. Willebrords, Z. Ristic, H. Lill, I. Dorange, J. Guillemont, Diarylquinolines target subunit c of mycobacterial ATP synthase, Nat. Chem. Biol. 3 (2007) 323–324.
[92] K. Andries, P. Verhasselt, J. Guillemont, H.W.H. Göhlmann, J.-M. Neefs, H. Winkler, J. Van Gestel, P. Timmerman, M. Zhu, E. Lee, A diarylquinoline drug active on the ATP synthase of Mycobacterium tuberculosis, Science (80) 307 (2005) 223–227.
[93] M. Lakshmanan, A.S. Xavier, Bedaquiline–The first ATP synthase inhibitor against multi drug resistant tuberculosis, J. Young Pharm. 5 (2013) 112–115.
[94] M.J. Lobo, R. Ray, G.G. Shenoy, Gaining deeper insights into the surface binding of bedaquiline analogues with the ATP synthase subunit C of Mycobacterium tuberculosis using molecular docking, molecular dynamics simulation and 3D-QSAR techniques, New J. Chem. 44 (2020) 18831–18852.
[95] H. Guo, G.M. Courbon, S.A. Bueler, J. Mai, J. Liu, J.L. Rubinstein, Structure of mycobacterial ATP synthase bound to the tuberculosis drug bedaquiline, Nature (2020) 1–5.
[96] A. Blaser, H.S. Sutherland, A.S.T. Tong, P.J. Choi, D. Conole, S.G. Franzblau, C.B. Cooper, A.M. Upton, M. Lotlikar, W.A. Denny, B.D. Palmer, Structure-activity relationships for unit C pyridyl analogues of the tuberculosis drug bedaquiline, Bioorg. Med. Chem. 27 (2019) 1283–1291, https://doi.org/10.1016/j.bmc.2019.02.025.
[97] S. Kumar, R. Mehra, S. Sharma, N.P. Bokolia, D. Raina, A. Nargotra, P.P. Singh, I.A. Khan, Screening of antitubercular compound library identifies novel ATP synthase inhibitors of Mycobacterium Tuberculosis, Tuberculosis (Oxford, United Kingdom) 108 (2018) 56–63, https://doi.org/10.1016/j.tube.2017.10.008.
[98] R.K. Munnaluri, V. Manga, In silico Quest guided by physico-chemical descriptors of bedaquiline for new scaffolds with potential inhibitory capacity against homology model of mycobacterium F1F0 ATP synthase, Asian J. Chem. 30 (2018) 904–912, https://doi.org/10.14233/ajchem.2018.21145.
[99] C. He, L. Preiss, B. Wang, L. Fu, H. Wen, X. Zhang, H. Cui, T. Meier, D. Yin, Structural simplification of bedaquiline: the discovery of 3-(4-(N,N-Dimethylaminomethyl)phenyl)quinoline-Derived antitubercular lead compounds, ChemMedChem 12 (2017) 106–119, https://doi.org/10.1002/cmdc.201600441.
[100] S.J. Tantry, S.D. Markad, V. Shinde, J. Bhat, G. Balakrishnan, A.K. Gupta, A. Ambady, A. Raichurkar, C. Kedari, S. Sharma, N.V. Mudugal, A. Narayan, C.N. Naveen Kumar, R. Nanduri, S. Bharath, J. Reddy, V. Panduga, K.R. Prabhakar, K. Kandaswamy, R. Saralaya, P. Kaur, N. Dinesh, S. Guptha, K. Rich, D. Murray, H. Plant, M. Preston, H. Ashton, D. Plant, J. Walsh, P. Alcock, K. Naylor, M. Collier, J. Whiteaker, R.E. McLaughlin, M. Mallya, M. Panda, S. Rudrapatna, V. Ramachandran, R. Shandil, V.K. Sambandamurthy, K. Mdluli, C.B. Cooper, H. Rubin, T. Yano, P. Iyer, S. Narayanan, S. Kavanagh, K. Mukherjee, V. Balasubramanian, V.P. Hosagrahara, S. Solapure, S. Ravishankar, S. Hameed P, Discovery of imidazo[1,2-a]pyridine ethers and squaramides as selective and potent inhibitors of mycobacterial adenosine triphosphate (ATP) synthesis, J. Med. Chem. 60 (2017) 1379–1399, https://doi.org/10.1021/acs.jmedchem.6b01358.
[101] Y.B. Surase, K. Samby, S.R. Amale, R. Sood, K.P. Purnapatre, P.K. Pareek, B. Das, K. Nanda, S. Kumar, A.K. Verma, Identification and synthesis of novel inhibitors of mycobacterium ATP synthase, Bioorg. Med. Chem. Lett 27 (2017) 3454–3459, https://doi.org/10.1016/j.bmcl.2017.05.081.
[102] S. Sellamuthu, A.H. Asseri, H.G. Goojani, G. Nath, S.K. Singh, Preliminary studies on ligand-based design and evaluation of new mycobacterial ATP synthase inhibitors, Curr. Drug Ther. 13 (2018) 56–73, https://doi.org/10.2174/1574885512666170911144732.
[103] S.J. Tantry, V. Shinde, G. Balakrishnan, S.D. Markad, A.K. Gupta, J. Bhat, A. Narayan, A. Raichurkar, L.K. Jena, S. Sharma, N. Kumar, R. Nanduri, S. Bharath, J. Reddy, V. Panduga, K.R. Prabhakar, K. Kandaswamy, P. Kaur, N. Dinesh, S. Guptha, R. Saralaya, M. Panda, S. Rudrapatna, M. Mallya, H. Rubin, T. Yano, K. Mdluili, C.B. Cooper, V. Balasubramanian, V.K. Sambandamurthy, V. Ramachandran, R. Shandil, S. Kavanagh, S. Narayanan, P. Iyer, K. Mukherjee, V.P. Hosagrahara, S. Solapure, S. Hameed P, S. Ravishankar, Scaffold morphing leading to evolution of 2,4-diaminoquinolines and aminopyrazolopyrimidines as inhibitors of the ATP synthesis pathway, Med. Chem. Comm. 7 (2016) 1022–1032, https://doi.org/

10.1039/C5MD00589B.
[104] S. Singh, K.K. Roy, S.R. Khan, V.K. Kashyap, A. Sharma, S. Jaiswal, S.K. Sharma, M.Y. Krishnan, V. Chaturvedi, J. Lal, S. Sinha, A. Dasgupta, R. Srivastava, A.K. Saxena, Novel, potent, orally bioavailable and selective mycobacterial ATP synthase inhibitors that demonstrated activity against both replicating and non-replicating M. tuberculosis, Bioorg. Med. Chem. 23 (2015) 742–752, https://doi.org/10.1016/j.bmc.2014.12.060.
[105] S.R. Khan, S. Singh, K.K. Roy, M.S. Akhtar, A.K. Saxena, M.Y. Krishnan, Biological evaluation of novel substituted chloroquinolines targeting mycobacterial ATP synthase, Int. J. Antimicrob. Agents 41 (2013) 41–46.
[106] A. Hotra, P. Seankongsuk, A. Harikishore, P. Sae-Lao, R.W. Bates, P. Ragunathan, S.W. Geok, J. Shin, C.N. Pradeep, H. Makhija, P. Droge, K. Pethe, P.S. Ng, J.P. Sarathy, T. Dick, U. Lakshmanan, A. Poulsen, J.H.L. Tan, N.P. Kalia, R. Kalyanasundaram, S. Anbarasu, K. Parthasarathy, G. Gruber, Discovery of a novel Mycobacterial F-ATP synthase inhibitor and its potency in combination with diarylquinolines, Angew Chem. Int. Ed. Engl. (2020).
[107] P. Pruksakorn, M. Arai, L. Liu, P. Moodley, W.R. Jacobs Jr., M. Kobayashi, Action-mechanism of trichoderin A, an anti-dormant mycobacterial aminolipopeptide from marine sponge-derived Trichoderma sp, Biol. Pharm. Bull. 34 (2011) 1287–1290, https://doi.org/10.1248/bpb.34.1287.
[108] P.A. Mak, S.P.S. Rao, M. Ping Tan, X. Lin, J. Chyba, J. Tay, S.H. Ng, B.H. Tan, J. Cherian, J. Duraiswamy, P. Bifani, V. Lim, B.H. Lee, N. Ling Ma, D. Beer, P. Thayalan, K. Kuhen, A. Chatterjee, F. Supek, R. Glynne, J. Zheng, H.I. Boshoff, C.E. Barry 3rd, T. Dick, K. Pethe, L.R. Camacho, A high-throughput screen to identify inhibitors of ATP homeostasis in non-replicating Mycobacterium tuberculosis, ACS Chem. Biol. 7 (2012) 1190–1197, https://doi.org/10.1021/cb2004884.
[109] K. Pethe, P.C. Sequeira, S. Agarwalla, K. Rhee, K. Kuhen, W.Y. Phong, V. Patel, D. Beer, J.R. Walker, J. Duraiswamy, J. Jiricek, T.H. Keller, A. Chatterjee, M.P. Tan, M. Ujjini, S.P.S. Rao, L. Camacho, P. Bifani, P.A. Mak, I. Ma, S.W. Barnes, Z. Chen, D. Plouffe, P. Thayalan, S.H. Ng, M. Au, B.H. Lee, B.H. Tan, S. Ravindran, M. Nanjundappa, X. Lin, A. Goh, S.B. Lakshminarayana, C. Shoen, M. Cynamon, B. Kreiswirth, V. Dartois, E.C. Peters, R. Glynne, S. Brenner, T. Dick, A chemical genetic screen in Mycobacterium tuberculosis identifies carbon-source-dependent growth inhibitors devoid of in vivo efficacy, Nat. Commun. 1 (2010), https://doi.org/10.1038/ncomms1060. Pet1/1-Pet1/8,SPet1/1-SPet1/2.
[110] K. Pethe, P.C. Sequeira, S. Agarwalla, K. Rhee, K. Kuhen, W.Y. Phong, V. Patel, D. Beer, J.R. Walker, J. Duraiswamy, J. Jiricek, T.H. Keller, A. Chatterjee, M.P. Tan, M. Ujjini, S.P.S. Rao, L. Camacho, P. Bifani, P.A. Mak, I. Ma, S.W. Barnes, Z. Chen, D. Plouffe, P. Thayalan, S.H. Ng, M. Au, B.H. Lee, B.H. Tan, S. Ravindran, M. Nanjundappa, X. Lin, A. Goh, S.B. Lakshminarayana, C. Shoen, M. Cynamon, B. Kreiswirth, V. Dartois, E.C. Peters, R. Glynne, S. Brenner, T. Dick, A chemical genetic screen in Mycobacterium tuberculosis identifies carbon-source-dependent growth inhibitors devoid of in vivo efficacy, Nat. Commun. 1 (2010), https://doi.org/10.1038/ncomms1060. Pet1/1-Pet1/8,SPet1/1-SPet1/2.
[111] B.S. Lee, N.P. Kalia, X.E.F. Jin, E.J. Hasenoehrl, M. Berney, K. Pethe, Inhibitors of energy metabolism interfere with antibiotic-induced death in mycobacteria, J. Biol. Chem. 294 (2019) 1936–1943.

Appendix 2

Squaric acid analogues in medicinal chemistry

Chasák, J.; Šlachtová, V.; Urban, M.; **Brulíková, L.***

Eur. J. Med. Chem. **2021**, *209*, 112872.

European Journal of Medicinal Chemistry 209 (2021) 112872

Contents lists available at ScienceDirect

European Journal of Medicinal Chemistry

journal homepage: http://www.elsevier.com/locate/ejmech

Review article

Squaric acid analogues in medicinal chemistry

Jan Chasák [a, 1], Veronika Šlachtová [a, 1], Milan Urban [b], Lucie Brulíková [a, *]

[a] Department of Organic Chemistry, Faculty of Science, Palacky University Olomouc, 17. listopadu 12, 771 46, Olomouc, Czech Republic
[b] Medicinal Chemistry, Institute of Molecular and Translational Medicine, Faculty of Medicine and Dentistry, Palacky University in Olomouc, Hněvotínská 5, 779 00, Olomouc, Czech Republic

ARTICLE INFO

Article history:
Received 18 August 2020
Received in revised form
12 September 2020
Accepted 21 September 2020
Available online 2 October 2020

Keywords:
Squaric acid
Squarate
Squaramide
Biological activity

ABSTRACT

In this review, we summarize the published data on squaric acid analogues with a special focus on their use in medicinal chemistry and as potential drugs. Squaric acid is an interesting small molecule with an almost perfectly square shape, and its analogues have a variety of biological activities that are enabled by the presence of significant H-bond donors and acceptors. Unfortunately, most of these compounds also exhibit reactive functionalities, and this deters the majority of medicinal chemists and pharmacologists from trying to use them in drug development. However, this group of compounds is experiencing a renaissance, and large numbers of them are being tested for antiprotozoal, antibacterial, antifungal, and antiviral activities. The most useful of these compounds exhibited IC_{50} values in the nanomolar range, which makes them promising drug candidates. In addition to these activities, their interactions with living systems were intensively explored, revealing that squaric acid analogues inhibit various enzymes and often serve as receptor antagonists and that the squaric acid moiety may be used as a non-classical isosteric replacement for other functional groups such as carboxylate. In summary, this review is focused on squaric acid and its analogues and their use in medicinal chemistry and should serve as a guide for other researchers in the field to demonstrate the potential of these compounds based on previous research.

Contents

* Corresponding author.
E-mail address: lucie.brulikova@upol.cz (L. Brulíková).
[1] These authors contributed equally.

https://doi.org/10.1016/j.ejmech.2020.112872
0223-5234/

1. Introduction

The squaric acid scaffold (Fig. 1) represents a unique moiety that has received considerable attention, especially during the last decade, due to its numerous synthetic [1–10], pharmaceutical [1–3,11,12], and other applications [1,2,13–17]. Squaric acid **1** (also known as quadratic acid; 3,4-dihydroxycyclobut-3-ene-1,2-dione) is a planar aromatic framework that received its special name because of its extraordinary, almost perfect square shape. The first cyclobutenediones were synthesized in the 1950s [18–20] and triggered this area of unique and versatile synthons in organic chemistry [10]. In the medicinal chemistry field, however, the squaric acid scaffold only came to the forefront in the last decade due to earlier concern about the risk of *in vivo* toxicity because of the scaffold's rather reactive functional groups. Squaric acid itself as well as its analogues features several unique physicochemical and pharmacokinetic properties described in more detail further.

1.1. Physicochemical properties

Squaric acid is a symmetrical planar diprotic four-membered oxocarbon compound that possesses unique 2π-*pseudo*-aromaticity [21]. Consequently, squaric acid features unusual high double acidity ($pK_{a1} = 0.54$; $pK_{a2} = 3.58$) due to the resonance stabilized squarate dianion (Fig. 1) [22]. Several physicochemical methods were employed to confirm the aromatic character of the squarate dianion (Fig. 1) by geometric (bond length, bond order), energetic (aromatic stabilization energies) and magnetic parameters (^{17}O-chemical shifts, nucleus-independent chemical shifts) [23,24].

Among the most common squaric acid analogues (Fig. 2), squaramides **5** have received considerable attention especially because of their interesting molecular structure capable of multiple interactions with biological targets *via* specific molecular recognition [2]. Squaramides can bind selectively through the four hydrogen bonds, acting both as hydrogen bond donors and acceptors. The potential of secondary squaramides to participate in hydrogen bonding is another significant feature which is one of the reasons for their high melting points of 275–300 °C and their low solubility in water [3]. Studies of squaramide-based artificial receptors used for the recognition of cations described that the capability to serve as a hydrogen bond acceptor is modulated by the increase in aromaticity [25]. The ability of squaramides to act as hydrogen bond donors to anionic species was investigated as well [26]. Squaramide-based artificial receptors designed to bind carboxylate anions proved hydrogen bond donor ability also due to enhanced aromaticity. Furthermore, electrostatic potentials suggest that the combined effect of two carbonyls enables squaramides to form strong acceptor interactions more efficiently in comparison with ureas [2].

Despite certain similarities between amides and squaramides, the rigid and planar structure of squaramides containing two coplanar carbonyls makes them a distinctive feature. sp^2-Hybridised nitrogens make this arrangement stable by providing their lone pairs to conjugation with the π-system orthogonal to the plane [2]. The mutual influence of a NH and carbonyl oxygen contributes to the formation of zwitterionic structures. Moreover, the dipole presented by a zwitterionic squaramide form is known to mimic the α-ammonium carboxylate motif and thus represents α-amino acid bioisosteres [27]. Amide-like restricted rotation around the C–N bonds forces a bis-secondary squaramide having two C–N bonds to prefer anti/anti conformation [2].

1.2. Pharmacological profile

In general, the main core of the squaric acid derivatives is chemically stable in water environment which these compounds encounter in the organism. Some studies revealed, that squaramides used as isosteres of amino acids may be more resistant against decarboxylases because they do not contain nucleophilic nitrogen important for the decarboxylation [2,27].

Although many derivatives were designed as potential drugs, the pharmacological profile was evaluated only in several of them and only the most promising lead compounds were selected for these advanced studies. As a result, several candidates have entered various stages of clinical trials (Fig. 3). Among them, perzinfotel **8**, discovered in 1999 [27] as a unique NMDA antagonist, had a favourable preclinical profile and therefore seemed to be a suitable lead structure for the development of a drug for the treatment of neurological disorders such as stroke and head trauma. In Ref. [27], the authors tried to improve its low bioavailability by synthesizing tetrazole analogue, which unfortunately failed in *in vivo* experiment designed to show neuroprotective potency (focal ischemia model involving occlusion of the middle cerebral artery in rats). Further attempts to modify perzinfotel **8** [28] afforded prodrug **9** that was adsorbed much better, it was enzymatically transformed to parent compound **8** and this significantly improved the perzinfotel half-life and potency *in vivo* (oral administration in a rodent model of inflammatory pain) [28].

Navarixin **10**, squaric acid dibutyl ester **11**, pibutidine **12** and BMY-25368 **13** (Fig. 3) are other examples of SQ analogues that entered clinical trials. Navarixin **10** (SCH527123, MK-7123) acts as an antagonist of the cysteine chemokine receptor (interleukin 8A receptor) and is under Phase II clinical trials for the treatment of solid tumours (combination therapy, late-stage disease, metastatic

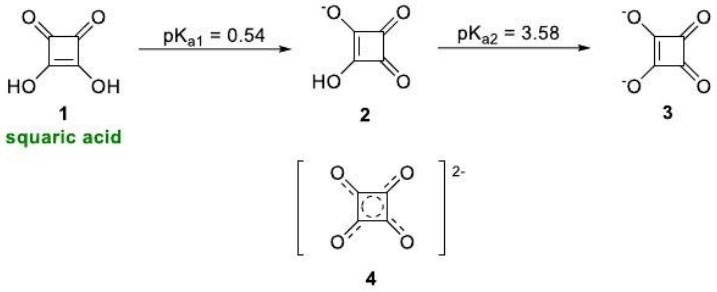

Fig. 1. Resonance stabilized squarate dianion.

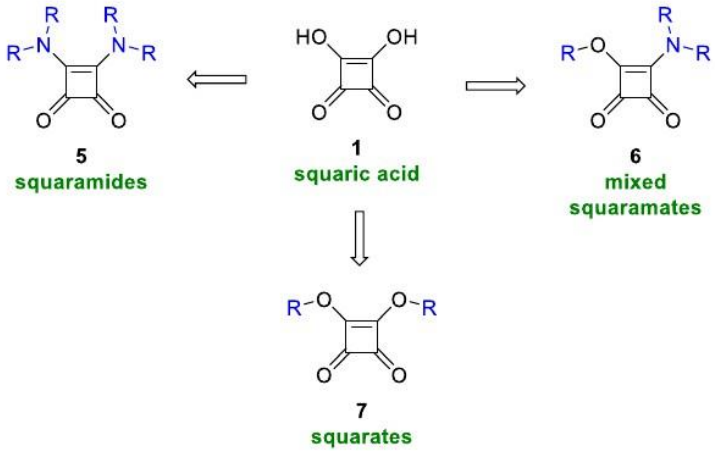

Fig. 2. Squaric acid analogues.

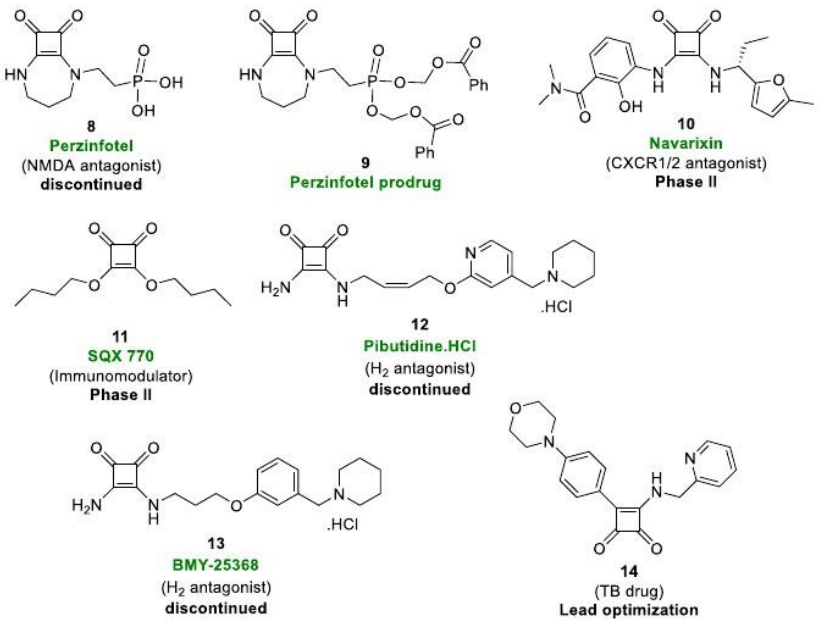

Fig. 3. Clinical/preclinical candidates containing a modified squaramide scaffold.

disease, second-line therapy or greater) in the USA and Israel [29]. Navarixin has also been investigated for the treatment of asthma, chronic obstructive pulmonary disease and psoriasis [30]. It was thought to reduce neutrophil migration to the diseased lung what should improve a participant's symptoms. However, this assumption was not proved, and this research has been discontinued. Squaric acid dibutyl ester **11** (SQX 770) was evaluated for its safety and efficacy for the treatment of herpes labialis in a clinical trial containing 54 patients and it was found that the compound is slightly effective in reducing the number of the disease outbreaks per year but it had non-serious adverse effects in more than 50% of the treated patients (mostly non-serious itching, redness, or swelling) [31,32]. Pibutidine **12** exhibited an H_2 antagonistic effect and was investigated as a gastrointestinal agent for ulcers [33–35]

by Taisho Pharmaceutical. In 2000, however, it was discontinued in Phase I due to cardiotoxicity and gastrointestinal toxicity [36]. BMY-25368 **13**, developed by Bristol-Myers Squibb, advanced as far as phase III clinical studies for duodenal and gastric ulcers. This compound acts as a histamine H_2 receptor antagonist [37,38].

Another example of pharmacokinetic and pharmacodynamic profiling for SA analogue was done in Ref. [39], where an antituberculotic compound **14** (Fig. 3) was developed. In **14**, high metabolic clearance was observed, which was likely caused by cytochromes. Therefore, the authors used pan CYP inhibitor (aminobenzotriazole, ABT) together with **14** in *in vivo* experiment (peroral administration in mice) and this caused a 300-fold increase in free plasma concentration when administered along with 100 mg/kg ABT. This provided plasma concentration above MIC for 15 h which was considered sufficient for further evaluation of pharmacodynamic profile in the acute model of tuberculosis infection. In general, it seems that some SA analogues may be enzymatically stable and other may be metabolized by various enzymes and therefore it is advisable to investigate the metabolic clearance for the most promising lead structures before they enter more expensive clinical trials.

Despite the importance of squaric acid analogues as privileged scaffolds in drug discovery, only two reviews have been published recently on this topic, both about squaramides [40,41]. The first [40] is a very comprehensive review about squaramides, their use in chemical biology, and especially their supramolecular properties. The second review [41] summarizes the synthetic approaches to squaramides. Older reviews on squaramides and squaric acid conjugates exist [2,3]. In contrast, this article presents an overview of squaric acid derivatives in general and focuses predominantly on their potential applications in drug development. The main purpose of this review is to provide an overview of the squaric scaffold-based derivatives as agents with remarkable potential in the medicinal chemistry field. Considerable attention is given to structure-activity relationship (SAR) studies and mechanism of action studies.

2. Squaric acid analogues in medicinal chemistry

Squaric acid analogues are significant in medicinal chemistry for many reasons. First, unlike many other compounds designed as potential drugs, they usually do not suffer from high lipophilicity and low solubility in water. Especially when squaric acid or the squaramide scaffold is combined with amine and carboxylic groups, the resulting compounds show increased solubility, and this makes them suitable therapeutic agents [42,43]. In addition, squaric acid analogues may serve as non-classical isosteres for carboxylates and amino acids during drug development [2]. For example, *N*-(hydroxydioxocyclobutenyl)-containing analogues of gamma-amino-butyric acid and L-glutamate were successfully used as analogues of compounds that are active towards amino acid receptors (AMPA and NMDA) in neurons [44].

Mono-amides of squaric acid (squaramates) are often used for bioconjugation with Lys and other amines. Diamides (squaramides) have been used as a phosphate group surrogate in nucleotide [45–47] or oligonucleotide (ON) analogues [48,49]. A chemically synthesized 2′-sugar-linked squaramate–RNA conjugate, prepared by the reaction of 2′-amino-modified RNA with diethyl squarate, was reported to cross-link to aminoacyl-transferase FemXWv [50], and this is the only example of the use of a squaric acid analogue in nucleic acid conjugation. Within the research aimed at base-functionalized nucleic acids for applications in chemical biology, the authors designed [51,52,123] novel squaramate-linked cytosine 2′-deoxyribonucleoside triphosphate (dNTP) for the enzymatic synthesis of modified DNA and cross-linking with proteins.

The use of squaric acid analogues in chemical biology is mostly represented by their bioconjugation to proteins or carbohydrates and by their use as ion receptors. In contrast, in medicinal chemistry, these compounds have numerous biological effects, including antiplasmodial, antichagasic, anticancer, and antibacterial activity, which makes them promising agents in drug development. In this chapter, various activities of squaric acid analogues will be summarized, and the advances towards their therapeutic use will be critically reviewed.

2.1. Antiprotozoal activity

Protozoans are unicellular eukaryotic organisms responsible for several serious human diseases, such as malaria, human African trypanosomiasis (HAT, sleeping sickness), leishmaniasis, and Chagas disease [53]. These four tropical diseases are endemic in many countries worldwide and together affect approximately 226 million people, particularly in developing countries [54]. Moreover, protozoal infections are among the most common life-threatening secondary infections in immunocompromised patients, e.g., patients with HIV or undergoing cancer chemotherapy. There are many antiparasitic compounds available; however, their use is often limited due to the emergence of drug resistance. An urgent need for novel efficient drugs that act by different mechanisms encourages global antiparasitic drug discovery. Squaric acid analogues might help to overcome the increasing antiparasitic drug resistance because many of these analogues have promising antiparasitic activities [42,55–58].

The first squaric acid analogues with activity against *Plasmodium falciparum*, the causative agent of malaria, appeared in 2013 [57]. The Santos group followed in their previous works [59,60] and synthesized a series of conjugates containing a squaric moiety and heterocycles of general structure **15** and **17** derived from known antimalarials (Fig. 4). Three compounds had nanomolar potency against chloroquine-resistant *P. falciparum* and approximately two-fold higher potency than the parent drug chloroquine. Moreover, they were not cytotoxic against NIH 3T3 or HEK 293T cells. The most interesting derivative **16** from this series is depicted in Fig. 4. Encouraged by these promising results, Ribeiro et al. synthesized other squaramides modified with aminoquinoline (Fig. 4) and tested them against liver-stage malaria parasites using human hepatoma cells (Huh7) infected by *Plasmodium berghei*. Compound **18** (Fig. 4) showed a 7.3-fold greater effect compared to the standard drug primaquine (the only available drug active against all *Plasmodium* exoerythrocytic forms). Overall, both papers by the Santos group [57,58] were focused on finding the most favourable linker between the substituted quinoline and squaramide parts. They tested various flexible alkyl chains, a rigid piperazine linker, and the direct binding of the heterocycle to the squaramide moiety. However, the rigid alkyl chain proved to be the most effective linker within the selected library. The direct binding of squaramide and aminoquinoline resulted in reduced activity [57]. Considering these interesting results, squaramide-modified aminoquinolines might represent a new class of antiplasmodial agents.

Squaramide-based compounds were also tested for their antileishmanial activity [55]. Leishmaniasis is a parasitic disease endemic in 98 countries worldwide. More than 1 million new cases are reported per year, and 350 million people are at risk of being infected [61]. The substances currently available for the treatment of this illness are pentavalent antimonials, paromomycin, amphotericin B, and miltefosine. Because these compounds are becoming less efficient due to the emergence of protozoal resistance, there are no effective substances to cure this parasitic disease. Considering the widespread resistance, there is an urgent need to identify new highly active antileishmanial drugs. Due to their interesting biological activity, modified squaramides have been explored as

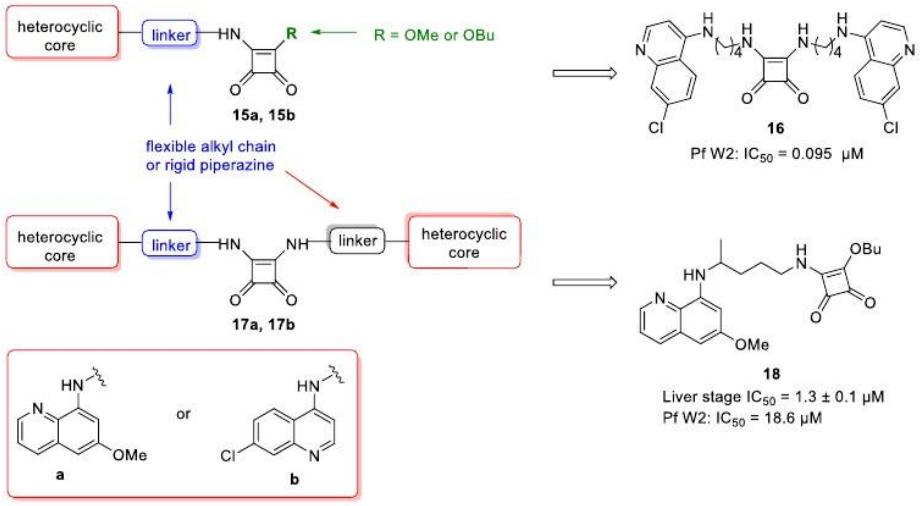

Fig. 4. Squaramides with antiplasmodial activity [57,58].

antileishmanial agents [55]. In 2016, the Sánchez-Moreno group reported the synthesis of variously substituted squaramides of general structures **19**–**21** (Fig. 5) and their antileishmanial activity on promastigote and amastigote forms of *Leishmania donovani*, *Leishmania infantum*, and *Leishmania braziliensis*. Three of the prepared compounds exhibited higher activity than the standard drug glucantime and were less toxic (Fig. 5). Among them, compound **23** (Fig. 5) was the most effective. Moreover, the authors observed certain alterations in the excretion products of all species indicating the leishmanicidal activity of the studied squaramides.

Of note, squaramide-based compounds have already been explored as highly efficient antichagasic agents [42,56]. Chagas disease (also known as American trypanosomiasis) is an insect-transmitted protozoal infection caused by *Trypanosoma cruzi*. The World Health Organization (WHO) has stated that an estimated 8 million people are infected with *Trypanosoma cruzi* worldwide, especially in Latin America, causing more than 10,000 deaths per year [62]. Current treatment is based on the use of nifurtimox (NFX) and benznidazole (BZN), compounds developed more than 40 years ago. Moreover, their mechanism of action is still under debate

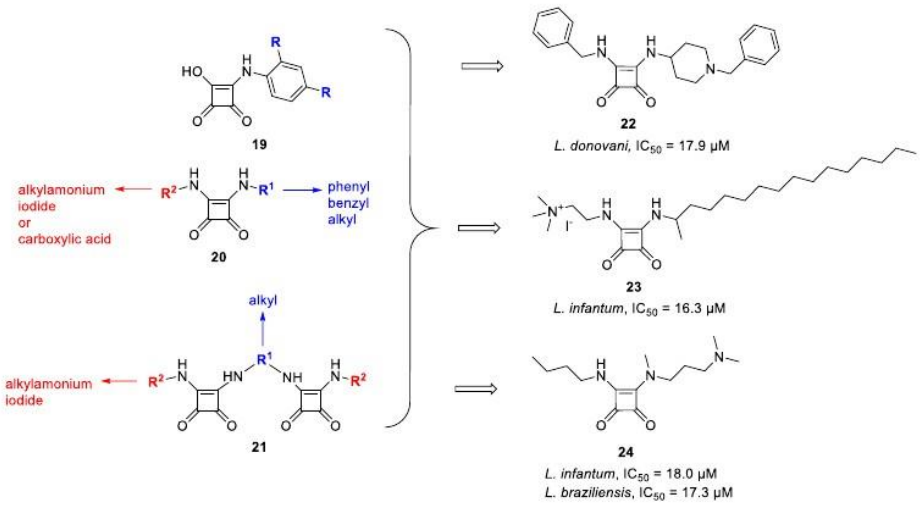

Fig. 5. Squaramides with antileishmanial activity [55].

[63,64]. Unfortunately, both agents are limited in their ability to eliminate *T. cruzi* from the body and have severe side effects such as vomiting, anorexia, and peripheral polyneuropathy due to their high toxicity [42]. For this reason, it is necessary to overcome the serious drawbacks of current antichagasic drugs and develop less toxic and more selective compounds.

During their research with novel squaramides, Olmo et al. found that some of the tested compounds of general structures **25** and **26** exhibited interesting antichagasic properties (Fig. 6) [42]. *In vitro* and *in vivo* studies of various structurally simple aminosquaramides revealed compound **27** (Fig. 6) to be the most active from the selected library in both the acute and chronic phases of Chagas disease. In immunosuppression experiments in a mouse model, the monitoring of total Ig-G in response to *T. cruzi* infection showed comparatively low levels in treated mice and confirmed compound **27** as an ideal candidate for preclinical studies.

The obtained knowledge triggered a study of similar squaramides of general structures **28** and **29** reported by Martín-Escolano et al., in 2019 (Fig. 6) [56]. Among various substitutions, a longer alkyl chain and a dimethylamino substituent showed efficacy against *T. cruzi* [42]. Therefore, the subsequent survey focused on the study of squaramides with longer alkyl chains [56]. To perform an SAR study, they evaluated derivatives with an increasing length of the linear aliphatic chain (C0–C16), compounds with different heteroatoms, and squaramides containing two or three basic nitrogens (Fig. 6). Based on the *in vitro* and *in vivo* studies, compound **30** was identified as the most potent form of the studied library. Interestingly, the authors attempted to determine the mechanism of action and suggested that compound **30** can depolarize the mitochondrial membrane, resulting in an energetic deficit and subsequent cell death by necrosis. Because selected compound **30** exhibited better trypanocidal properties *in vitro* and lower toxicity compared to the standard drug BZN, it is worth further investigation in the preclinical phase.

2.2. Antibacterial activity

Bacterial infections represent one of the greatest public health problems, especially when we consider the increasing antibiotic resistance. This rapid emergence of resistant bacteria is occurring worldwide; therefore, it is essential to extend the spectrum of existing antibiotics. From this point of view, many compounds derived from squaric acid have been studied.

The first reports of antibacterial activity associated with the squarate scaffold associated emerged in 1996 [65] when the Kojima group noted that several squaramides of general structure **31** could act as H_2 antagonists (Fig. 7). Moreover, some of the tested derivatives such as **32** exhibited moderate to weak inhibitory activity

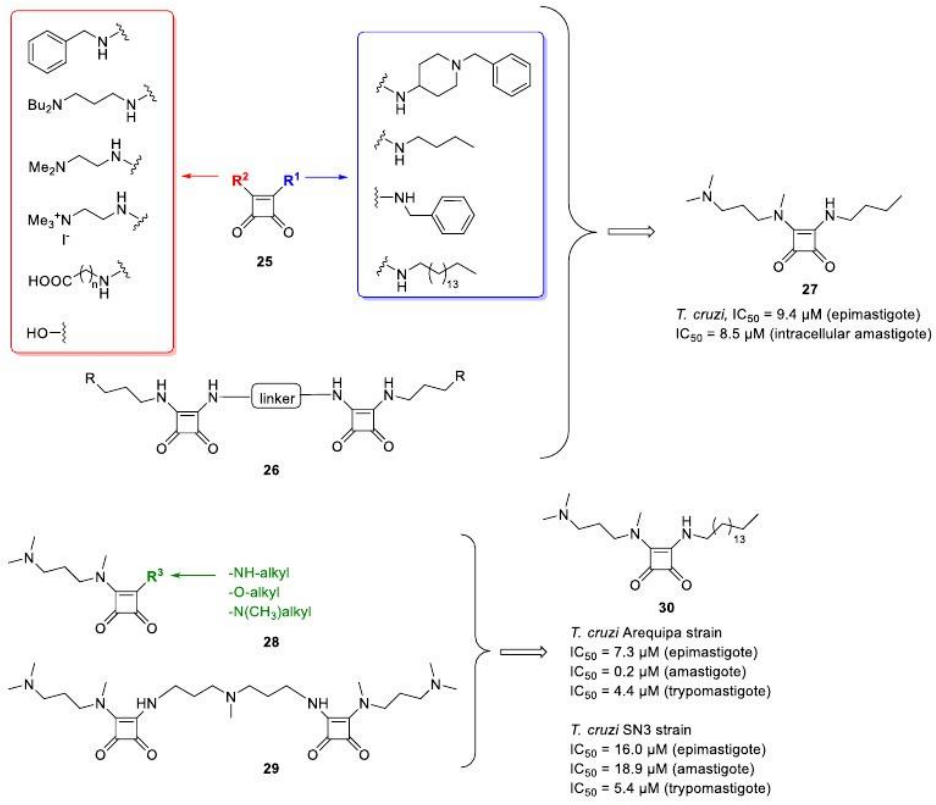

Fig. 6. Squaramides with antichagasic activity [42,56].

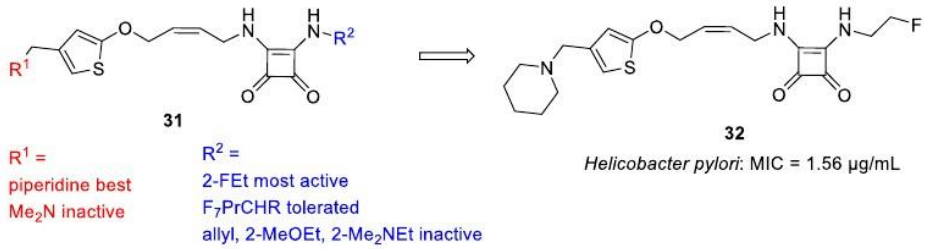

Fig. 7. Squaramides acting as H_2 antagonists [65,66].

against *Helicobacter pylori*. Later, this observation resulted in the synthesis of other potent H_2 antagonists and their progression to human clinical trials (as mentioned above with Pibutidine and BMY-25368, Fig. 3) [66].

Lindhorst and co-workers described the interesting behaviour of mannosidic squaric acid monoamides **33** and **34** (Fig. 8) [67,68]. Bacteria use fimbriae (also known as pili) to connect to the host cell [69], and synthetic mannosides based on the squarate structure can inhibit type 1 fimbriae-mediated mannose-specific bacterial adhesion that normally proceeds through the lectin FimH. Synthetic squarate **33** showed high affinity to FimH and exhibited ~50-fold greater inhibitory potency than the standard agent *p*NPMan [67].

The high potency of squaramides within the medicinal chemistry field was recently confirmed by work published in *J. Med. Chem.* [70]. During the search for novel antibacterial agents, the Murakami team focused on the large antibacterial target, RNA polymerase, which is essential for gene expression, cell growth, and viability [71]. Using a high-throughput screening of a corporate compound library, the Murakami team identified a highly active novel structural framework of general structure **35** based on the squaramide moiety (Fig. 9). This squaramide was shown to bind to the RNA polymerase switch region and result in the dysfunction of the region with consequent transcriptional inhibition. Detailed SAR studies indicated that the terminal isoxazole and benzyl rings are essential for specific binding to pockets in the switch region. Nevertheless, there are further structural modifications to be explored.

Recently, the groups of Gupta and Ravishankar reported one of the most active compounds against *Mycobacterium tuberculosis* (*Mtb*) based on the unique squaramide feature acting as a mycobacterial ATP synthase inhibitor (Fig. 10) [39]. ATP synthase is a ubiquitous key enzyme in the energetics and metabolism of bacteria that utilizes the energy stored in as transmembrane electrochemical potential for the production of ATP [72]. ATP synthase in *Mtb* has recently been validated as a highly promising target of antibacterial compounds. It is noteworthy that these research groups screened approximately 900,000 compounds in cooperation with AstraZeneca to identify hits and proceed with lead optimization (Fig. 10). The lead series of squaramides **37** was very specific and selective while lacking cytotoxicity [73]. Interestingly, a comparison of squaramide **14** with bedaquiline (an approved drug for tuberculosis treatment that acts as an ATP synthase inhibitor) showed the absence of cross-resistance in bedaquiline-resistant mutants. This finding suggests that squaramide **14** interacts with an ATP synthase site distinct from that with which bedaquiline interacts. These observations indicate the high potency of squaramide **14** in the identification of novel drug candidates active against drug-resistant mutants of *Mtb*.

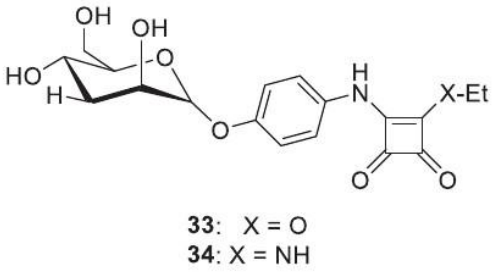

Fig. 8. Squarates as inhibitors of bacterial adhesion [67].

2.3. Cytotoxic activity

The treatment of cancer remains a hot topic. Many researchers explore how to reduce the inherent toxicity of currently used drugs, limit adverse effects on the human body, and improve drug targeting. The most commonly used chemotherapeutics (many approved more than 40 years ago) suffer from low bioavailability due to low water solubility or poor membrane permeability and thus require high dosage. Furthermore, the majority of these compounds have led to the development of multidrug resistance along with fatal side effects. Therefore, the discovery of novel effective anticancer agents with different mechanisms of action has become one of the main research goals worldwide.

Squaric acid analogues have received special attention as potent anticancer agents especially in the last decade [45,74–79]. However, the first report on cytotoxic squaramides appeared as early as 2005 [80], when Grabner et al. studied the complex compound $[Pt_3(\mu_2\text{-}C_4O_4)_3(H_2NPr^i)_6]\cdot 3H_2O$ **38** (Fig. 11) obtained by the reaction of *cis*-$[Pt(H_2O)_2(H_2NPr^i)_2]SO_4$ with barium squarate in a 1:1 M ratio and found that it exhibited interesting cytotoxic properties. In this complex, platinum atoms are joined by squarate ligands that occupy a rather significant distance (approximately 2 Å) between platinum atoms (so-called trinuclear complex); the distance between oxygen atoms is relatively short in comparison (approximately 3.1–3.2 Å). 3D structure is deposited in the published paper as Supplementary data [80]. The cytotoxicity of this compound was tested on T24 cells, which exhibited slightly reduced size after exposure to this compound. This complex has not achieved cytotoxicity similar to cisplatin; however, future studies with squarate complexes might help to overcome the inherent cytotoxicity of platinum complexes.

In 2012, Villalonga et al. reported the synthesis of oligosquaramide-based macrocycles with anticancer properties of

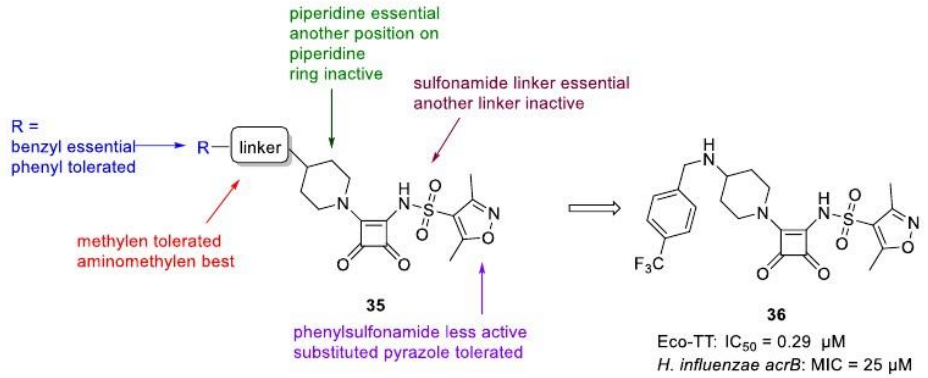

Fig. 9. Squaramides as RNA polymerase inhibitors [70].

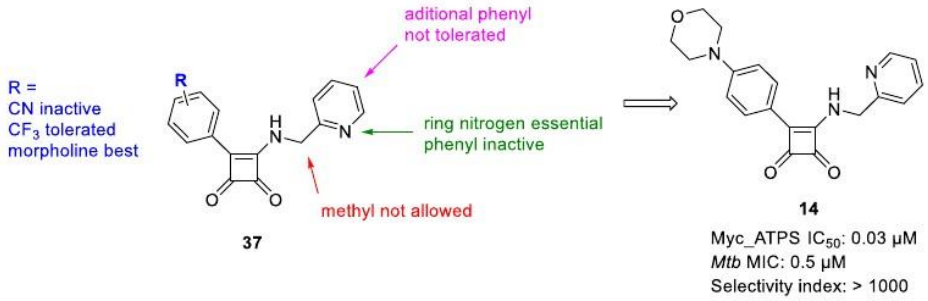

Fig. 10. Squaramides acting as mycobacterial ATP synthase inhibitors [39].

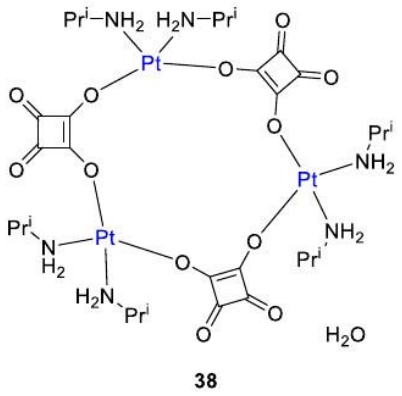

Fig. 11. Structure of trinuclear complex.

general structure **39** (Fig. 12) [79]. They prepared various oligomer cyclosquaramides and acyclic oligosquaramides and tested their anticancer activity primarily on mantle cell lymphoma (MCL) cell lines Jeko-1 and Z-138. Interestingly, the appropriate size of the macrocycle was crucial for antiproliferative activity. The most interesting oligomer comprises five squaramide scaffolds (**40**, n = 3) connected with appropriate linkers (Fig. 12) and displays a well-defined structure with a certain level of conformational pre-organization and flexibility that is very important for ligand binding on the desired target. In contrast, corresponding acyclic oligosquaramides and smaller cyclosquaramides containing 2–4 squaramides did not show any anticancer activity. The oligosquaramide **40** exhibited significant antiproliferative activity against both Jeko-1 and Z-138 cells and was subsequently tested against the NCI-60 human tumour cell line panel. Moreover, oligosquaramide **40** did not show toxicity against controlled nontransformed NIH3T3 fibroblasts. Although the biological target of cyclosquaramides remains unknown to date, the authors speculated that target proteins may include kinases. However, determining the exact mechanism of action will require more information and consistent studies in the future.

The anticancer SAR of squaric acid analogues inspired by the structure of the known antimitotic agent combretastatin A4 (CA4) demonstrated the potency of this motif (Fig. 13) [75]. Liu et al. synthesized various 3,4-diaryl squaric acid analogues **43** as CA4 mimetics incorporating the squaric scaffold as a *cis*-restricted linker and studied their cytotoxicity. All the compounds were tested

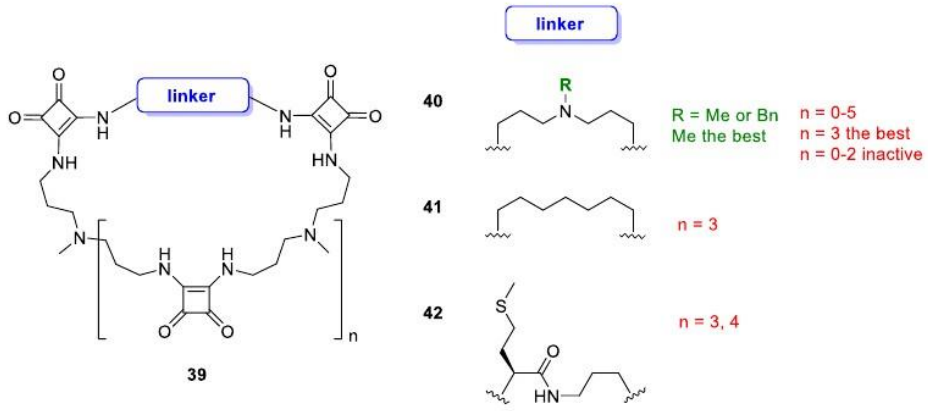

Fig. 12. Cyclosquaramides with antiproliferative activity [79].

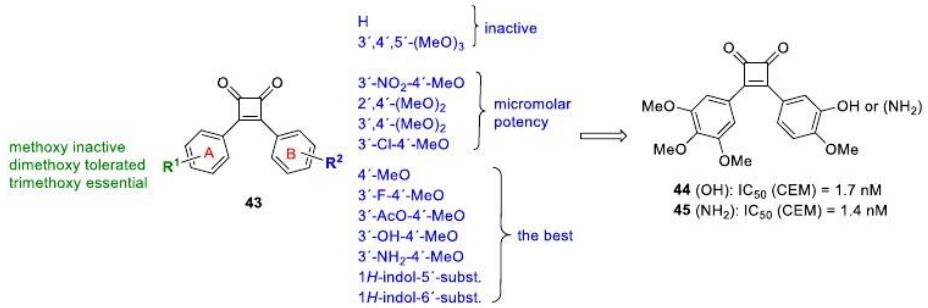

Fig. 13. Squaric acid analogues with antimitotic activity [75].

against the non-solid human CEM cell line and further evaluated against a panel of human tumour cell lines, including Bel-7402, HepG2, and SMMC-7221 human liver cancer cells, MCF-7 human breast cancer cells, SW-1990 human pancreatic cancer cells, HCT116 human colon adenocarcinoma cells, and CEM human leukaemia cells, with CA4 employed as a positive control. The extended SAR study revealed that some of the tested compounds exhibited nanomolar activities against human leukaemia cells and potent activities against a panel of human tumour cell lines. Of note, compounds **44** and **45** exhibited activities comparable to the standard drug CA4 (IC_{50} (CEM) = 1.6 nM). Moreover, the reported SAR study showed that all three methoxy groups of the A ring are essential, whereas the substitution of the B ring can be more varied. The authors also reported preliminary mechanism of action studies revealing that compounds **44** and **45** cause cell cycle arrest tumour cells in G2-M phase and interact with the colchicine binding site on microtubules.

In 2016, Quintana et al. reported the cytotoxicity of various squaramates and squaramides of general structure **46** (Fig. 14) evaluated on different tumour cell lines (especially HeLa, cervical carcinoma, and HGC-27, gastric carcinoma) [78]. The reported anticancer SAR of all hybrids depicted in Fig. 14 demonstrates the necessity of both NH groups (squaramates did not show any significant activity). Interestingly, squaramides with cinchona-based substituents exhibited micromolar potency with IC_{50} values of 3–12 μM in HGC-27 or HeLa cells. The best candidate from the evaluated library was compound **47** with an IC_{50} value of 1.81 μM in HGC-27 cells and 34.63 μM in HeLa cells. Squaramide **47** was further tested on different cell lines such as T98 and U87 glioblastoma cells (the most aggressive cell type causing brain cancer), HEK293 transformed human kidney cells, MDCK cells (epithelial cells) and Vero (African green monkey kidney cell). The results confirm cell type-dependent toxicity (IC_{50} values of 60.25 μM and 7.15 μM for glioblastoma cell lines U87 and T98, respectively, 9.03 μM for HEK293, 70.20 μM for MDCK, and 33.40 μM for Vero). Furthermore, the authors found out that the inhibitory effect of **47** is associated with cell cycle arrest at the G1 phase and the induction of caspase-dependent apoptosis. Based on these results, squaramide **47** could act as a hit for further optimization.

In 2016, Soukarieh et al. designed novel cap-binding inhibitors of 4E factor (eIF4E) based on the squaramide scaffold [45]. The factor eIF4E is a component of the eukaryotic translation initiation factor 4F complex, which recognizes the 7-methylguanosine cap structure at the 5′ end of messenger RNAs and is a key player in the regulation of translation. eIF4E activity is implicated in mitosis, embryogenesis, and apoptosis. Interestingly, eIF4E is overexpressed in numerous human tumours, which makes it an interesting target for anticancer therapy. Based on the known crystal structure of

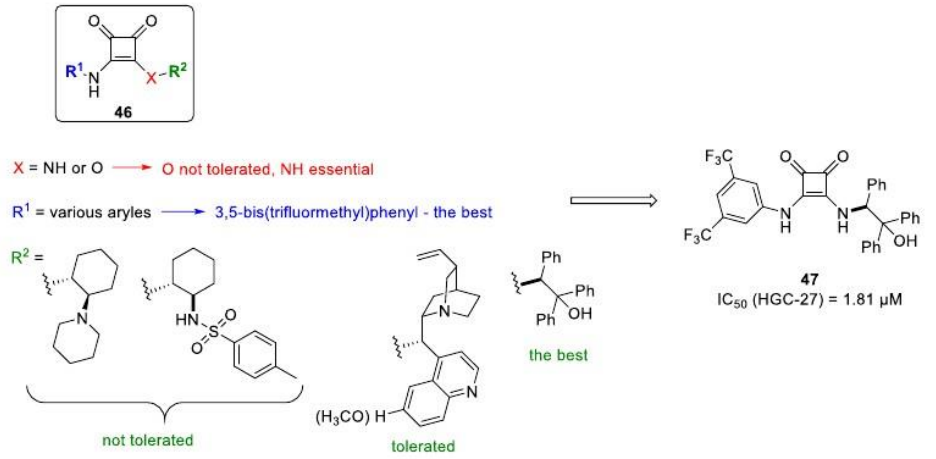

Fig. 14. Squaramates and squaramides evaluated for their cytotoxicity [78].

eIF4E and in consideration of the cellular bioavailability of potent drugs, Soukarieh et al. designed and synthesized novel eIF4E cap-binding inhibitors, some of which contain the squaramate scaffold (Fig. 15). Most of the tested squaramates did not show any significant activity; only compounds **49** and **50** exhibited modest inhibitory effects (Fig. 15). Moreover, these two depicted squaramates were co-crystallized with eIF4E. The obtained crystal structures showed similar binding modes to cap derivatives reported previously.

Carbocyclic nucleosides **51**–**53** incorporating the squaric acid scaffold synthesized by Lu et al. (Fig. 16) were examined for their anticancer activity in a National Cancer Institute battery of human tumour cell lines [77]. All three derivatives exhibited modest anticancer activity against non-small cell lung cancer (NCI–H522) at 10 μM. Squaramide **51** and squaramate **52** showed micromolar potency against renal cancer (UO-31). Moreover, compound **51** exhibited modest anticancer activity against ovarian cancer (OVCAR-8) and leukaemia (CCRF-CEM), whereas compound **52** was potent against colon cancer (KM12) and melanoma (UACC-257) at 10 μM. Interestingly, derivative **53** showed moderate growth inhibition of CNS cancer (SF-295) at 10 μM. Furthermore, all three analogues were tested for toxicity to HeLa cells. However, none of the tested compounds showed better inhibitory effects compared with the standard drug cisplatin. Overall, the tested squaric acid analogues exhibited moderate anticancer activity with a selective effect on some of the tested cell lines. However, more studies are needed to demonstrate the potency of the presented carbocyclic nucleosides as non-classical bioisosteres for the heterocyclic base in cancer treatment.

The squaric acid scaffold was also incorporated into the structure of nucleosides designed as inhibitors of SNM1A [81]. SNM1A (sensitive to nitrogen mustard 1A) is a DNA repair enzyme that plays a crucial role in the repair of interstrand crosslinks. The enzyme is considered a potential therapeutic target for the treatment of cancer that is resistant to DNA crosslinking agents. Because the active site of SNM1A contains a zinc atom, Doherty et al. proposed that a molecule modified with a zinc-binding group might block this enzyme and inhibit the repair of interstrand crosslinks. Because squarate or the squaramide ring can selectively bind through hydrogen bonds acting as hydrogen bond donors or

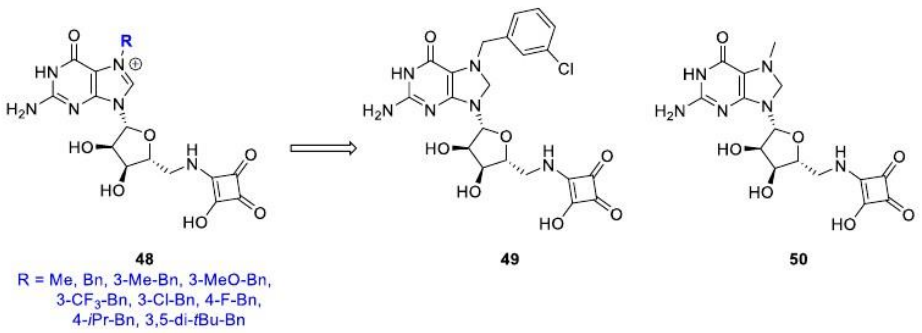

Fig. 15. Squaramates as eIF4E inhibitors [45].

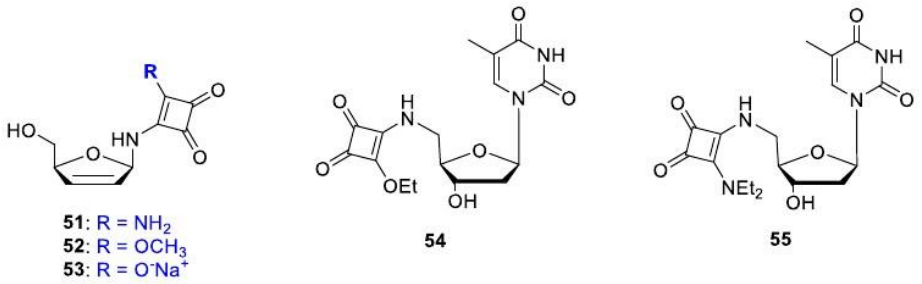

Fig. 16. Carbocyclic nucleosides incorporating the squaramate scaffold [77] and nucleosides designed as inhibitors of SNM1A [81].

acceptors, this nucleoside modification was selected as a suitable zinc-binding group (Fig. 16). Unfortunately, neither squarate **54** nor squaramide **55** showed any activity in the performed assay.

Squaric acid derivatives as cytotoxic agents were further described by Fernández-Moreira et al. [74]. They studied several squarates and squaramides for their cytotoxicity against HeLa cervical cancer cells (Fig. 17). Compound **57** exhibited the greatest cytotoxicity (IC_{50} = 0.88 μM). Moreover, the cyclobutenedione ring was modified with various fluorophores for potential application in cell imaging studies, and the novel luminescent compounds were visualized using fluorescence cell microscopy. The authors observed lysosomal and nuclear localization. Squarate compound **58** was the most promising candidate from the evaluated library. Compound **58** enters the cell and accumulates in the nucleus. These results indicate the high potential of squaramide-based transporters, which merit further investigation.

2.4. Antiviral activity

Among all the viral diseases, acquired immunodeficiency syndrome (AIDS) caused by the human immunodeficiency virus (HIV) continues to be a major global health issue, having claimed almost 33 million lives. Due to gaps in HIV services, 690,000 people died from HIV-related causes in 2019, and 1.7 million people were newly infected [82]. The emergence of resistance and/or a lack of tolerability in individual patients requires a wider range of treatment options. As a result, the development of new anti-HIV agents with improved safety, better resistance profiles, and new mechanisms of

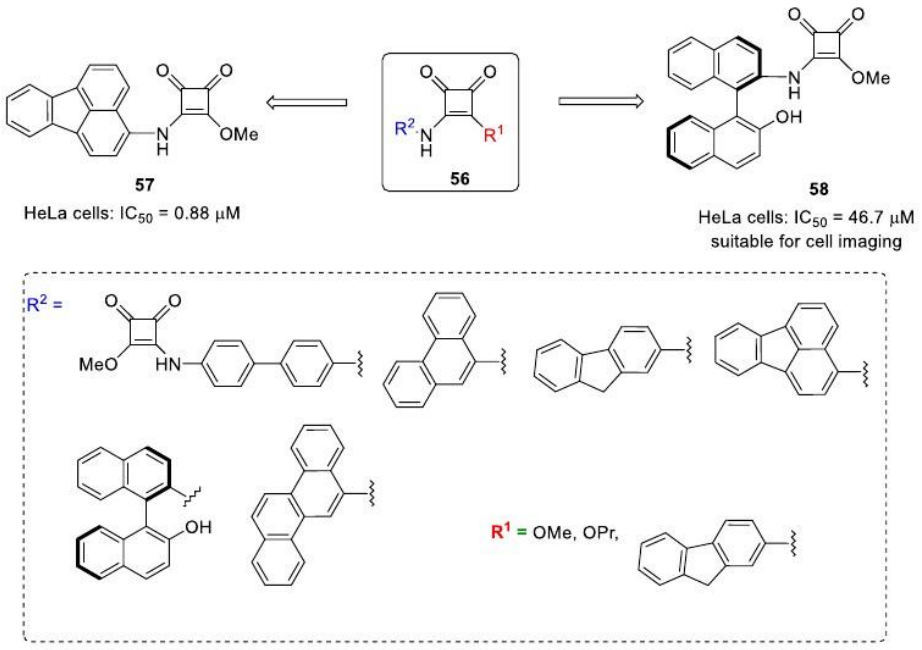

Fig. 17. Luminescent derivatives studied for their cytotoxicity against HeLa cells [74].

action is gaining attention [83]. Squaric acid analogues offer interesting opportunities within this research area.

In contrast to their significant antibacterial properties, the antiviral activity of squaric acid analogues has not been explored extensively. Most attention has been paid to analogues with anti-HIV activity. In 2005, Lee et al. screened a novel series of peptidomimetics containing a squaramide scaffold of general structure **59** (Fig. 18) as bioisosteric replacement for guanidine. These compounds were studied for their ability to inhibit the Tat-TAR interaction required for the conversion of arrested RNA polymerase II into a form needed for successful viral transcription. Derivative **60** was able to bind TAR RNA with high affinity (K_D = 7.7 μM) [84].

Another series of anti-HIV squaramides of general structure of **61** was synthesized and studied by Ghosh et al., in 2019 [85]. All the HIV-1 protease inhibitors contain a squaramide-derived scaffold as the P2 ligand combined with an (*R*)-hydroxyethylamine sulfonamide isostere (Fig. 18). Compound **62** with an *N*-methyl-3-(*R*)-aminotetrahydrofuranyl squaramide P2 ligand exhibited the best HIV-1 protease inhibitory K_i value of 0.51 nM. To explain the inhibitory potency, an energy-minimized active site model of inhibitor **62** was employed, and this model revealed several key interactions with Asp29 and Asp30 [85].

Previously mentioned carbocyclic nucleosides **51**–**53** incorporating the squaric acid scaffold synthesized by Lu et al. (Fig. 16) were examined for their antiviral activity [77]. However, no antiviral activity was observed for any of the analogues against a National Institute of Allergy and Infectious Diseases (NIAID) panel of 25 viruses [77].

2.5. CXCR2 receptor antagonists

CXCR1 and CXCR2 receptors are G protein-coupled receptors activated by growth-related protein-α (CXCL1) and interleukin-8 (CXCL8) [86]. These receptors are expressed on many different inflammatory and structural cells, where they regulate pulmonary functions. Therefore, CXCR2 is involved in the pathology of various lung diseases such as chronic obstructive pulmonary disease (COPD), asthma, acute respiratory distress syndrome, and cystic and pulmonary fibrosis [87–89]. Due to the key role of CXCR2 in a number of inflammatory disorders, potent selective CXCR2 antagonists have been developed over the past decade as promising anti-inflammatory agents [90].

In 2007, Gonsiorek et al. confirmed the pharmacological specificity of Sch527123 as a novel, potent, and allosteric CXCR2 antagonist with potential therapeutic utility in a variety of inflammatory conditions (Fig. 19) [91]. To measure compound affinity, [^{3}H] Sch527123 was characterized in both equilibrium and nonequilibrium binding analyses. Its binding to CXCRs was both saturable and reversible. Although Navarixin **10** bound to CXCR1 with good affinity (K_d = 3.9 ± 0.3 nM), the compound is CXCR2-selective (K_d = 0.049 ± 0.004 nM). The extraordinary picomolar potency of Sch527123 binding to hCXCR2 arises from slow (approximately 24 h at room temperature) dissociation from the receptor [91].

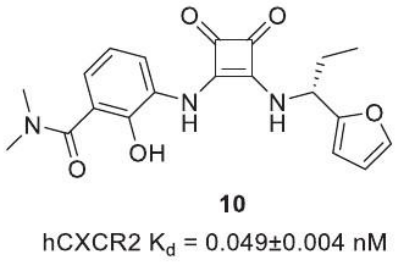

Fig. 19. Navarixin (Sch527123) [91].

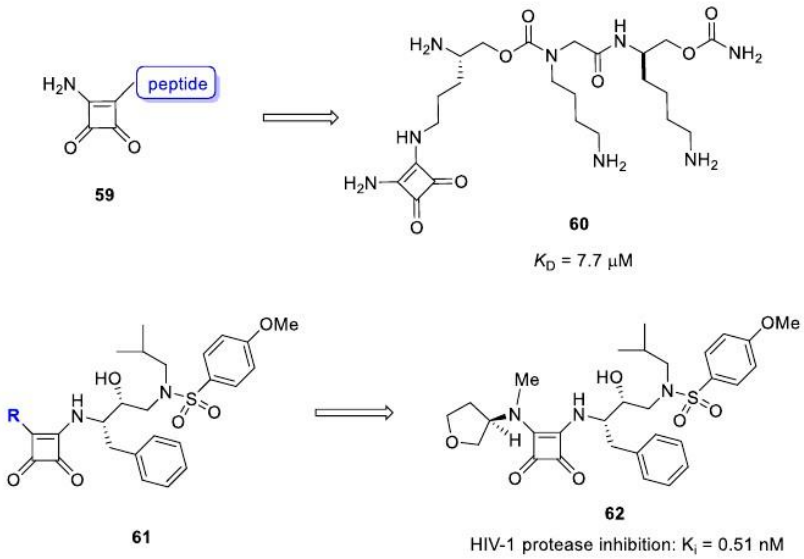

Fig. 18. Anti-HIV peptidomimetics containing squaramide scaffold [84] and squaramides as HIV-1 protease inhibitors [85].

N,N′-diarylsquaramides **63** were identified by McCleland and co-workers as selective and potent CXCR2 antagonists (Fig. 20) [92]. They studied squaramides as bioisosteric replacements of previously synthesized *N,N′*-diarylureas and *N,N′*-diaryl (cyano)guanidine-type CXCR2 antagonists. Based on SAR, NHs and the phenolic group are essential. In contrast, diarylsquaramides are insensitive to the ionization state of the phenol. The 3-position adjacent to the phenol is tolerant to the modulation of physicochemical parameters by the introduction of solubilizing sulfonamides and amides. All the other aromatic substituents have limited effects on solubility. Within the series, squaramide **64** (Fig. 20) displays the best activity and most desirable pharmacokinetic profile [92].

Another isosteric urea replacement by *N,N′*-diarylsquaramide moiety, which has received an increased attention, was disclosed in three patents by Glaxo-SmithKline in 2001 and 2002 (Fig. 21) [93]. Additionally, there was a joint application from Pharmacopeia and Schering-Plough in 2002 covering phenol-containing squaramides such as compound **65** with the typical aryl right-hand side, compound **69** bearing a branched alkyl group, and compound **70** containing a benzyl-type group (Fig. 21). The preference of a 3-(*N,N*-dimethylcarboxamido)-2-hydroxyphenyl left-hand side indicates this as an optimal group for this class of squaramides. All these phenol-containing CXCR2 antagonists play an important role in the resurgence of chemokine receptor antagonists and demonstrate efficacy in complex chronic diseases such as COPD and cystic fibrosis [93].

Extended SAR studies conducted with the diaryl cyclobutenedione series comprising general structures **71** resulted in compound **72** (Fig. 22), which demonstrated significant affinity in the CXCR2 binding assay (IC_{50} = 36 nM) [94]. Due to concerns about the metabolic fate of the 4-NO_2 group, the 3-dimethylcarboxamide derivative **73** (Fig. 22) was created and showed excellent *in vitro* potency (CXCR2 IC_{50} = 15 nM) and good functional activity in a CXCR2 chemotaxis assay (IC_{50} = 19 nM). Moreover, compound **73** showed improved organic solubility and better predicted absorption. Further SAR studies focused on the exploration of the right-hand benzylic functionality. The (*R*)-ethyl analogue **74** (Fig. 22) demonstrated superior binding affinities (CXCR2 IC_{50} = 6.8 nM) and a high level of oral bioavailability. However, the best potency (CXCR2 IC_{50} = 2.6 nM) was observed upon replacement of the phenyl ring of **74** with heterocyclic rings affording the previously mentioned clinical candidate Sch527123 (Fig. 19) [94].

Novartis is developing the CXCR2 selective antagonist **75** (Fig. 23) with the potential to become the first anti-inflammatory treatment for COPD. Recently, Martin and co-workers developed a manufacturing concept for the choline salt of a nonsymmetric squaramide as a potent CXCR2 antagonist to increase drug substance quality [95]. Progress was outlined in terms of yield improvement as well as purging strategies for key impurities. Furthermore, an alternative sequence has been explored to avoid the switching of the phenolate salt from triethylammonium to free acid to a choline salt, providing significant cost reduction [95].

2.6. Bioisosteres

The concept of isosterism between relatively simple chemical entities was originally contemplated by James Moir in 1909 [96]. The term "bioisostere" was introduced in 1950 by Harris Friedman, who defined bioisosteres as compounds eliciting a similar biological effect [97]. Bioisosteres are usually less than exact structural mimetics and are often more alike in biological rather than physical properties. Consequently, bioisosteres introduce structural changes that can be beneficial for the design and development of drug candidates, and thus they have become a fundamental tactical approach in medicinal chemistry [98]. In this context, squaric acid derivatives were also explored as non-classical bioisosteres.

First, squaric acids were identified as useful isosteres of carboxylic acids and tetrazoles in angiotensin II antagonists due to their high intrinsic acidity. Squarate **76** (Fig. 24) reduced blood pressure in Goldblatt hypertensive rats, although efficacy was lower than the analogous tetrazole [99].

In an elegant example of isostere design, diaminosquaric acid derivatives **77** were conceived as achiral mimetics of glutamic acid [100]. Some of these molecules exhibited modest affinity for the *N*-methyl-D-aspartate (NMDA) glutamate receptor. The phosphonate derivative **78** (Fig. 24) was the most potent NMDA ligand, although it showed lower affinity than glutamic acid with an IC_{50} = 70 nM [100].

Butera et al. studied bioisosteric replacement of *N*-cyanoquanidine with a squaramide moiety to identify structurally novel adenosine 5′-triphosphate-sensitive potassium (K_{ATP}) channel openers of general structure **79** to treat urge urinary incontinence (UUI) [101]. A systematic SAR study on aryl and alkylamidine groups produced definitive trends summarized in Fig. 24. Mechanistic studies were performed within the series, and compound **80** (Fig. 24) showed significant K_{ATP} hyperpolarization and thus represents an attractive development candidate for the treatment of UUI [101].

Additionally, squaramide-type nucleotide analogues **81** and **82** were evaluated as phosphate isosteres. NMR analysis of compound **83** (Fig. 25) revealed its *N*-type form of ribose puckering identical to that in cAMP and cGMP. Due to their acidity (pK_a = 2.3) and conformational properties, they are interesting as potential antiviral and anticancer agents [102].

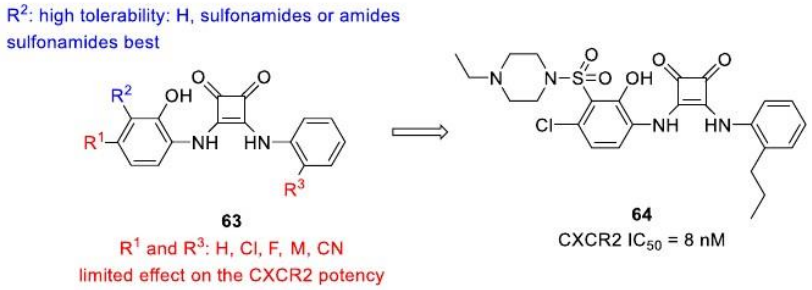

Fig. 20. N,N′-diarylsquaramides as antagonists of CXCR2 receptor [92].

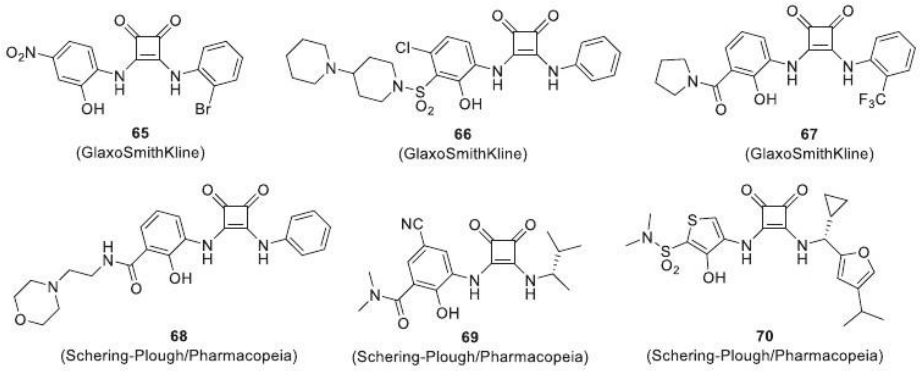

Fig. 21. N,N′-diarylsquaramide CXCR2 antagonists [93].

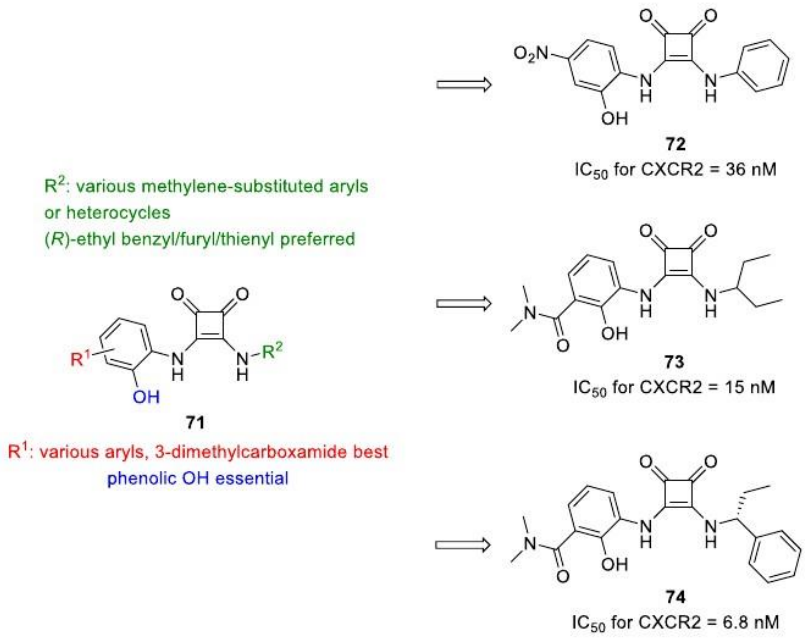

Fig. 22. Phenol-containing *N,N′*-squaramide CXCR2 antagonists [94].

Additional squaramide-based phosphate bioisosteres **84** were described by Xie et al. [103]. They showed that the squaric acid moiety could be incorporated in protein tyrosine phosphatase inhibitors as a phosphate bioisostere. As a result, compounds **85** and **86** (Fig. 26) were developed and showed moderate inhibitory activity against *Yersinia pestis* protein tyrosine phosphatase with IC_{50} s at pH 5.5 of 120 ± 20 and 350 ± 40 μM, respectively [103].

2.7. Vaccines

The introduction of vaccination against bacterial infections represents a breakthrough in human medicine [104]. Instead of a curing effect, an immunological memory is installed. In the field of vaccine development, the squaric acid moiety was initially used to prepare glycoconjugates from synthetic linker-equipped carbohydrates [105,106].

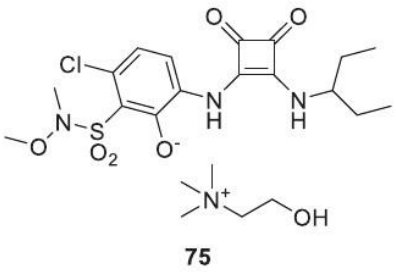

Fig. 23. A selective CXCR2 antagonist in development at Novartis [95].

In the context of cancer immunotherapy, Palitzsch et al. synthesized muci MUC1-glycopeptide vaccines with TTox as the immune-stimulating carrier and analysed their SAR in immunizations. Diethyl squarate has been used to couple glycopeptide antigens to carrier proteins. As a result, a synthetic glycopeptide vaccine inducing tumour-associated MUC1- specific IgG monoclonal antibodies that differentiate between normal and tumour mammary cells has been generated [105].

Peng and co-workers studied factors affecting the conjugation of bacterial polysaccharides to protein carriers employing squaric acid chemistry. Based on the identification of efficient conjugation to bovine serum albumin (BSA) and recombinant tetanus toxin fragment C (rTT-Hc) at pH 8.5, 9.0, and 9.5, higher-quality labelling of the O-SP-core (O-SPcNH$_2$) polysaccharide antigen with methyl squarate has been achieved. The novelty of the described approach is based primarily on the direct conjugation without the introduction of linkers to the molecule. Overall, the results indicate an increased efficiency of conjugation of the *Vibrio cholerae* O1 lipopolysaccharide (LPS) to BSA from 25% to 51% [106].

2.8. Various receptor antagonists

In 1992, Kinney et al. described a series of squaramide-based NMDA antagonists. These compounds inhibit excitatory amino acids (EEAs) such as a glutamic acid neurotransmitter that can lead to neuronal cell death [100]. Therefore, NMDA antagonists have been considered for the treatment of epilepsy, stroke, and neurodegenerative disorders [107]. Among all the studied isosteres, phosphonic acid **87** provided protection against NMDA-induced lethality in mice (Fig. 27) [100].

The squarate scaffold has also been used as a carboxylic acid bioisostere for the design of a potent, non-peptidic, non-tetrazole

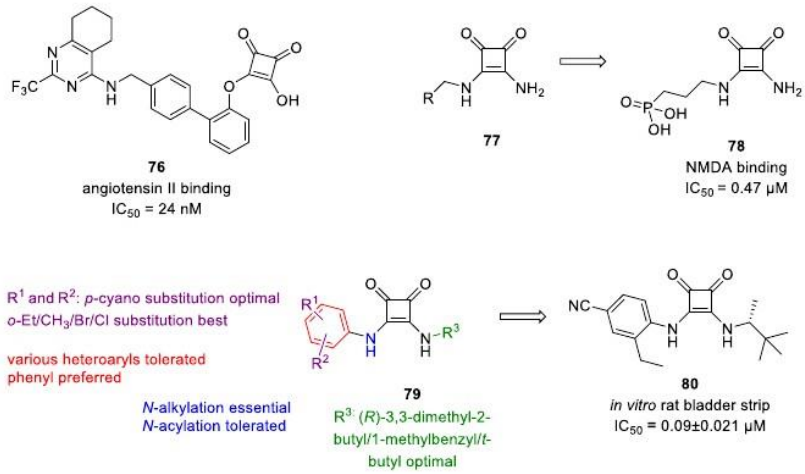

Fig. 24. Squaric acid isostere **76** as angiotensin II receptor antagonist [99], diaminosquaric acid-based NMDA antagonists **78** [100], and *N*-cyanoguanidine bioisosteres **80** as K_{ATP} channel openers [101].

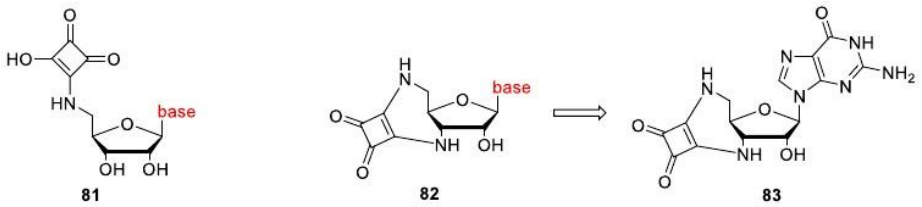

Fig. 25. Squaramide-type nucleotide analogues [102].

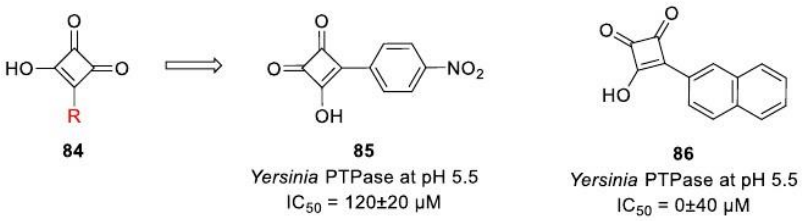

Fig. 26. Squaric acid-based protein tyrosine phosphatase inhibitors [103].

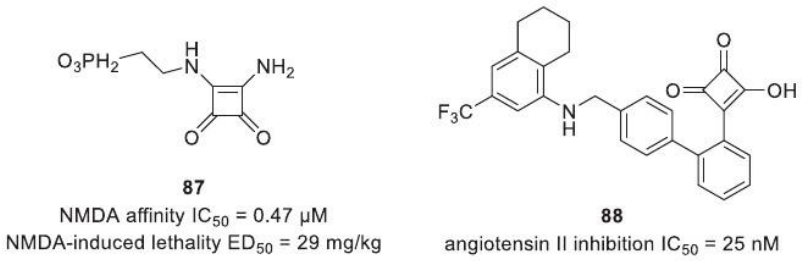

Fig. 27. Phosphonoalkyl squaramide-based NMDA antagonist **87** [100] and squarate-derived angiotensin II inhibitor **88** [99].

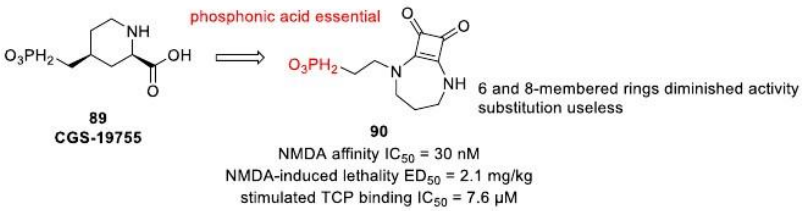

Fig. 28. Fused phosphonoalkyl squaramides as NMDA antagonists [27].

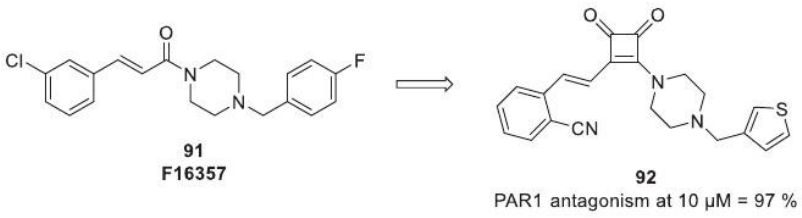

Fig. 29. Squarate-type cinnamoylpiperazine PAR1 antagonists [108].

angiotensin II antagonist [99]. The main purpose of this study was to assess *in vitro* potency as angiotensin II antagonists and the *in vivo* antihypertensive profile of various carboxylic acid bioisosteres including squarates compared with losartan. Unfortunately, squarate **88** was less potent in lowering blood pressure than losartan (Fig. 27) [99].

In another series of NMDA antagonists, the diazabicyclic amino acid phosphonate **90** was found to have equivalent potency as GCS-19755 **89** in the [^{3}H]CPP binding assay, the stimulated [^{3}H]TCP binding assay, and the NMDA-induced lethality model in mice [27]. Compound **90** is a unique NMDA antagonist with a favourable preclinical profile offering an opportunity for the treatment of several neurological disorders (Fig. 28). Extensive SAR exploration indicated that the 6- or 8-membered ring compounds possessed diminished activity and revealed that a 2-carbon side chain is optimal for NMDA receptor affinity. Substitution on the ring was

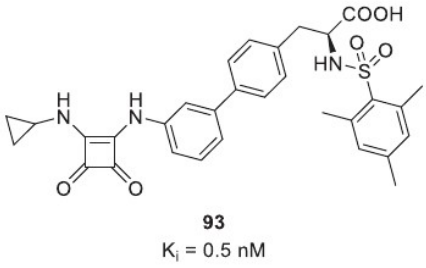

Fig. 30. Biphenyl squaramide as a vitronectin receptor antagonist [109].

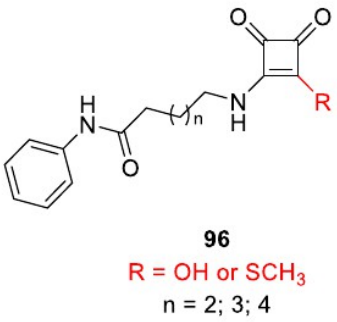

Fig. 32. Squaric acid derivatives as potential HDAC inhibitors [112].

not beneficial, and replacement of the phosphonic acid group was also ineffective [27].

Planty and co-workers synthesized squarate-type cinnamoylpiperazines as new protease activated receptor 1 (PAR1) antagonists [108]. Because human PAR1 is involved in thrombin-induced platelet aggregation, its antagonism should result in novel antiplatelet drugs. Additionally, PAR1 antagonists do not affect thrombin's role in the coagulation cascade and thus have a limited impact on bleeding. All the reported squarate analogues were derived from the cinnamoylpiperazine PAR1 inhibitor F16357 **91** (Fig. 29). Replacement of the carbonyl scaffold by a squarate bioisostere led to very potent PAR1 antagonists such as compound **92**, which showed 97% antagonism at 10 μM (Fig. 29). In contrast, no anti-aggregant properties were detected in an *in vitro* human platelet model [108].

In 2007, other squaramides were investigated as arginine mimetic moieties acting as vitronectin receptor ($\alpha_V\beta_3$) antagonists by Klaus et al. [109]. Squaramide **93** proved to be a subnanomolar $\alpha_V\beta_3$ antagonist (K_i of 0.5 nM) and could be used as a new treatment of restenosis after balloon angioplasty (Fig. 30) [109].

Finally, phosphoglycolipid analogues modified by the squaryl group were studied by Ding and co-workers for their modulatory activity towards the class A G-protein coupled receptor (GPR) 55 [110]. Localized in spinal cord sensory axons, GPR55 plays a key role in neuropathic pain, cancer, and inflammation [111]. In this study, the endogenous ligand lyso-phosphatidyl-β-D-glucoside (LPGlc)-derived analogues with a squaryl diamide group were developed as GPR55 modulators. Compound **95** showed LPGlc-like behaviour and repelled dorsal root ganglion (DRG) nociceptive axons (Fig. 31) [110].

2.9. Various enzyme inhibitors

The first enzyme to highlight in association with squaric acid inhibitors is histone deacetylase (HDAC) [112]. HDAC catalyses the deacetylation of the lysine residues, thereby affecting the chromatin remodelling process, and its inhibition has antiproliferative effects. To prepare suberoylanilide hydroxamic acid (SAHA) analogues as HDAC inhibitors, Hannesian et al. replaced the Zn-binding group (ZBG) with squaric acid, *N*-hydroxyurea, and 4-hydroxymethyl oxazoline moieties (Fig. 32). Subsequently, they tested the inhibitory activity against HADC. Unfortunately, no inhibitory activity against HDAC was observed at concentrations less than 1.0 μM, and no cytotoxicity to tumour cell lines was observed below 20 μM [112].

Another series of squaramide-based hydroxamic acids of general structure **97** were studied as novel class I and IIB HDAC inhibitors for the topical treatment of cutaneous t-cell lymphoma (CTCL) [113]. Fournier et al. targeted *mycosis fungoides*, an early form of CTCL, by a topical approach with HDAC inhibitors with an improved safety profile. As a result, a novel scaffold binding to class I, IIB, and IV HDACs include a hydroxamic acid as ZBG and a squaramide that pinches the Asp104 carboxylate. SAR studies revealed that a *para*-substituted phenyl improves potency and metabolic clearance, whereas a benzylic side chain decreases potency. Additionally, aliphatic branching with small substituents improves organic and aqueous solubility and further increases metabolic clearance. Docking studies also predicted that 5- or 6-carbon linkers would provide the best inhibitory activity. Lead compound **98** showed good potency with an IC_{50} of 7.3 nM in the Hut78 cell line, which was comparable to those of approved drugs (Fig. 33) [113].

The second potential target for tacrine-squaramide inhibitors is acetylcholinesterase (AChE) [114]. This serine protease catalyses the hydrolysis of the acetylcholine (Ach) neurotransmitter to produce choline and acetic acid, which are associated with cognitive impairment and dementia. Because tacrine is a central reversible AChE inhibitor marketed in 1993 for Alzheimer's disease treatment, a series of tacrine-squaramide homodimers was evaluated for their

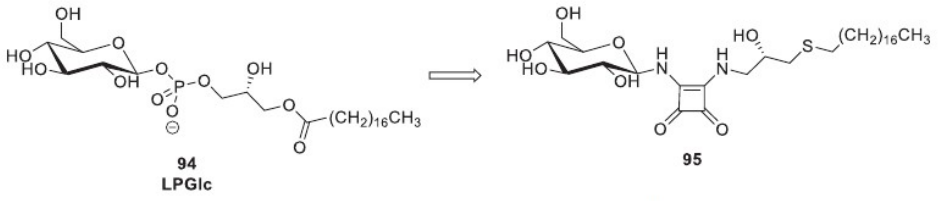

Fig. 31. Squaramide analogue of LPGlc as a GPR55 modulator [110].

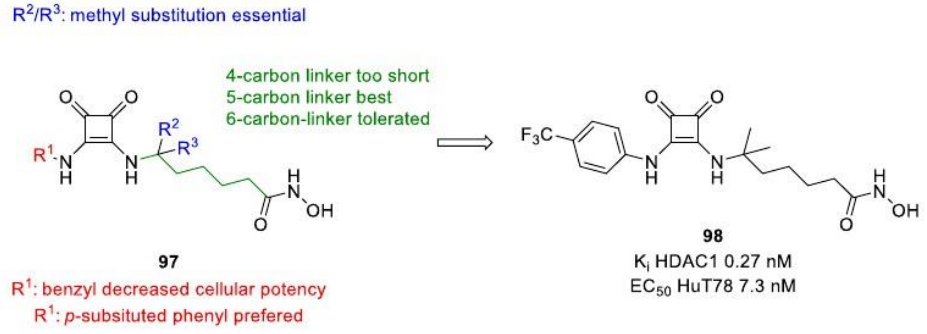

Fig. 33. Squaramide-type inhibitors of class I and IIB HDAC [113].

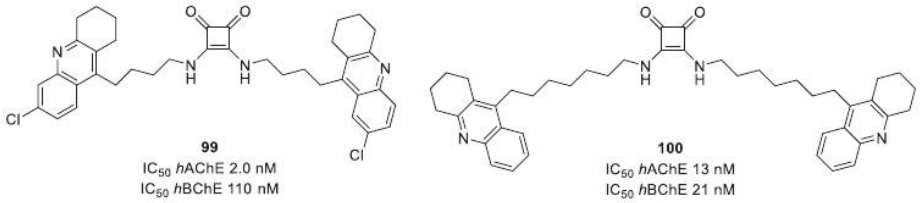

Fig. 34. Tacrine-squaramide cholinesterase inhibitors [114].

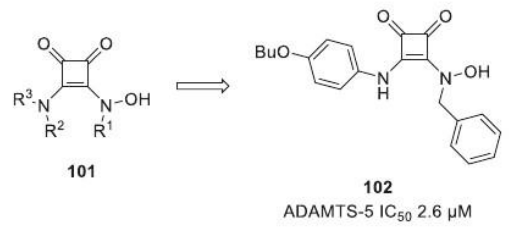

Fig. 35. Squaric acid *N*-hydroxylamide amides as ADAMTS-5 inhibitors [115].

anti-cholinesterase activity to find less toxic analogues. Compounds **99** and **100** exhibited the best inhibition of *h*AChE of 2.0 and 13 nM, respectively, and inhibition of *h*BChE of 110 and 21 nM, respectively (Fig. 34). Moreover, both inhibitors possessed the lowest cytotoxicity to HepG2 cells [114].

In 2018, the parallel synthesis of 200 squaric acid *N*-hydroxylamide amides was performed by Charton et al. [115]. Subsequently, the library was screened against the zinc metalloenzyme ADAMTS-5, thus allowing the identification of the totally new micromolar inhibitor **102** with an IC_{50} of 2.6 μM (Fig. 35) [115].

A series of squaric acid-peptide conjugates of general structures **103** was synthesized and studied as matrix metalloprotease-1 (MMP-1) inhibitors [116]. In general, MMPs are structurally related endopeptidases remodelling the extracellular matrix. Their overexpression is associated with a wide range of pathological conditions such as multiple sclerosis [117], rheumatoid arthritis [118], angiogenesis [119], and metastasis [120]. The squaric acid moiety of all the studied compounds was substituted in the 3-position with various zinc-binding functional groups, and the 4-position was modified with monopeptides or dipeptides interacting with S1′ and

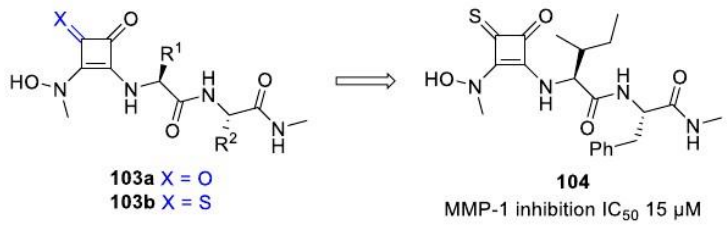

Fig. 36. Squaric acid-based peptidic inhibitors of MMP-1 [116].

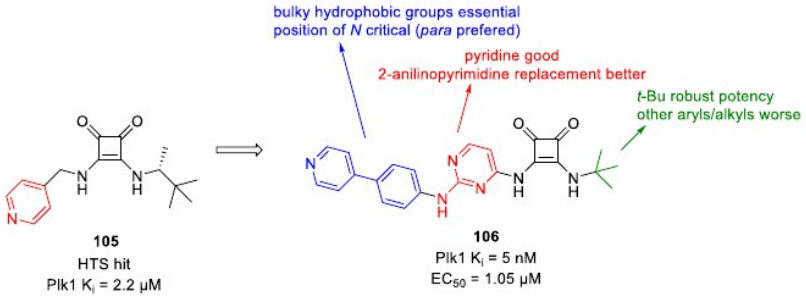

Fig. 37. Squarate-containing polo-like inhibitors [121].

Table 1
The most potent squaric acid analogues with submicromolar biological activity.

Compound	Target(s)	IC_{50} or Ki value(s)
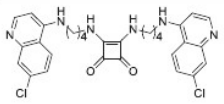	*Mtb* ATP synthase (Myc_ATPS)	IC_{50} = 30 nM
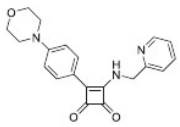	*P. falciparum* (PfW2)	IC_{50} = 95 nM
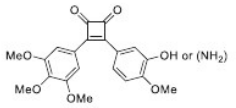	Human leukaemia cells (CEM)	IC_{50} = 1.7 or 1.4 nM
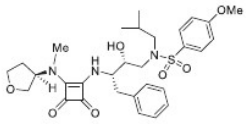	HIV-1 protease	K_i = 0.51 nM
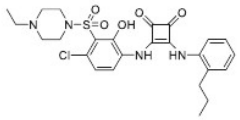	CXCR2	IC_{50} = 8 nM
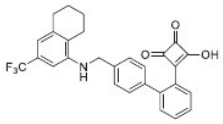	Angiotensin II	IC_{50} = 25 nM
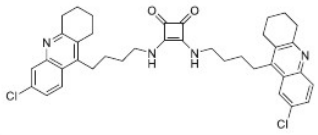	Human acetylcholinesterase (*h*AChE)	IC_{50} = 2.0 nM

S2' enzymatic subsites. Positional scanning revealed that the combination of an −N (Me)OH chelating group and Leu-Tle-NHMe peptide was the best (Fig. 36). Moreover, the conversion of one carbonyl to thiocarbonyl resulted in an 18-fold increase in potency, providing compound **104** with an IC_{50} of 15 μM (Fig. 36) [116].

The last enzyme group known to be influenced by squarate-containing inhibitors are polo-like kinases (Plks) [121]. Plks are serine/threonine kinases involved in the regulation of cell cycle *via* G2 and mitosis, thus controlling cell proliferation. Recently, ATP-competitive Plk1 inhibitors have inspired Zhang et al. to perform hit-to-lead optimization of an initial HTS hit **105** (Fig. 37). Molecular modelling revealed the importance of a hydrophobic aromatic amine side chain that enables H-binding. However, the incorporation of a 2-anilinepyrimidine moiety as a replacement for the 4-pyridyl significantly improved kinase affinity. Considering the substitution of the 2-aniline pyrimidine scaffold, hydrophobic aromatic cores interacting along the sidechain of Arg136 were beneficial. To attain acceptable pharmacokinetic properties, a simple *t*-butyl aliphatic right-hand side chain showed robust potency. Moreover, the position of the pyridine nitrogen was a critical parameter with the *para* position preferred. Finally, extensive SAR studies led to inhibitor **106** with Plk1 $K_i = 5$ nM and $ED_{50} = 1.05$ μM and moderate efficacy at 100 mpk in a MiaPaCa tumour model [121].

3. Conclusions and future perspectives

Squaric acid derivatives, squaramides, squaramines, and squarates are very simple, yet highly useful molecules. Despite these structures being discovered many decades ago by synthetic organic chemists, their use as potential therapeutics has only been explored quite recently. The main reason for this was their appearance; the structures include highly reactive functionalities that are usually associated with negative side-effects, such as toxicity, lack of selectivity, and promiscuity towards various molecular targets. Such compounds are generally not appreciated by pharmaceutical companies and regulatory organizations despite their superior pharmacological activity, because they often fail in late phases of drug development after large investments have been made and, in some of the worst cases, after they cause severe damage to the health of the first patients. However, such a strict selection of compounds entering the primary screening along with growing drug resistance emerging for the majority of infectious agents, cancers, etc. has resulted in a lack of effective drugs for some of the most prevalent illnesses. This environment has led to renewed attention to some of the previously overlooked compounds, including derivatives of squaric acid. These compounds have a variety of biological activities in low concentrations (often submicromolar), such as antiparasitic, antibacterial, cytotoxic, and antiviral activity, and some have known mechanisms of action (they inhibit certain receptors, enzymes, etc.), which makes them potentially useful in drug development. Ongoing research covering diverse fields of medicinal chemistry has revealed several small squaric acid analogues with significant biological activity; the most potent scaffolds from each group are summarized in Table 1.

Therefore, several compounds have passed clinical trials, and although none are on the market yet, it is very likely that this will change soon. Squaric acid analogues have been overlooked by medicinal chemists for some time but this has changed. In the future, all of the synthesized analogues of squaric acid should be tested for possible biological activities, and if they are selected for the development of a potential new drug, their toxicity should be carefully evaluated using *in vitro* experiments initially. Advanced *in vivo* toxicology experiments should follow as soon as possible to distinguish between compounds with selective activity to a druggable target and compounds with toxic side effects.

Declaration of competing interest

The authors declare that they have no known competing financial interests or personal relationships that could have appeared to influence the work reported in this paper.

Acknowledgement

This work was supported by grant no. JG_2019_002 and by an internal grant (IGA_PrF_2020_012) from Palacký University in Olomouc, Czech Republic.

References

[1] X. Han, H. Zhou, C. Dong, Applications of chiral squaramides: from asymmetric organocatalysis to biologically active compounds, Chem. Rec. 16 (2016) 897–906.
[2] R.I. Storer, C. Aciro, L.H. Jones, Squaramides: physical properties, synthesis and applications, Chem. Soc. Rev. 40 (2011) 2330–2346.
[3] F.R. Wurm, H.-A. Klok, Be squared: expanding the horizon of squaric acid-mediated conjugations, Chem. Soc. Rev. 42 (2013) 8220–8236.
[4] A. Mukkanti, M. Periasamy, Methods of synthesis of cyclobutenediones, Arkivoc 11 (2005) 48–77.
[5] S. Sopeña, E. Martin, E.C. Escudero-Adán, A.W. Kleij, Pushing the limits with squaramide-based organocatalysts in cyclic carbonate synthesis, ACS Catal. 7 (2017) 3532–3539.
[6] D.E. Lynch, D.G. Hamilton, Microreview: pyrrol-3-yl squaraines (including indol-3-yl squaraines), J. Heterocycl. Chem. 55 (2018) 1249–1262.
[7] J.P. Malerich, K. Hagihara, V.H. Rawal, Chiral squaramide derivatives are excellent hydrogen bond donor catalysts, J. Am. Chem. Soc. 130 (2008) 14416–14417.
[8] A. Rouf, C. Tanyeli, Squaramide based organocatalysts in organic transformations, Curr. Org. Chem. 20 (2016) 2996–3013.
[9] S. Karahan, C. Tanyeli, Squaramide catalyzed α-chiral amine synthesis, Tetrahedron Lett. 59 (2018) 3725–3737.
[10] P. Chen, G. Dong, Cyclobutenones and benzocyclobutenones: versatile synthons in organic synthesis, Chemistry 22 (2016) 18290.
[11] T.S. Elliott, A. Slowey, Y. Ye, S.J. Conway, The use of phosphate bioisosteres in medicinal chemistry and chemical biology, Med. Chem. Comm. 3 (2012) 735–751.
[12] P. Kováč, P. Xu, Controlled and highly efficient preparation of carbohydrate-based vaccines: squaric acid chemistry is the way to go, Carbohydr. Chem. 42 (2017) 83–115.
[13] M.D. Laramie, A. Levitz, M. Henary, Cyanine and squaric acid metal sensors, Sensor. Actuator. B Chem. 243 (2017) 1191–1204.
[14] C. Tong, T. Liu, V. Saez Talens, W.E.M. Noteborn, T.H. Sharp, M.M.R.M. Hendrix, I.K. Voets, C.L. Mummery, V.V. Orlova, R.E. Kieltyka, Squaramide-based supramolecular materials for three-dimensional cell culture of human induced pluripotent stem cells and their derivatives, Biomacromolecules 19 (2018) 1091–1099.
[15] X. Qian, C. Jin, X. Zhang, Y. Jiang, C. Lin, L. Wang, Squaramide derivatives and their applications in ion recognition, Prog. Chem. 26 (2014) 1701.
[16] I. Castro, M.L. Calatayud, J. Sletten, M. Julve, F. Lloret, Squarate and croconate in designing one-and two-dimensional oxamidato-bridged copper (II) complexes: synthesis, crystal structures and magnetic properties of $[Cu_2(apox)(C_4O_4)(H_2O)_2]_n \cdot nH_2O$ and $[Cu_4(apox)_2(C_5O_5)_2] \cdot 6H_2O$, Comptes Rendus l'Académie Des Sci. IIC-Chemistry 4 (2001) 235–243.
[17] W. Cheuquepán, J. Martínez-Olivares, A. Rodes, J.M. Orts, Squaric acid adsorption and oxidation at gold and platinum electrodes, J. Electroanal. Chem. 819 (2018) 178–186.
[18] E.J. Smutny, J.D. Roberts, Phenylcyclobutadienoquinone, J. Am. Chem. Soc. 77 (1955) 3420.
[19] M. Julia, A. Rouault, Synthesis of cyclobutanecarboxylic acids, Bull. Soc. Chim. Fr. (1959) 1833–1840.
[20] S. Cohen, J.R. Lacher, J.D. Park, Diketocyclobutenediol, J. Am. Chem. Soc. 81 (1959) 3480.
[21] S.L. Kitson, Squaryl molecular metaphors-application to rational drug design and imaging agents, J. Diagnostic Imaging Ther 4 (2017) 35–75.
[22] L.M. Schwartz, L.O. Howard, Conductance study of squaric acid aqueous dissociation, J. Phys. Chem. 75 (1971) 1798–1803.
[23] P. von R. Schleyer, C. Maerker, A. Dransfeld, H. Jiao, N.J.R. van Eikema Hommes, Nucleus-independent chemical shifts: a simple and efficient aromaticity probe, J. Am. Chem. Soc. 118 (1996) 6317–6318.
[24] P. von R. Schleyer, K. Najafian, B. Kiran, H. Jiao, Are oxocarbon dianions aromatic? J. Org. Chem. 65 (2000) 426–431.
[25] D. Quiñonero, A. Frontera, P. Ballester, P.M. Deyà, A theoretical study of aromaticity in squaramide and oxocarbons, Tetrahedron Lett. 41 (2000) 2001–2005.
[26] C. Garau, A. Frontera, P. Ballester, D. Quiñonero, A. Costa, P.M. Deyà, A theoretical ab initio study of the capacity of several binding units for the

molecular recognition of anions, Eur. J. Org. Chem. 2005 (2005) 179–183.
[27] W.A. Kinney, M. Abou-Gharbia, D.T. Garrison, J. Schmid, D.M. Kowal, D.R. Bramlett, T.L. Miller, R.P. Tasse, M.M. Zaleska, J.A. Moyer, Design and synthesis of [2-(8,9-Dioxo-2,6-diazabicyclo[5.2.0]non-1(7)-en-2-yl)-ethyl] phosphonic acid (EAA-090), a potent *N*-Methyl-D-aspartate antagonist, via the use of 3-cyclobutene-1, 2-dione as an achiral α-amino acid bioisostere, J. Med. Chem. 41 (1998) 236–246.
[28] R.B. Baudy, J.A. Butera, M.A. Abou-Gharbia, H. Chen, B. Harrison, U. Jain, R. Magolda, J.Y. Sze, M.R. Brandt, T.A. Cummons, Prodrugs of perzinfotel with improved oral bioavailability, J. Med. Chem. 52 (2009) 771–778.
[29] K. Jaeger, S. Bruenle, T. Weinert, W. Guba, J. Muehle, T. Miyazaki, M. Weber, A. Furrer, N. Haenggi, T. Tetaz, Structural basis for allosteric ligand recognition in the human CC chemokine receptor 7, Cell 178 (2019) 1222–1230.
[30] S.I. Rennard, D.C. Dale, J.F. Donohue, F. Kanniess, H. Magnussen, E.R. Sutherland, H. Watz, S. Lu, P. Stryszak, E. Rosenberg, CXCR2 antagonist MK-7123. A phase 2 proof-of-concept trial for chronic obstructive pulmonary disease, Am. J. Respir. Crit. Care Med 191 (2015) 1001–1011.
[31] M.A. Palli, H. McTavish, A. Kimball, T.D. Horn, Immunotherapy of recurrent herpes labialis with squaric acid, JAMA Dermatol. 153 (2017) 828–829.
[32] A.L.S. Chang, G. Honari, L. Guan, L. Zhao, M.A. Palli, T.D. Horn, A.Z. Dudek, H. McTavish, A phase 2, Multi-center, Placebo-controlled study of single dose squaric acid dibutyl ester (SADBE) to reduce frequency of outbreaks in subjects with recurrent herpes labialis, J. Am. Acad. Dermatol. (2020). https://www.sciencedirect.com/science/article/abs/pii/S0190962220305612.
[33] S. Okabe, T. Nishida, H. Igata, K. Takagi, Effects of IT-066, a new histamine H2-receptor antagonist, on gastric acid secretion and experimental gastric ulcers in rats and dogs, Nihon Yakurigaku Zasshi 95 (1990) 247.
[34] Y. Naito, T. Yoshikawa, K. Matsuyama, N. Yagi, M. Arai, Y. Nakamura, T. Kaneko, N. Yoshida, M. Kondo, Effect of a novel histamine H2 receptor antagonist, IT-066, on acute gastric injury induced by ischemia-reperfusion in rats, and its antioxidative properties, Eur. J. Pharmacol. 294 (1995) 47–54.
[35] K. Kato, S. Jingu, N. Ogawa, S. Higuchi, Development and validation of a liquid chromatographic–tandem mass spectrometric method for the determination of pibutidine in human urine, J. Chromatogr. B Biomed. Sci. Appl. 740 (2000) 187–193.
[36] T. Oshima, Repeated dose toxicity study of 3-amino-4-[[(Z)-4-[[4-(piperidiomethyl)-2-pyridyl] oxy]-2-butenyl] amino]-3-cyclobutene-1, 2-dione monohydrochloride (Pibutidine hydrochloride) in rats (1): 13-week oral toxicity study with 4-week recovery test, Jpn. Pharmacol. Ther. 27 (1999) 331–345.
[37] C.J. Gavey, J.T.L. Smith, C.U. Nwokolo, R.E. Pounder, The effect of SK&F 94482 (BMY-25368) on 24-hour intragastric acidity and plasma gastrin concentration in healthy subjects, Aliment. Pharmacol. Ther. 3 (1989) 557–564.
[38] R.L. Cavanagh, J.P. Buyniski, Effect of BMY-25368, a potent and long-acting histamine H2-receptor antagonist, on gastric secretion and aspirin-induced gastric lesions in the dog, Aliment. Pharmacol. Ther. 3 (1989) 299–313.
[39] S.J. Tantry, S.D. Markad, V. Shinde, J. Bhat, G. Balakrishnan, A.K. Gupta, A. Ambady, A. Raichurkar, C. Kedari, S. Sharma, N.V. Mudugal, A. Narayan, C.N. Naveen Kumar, R. Nanduri, S. Bharath, J. Reddy, V. Panduga, K.R. Prabhakar, K. Kandaswamy, R. Saralaya, P. Kaur, N. Dinesh, S. Guptha, K. Rich, D. Murray, H. Plant, M. Preston, H. Ashton, D. Plant, J. Walsh, P. Alcock, K. Naylor, M. Collier, J. Whiteaker, R.E. McLaughlin, M. Mallya, M. Panda, S. Rudrapatna, V. Ramachandran, R. Shandil, V.K. Sambandamurthy, K. Mdluli, C.B. Cooper, H. Rubin, T. Yano, P. Iyer, S. Narayanan, S. Kavanagh, K. Mukherjee, V. Balasubramanian, V.P. Hosagrahara, S. Solapure, S. Ravishankar, S. Hameed, P, discovery of imidazo[1,2-a]pyridine ethers and squaramides as selective and potent inhibitors of mycobacterial adenosine triphosphate (ATP) synthesis, J. Med. Chem. 60 (2017) 1379–1399, https://doi.org/10.1021/acs.jmedchem.6b01358.
[40] L.A. Marchetti, L.K. Kumawat, N. Mao, J.C. Stephens, R.B.P. Elmes, The versatility of squaramides: from supramolecular chemistry to chemical biology, Chem. 5 (2019) 1398–1485.
[41] S. Nagy, P. Kisszékelyi, J. Kupai, Synthesis and application of thiosquaramides and their derivatives: a review, period, Polytech. Chem. Eng 62 (2018) 467–475.
[42] F. Olmo, C. Rotger, I. Ramírez-Macías, L. Martínez, C. Marín, L. Carreras, K. Urbanova, M. Vega, G. Chaves-Lemaur, A. Sampedro, Synthesis and biological evaluation of N, N′-squaramides with high in vivo efficacy and low toxicity: toward a low-cost drug against Chagas disease, J. Med. Chem. 57 (2014) 987–999.
[43] D. Cui, D. Prashar, P. Sejwal, Y.-Y. Luk, Water-driven ligations using cyclic amino squarates: a class of useful SN1-like reactions, Chem. Commun. 47 (2011) 1348–1350.
[44] P.C.M. Chan, R.J. Roon, J.F. Koerner, N.J. Taylor, J.F. Honek, A 3-Amino-4-hydroxy-3-cyclobutene-1, 2-dione-Containing glutamate analog exhibiting high affinity to excitatory amino acid receptors, J. Med. Chem. 38 (1995) 4433–4438.
[45] F. Soukarieh, M.W. Nowicki, A. Bastide, T. Pöyry, C. Jones, K. Dudek, G. Patwardhan, F. Meullenet, N.J. Oldham, M.D. Walkinshaw, Design of nucleotide-mimetic and non-nucleotide inhibitors of the translation initiation factor eIF4E: synthesis, structural and functional characterisation, Eur. J. Med. Chem. 124 (2016) 200–217.
[46] S. Niewiadomski, Z. Beebeejaun, H. Denton, T.K. Smith, R.J. Morris, G.K. Wagner, Rationally designed squaryldiamides–a novel class of sugar-nucleotide mimics? Org. Biomol. Chem. 8 (2010) 3488–3499.
[47] Y. Zhang, M. Jumppanen, M.M. Maksimainen, S. Auno, Z. Awol, L. Ghemtio, H. Venkannagari, L. Lehtiö, J. Yli-Kauhaluoma, H. Xhaard, Adenosine analogs bearing phosphate isosteres as human MDO1 ligands, Bioorg. Med. Chem. 26 (2018) 1588–1597.
[48] E. Dürr, W. Doherty, S.Y. Lee, A.H. El-Sagheer, A. Shivalingam, P.J. McHugh, T. Brown, J.F. McGouran, Squaramide-based 5′-phosphate replacements bind to the DNA repair exonuclease SNM1A, ChemistrySelect 3 (2018) 12824–12829.
[49] K. Sato, K. Seio, M. Sekine, Squaryl group as a new mimic of phosphate group in modified oligodeoxynucleotides: synthesis and properties of new oligodeoxynucleotide analogues containing an internucleotidic squaryldiamide linkage, J. Am. Chem. Soc. 124 (2002) 12715–12724.
[50] M. Fonvielle, N. Sakkas, L. Iannazzo, C. Le Fournis, D. Patin, D. Mengin-Lecreulx, A. El-Sagheer, E. Braud, S. Cardon, T. Brown, Electrophilic RNA for peptidyl-RNA synthesis and site-specific cross-linking with tRNA-binding enzymes, Angew. Chemie 128 (2016) 13751–13755.
[51] M. Hocek, Synthesis of base-modified 2′-deoxyribonucleoside triphosphates and their use in enzymatic synthesis of modified DNA for applications in bioanalysis and chemical biology, J. Org. Chem. 79 (2014) 9914–9921.
[52] M. Hocek, Enzymatic synthesis of base-functionalized nucleic acids for sensing, cross-linking, and modulation of protein–DNA binding and transcription, Acc. Chem. Res. 52 (2019) 1730–1737.
[53] K.T. Andrews, G. Fisher, T.S. Skinner-Adams, Drug repurposing and human parasitic protozoan diseases, Int. J. Parasitol. Drugs Drug Resist 4 (2014) 95–111.
[54] W.H. Organization, Chagas disease in Latin America: an epidemiological update based on 2010 estimates, Wkly. Epidemiol. Rec. Relev. Épidémiologique Hebd 90 (2015) 33–44.
[55] C. Marín, M. Ximenis, I. Ramirez-Macías, C. Rotger, K. Urbanova, F. Olmo, R. Martín-Escolano, M.J. Rosales, R. Cañas, R. Gutierrez-Sánchez, Effective anti-leishmanial activity of minimalist squaramide-based compounds, Exp. Parasitol. 170 (2016) 36–49.
[56] R. Martín-Escolano, C. Marín, M. Vega, Á. Martin-Montes, E. Medina-Carmona, C. López, C. Rotger, A. Costa, M. Sánchez-Moreno, Synthesis and biological evaluation of new long-chain squaramides as anti-chagasic agents in the BALB/c mouse model, Bioorg. Med. Chem. 27 (2019) 865–879.
[57] C.J.A. Ribeiro, S.P. Kumar, J. Gut, L.M. Goncalves, P.J. Rosenthal, R. Moreira, M.M.M. Santos, Squaric acid/4-aminoquinoline conjugates: novel potent antiplasmodial agents, Eur. J. Med. Chem. 69 (2013) 365–372.
[58] C.J.A. Ribeiro, M. Espadinha, M. Machado, J. Gut, L.M. Gonçalves, P.J. Rosenthal, M. Prudêncio, R. Moreira, M.M.M. Santos, Novel squaramides with in vitro liver stage antiplasmodial activity, Bioorg. Med. Chem. 24 (2016) 1786–1792.
[59] S.P. Kumar, P.M.C. Glória, L.M. Gonçalves, J. Gut, P.J. Rosenthal, R. Moreira, M.M.M. Santos, Squaric acid: a valuable scaffold for developing antimalarials? Med. Chem. Comm. 3 (2012) 489–493.
[60] P.M.C. Glória, J. Gut, L.M. Gonçalves, P.J. Rosenthal, R. Moreira, M.M.M. Santos, Aza vinyl sulfones: synthesis and evaluation as antiplasmodial agents, Bioorg. Med. Chem. 19 (2011) 7635–7642.
[61] A.S. Nagle, S. Khare, A.B. Kumar, F. Supek, A. Buchynskyy, C.J.N. Mathison, N.K. Chennamaneni, N. Pendem, F.S. Buckner, M.H. Gelb, Recent developments in drug discovery for leishmaniasis and human African trypanosomiasis, Chem. Rev. 114 (2014) 11305–11347.
[62] W.H. Organization, Chagas disease-epidemiology, WHO, 2018. WHO. Available, Https//www.Who.Int/Chagas/Epidemiology/En/. (Accessed 1 August 2019).
[63] J.D. Maya, B.K. Cassels, P. Iturriaga-Vásquez, J. Ferreira, M. Faúndez, N. Galanti, A. Ferreira, A. Morello, Mode of action of natural and synthetic drugs against Trypanosoma cruzi and their interaction with the mammalian host, Comp. Biochem. Physiol. Part A Mol. Integr. Physiol 146 (2007) 601–620.
[64] S.R. Wilkinson, C. Bot, J.M. Kelly, B.S. Hall, Trypanocidal activity of nitroaromatic prodrugs: current treatments and future perspectives, Curr. Top. Med. Chem. 11 (2011) 2072–2084.
[65] K. Kojima, K. Nakajima, H. Kurata, K. Tabata, Y. Utsui, Synthesis of a piperidinomethylthiophene derivative as H2-antagonist with inhibitory activity against Helicobacter pylori, Bioorg. Med. Chem. Lett 6 (1996) 1795–1798.
[66] H. Kijima, Y. Isobe, M. Muramatsu, S. Yokomori, M. Suzuki, S. Higuchi, Structure–activity characterization of an H2-receptor antagonist, 3-Amino-4-[4-[4-(1-piperidinomethyl)-2-pyridyloxy]-cis-2-butenylamino]-3-cyclobutene-1, 2-dione hydrochloride (IT-066), involved in the insurmountable Antagonism against histamine-induced P, Biochem. Pharmacol. 55 (1998) 151–157.
[67] C. Grabosch, M. Hartmann, J. Schmidt-Lassen, T.K. Lindhorst, Squaric acid monoamide mannosides as ligands for the bacterial lectin FimH: covalent inhibition or not? Chembiochem 12 (2011) 1066–1074.
[68] T.K. Lindhorst, K. Bruegge, A. Fuchs, O. Sperling, A bivalent glycopeptide to target two putative carbohydrate binding sites on FimH, Beilstein J. Org. Chem. 6 (2010) 801–809.
[69] K. Ohlsen, T.A. Oelschlaeger, J. Hacker, A.S. Khan, Carbohydrate receptors of bacterial adhesins: implications and reflections, in: Glycosci. Microb. Adhes, Springer, 2008, pp. 17–65.
[70] V. Molodtsov, P.R. Fleming, C.J. Eyermann, A.D. Ferguson, M.A. Foulk, D.C. McKinney, C.E. Masse, E.T. Buurman, K.S. Murakami, X-ray crystal

structures of Escherichia coli RNA polymerase with switch region binding inhibitors enable rational design of squaramides with an improved fraction unbound to human plasma protein, J. Med. Chem. 58 (2015) 3156–3171.
[71] E.T. Buurman, M.A. Foulk, N. Gao, V.A. Laganas, D.C. McKinney, D.T. Moustakas, J.A. Rose, A.B. Shapiro, P.R. Fleming, Novel rapidly diversifiable antimicrobial RNA polymerase switch region inhibitors with confirmed mode of action in Haemophilus influenzae, J. Bacteriol. 194 (2012) 5504–5512.
[72] K. Andries, P. Verhasselt, J. Guillemont, H.W.H. Göhlmann, J.-M. Neefs, H. Winkler, J. Van Gestel, P. Timmerman, M. Zhu, E. Lee, A diarylquinoline drug active on the ATP synthase of Mycobacterium tuberculosis, Science (80-.) 307 (2005) 223–227.
[73] C. Geadas, S.K. Stoszek, D. Sherman, B.B. Andrade, S. Srinivasan, C.D. Hamilton, J. Ellner, Advances in basic and translational tuberculosis research: proceedings of the first meeting of RePORT international, Tuberculosis 102 (2017) 55–67.
[74] V. Fernández-Moreira, J.V. Alegre-Requena, R.P. Herrera, I. Marzo, M.C. Gimeno, Synthesis of luminescent squaramide monoesters: cytotoxicity and cell imaging studies in HeLa cells, RSC Adv. 6 (2016) 14171–14177.
[75] Z. Liu, Y. Wang, Y. Han, L. Liu, J. Jin, H. Yi, Z. Li, J. Jiang, D.W. Boykin, Synthesis and antitumor activity of novel 3, 4-diaryl squaric acid analogs, Eur. J. Med. Chem. 65 (2013) 187–194.
[76] K.A. López, M.N. Pina, R. Alemany, O. Vögler, F. Barcelo, J. Morey, Antifolate-modified iron oxide nanoparticles for targeted cancer therapy: inclusion vs. covalent union, RSC Adv. 4 (2014) 19196–19204.
[77] M. Lu, Q.-B. Lu, J.F. Honek, Squarate-based carbocyclic nucleosides: syntheses, computational analyses and anticancer/antiviral evaluation, Bioorg. Med. Chem. Lett 27 (2017) 282–287.
[78] M. Quintana, J.V. Alegre-Requena, E. Marqués-López, R.P. Herrera, G. Triola, Squaramides with cytotoxic activity against human gastric carcinoma cells HGC-27: synthesis and mechanism of action, Med. Chem. Comm. 7 (2016) 550–561.
[79] P. Villalonga, S.F. de Mattos, G. Ramis, A. Obrador-Hevia, A. Sampedro, C. Rotger, A. Costa, Cyclosquaramides as kinase inhibitors with anticancer activity, ChemMedChem 7 (2012) 1472–1480.
[80] S. Grabner, B. Modec, M. Čemažar, N. Bukovec, Crystal structures and cytotoxicity of isopropylamine Pt (II) complexes: a trinuclear squarato-bridged [Pt3 (μ2-C4O4) 3 (H2NPri) 6]· 3H2O and a mononuclear cis-[Pt (NO3) 2 (H2NPri) 2], J. Inorg. Biochem. 99 (2005) 1465–1471.
[81] W. Doherty, E.-M. Dürr, H.T. Baddock, S.Y. Lee, P.J. McHugh, T. Brown, M.O. Senge, E.M. Scanlan, J.F. McGouran, A hydroxamic-acid-containing nucleoside inhibits DNA repair nuclease SNM1A, Org. Biomol. Chem. 17 (2019) 8094–8105.
[82] W.H. Organization, Hiv/Aids Key Facts, 2018, 2018. Available Online WHO, Https//www.Who.Int/News-Room/Fact-Sheets/Detail/Hiv-Aids. (Accessed 5 August 2019).
[83] T. Cihlar, M. Fordyce, Current status and prospects of HIV treatment, Curr. Opin. Virol 18 (2016) 50–56.
[84] C.-W. Lee, H. Cao, K. Ichiyama, T.M. Rana, Design and synthesis of a novel peptidomimetic inhibitor of HIV-1 Tat–TAR interactions: squaryldiamide as a new potential bioisostere of unsubstituted guanidine, Bioorg. Med. Chem. Lett 15 (2005) 4243–4246.
[85] A.K. Ghosh, J.N. Williams, S. Kovela, J. Takayama, H.M. Simpson, D.E. Walters, S. Hattori, M. Aoki, H. Mitsuya, Potent HIV-1 protease inhibitors incorporating squaramide-derived P2 ligands: design, synthesis, and biological evaluation, Bioorg. Med. Chem. Lett 29 (2019) 2565–2570.
[86] R. Feniger-Barish, I. Yron, T. Meshel, E. Matityahu, A. Ben-Baruch, IL-8-induced migratory responses through CXCR1 and CXCR2: association with phosphorylation and cellular redistribution of focal adhesion kinase, Biochemistry 42 (2003) 2874–2886.
[87] R.W. Chapman, J.E. Phillips, R.W. Hipkin, A.K. Curran, D. Lundell, J.S. Fine, CXCR2 antagonists for the treatment of pulmonary disease, Pharmacol. Ther. 121 (2009) 55–68.
[88] D.J. Nicholls, N.P. Tomkinson, K.E. Wiley, A. Brammall, L. Bowers, C. Grahames, A. Gaw, P. Meghani, P. Shelton, T.J. Wright, Identification of a putative intracellular allosteric antagonist binding-site in the CXC chemokine receptors 1 and 2, Mol. Pharmacol. 74 (2008) 1193–1202.
[89] K. Salchow, M.E. Bond, S.C. Evans, N.J. Press, S.J. Charlton, P.A. Hunt, M.E. Bradley, A common intracellular allosteric binding site for antagonists of the CXCR2 receptor, Br. J. Pharmacol. 159 (2010) 1429–1439.
[90] L.E. Donnelly, P.J. Barnes, Chemokine receptors as therapeutic targets in chronic obstructive pulmonary disease, Trends Pharmacol. Sci. 27 (2006) 546–553.
[91] W. Gonsiorek, X. Fan, D. Hesk, J. Fossetta, H. Qiu, J. Jakway, M. Billah, M. Dwyer, J. Chao, G. Deno, Pharmacological characterization of Sch527123, a potent allosteric CXCR1/CXCR2 antagonist, J. Pharmacol. Exp. Therapeut. 322 (2007) 477–485.
[92] B.W. McCleland, R.S. Davis, M.R. Palovich, K.L. Widdowson, M.L. Werner, M. Burman, J.J. Foley, D.B. Schmidt, H.M. Sarau, M. Rogers, Comparison of N, N′-diarylsquaramides and N, N′-diarylureas as antagonists of the CXCR2 chemokine receptor, Bioorg. Med. Chem. Lett 17 (2007) 1713–1717.
[93] J. Busch-Petersen, Y. Wang, Phenol-containing antagonists of the CXCR2 receptor, Expert Opin. Ther. Pat. 18 (2008) 629–637.
[94] M.P. Dwyer, P. Biju, Discovery of 3, 4-diaminocyclobut-3-ene-1, 2-dione-based CXCR2 receptor antagonists for the treatment of inflammatory disorders, Curr. Top. Med. Chem. 10 (2010) 1339–1350.
[95] B. Martin, X. Lai, U. Baettig, E. Neumann, T. Kuhnle, D. Porter, R. Robinson, J. Hatto, A.-M. D'Souza, O. Steward, Early process development of a squaramide-based CXCR2 receptor antagonist, Org. Process Res. Dev. 19 (2015) 1038–1043.
[96] N.A. Meanwell, Synopsis of some recent tactical application of bioisosteres in drug design, J. Med. Chem. 54 (2011) 2529–2591.
[97] H.L. Friedman, Influence of isosteric replacements upon biological activity, Nasnrs 206 (1951) 295–358.
[98] L.M. Lima, E.J. Barreiro, Bioisosterism: a useful strategy for molecular modification and drug design, Curr. Med. Chem. 12 (2005) 23–49.
[99] R.M. Soll, W.A. Kinney, J. Primeau, L. Garrick, R.J. McCaully, T. Colatsky, G. Oshiro, C.H. Park, D. Hartupee, V. White, 3-hydroxy-3-cyclobutene-1, 2-dione: application of novel carboxylic acid bioisostere to an in-vivo active non-tetrazole angiotensin-II antagonist, Bioorg. Med. Chem. Lett 3 (1993) 757–760.
[100] W.A. Kinney, N.E. Lee, D.T. Garrison, E.J. Podlesny Jr., J.T. Simmonds, D. Bramlett, R.R. Notvest, D.M. Kowal, R.P. Tasse, Bioisosteric replacement of the. alpha.-amino carboxylic acid functionality in 2-amino-5-phosphonopentanoic acid yields unique 3, 4-diamino-3-cyclobutene-1, 2-dione containing NMDA antagonists, J. Med. Chem. 35 (1992) 4720–4726.
[101] J.A. Butera, M.M. Antane, S.A. Antane, T.M. Argentieri, C. Freeden, R.F. Graceffa, B.H. Hirth, D. Jenkins, J.R. Lennox, E. Matelan, Design and SAR of novel potassium channel openers targeted for urge urinary incontinence. 1. N-Cyanoguanidine bioisosteres possessing in vivo bladder selectivity, J. Med. Chem. 43 (2000) 1187–1202.
[102] K. Seio, T. Miyashita, K. Sato, M. Sekine, Synthesis and properties of new nucleotide analogues possessing squaramide moieties as new phosphate isosters, Eur. J. Org Chem. 2005 (2005) 5163–5170.
[103] J. Xie, A.B. Comeau, C.T. Seto, Squaric acids: a new motif for designing inhibitors of protein tyrosine phosphatases, Org. Lett. 6 (2004) 83–86.
[104] E. Von Behring, S. Kitasato, The mechanism of diphtheria immunity and tetanus immunity in animals. 1890, Mol. Immunol. 28 (1991) 1317–1319.
[105] B. Palitzsch, N. Gaidzik, N. Stergiou, S. Stahn, S. Hartmann, B. Gerlitzki, N. Teusch, P. Flemming, E. Schmitt, H. Kunz, A synthetic glycopeptide vaccine for the induction of a monoclonal antibody that differentiates between normal and tumor mammary cells and enables the diagnosis of human pancreatic cancer, Angew. Chemie Int. Ed. 55 (2016) 2894–2898.
[106] P. Xu, M. Kelly, W.F. Vann, F. Qadri, E.T. Ryan, P. Kováč, Conjugate vaccines from bacterial antigens by squaric acid chemistry: a closer look, Chembiochem 18 (2017) 799–815.
[107] B. Engelsen, Neurotransmitter glutamate: its clinical importance, Acta Neurol. Scand. 74 (1986) 337–355.
[108] B. Planty, C. Pujol, M. Lamothe, C. Maraval, C. Horn, B. Le Grand, M. Perez, Exploration of a new series of PAR1 antagonists, Bioorg. Med. Chem. Lett 20 (2010) 1735–1739.
[109] K. Urbahns, M. Härter, M. Albers, D. Schmidt, B. Stelte-Ludwig, U. Brüggemeier, A. Vaupel, C. Gerdes, Biphenyls as potent vitronectin receptor antagonists, Bioorg. Med. Chem. Lett 12 (2002) 205–208.
[110] F. Ding, A.T. Guy, P. Greimel, Y. Hirabayashi, H. Kamiguchi, Y. Ito, Squaryl group modified phosphoglycolipid analogs as potential modulators of GPR55, Chem. Commun. 54 (2018) 8470–8473.
[111] A.T. Guy, Y. Nagatsuka, N. Ooashi, M. Inoue, A. Nakata, P. Greimel, A. Inoue, T. Nabetani, A. Murayama, K. Ohta, Glycerophospholipid regulation of modality-specific sensory axon guidance in the spinal cord, Science 349 (2015) 974–977.
[112] S. Hanessian, V. Vinci, L. Auzzas, M. Marzi, G. Giannini, Exploring alternative Zn-binding groups in the design of HDAC inhibitors: squaric acid, N-hydroxyurea, and oxazoline analogues of SAHA, Bioorg. Med. Chem. Lett 16 (2006) 4784–4787.
[113] J.-F. Fournier, Y. Bhurruth-Alcor, B. Musicki, J. Aubert, M. Aurelly, C. Bouix-Peter, K. Bouquet, L. Chantalat, M. Delorme, B. Drean, Squaramides as novel class I and IIB histone deacetylase inhibitors for topical treatment of cutaneous t-cell lymphoma, Bioorg. Med. Chem. Lett 28 (2018) 2985–2992.
[114] B. Svobodova, E. Mezeiova, V. Hepnarova, M. Hrabinova, L. Muckova, T. Kobrlova, D. Jun, O. Soukup, M.L. Jimeno, J. Marco-Contelles, Exploring structure-activity relationship in tacrine-squaramide derivatives as potent cholinesterase inhibitors, Biomolecules 9 (2019) 379.
[115] J. Charton, B.P. Déprez, R.F. Déprez-Poulain, Synthesis of a 200-member library of squaric acid N-hydroxylamide amides, Bioorg. Med. Chem. Lett 18 (2008) 4968–4971.
[116] M.B. Onaran, A.B. Comeau, C.T. Seto, Squaric acid-based peptidic inhibitors of matrix metalloprotease-1, J. Org. Chem. 70 (2005) 10792–10802.
[117] W. Liedtke, B. Cannella, R.J. Mazzaccaro, J.M. Clements, K.M. Miller, K.W. Wucherpfenning, A.J.H. Gearing, C.S. Raine, Effective treatment of models of multiple sclerosis by matrix metalloproteinase inhibitors, Ann. Neurol. Off. J. Am. Neurol. Assoc. Child Neurol. Soc. 44 (1998) 35–46.
[118] C. Jackson, M. Nguyen, J. Arkell, P. Sambrook, Selective matrix metalloproteinase (MMP) inhibition in rheumatoid arthritis-targetting gelatinase A activation, Inflamm. Res. 50 (2001) 183–186.
[119] C. Fisher, S. Gilbertson-Beadling, E.A. Powers, G. Petzold, R. Poorman, M.A. Mitchell, Interstitial collagenase is required for angiogenesis in vitro, Dev. Biol. 162 (1994) 499–510.
[120] M. Whittaker, C.D. Floyd, P. Brown, A.J.H. Gearing, Design and therapeutic application of matrix metalloproteinase inhibitors, Chem. Rev. 99 (1999)

2735–2776.
[121] Q. Zhang, Z. Xia, M.J. Mitten, L.M. Lasko, V. Klinghofer, J. Bouska, E.F. Johnson, T.D. Penning, Y. Luo, V.L. Giranda, Hit to Lead optimization of a novel class of squarate-containing polo-like kinases inhibitors, Bioorg. Med. Chem. Lett 22 (2012) 7615–7622.
[123] Ivana Ivancová, et al., Squaramate-Modified Nucleotides and DNAfor Specific Cross-Linking with Lysine-Containing Peptides and Proteins, Angewandte Chemie (2019), https://doi.org/10.1002/anie.201906737.

Appendix 3

Novel thiazolidinedione-hydroxamates as inhibitors of Mycobacterium tuberculosis virulence factor Zmp1

Šlachtová, V.; Šebela, M.; Torfs, E.; Oorts, L.; Cappoen, D.; Berka, K.; Bazgier, V.; **Brulíková, L.***

Eur. J. Med. Chem. **2020**, *185,* 111812.

European Journal of Medicinal Chemistry 185 (2020) 111812

Contents lists available at ScienceDirect

European Journal of Medicinal Chemistry

journal homepage: http://www.elsevier.com/locate/ejmech

Research paper

Novel thiazolidinedione-hydroxamates as inhibitors of *Mycobacterium tuberculosis* virulence factor Zmp1

Veronika Šlachtová [a], Marek Šebela [b], Eveline Torfs [c], Lauren Oorts [c], Davie Cappoen [c], Karel Berka [d], Václav Bazgier [d], Lucie Brulíková [a, *]

[a] Department of Organic Chemistry, Faculty of Science, Palacký University, 17. listopadu 12, 771 46, Olomouc, Czech Republic
[b] Department of Protein Biochemistry and Proteomics, Centre of the Region Haná for Biotechnological and Agricultural Research, Faculty of Science, Palacký University, Šlechtitelů 27, 783 71, Olomouc, Czech Republic
[c] Laboratory of Microbiology, Parasitology and Hygiene (LMPH), S7, Faculty of Pharmaceutical, Biomedical and Veterinary Sciences, University of Antwerp, Wilrijk, Belgium
[d] Department of Physical Chemistry, Regional Centre of Advanced Technologies and Materials, Faculty of Science, Palacky University, 17. listopadu 12, 771 46, Olomouc, Czech Republic

ARTICLE INFO

Article history:
Received 2 May 2019
Received in revised form
7 August 2019
Accepted 23 October 2019
Available online 5 November 2019

Keywords:
Zmp1
Mycobacterium tuberculosis
Thiazolidinediones
Hydroxamates
MALDI-TOF

ABSTRACT

Zinc metalloprotease 1 (Zmp1) is an extracellular enzyme, which has been found essential for the intracellular survival and pathogenesis of *Mycobacterium tuberculosis*. In this work, we designed and synthesized a series of novel thiazolidinedione-hydroxamates and evaluated *in silico* their drug-likeness behavior. Then, their inhibitory properties towards a recombinant Zmp1 from *Mycobacterium tuberculosis* were analyzed by MALDI-TOF MS. Nine of the tested compounds were found to inhibit the enzymatic reaction more effectively than the generic metalloprotease inhibitor phosphoramidon. Furthermore, the synthesized thiazolidinedione-hydroxamate hybrids were evaluated for their *in vitro* antimycobacterial activity and acute cytotoxicity using whole-cell assays. Results showed that none of the hybrids exhibited acute cytotoxicity against RAW264.7 macrophages. Whereas extracellular antimycobacterial activity was limited, RAW264.7 macrophage infection results showed that a majority of the hybrids inhibited the intracellular growth of *Mycobacterium tuberculosis* at a concentration of 100 and 10 μM. The thiazolidinedione-hydroxamate compound **2n** was considered to be the best candidate of the evaluated library.

1. Introduction

Tuberculosis (TB), an infectious disease predominantly caused by the bacillus *Mycobacterium tuberculosis (Mtb)* still poses a major and enduring global health threat [1]. The infectious disease remains one of the top 10 causes of death and is, additionally, the leading cause of death due to a single infectious agent. In 2017, approximately 10 million people developed active TB disease and over 1.6 million persons died as a result [2]. Furthermore, the epidemic is fueled by the current HIV/AIDS pandemic and ever-increasing emergence of anti-TB drug resistance [2]. Moreover, there is only a limited number of drugs available on the market for the treatment of multidrug-resistant (MDR) and extensively drug-resistant (XDR) TB. Additionally, treatment is less efficient and associated with serious side effects [3]. Without doubt, the discovery of entirely new compounds with an alternative mechanism of action to the existing therapeutics and directed towards unknown targets of *Mtb* becomes more and more desirable [4,5].

One attractive mycobacterial target is represented by the promising and validated 20S proteasome protein, which is necessary for persistence in mice and vitality of the bacterium in pathogenesis as it protects *Mtb* against nitrosative stress from the host [6]. More recently, another interesting mycobacterial enzyme with protease activity was identified, i.e. zinc metalloprotease 1 (Zmp1). The enzyme is found to be essential for the intracellular survival and pathogenesis of *Mtb* [7–11]. In 2008, Master et al. illustrated that Zmp1 affects the macrophage phagosome maturation via suppression of inflammasome activation and subsequent phagolysosome formation, desired for the full clearance of the invalid pathogens (Fig. 1). The exact action mechanism of Zmp1 in the

* Corresponding author.
E-mail address: lucie.brulikova@upol.cz (L. Brulíková).

https://doi.org/10.1016/j.ejmech.2019.111812
0223-5234/

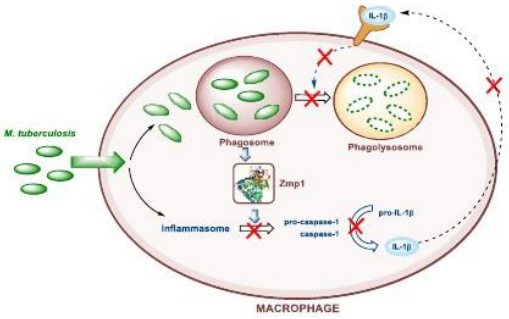

Fig. 1. Inhibition of the phagosome maturation process by mycobacterial Zmp1 (this figure was adopted from Ferraris and Rizzi) [11].

pathogenesis, however, has not been fully elucidated. Though, there is evidence that the zinc metalloprotease, a type of enzyme which can carry out diverse functions in pathogenic microorganisms, may be released from *Mtb* and act on the activation of the caspase-1/interleukin-1β inflammasome, ultimately disrupting phagolysosome formation and *Mtb* clearance [8]. Therefore, Zmp1 and its inhibition leading to virulence attenuation may also represent a potentially useful drug target and are worthy of further investigation.

The molecular structures of the mycobacterial 20S proteasome and Zmp1 are markedly different. Unlike the monomeric Zmp1 [7], 20S proteasome is a large barrel-shaped oligomer: 7 α-subunits are arranged into an α-ring and 7 β-subunits form a β-ring. These rings are stacked to a symmetric complex of $\alpha_{1\text{-}7}\,\beta_{1\text{-}7}\,\beta_{1\text{-}7}\,\alpha_{1\text{-}7}$ [12]. The active site of Zmp1 appears between the two structural domains rich in α-helices and contains a catalytic zinc ion in tetrahedral coordination. Because of the presence of hydrophobic residues, peptide substrates with a large hydrophobic P1' side chain (e.g. Phe, Leu, Ile) are well accommodated. There is also a secondary binding pocket available at the active site, with arginine residues, which has been suggested a promising docking site for inhibitors [7]. Conversely, the proteolytic mechanism of 20S proteasome involves the N-terminal threonine residue of each β-subunit [13]. The arrangement of the substrate binding pocket in *M. tuberculosis* 20S proteasome allows versatility in degrading of hydrophobic, basic as well as acidic peptide substrates [12]. The enzyme shows not only a different mechanism but also substrate and cleavage specificity compared to Zmp1. Thus, it is clear that the designing of new inhibitors of these two enzyme targets has to follow unique principles and approaches.

To date, only a few examples of Zmp1 inhibitors are known [14–18]. In 2014, the first selective *Mtb* Zmp1 inhibitors emerged, when the Botta group identified active structures by combining an *in silico* structure-based inhibitor design and biochemical studies (Fig. 2) [14]. Most of the defined structures in their study comprised the rhodanine skeleton that further served as a basic structural motif for the development of other Zmp1 inhibitors [15–18]. The most potent Zmp1 inhibitor to date was identified in the latest study from 2018 [16] when Paolino et al. described a series of 8-hydroxyquinolines modified with a hydroxamate substitution as the zinc-binding group.

In the present study, a protocol for synthetic preparation of thiazolidinedione-hydroxamates was developed. All synthesized compounds were evaluated for their antimycobacterial activity. In addition, the inhibitory properties of the studied compounds towards a recombinant Zmp1 from *Mycobacterium tuberculosis* were analyzed by MALDI-TOF MS.

2. Results and discussion

Based on the biological significance of both thiazolidinedione scaffold [19–21] and known hydroxamate-based zinc-binding group (ZBG) [22,23], a new library of thiazolidinedione-hydroxamate hybrids was designed and synthesized (Fig. 3). Two lipophilic hydroxamates as privileged scaffolds in a multitude of medicinally useful agents were selected for our initial studies [23–25]. Thiazolidinedione heterocycle may further be modified by various benzylidenes or alkylidenes according to various known biologically active structures [19]. Furthermore, the thiazolidinedione and hydroxamate scaffolds are connected via an appropriate linker R^2, where two simple variants were selected for the initial study.

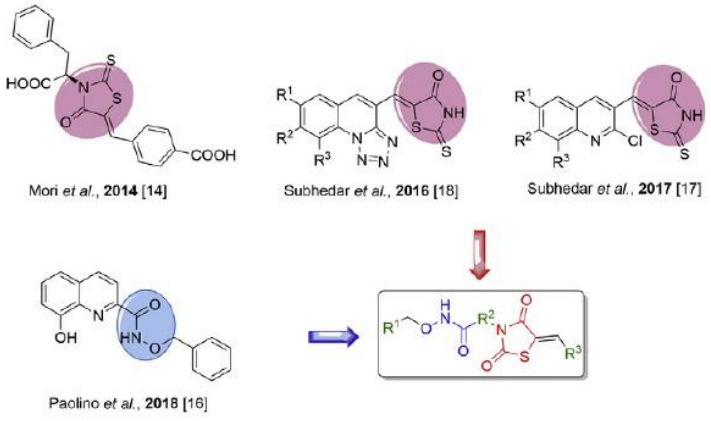

Fig. 2. Examples of known Zmp1 inhibitors and design of novel compounds.

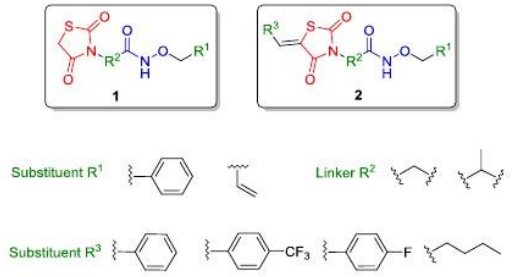

Fig. 3. Structures selected for the study.

3. Chemistry

First, simple thiazolidinedione-unsubstituted hydroxamates **1** were generated (Scheme 1). The initial thiazolidinedione **3** was synthesized according to a previously described procedure [26] and reacted with methyl bromoacetate or methyl 2-bromopropionate giving compounds **4**. This step was followed by the acid-catalyzed hydrolysis resulting in carboxylic acids **5.** The desired compounds **1** were obtained after a coupling reaction of the carboxylic acids **5** with either *O*-allylhydroxylamine hydrochloride or *O*-benzylhydroxylamine hydrochloride using *N*-(3-dimethylaminopropyl)-*N*′-ethyl carbodiimide hydrochloride (EDC.HCl) under aqueous conditions in moderate yields (see Table 1).

Next, hydroxamates **2** were synthesized (Scheme 1). The synthetic procedure was initiated with Knoevenagel condensation of thiazolidinedione **4** with various aldehydes to reach compounds **6**. Then a substitution with methyl bromoacetate or methyl 2-bromopropionate gave compounds **7**. After the acid-mediated hydrolysis of **7,** the resulting carboxylic acids **8** were coupled with either *O*-allylhydroxylamine hydrochloride or *O*-benzylhydroxylamine hydrochloride using EDC.HCl to give hydroxamates **2** in yields ranging from 31 to 75% (see Table 2). The lower yields were caused by losses during column chromatography.

Finally, we assessed the stereochemical outcome of our synthetic protocol. The formation of two geometrical isomers *E* or *Z* after Knoevenagel condensation is possible. These two isomers can easily be distinguished by their ^{1}H NMR spectral characteristics. It is well known that the benzylidine proton appears above 7.90 ppm for *Z* isomer and below 7.42 ppm for *E* isomer [27,28]. The measured NMR data confirmed the formation of *Z* isomers for all our products. Moreover, the final compounds containing a stereogenic centre were analyzed by supercritical fluid chromatography (SFC). All analyses confirmed the racemic form of both mentioned derivatives (See Supplementary).

3.1. In silico prediction of drug-likeness properties

To select those compounds suitable for further screening, *in silico* physicochemical and pharmacokinetic parameters of the thiazolidinedione-hydroxamates were predicted using the knowledge-based FAF*Drugs*4 [29] and admetSAR [30] software tools [6,31]. Narrowing the library to a series of compounds with a favourable drug-likeness and no toxicity alerts avoids futile investment in compounds with possible undesirable effects in later stages of the drug discovery and development cascade. For each hybrid, the predicted drug-likeness parameters are shown in Table 3, whereas ranges of such parameters followed by 95% of known drugs are also added in the footnotes [32,33]. The results revealed that the synthesized thiazolidinedione-hydroxamates meet the Lipinski's rule of five as the predicted values of the molecular weight, *n*-octanol, and water partition coefficient, hydrogen bond acceptors and hydrogen-bond donors parameters fall within the prescribed ranges. Furthermore, the number of atoms was also found within the range, improving drug-likeness [29]. Aqueous solubility was forecasted to be good for all thiazolidinedione-hydroxamates, except for **2g**, for which it was predicted to be reduced with a $\log S^W$ of −5.22. The thiazolidinedione-hydroxamates were also considered to have a good oral bioavailability, based on Verber's rule [34]. All hybrids were designated to class III considering acute oral toxicity, which reveals that the compounds should possess fairly high lethal doses (i.e. $LD_{50} = 0.5-5$ g/kg) and can be considered druggable. As for mutagenicity (Ames test), there were no alerts indicated. In contrast, another rule of thumb such as the GSK 4/400 rule, which anticipates higher risks of toxicity, interactions with off-targets or difficulties during development if the logP and the molecular weight is larger than 4 and 400, respectively, suggested that **2e** and **2g** could be less druggable [29]. Though, the overall results indicate that the synthesized thiazolidinedione-hydroxamates generally do possess drug-likeness behavior. Therefore, all derivatives are selected for further investigation, except the compounds **2e** and **2g**.

3.2. Inhibitory activity towards Zmp1

The inhibitory properties of the studied compounds towards a recombinant zinc metallopeptidase (Zmp1) from *Mtb* were

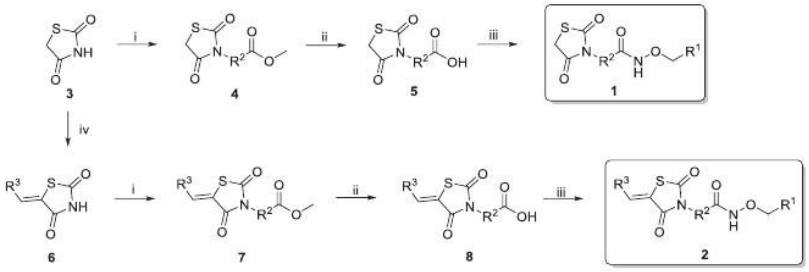

Scheme 1. Synthesis of model compounds **1** and **2**.
Reagents and conditions: (i) methyl bromoacetate or methyl 2-bromopropionate, NaH, DMF dry, rt, on; (ii) HBr (40%), reflux, 5 h; (iii) *O*-allylhydroxylamine hydrochloride or *O*-benzylhydroxylamine hydrochloride, EDC.HCl, H_2O, rt, 2 h; (iv) aldehyde, piperidine, EtOH, reflux, 5 h.

Table 1
Overview of synthesized products **1**.

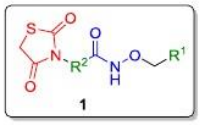

Entry	R^1	R^2	Yield[a] [%]
1a			49
1b			55
1c			61
1d			52

[a] Isolated yield after purification.

analyzed by matrix-assisted laser desorption/ionization-time of flight mass spectrometry (MALDI-TOF MS). The reaction mixture contained human angiotensin II as a substrate and the respective inhibitor. The proteolytic digestion of angiotensin II (*m/z* 1046) produced two peptide fragments providing characteristic signals in the mass spectrum, namely DRVY (*m/z* 552) and IHPF (*m/z* 513), in accordance with the literature [35] and as confirmed by tandem MS (MS/MS) analyses (not shown). The production of the fragments was accompanied by a simultaneous decrease in the angiotensin II signal (Supplementary Figs. S1–2).

MALDI is generally not considered a robust ionization technique for quantitative measurements, but a growing number of reports have documented its applicability for quantifying peptides [36]. This stems from reduced experimental difficulties because of the ongoing technological improvement of the instruments [37]. In this work, we eliminated both sample-to-sample and shot-to-shot variability of peak intensities by reading intensity ratios of the reaction product at *m/z* 552 and substrate at *m/z* 1046 in mass spectra averaged from 1000 laser shots. Finally, the inhibition rate was calculated from the ratio of the determined time-dependence slopes for inhibited and control reaction (Supplementary Table S1). Fig. 4 shows the obtained results. All compounds were found to inhibit the enzymatic reaction but the existing structural differences were reflected in their inhibitory strength. The most potent inhibitors were **2c**, **2k-m**, and **1b** (which inhibited almost completely), whereas **2d** and **2g** inhibited only by less than 20%.

Using the measured inhibition percentages, IC_{50} (half-maximal inhibitory concentration) values of the inhibitors can be estimated (100% activity for $[I] = 0\ \mu M$) and they appear in the range of 20–160 μM. Experimental IC_{50} values were obtained with three different inhibitor concentrations for **2n** (18 μM) and **2e** (38 μM), which represent highly efficient and medium-efficient inhibitors from the studied group, respectively. These numbers correspond to inhibition constants described for some other Zmp1 inhibitors [6,14,38].

Supplementary table (Table S2) shows a graphic interpretation of the influence of chemical functional groups on the inhibitory properties. The analyzed hybrid compounds can be divided into five clusters according to the substituent at the thiazolidinedione moiety (R^3): without any substitution, with a benzylidene, fluorobenzylidene, trifluorobenzylidene, and pentylidene substituting group. In each cluster, the presence of either a benzyl or allyl

Table 2
Overview of synthesized products **2**.

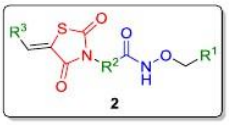

Entry	R^1	R^2	R^3	Yield[a] [%]
2a				58
2b				51
2c				64
2d				62
2e	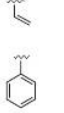			49
2f				50
2g			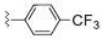	48
2h			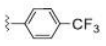	31
2i				35
2j				40
2k				60
2l				56
2m				75
2n				75
2o				45
2p				45

[a] Isolated yield after purification.

substitution at the hydroxamate moiety (R^1) was considered, plus a possible methyl group in the linker (R^2). As can be seen, the benzyl group at the hydroxamate function resulted predominantly in a lower inhibition potency compared to the allyl group at this position for the hybrid compounds with both non-substituted and trifluorbenzylidene-substituted thiazolidinedione ring. An opposite trend was found for those containing the benzylidene-substituted thiazolidinedione ring, whereas no clear trend was observed for the other two clusters. The methyl group presence in

Table 3
In silico predicted physicochemical and pharmacokinetic parameters of the thiazolidinedione-hydroxamates.

Compound	MW[a]	LogP[b]	HBD[c]	HBA[d]	No. of atoms[e]	Rotatable bonds[f]	logSw[g]	Solubility Forecast Index	Oral bioavailability (Veber's rule]	4/400	Ames test toxicity	Acute oral toxicity
1a	280.3	1.14	1	6	19	5	−2.11	Good	Good	Good	Non	III
1b	230.24	0.29	1	6	15	5	−1.12	Good	Good	Good	Non	III
1c	294.33	1.54	1	6	20	5	−2.44	Good	Good	Good	Non	III
1d	244.27	0.69	1	6	16	5	−1.46	Good	Good	Good	Non	III
2a	368.41	3.26	1	6	26	6	−3.99	Good	Good	Good	Non	III
2b	318.35	2.41	1	6	22	6	−3.06	Good	Good	Good	Non	III
2c	382.43	3.67	1	6	27	6	−4.32	Good	Good	Good	Non	III
2d	332.37	2.82	1	6	23	6	−3.4	Good	Good	Good	Non	III
2e	436.41	4.15	1	6	30	7	−4.9	Good	Good	Bad	Non	III
2f	386.35	3.30	1	6	26	7	−3.97	Good	Good	Good	Non	III
2g	450.43	4.55	1	6	31	7	−5.22	Reduced	Good	Bad	Non	III
2h	400.37	3.70	1	6	27	7	−4.3	Good	Good	Good	Non	III
2i	386.4	3.36	1	6	27	6	−4.17	Good	Good	Good	Non	III
2j	336.34	2.51	1	6	23	6	−3.23	Good	Good	Good	Non	III
2k	400.42	3.77	1	6	28	6	−4.5	Good	Good	Good	Non	III
2l	350.36	2.92	1	6	24	6	−3.57	Good	Good	Good	Non	III
2m	348.42	3.52	1	6	24	8	−3.79	Good	Good	Good	Non	III
2n	298.36	2.67	1	6	20	8	−2.84	Good	Good	Good	Non	III
2o	362.44	3.92	1	6	25	8	−4.12	Good	Good	Good	Non	III
2p	312.38	3.07	1	6	21	8	−3.18	Good	Good	Good	Non	III

[a] Molecular Weight (MW; 130 to 725).
[b] Log partition coefficient between *n*-octanol and water (−2 to 6.5).
[c] Number of hydrogen bond donors (0−6).
[d] Number of hydrogen acceptors (2−20).
[e] Number of atoms (20−70).
[f] Number of rotatable bonds (0−15).
[g] Log aqueous solubility (−6.5 to 0.5).

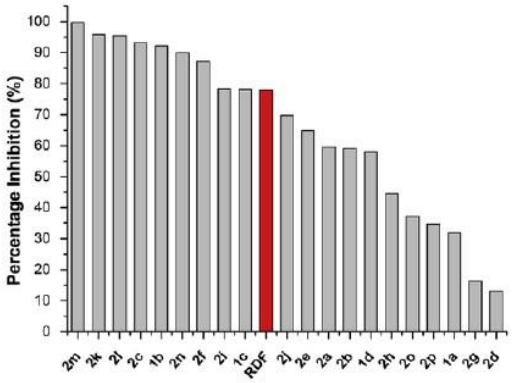

Fig. 4. Inhibitory activity toward Zmp1. Inhibition rate at a given inhibitor concentration of 40 μM was calculated by inverting the ratio of slopes for inhibited and control reaction. Phosphoramidon (RDF) was used as a reference at a final concentration of 40 μM [16].

the linker resulted in lower inhibitory properties when compared to the counterparts without this group, for the compounds with pentylidene and trifluorbenzylidene substitutions at the thiazolidinedione ring. It was the opposite for those with the fluorobenzylidene substitution. Generally, this interpretation indicates that the measured inhibition data reflect a structure-based interaction with the enzyme molecule as they are not fully random.

3.3. In vitro biological activity

Following the synthesis and enzymatic assays, the thiazolidinedione-hydroxamate hybrids were evaluated for their *in vitro* activity against *Mycobacterium tuberculosis* H37Ra using a whole-cell assay. Antimycobacterial potency was assessed using resazurin, as previously reported [39]. The results were expressed as the IC_{50}, and also minimal inhibitory concentration (MIC) at which the mycobacterial growth is reduced by 90% (Table 4). In parallel, the acute cytotoxicity of the thiazolidinedione-hydroxamates against the eukaryotic RAW264.7 macrophage cell line was studied using a previously reported neutral red uptake (NRU) assay [40]. The cytotoxic concentration (CC_{50}) of a compound is defined as the concentration at which the NRU by the cells is reduced by 50% (Table 4). The selectivity index (SI) of the synthesized compounds was calculated by dividing the CC_{50} with the MIC (Table 4). Results showed that most of the thiazolidinedione-hydroxamates showed no significant antimycobacterial activity against extracellular *Mtb* H37Ra, i.e. IC_{50} and MIC values > 64 μM (Table 4). The hybrids **2f**, **2k**, **2l**, **2m** and **2n** showed a low antimycobacterial potency with IC_{50} values of 51.7, 44.4, 60.0, 55.0 and 42.2 respectively. For **2n**, a MIC value of 61.8 could be calculated. Except for **2o**, none of the compounds exhibited acute cytotoxicity against RAW264.7 macrophages, i.e. CC_{50} values > 128 μM (Table 4). Only **2o** showed a low cytotoxic effect with a CC_{50} value of 43.9 μM. Though, this effect did not exceed the cytotoxic effect of the reference drug tamoxifen (CC_{50} = 11.1 μM). As a result, a SI of at least 2.1 and 0.7, respectively, could be calculated for **2n** and **2o**. Although only a low antimycobacterial activity against extracellular *Mtb* H37Ra was present, **2n** showed to be the most potent of the evaluated hybrids. Interestingly, this compound belonged to those providing the strongest inhibitory properties towards the mycobacterial enzyme Zmp1.

As the thiazolidinedione-hydroxamate hybrids were designed as Zmp1-inhibitors, the *in vitro* antimycobacterial activity of the compounds against intracellular residing *Mtb* H37Ra bacilli was assessed as well. The intracellular activity was studied using a luminometric macrophage infection assay [41]. Based on the luminescent signal of the synthesized compounds and untreated control, the obtained results were expressed as inhibition

Table 4
In vitro antimycobacterial activity and acute cytotoxicity results.

Compound	IC_{50} (μM)[a]	MIC (μM)[b]	CC_{50} (μM)[c]	SI[d]
1a	>64	>64	>128	ND
1b	>64	>64	>128	ND
1c	>64	>64	>128	ND
1d	>64	>64	>128	ND
2a	>64	>64	>128	ND
2b	>64	>64	>128	ND
2c	>64	>64	>128	ND
2d	>64	>64	>128	ND
2e	59.5	>64	>128	ND
2f	51.7	>64	>128	ND
2g	>64	>64	>128	ND
2h	>64	>64	>128	ND
2i	>64	>64	>128	ND
2j	>64	>64	>128	ND
2k	>64	>64	>128	ND
2l	60.0	>64	>128	ND
2m	55.0	>64	>128	ND
2n	42.2	61.8	>128	>2.1
2o	44.4	>64	43.9	>0.7
2p	>64	>64	>128	ND
Isoniazid	0.1	0.3	ND	ND
Tamoxifen	ND	ND	11.1	ND

ND, not done.
[a] Fifty percent inhibitory concentration.
[b] Minimum inhibitory concentration.
[c] Fifty percent cytotoxicity concentration.
[d] Selectivity index (CC_{50}/MIC).

percentages. As depicted in Fig. 5, sixteen of the thiazolidinedione-hydroxamates were found antimycobacterial at a final test concentration of 100 μM. Only **2f**, **2h**, **2m** and **2o** completely lacked intracellular activity. Considering a final concentration of 10 μM, eight of the thiazolidinedione-hydroxamates showed an antimycobacterial activity in this experimental arrangement, namely **1b**, **1d**, **2a**, **2c**, **2e**, **2g**, **2i**, and **2k**. The percentage inhibition was 30.2, 21.6, 38.3, 46.9, 48.8, 19.4, 20.6 and 25.1%, respectively. This indicates that the existing structural differences not only influence the enzymatic inhibitory strength towards Zmp1 but also affect less straightforward biological properties such as cell membrane penetration. The hybrid **2n**, which showed only a low antimycobacterial activity against extracellular *Mtb* H37Ra, exhibited intracellular activity at the relatively high 100-μM concentration. In

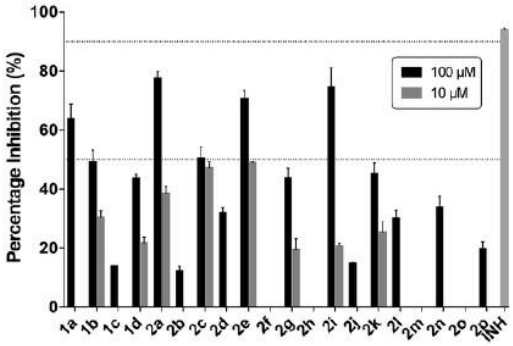

Fig. 5. Intracellular antimycobacterial activity of the thiazolidinedione-hydroxamates. The growth inhibition of Mtb H37Ra^{lux} inside RAW264.7 macrophages upon 24 h of exposure to 100 and 10 μM of the hybrids was expressed as the percentage inhibition. Isoniazid (INH) was used as a reference at a final test concentration of 0.1 μM. Results are presented as the mean ± SD.

contrast, **2e** excels in antimycobacterial activity against intracellular residing *Mtb* H37Ra, even at the lower concentration of 10 μM, whereas it lacks a significant extracellular activity. Structure-activity relationship deductions indicate that the R^2 linker, connecting the thiazolidinedione and hydroxamate moieties, did not influence *in vitro* intracellular activity too much. In contrast, the R^1 substitution appeared largely influential. For example, for the simple thiazolidinedione-unsubstituted hydroxamates **1**, the benzyl-substitution (**1a** and **1c**) reduced intracellular antimycobacterial activity at lower concentrations. In contrast, the R^1 benzyl-substitution of the thiazolidinedione-hydroxamates **2** increased their *in vitro* potency against intracellular residing *Mtb* H37Ra. For the latter group, the R^3 substitution also showed to be important: the presence of an alkyl reduced the antimycobacterial activity at low concentrations, whereas substitution with either an unsubstituted benzyl group or fluorinated benzyl group increased the inhibition percentage in the intracellular test. Hybrid **2e** was selected as the most potent inhibitor of intracellular residing *Mtb* H37Ra, with an inhibition percentage of 70.4 and 48.8% at 100 and 10 μM, respectively. Hybrid **2n**, however, was selected as the most optimal compound considering the overall results, including the *in silico* drug-likeness predictions and target-based enzymatic assays.

3.4. Pose identification with in silico molecular docking

In order to explain the inhibitory effect of the thiazolidinedione-hydroxamates, we have employed a molecular docking of **2n** into the internal central cavity of *Mycobacterium tuberculosis* zinc metalloprotease Zmp1 structure (PDB ID: 3ZUK) [7]. The compound mimics the interactions of the indole part of phosphoramidon inhibitor crystal pose as shown in Fig. 6A. Both aromatic moieties, the indole of phosphoramidon and thiazolidinedione of compound **2n**, interact via a π-π interaction with the phenyl ring of F48. They also share the H-bond with R628 and the hydrophobic interactions with the aliphatic chain in the cleft formed by F48 and W604. Phosphoramidon, however, shows a direct interaction with the zinc atom and its surroundings leading towards much stronger inhibition ($K_i = 35$ nM according to PDBBIND) [42]. Compound **2n** shows additional polar contacts with the cavity entrance at R616. This is in agreement with the previous suggestion of designing such promising inhibitors, which would target the secondary binding pocket at the active site of Zmp1 [7].

The reasons for a good performance of the compound **2n** seem to be i) nonpolar aliphatic chain interaction with the hydrophobic cleft, where larger moieties do not fit, ii) unbranched linker joining the polar moiety of **2n** to the thiazolidinedione ring, which allows more flexibility towards the polar part of the entrance into the cavity and iii) polar interactions with highly populated charged residues within the entrance.

The studied thiazolidinedione-hydroxamates are thus expected to occupy the entrance into the central cavity, approximately 7 Å apart of the zinc-binding catalytic site (Fig. 6B). This is probably the reason for their lower efficiency than it could have been expected from their rational design (combining structural features of previously described potent inhibitors) as they are only gate-keeping the entry/exit of the peptidic substrate and do not further interfere with the reaction on the zinc atom. In contrast, as shown in crystal structures, phosphoramidon interacts directly with the zinc catalytic site and this allows the compound to inhibit also human zinc metallopeptidase neprilysin (NEP) structure (PDB ID: 1DMT) [43] as shown in Fig. 6C. NEP is able to cleave peptide bonds between hydrophobic residues in a variety of peptides such as opioid Met- and Leu-enkephalins [44] or angiotensins (e.g. angiotensin II). However, while the cleft surrounding the zinc-binding catalytic site is structurally identical, the entrance into the cavity differs

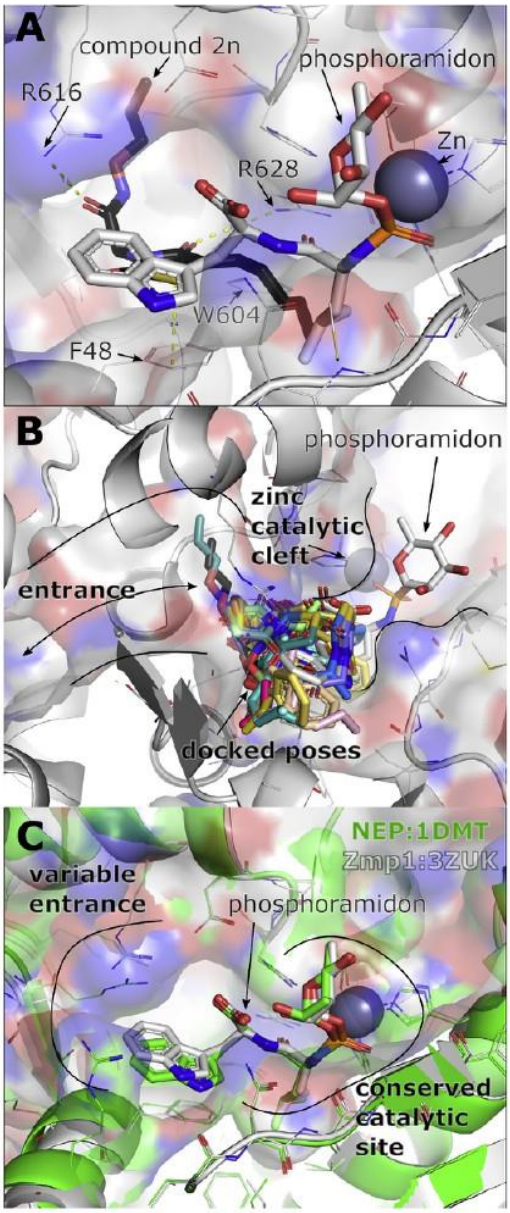

Fig. 6. Pose identification with molecular docking. A – a comparison of the docked pose of **2n** with that of phosphoramidon (from the crystal structure, PDB ID: 3ZUK) at the catalytic site of Zmp1; B – the docked poses of thiazolidinedione-hydroxamates in the entrance compared to the crystal structure pose of phosphoramidon blocking the entrance and also occupying the catalytic site of Zmp1; C – a comparison of the binding of phosphoramidon in the cavity of Zmp1 (PDB ID: 3ZUK) and neprilysin (NEP; PDB ID: 1DMT) [43]. Notice the conserved amino acids around the zinc-binding catalytic site; on the contrary, the entrance shows a variability in the constituting amino acids.

dramatically between the *Mycobacterium* and human zinc metallopeptidases.

4. Conclusion

In conclusion, we have developed an efficient synthetic protocol for the preparation of a series of thiazolidinedione-hydroxamates and assessed their inhibitory properties towards a recombinant Zmp1 from *Mycobacterium tuberculosis* by MALDI-TOF MS. This characterization was completed by whole-cell biological activity and cytotoxicity tests. Results showed that none of the synthesized thiazolidinedione-hydroxamates possessed acute cytotoxic effects against RAW264.7 macrophages. The extracellular anti-mycobacterial activity was rather limited, whereas anti-mycobacterial activity against intracellular residing bacilli was present for the majority of the tested hybrid library. The existing structural differences were reflected in the variability of the *in silico* predicted parameters and biologically determined responses. When looking for a synergic behavior of the studied synthetic compounds in all performed experimental tests, the compound **2n**, which does not contain aromatic R^1 and R^3 substituents as well as a branched R^2 linker, was found the most optimal.

5. Experimental section

5.1. Materials and methods

Solvents and chemicals were purchased from Sigma-Aldrich (www.sigmaaldrich.com) and Fluorochem (www.fluorochem.co.uk). All reactions were carried out at ambient temperature (21 °C) unless stated otherwise. Analytical thin-layer chromatography (TLC) was performed using aluminum plates precoated with silica gel (silica gel 60 F254).

The LC-MS analyses were carried out on UHPLC-MS system consisting of UHPLC chromatograph Accela with photodiode array detector and triple quadrupole mass spectrometer TSQ Quantum Access (Thermo Scientific, CA, USA), using Nucleodur Gravity C18 column (dimensions 1.8 μm, 2.1 × 50 mm at 30 °C and a flow rate of 800 μl/min (Macherey-Nagel, Germany). The mobile phase was (A) 0.1% ammonium acetate in water, and (B) 0.1% ammonium acetate in acetonitrile, linearly programmed from 10% to 80% B over 2.5 min, kept for 1.5 min. The column was re-equilibrated with 10% of solution B for 1 min. The APCI source operated at a discharge current of 5 μA, vaporizer temperature of 400 °C and a capillary temperature of 200 °C.

NMR 1H/13C spectra were recorded on JEOL ECX-500SS (500 MHz) or JEOL ECA400II (400 MHz) spectrometer at magnetic field strengths of 11.75 T (with operating frequencies 500.16 MHz for 1H and 125.77 MHz for 13C) and 9.39 T (with operating frequencies 399.78 MHz for 1H and 100.53 MHz for 13C) at ambient temperature (~21 °C). Chemical shifts (δ) are reported in parts per million (ppm), and coupling constants (J) are reported in Hertz (Hz). NMR spectra were recorded at ambient temperature (21 °C) in DMSO-d_6 and referenced to the resonance signal of the solvent.

HRMS analysis was performed with LC-MS and an Orbitrap high-resolution mass spectrometer (Dionex, Ultimate 3000, Thermo Exactive plus, MA, USA) operating in positive full scan mode in the range of 80–1200 *m/z*. The settings for electrospray ionization were as follows: 150 °C oven temperature and 3.6 kV source voltage. The acquired data were internally calibrated with phthalate as a contaminant in methanol (*m/z* 297.15909). Samples were diluted to a final concentration of 0.1 mg/ml in a solution of water and acetonitrile (50:50, v/v). The samples were injected into the mass spectrometer following HPLC separation on a Kinetex C18 column (2.6 μm, 100 A, 50 × 3.0 mm) using an isocratic mobile

phase of 0.01M acetonitrile/ammonium acetate (80/20) at a flow rate of 0.3 ml min^{-1}.

SFC chiral analyses were performed using an Acquity UPC system (Waters) consisting of a binary solvent manager, sample manager, column manager, column heater, convergence manager, PDA detector 2998, QDA mass detector and chiral analytical columns CHIRALPAK IA3, IB3, IC3 and ID3 (4,6 × 100 mm, 3 μm particle size). The chromatographic runs were performed at a flow rate of 2.2 ml min^{-1}, column temperature of 38 °C and ABPR 2000 psi.

5.2. Chemistry

5.2.1. General procedure for Knoevenagel condensation

A mixture of thiazolidinedione **3**, aldehyde (1 eq), piperidine (0.8 eq) and EtOH (130 ml/17 mmol) was refluxed on (16–20 h) and worked up according to *method A* or *B*.

Method A: The reaction mixture was poured into H_2O (200 ml), acidified with AcOH (10 ml) and filtered affording compounds **6**.

Method B: The product was concentrated *in vacuum* and purified by column chromatography (mobile phase: hexane/EtOAc 6:2) affording compounds **6**.

5.2.2. General procedure for reaction with bromoester

Thiazolidinedione **3** or **6** was dissolved in dry DMF (10 ml/8 mmol). NaH (1 eq) was slowly added to the reaction mixture followed by stirring and stirred for 10 min. Bromoester (1 eq) was added dropwise. After stirring overnight (24 h), the reaction mixture was diluted with water (50 ml). The product was extracted with DCM (5 × 50 ml), organic layers were washed with 5% HCl, brine, dried over Na_2SO_4 and concentrated in vacuum.

5.2.3. Methyl 2-(2,4-dioxo-5-pentylidenethiazolidin-3-yl)acetate 7a

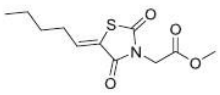

Orange oil. Yield: 81% (822 mg). ^{1}H NMR (500 MHz, DMSO-d_6): δ 7.12 (t, J = 7.7 Hz, 1H), 4.44 (s, 2H), 3.70 (s, 3H), 2.28–2.23 (m, 2H), 1.53–1.47 (m, 2H), 1.32 (dd, J = 14.9, 7.4 Hz, 2H), 0.89 (t, J = 7.3 Hz, 3H). ^{13}C NMR (126 MHz, DMSO-d_6): δ 167.17, 166.63, 163.57, 140.10, 123.92, 52.58, 41.83, 31.01, 29.23, 21.74, 13.56. HRMS: *m/z*: calcd for $C_{11}H_{15}NO_4S$: 258.0795 $[M+H]^+$; found: 258.0796.

5.2.4. Methyl 2-(2,4-dioxo-5-pentylidenethiazolidin-3-yl) propanoate 7b

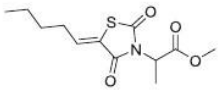

Mobile phase: DCM/MeOH 98:2. Brown solid. Yield: 44% (467 mg). ^{1}H NMR (500 MHz, DMSO-d_6): δ 7.10 (t, J = 7.7 Hz, 1H), 5.07 (q, J = 7.1 Hz, 1H), 3.65 (s, 3H), 2.24 (dd, J = 14.8, 7.5 Hz, 2H), 1.51–1.46 (m, 5H), 1.32 (dd, J = 14.9, 7.4 Hz, 2H), 0.89 (t, J = 7.3 Hz, 3H). ^{13}C NMR (126 MHz, DMSO-d_6): δ 169.02, 166.42, 163.42, 140.12, 123.77, 52.57, 49.98, 30.99, 29.24, 21.76, 13.95, 13.57. HRMS: *m/z*: calcd for $C_{12}H_{17}NO_4S$: 272.0951 $[M+H]^+$; found: 272.0952.

5.2.5. Ester hydrolysis

Ester **4/7** was dissolved in HBr 40% (8 ml/5 mmol) and refluxed for 5 h. The mixture was cooled down to rt and diluted with water (50 ml) and worked up according to *method A* or *B*.

Method A: The resulting suspension was filtered and washed with water.

Method B: The product was extracted with EtOAc (3 × 50 ml), washed with brine, dried over Na_2SO_4 and concentrated in vacuum.

5.2.6. 2-(2,4-Dioxo-5-(4-trifluoromethyl)benzylidene)thiazolidin-3-yl)propanoic acid 8a

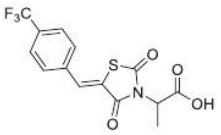

Method A. Brown solid. Yield: 55% (734 mg). ^{1}H NMR (500 MHz, DMSO-d_6): δ 13.28 (s, 1H), 8.06 (s, 1H), 7.91 (d, J = 8.4 Hz, 2H), 7.86 (d, J = 8.1 Hz, 2H), 5.03 (q, J = 7.2 Hz, 1H), 1.52 (d, J = 7.2 Hz, 3H). ^{13}C NMR (126 MHz, DMSO-d_6): δ 169.89, 166.32, 164.63, 136.83, 131.89, 130.63, 130.01 (q, J = 32.7 Hz), 126.12, 123.79 (q, J = 272.1 Hz), 123.68, 50.49, 13.87. HRMS: *m/z*: calcd for $C_{14}H_{10}F_3NO_4S$: 346.0355 $[M+H]^+$; found: 346.0358.

5.2.7. 2-(2,4-Dioxo-5-pentylidenethiazolidin-3-yl)propanoic acid 8b

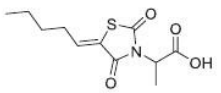

Method B. Brown solid. Yield: 83% (415 mg). ^{1}H NMR (500 MHz, DMSO-d_6): δ 13.16 (s, 1H), 7.08 (t, J = 7.7 Hz, 1H), 4.93 (q, J = 7.2 Hz, 1H), 2.24 (dd, J = 14.8, 7.5 Hz, 2H), 1.51–1.45 (m, 5H), 1.32 (dd, J = 14.9, 7.4 Hz, 2H), 0.89 (t, J = 7.3 Hz, 3H). ^{13}C NMR (126 MHz, DMSO-d_6): δ 169.97, 166.48, 163.58, 139.59, 123.94, 50.06, 30.96, 29.26, 21.76, 13.91, 13.57. HRMS: *m/z*: calcd for $C_{11}H_{15}NO_4S$: 258.0795 $[M+H]^+$; found: 258.0795.

5.2.8. Reaction with hydroxylamine.HCl

Carboxylic acid (1 eq) **5/8** was suspended in water (20 ml/1 mmol). Hydroxylamine.HCl (1.5 eq) was dissolved in water (20 ml/1 mmol). The amine mixture was added to the acid mixture and the pH was adjusted to 4.5 with 1M NaOH. THF was added until a homogeneous solution was obtained. EDC.HCl (3 eq) was dissolved in water (10 ml/1 mmol) and added in aliquots (4 ml/1 min) to the reaction mixture. The reaction was stirred for 2 h and worked up according to the *method A* or *B*.

Method A: The reaction was filtered and the solid was dried overnight.

Method B: The product was extracted with EtOAc (3 × 40 ml), washed with saturated $NaHCO_3$, brine, dried over Na_2SO_4 and concentrated *in vacuum*.

5.2.9. N-(benzyloxy)-2-(2,4-dioxothiazolidin-3-yl)acetamide 1a

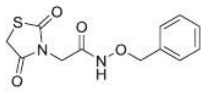

Method A. Mobile phase: DCM/MeOH 90:10. White solid. Yield: 49% (277 mg). ^{1}H NMR (500 MHz, DMSO-d_6): δ 11.22 (s, 1H), 7.42−7.35 (m, 5H), 4.82 (s, 2H), 4.25 (s, 2H), 4.10 (s, 2H). ^{13}C NMR (126 MHz, DMSO-d_6): δ 171.84, 171.46, 162.66, 135.65, 128.87, 128.32, 77.05, 41.14, 33.97. HRMS: *m/z*: calcd for $C_{12}H_{12}N_2O_4S$: 281.0591 $[M+H]^+$; found: 281.0592.

5.2.10. N-(allyloxy)-2-(2,4-dioxothiazolidin-3-yl)acetamide 1b

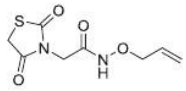

Method B. Mobile phase: $CHCl_3$/MeOH 90:10. Yellow oil. Yield: 55% (257 mg). ^{1}H NMR (500 MHz, DMSO-d_6): δ 11.35 (s, 1H), 5.95−5.87 (m, 1H), 5.31 (d, J = 17.3 Hz, 1H), 5.26 (d, J = 10.4 Hz, 1H), 4.27 (s, 4H), 4.03 (s, 2H). ^{13}C NMR (126 MHz, DMSO-d_6): δ 171.82, 171.44, 162.49, 132.70, 119.48, 76.05, 41.11, 33.96. HRMS: *m/z*: calcd for $C_8H_{10}N_2O_4S$: 231.0434 $[M+H]^+$; found: 231.0435.

5.2.11. N-(benzyloxy)-2-(2,4-dioxothiazolidin-3-yl)propanamide 1c

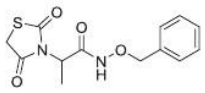

Method B. Mobile phase: DCM/MeOH 90:10. Yellow oil. Yield: 61% (342 mg). ^{1}H NMR (500 MHz, DMSO-d_6): δ 11.35 (s, 1H), 7.40−7.38 (m, 4H), 7.37−7.36 (m, 1H), 4.75 (d, J = 7.1 Hz, 2H), 4.68 (q, J = 7.1 Hz, 1H), 4.16 (s, 2H), 1.40 (d, J = 7.2 Hz, 3H). ^{13}C NMR (126 MHz, DMSO-d_6): δ 171.71, 171.31, 165.08, 135.67, 128.94, 128.28, 76.90, 49.39, 34.03, 13.61. HRMS: *m/z*: calcd for $C_{13}H_{14}N_2O_4S$: 295.0747 $[M+H]^+$; found: 295.0749.

5.2.12. N-(allyloxy)-2-(2,4-dioxothiazolidin-3-yl)propanamide 1d

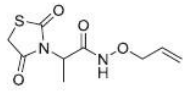

Method B. Mobile phase: $CHCl_3$/MeOH 90:10. Yellow oil. Yield: 52% (240 mg). ^{1}H NMR (500 MHz, DMSO-d_6): δ 11.24 (s, 1H), 5.94−5.86 (m, 1H), 5.30 (dd, J = 17.3, 1.6 Hz, 1H), 5.24 (d, J = 10.5 Hz, 1H), 4.65 (q, J = 7.1 Hz, 1H), 4.25−4.23 (m, 2H), 4.16 (s, 2H), 1.38 (d, J = 7.2 Hz, 3H). ^{13}C NMR (126 MHz, DMSO-d_6): δ 171.66, 171.29, 164.87, 132.80, 119.24, 75.83, 49.33, 34.02, 13.59. HRMS: *m/z*: calcd for $C_9H_{12}N_2O_4S$: 245.0591 $[M+H]^+$; found: 245.0593.

5.2.13. 2-(5-benzylidene-2,4-dioxothiazolidin-3-yl)-N-(benzyloxy) acetamide 2a

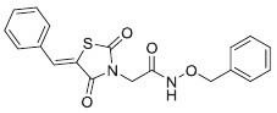

Method A. White solid. Yield: 58% (451 mg). ^{1}H NMR (500 MHz, DMSO-d_6): δ 11.34 (s, 1H), 7.96 (s, 1H), 7.65 (d, J = 7.3 Hz, 2H), 7.56 (t, J = 7.3 Hz, 2H), 7.52 (d, J = 7.1 Hz, 1H), 7.42−7.37 (m, 5H), 4.84 (s, 2H), 4.28 (s, 2H). ^{13}C NMR (126 MHz, DMSO-d_6): δ 166.96, 165.15, 162.54, 135.64, 133.50, 132.83, 130.77, 130.15, 129.39, 128.91, 128.33, 121.00, 77.10, 41.50. HRMS: *m/z*: calcd for $C_{19}H_{16}N_2O_4S$: 369.0904 $[M+H]^+$; found: 369.0907.

5.2.14. N-(allyloxy)-2-(5-benzylidene-2,4-dioxothiazolidin-3-yl) acetamide 2b

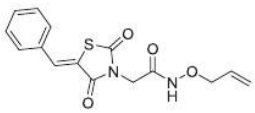

Method A. White solid. Yield: 51% (339 mg). ^{1}H NMR (500 MHz, DMSO-d_6): δ 11.26 (s, 1H), 7.96 (s, 1H), 7.64 (d, J = 6.0 Hz, 2H), 7.58−7.51 (m, 3H), 5.96 (s, 1H), 5.35 (d, J = 17.2 Hz, 1H), 5.28 (d, J = 9.2 Hz, 1H), 4.30 (d, J = 28.8 Hz, 4H). ^{13}C NMR (126 MHz, DMSO-d_6): δ 166.94, 165.13, 162.38, 133.48, 132.82, 132.69, 130.77, 130.14, 129.39, 120.99, 119.54, 76.09, 41.46. HRMS: *m/z*: calcd for $C_{15}H_{14}N_2O_4S$: 319.0747 $[M+H]^+$; found: 319.0749.

5.2.15. 2-(5-benzylidene-2,4-dioxothiazolidin-3-yl)-N-(benzyloxy) propanamide 2c

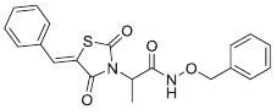

Method B. Mobile phase: DCM/MeOH 98:2. Yellow solid. Yield: 64% (373 mg). ^{1}H NMR (500 MHz, DMSO-d_6): δ 11.46 (s, 1H), 7.94 (s, 1H), 7.65 (d, J = 7.4 Hz, 2H), 7.58−7.50 (m, 3H), 7.40−7.34 (m, 5H), 4.87 (q, J = 7.1 Hz, 1H), 4.77 (q, J = 10.7 Hz, 2H), 1.50 (d, J = 7.2 Hz, 3H). ^{13}C NMR (126 MHz, DMSO-d_6): δ 166.75, 164.99, 164.90, 135.69, 132.96, 130.63, 130.05, 129.40, 128.97, 128.27, 121.36, 76.92, 49.85, 13.86. HRMS: *m/z*: calcd for $C_{20}H_{18}N_2O_4S$: 383.1060 $[M+H]^+$; found: 383.1058.

5.2.16. N-(allyloxy)-2-(5-benzylidene-2,4-dioxothiazolidin-3-yl) propanamide 2d

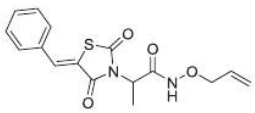

Method B. Mobile phase: DCM/MeOH 98:2. Yellow solid. Yield: 62% (314 mg). ^{1}H NMR (500 MHz, DMSO-d_6): δ 11.36 (s, 1H), 7.94 (s, 1H), 7.64 (d, J = 7.4 Hz, 2H), 7.58−7.51 (m, 3H), 5.91 (dq, J = 10.7,

6.1 Hz, 1H), 5.31 (d, J = 17.3 Hz, 1H), 5.24 (d, J = 11.7 Hz, 1H), 4.85 (q, J = 7.1 Hz, 1H), 4.26 (t, J = 5.2 Hz, 2H), 1.48 (d, J = 7.2 Hz, 3H). ^{13}C NMR (126 MHz, DMSO-d_6): δ 166.72, 164.98, 164.70, 132.95, 132.82, 130.63, 130.05, 129.39, 121.36, 119.30, 75.87, 49.81, 13.85. HRMS: m/z: calcd for $C_{16}H_{16}N_2O_4S$: 333.0904 $[M+H]^+$; found: 333.0905.

5.2.17. N-(benzyloxy)-2-(2,4-dioxo-5-(4-trifluoromethyl) benzylidene)thiazolidin-3-yl)acetamide 2e

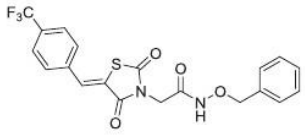

Method A. White solid. Yield: 49% (298 mg). ^{1}H NMR (500 MHz, DMSO-d_6): δ 11.35 (s, 1H), 8.04 (s, 1H), 7.87 (dd, J = 19.3, 8.2 Hz, 4H), 7.43–7.37 (m, 5H), 4.85 (s, 2H), 4.29 (s, 2H). ^{13}C NMR (126 MHz, DMSO-d_6): δ 166.62, 164.93, 162.45, 136.81, 135.63, 131.67, 129.97 (q, J = 31.5 Hz), 128.92, 128.33, 126.13, 124.00, 123.79 (q, J = 273.4 Hz), 77.11, 41.63. HRMS: m/z: calcd for $C_{20}H_{15}F_3N_2O_4S$: 437.0777 $[M+H]^+$; found: 437.0775.

5.2.18. N-(allyloxy)-2-(2,4-dioxo-5-(4-trifluoromethyl) benzylidene)thiazolidin-3-yl)acetamide 2f

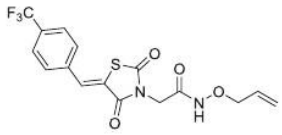

Method A. Yellow solid. Yield: 50% (289 mg). ^{1}H NMR (500 MHz, DMSO-d_6): δ 11.27 (s, 1H), 8.03 (s, 1H), 7.89 (d, J = 8.4 Hz, 2H), 7.85 (d, J = 8.4 Hz, 2H), 5.96 (dd, J = 16.1, 9.9 Hz, 1H), 5.35 (d, J = 17.2 Hz, 1H), 5.28 (d, J = 10.1 Hz, 1H), 4.33 (s, 4H). ^{13}C NMR (126 MHz, DMSO-d_6): δ 166.60, 164.91, 162.29, 136.81, 132.69, 131.66, 130.63, 129.97 (q, J = 31.5 Hz), 126.16, 124.00, 123.81 (q, J = 272.1 Hz), 119.56, 76.11, 41.59. HRMS: m/z: calcd for $C_{16}H_{13}F_3N_2O_4S$: 387.0621 $[M+H]^+$; found: 387.0621.

5.2.19. N-(benzyloxy)-2-(2,4-dioxo-5-(4-trifluoromethyl) benzylidene)thiazolidin-3-yl)propanamide 2g

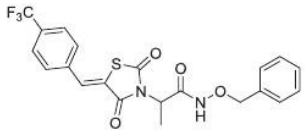

Method B. Mobile phase: DCM/MeOH 95:5. White solid. Yield: 48% (126 mg). ^{1}H NMR (500 MHz, DMSO-d_6): δ 11.47 (s, 1H), 8.03 (s, 1H), 7.91 (d, J = 8.3 Hz, 2H), 7.86 (d, J = 8.1 Hz, 2H), 7.41–7.34 (m, 5H), 4.88 (q, J = 7.0 Hz, 1H), 4.77 (q, J = 8.4 Hz, 2H), 1.50 (d, J = 7.1 Hz, 3H). ^{13}C NMR (126 MHz, DMSO-d_6): δ 166.41, 164.82, 164.78, 136.94, 135.67, 131.05, 130.53, 129.85 (q, J = 32.7), 128.98, 128.28, 126.16, 124.41, 123.80 (q, J = 273.4 Hz), 49.95, 13.82. HRMS: m/z: calcd for $C_{21}H_{17}F_3N_2O_4S$: 451.0934 $[M+H]^+$; found: 451.0934.

5.2.20. N-(allyloxy)-2-(2,4-dioxo-5-(4-trifluoromethyl) benzylidene)thiazolidin-3-yl)propanamide 2h

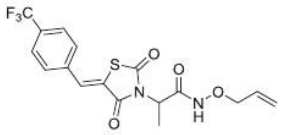

Method B. Mobile phase: DCM/MeOH 98:2. White solid. Yield: 31% (127 mg). ^{1}H NMR (500 MHz, DMSO-d_6): δ 11.37 (s, 1H), 8.02 (s, 1H), 7.91 (d, J = 8.3 Hz, 2H), 7.85 (d, J = 8.2 Hz, 2H), 5.91 (qd, J = 11.8, 6.1 Hz, 1H), 5.31 (d, J = 17.3 Hz, 1H), 5.24 (d, J = 10.4 Hz, 1H), 4.86 (q, J = 6.9 Hz, 1H), 4.26 (t, J = 5.1 Hz, 2H), 1.49 (d, J = 7.1 Hz, 3H). ^{13}C NMR (126 MHz, DMSO-d_6): δ 166.38, 164.76, 164.62, 136.94, 132.81, 131.04, 130.54, 129.85 (q, J = 31.5 Hz), 126.18, 124.41, 123.80 (q, J = 272.1 Hz), 119.34, 75.89, 49.92, 13.79. HRMS: m/z: calcd for $C_{17}H_{15}F_3N_2O_4S$: 401.0777 $[M+H]^+$; found: 401.0775.

5.2.21. N-(benzyloxy)-2-(5-(4-fluorobenzylidene)-2,4-dioxothiazolidin-3-yl)acetamide 2i

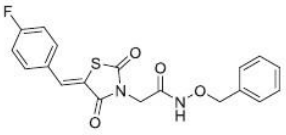

Method A. Yellow solid. Yield: 75% (617 mg). ^{1}H NMR (500 MHz, DMSO-d_6): δ 11.33 (s, 1H), 7.97 (d, J = 7.0 Hz, 1H), 7.71 (dd, J = 12.5, 6.7 Hz, 2H), 7.42–7.36 (m, 7H), 4.84 (s, 2H), 4.27 (s, 2H). ^{13}C NMR (126 MHz, DMSO-d_6): δ 166.85, 165.11, 164.06, 162.53, 162.06, 135.64, 132.66, 132.47, 129.51, 128.99, 128.82, 128,41, 128.26, 120.70, 116.74, 116.67, 116.43, 77.10, 41.51. HRMS: m/z: calcd for $C_{19}H_{15}FN_2O_4S$: 387.0809 $[M+H]^+$; found: 387.0813.

5.2.22. N-(allyloxy)-2-(5-(4-fluorobenzylidene)-2,4-dioxothiazolidin-3-yl)acetamide 2j

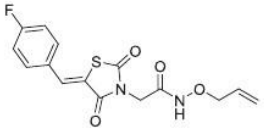

Method A. Yellow solid. Yield: 75% (432 mg). ^{1}H NMR (500 MHz, DMSO-d_6): δ 11.25 (s, 1H), 7.97 (s, 1H), 7.74–7.69 (m, 2H), 7.38 (t, J = 8.4 Hz, 2H), 5.95 (s, 1H), 5.35 (d, J = 17.1 Hz,2H), 5.28 (d, J = 9.5 Hz, 2H), 4.32 (br s, 4H). ^{13}C NMR (126 MHz, DMSO-d_6): δ 166.82, 165.10, 162.37, 162.06, 132.70, 132.62, 132.43, 129.50, 119.54, 116.72, 116.61, 116.55, 116.44, 76.09, 41.47. HRMS: m/z: calcd for $C_{15}H_{13}FN_2O_4S$: 337.0653 $[M+H]^+$; found: 337.0653.

5.2.23. N-(benzyloxy)-2-(5-(4-fluorobenzylidene)-2,4-dioxothiazolidin-3-yl)propanamide 2k

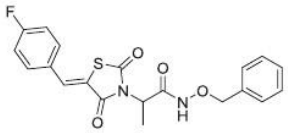

Method B. Mobile phase: DCM/MeOH 98:2. Green solid. Yield: 45% (62 mg). ^{1}H NMR (500 MHz, DMSO-d_6): δ 11.46 (s, 1H), 7.96 (s, 1H), 7.72 (dd, J = 8.5, 5.5 Hz, 2H), 7.43–7.34 (m, 7H), 4.87 (q, J = 7.1 Hz, 1H), 4.77 (d, J = 8.2 Hz, 2H), 1.49 (d, J = 7.2 Hz, 3H). ^{13}C NMR (126 MHz, DMSO-d_6): δ 166.63, 164.95, 164.89, 163.97, 161.97, 135.69, 132.59, 131.89, 129.62, 128.97, 128.27, 121.07, 116.68, 116.50, 76.92, 49.88, 13.86. HRMS: m/z: calcd for $C_{20}H_{17}FN_2O_4S$: 401.0966 $[M+H]^+$; found: 401.0968.

5.2.24. N-(allyloxy)-2-(5-(4-fluorobenzylidene)-2,4-dioxothiazolidin-3-yl)propanamide 2l

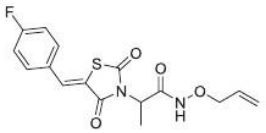

Method B. Mobile phase: DCM/MeOH 95:5. Green solid. Yield: 45% (54 mg). ^{1}H NMR (500 MHz, DMSO-d_6): δ 11.35 (s, 1H), 7.95 (s, 1H), 7.72 (dd, J = 8.7, 5.4 Hz, 2H), 7.41 (t, J = 8.8 Hz, 2H), 5.95–5.87 (m, 1H), 5.30 (d, J = 16.0 Hz, 1H), 5.24 (d, J = 10.4 Hz, 1H), 4.84 (q, J = 7.0 Hz, 1H), 4.26 (t, J = 5.2 Hz, 2H), 1.48 (d, J = 7.2 Hz, 3H). ^{13}C NMR (126 MHz, DMSO-d_6): δ 166.59, 164.94, 164.69, 161.97, 132.81, 132.59, 132.52, 131.88, 129.64, 121.07, 119.31, 116.67, 116.50, 75.88, 49.84, 13.84. HRMS: m/z: calcd for $C_{16}H_{15}FN_2O_4S$: 351.0809 $[M+H]^+$; found: 351.0811.

5.2.25. N-(benzyloxy)-2-(2,4-dioxo-5-pentylidenethiazolidin-3-yl) acetamide 2m

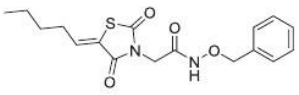

Method B. Brown solid. Yield: 35% (174 mg). ^{1}H NMR (500 MHz, DMSO-d_6): δ 11.29 (s, 1H), 7.43–7.37 (m, 5H), 7.09 (dt, J = 11.2, 7.6 Hz, 1H), 4.83 (d, J = 8.5 Hz, 2H), 4.21 (s, 2H), 2.27 (dq, J = 11.2, 7.4 Hz, 2H), 1.53 (dd, J = 14.5, 10.9 Hz, 2H), 1.36 (ddd, J = 14.5, 11.1, 7.5 Hz, 2H), 0.92 (t, J = 11.3, 7.3 Hz, 3H). ^{13}C NMR (126 MHz, DMSO-d_6): δ 166.79, 163.86, 162.60, 139.33, 135.64, 128.86, 128.33, 124.32, 77.07, 41.19, 30.95, 29.28, 21.75, 13.57. HRMS: m/z: calcd for $C_{17}H_{20}N_2O_4S$: 349.1217 $[M+H]^+$; found: 349.1217.

5.2.26. N-(allyloxy)-2-(2,4-dioxo-5-pentylidenethiazolidin-3-yl) acetamide 2n

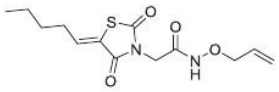

Method B. Mobile phase: hex/EtOAc 60:40. Yellow solid. Yield: 40% (178 mg). ^{1}H NMR (500 MHz, DMSO-d_6): δ 11.40 (s, 1H), 7.08 (t, J = 7.7 Hz, 1H), 5.91 (ddd, J = 16.5, 11.3, 6.0 Hz, 1H), 5.32 (d, J = 17.3 Hz, 1H), 5.26 (d, J = 10.4 Hz, 1H), 4.35–4.13 (m, 4H), 2.24 (dd, J = 14.7, 7.4 Hz, 2H), 1.50 (dt, J = 15.0, 7.4 Hz, 2H), 1.32 (dd, J = 14.9, 7.4 Hz, 2H), 0.89 (t, J = 7.3 Hz, 3H). ^{13}C NMR (126 MHz, DMSO-d_6): δ 166.76, 163.85, 162.43, 139.28, 132.70, 124.31, 119.48, 76.06, 41.16, 30.94, 29.27, 21.74, 13.57. HRMS: m/z: calcd for $C_{13}H_{18}N_2O_4S$: 299.1060 $[M+H]^+$; found: 299.1060.

5.2.27. N-(benzyloxy)-2-(2,4-dioxo-5-pentylidenethiazolidin-3-yl) propanamide 2o

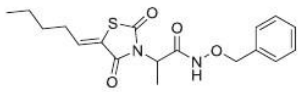

Method B. Mobile phase: DCM/MeOH 95:5. Yellow oil. Yield: 60% (160 mg). ^{1}H NMR (500 MHz, DMSO-d_6): δ 11.41 (s, 1H), 7.39–7.34 (m, 5H), 7.04 (t, J = 7.7 Hz, 1H), 4.76 (t, J = 8.8 Hz, 3H), 2.23 (q, J = 7.4 Hz, 2H), 1.51–1.48 (m, 2H), 1.45 (d, J = 7.2 Hz, 3H), 1.33 (dd, J = 14.9, 7.4 Hz, 2H), 0.89 (t, J = 7.3 Hz, 3H). ^{13}C NMR (126 MHz, DMSO-d_6): δ 166.59, 164.94, 163.73, 138.64, 135.68, 128.95, 128.26, 124.51, 76.89, 49.64, 30.87, 29.32, 21.75, 13.85, 13.59. HRMS: m/z: calcd for $C_{18}H_{22}N_2O_4S$: 363.1373 $[M+H]^+$; found: 363.1372.

5.2.28. N-(allyloxy)-2-(2,4-dioxo-5-pentylidenethiazolidin-3-yl) propanamide 2p

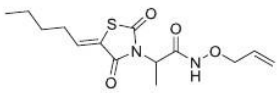

Method B. DCM/MeOH 85:15. Yellow oil. Yield: 56% (129 mg). ^{1}H NMR (500 MHz, DMSO-d_6): δ 11.31 (s, 1H), 7.04 (s, 1H), 5.91 (ddd, J = 17.0, 11.2, 5.9 Hz, 1H), 5.29 (d, J = 15.8 Hz, 1H), 5.23 (d, J = 8.8 Hz, 1H), 4.76 (q, J = 7.1 Hz, 1H), 4.24 (s, 2H), 2.23 (dd, J = 14.8, 7.4 Hz, 2H), 1.51–1.47 (m, 2H), 1.43 (d, J = 7.2 Hz, 3H), 1.33 (dd, J = 14.9, 7.4 Hz, 2H), 0.89 (t, J = 7.3 Hz, 3H). ^{13}C NMR (126 MHz, DMSO-d_6): δ 166.54, 164.74, 163.71, 138.63, 132.81, 119.25, 75.84, 49.59, 30.87, 29.32, 21.75, 13.84, 13.58. HRMS: m/z: calcd for $C_{14}H_{20}N_2O_4S$: 313.1217 $[M+H]^+$; found: 313.1215.

5.3. In silico prediction of drug-likeness properties

Physicochemical and pharmacokinetic parameters of the thiazolidinedione-hydroxamates were *in silico* predicted using the FAF*Drugs*4 [29] and admetSAR tools [30]. The different parameters predicted were as follows: molecular weight, octanol/water partition coefficient, number of hydrogen donors, number of hydrogen acceptors, number of atoms, number of rotatable bonds, aqueous solubility, Solubility Forecast Index, oral bioavailability via Veber's rule, 4/400 GSK rule, Ames toxicity and acute oral toxicity.

5.4. Zmp1 inhibition assay

Human angiotensin II (Sigma-Aldrich, Cat. No. A9525) was dissolved in LC-MS-quality water to a concentration of 4 nmol/ml. Aliquots (24 µl) of the stock solution were mixed with 1 µl of 2M NH_4HCO_3 in 0.5-ml test tubes. This was followed by pipetting either

1 μl of neat acetone (control) or 1 μl of 1 mM inhibitor solution in acetone (sample). After pre-incubation in a thermostat at 37 °C for 3 min, the reaction was started by adding 1 μl of a recombinant Zmp1 metallopeptidase from *Mycobacterium tuberculosis* (ProSci, Poway, CA, USA; Cat. No. 90−361; diluted 1:4, *v/v*, with cold 50 mM NH_4HCO_3 and kept on ice during the measurements) and proceeded at 37 °C for 20 min. Aliquots (0.5 μl) of the reaction mixture were aspirated by a pipette each 2 min, spotted onto the MALDI target (an MSP BigAnchor 96 BC; Bruker Daltonik, Bremen, Germany), immediately overlaid with matrix solution (α-cyano-4-hydroxycinnamic acid, 5 mg/ml in acetonitrile: 2.5% (v/v) trifluoroacetic acid, 7:3, v/v), and left to dry and crystallize.

MALDI-TOF MS measurements were carried out on a Microflex LRF 20 instrument equipped with a 60-Hz nitrogen laser operating at $\lambda_{max} = 337$ nm (Bruker Daltonik). Mass spectra were accumulated from 1000 laser shots in the reflectron positive ion mode using an acceleration voltage (IS1) of 18.0 kV, extraction voltage (IS2) of 15.5 kV, lens voltage of 9.3 kV, reflectron voltage of 19.0 kV, detector voltage of 1590 V and pulsed ion extraction delay time of 350 ns The instrument was calibrated externally with a peptide mixture (Peptide Calibration Standard II; Bruker Daltonik).

The enzymatic reaction was monitored by the hydrolysis of angiotensin II yielding a peptide DRVY (*m/z* 552.3), which is accompanied by a simultaneous decrease in the angiotensin II signal (DRVYIHPF; *m/z* 1046.5). The ratio of *m/z* 552 versus *m/z* 1046 signal intensities was plotted against the reaction time to achieve an increasing linear dependence. The inhibition rate at the given inhibitor concentration of 40 μM was finally calculated by inverting the ratio of slopes for inhibited and control reaction. Phosphoramidone (RDF) was used as a reference inhibitor [16]. Three different inhibitor concentrations in the range of 20−80 μM were used to determine the corresponding IC_{50} value. The measured responses (percentages of inhibition) were plotted against the respective concentrations. All data points obtained for a single inhibitor were fitted by a straight line (linear regression equation: y = a*x + b) and then IC_{50} (in μM) was obtained as a result of calculating formula (50 - b)/a.

5.5. In vitro antimycobacterial activity

In vitro activity of the synthesized hybrids against *Mtb* H37Ra (ATCC® 25177™) was evaluated by a resazurin assay. The thiazolidinedione-hydroxamates were solubilized in DMSO (Sigma-Aldrich) at stock concentration of 10 mM. A two-fold serial dilution of each compound was made in liquid Middlebrook 7H9 broth (Sigma-Aldrich) with 10% oleic acid, albumin, dextrose, catalase (OADC) enrichment (BD Biosciences; complete 7H9 broth) with final concentrations ranging from 64 to 0.25 μM. Volumes of 100 μl of the serial dilutions were added in triplicate to flat-bottomed 96-well plates. A mycobacterial suspension was prepared by thawing and dissolving a frozen glycerol-stock of *Mtb* H37Ra and, subsequently, diluting it in complete 7H9 broth to obtain a suspension with an appropriate inoculum size. A volume of 100 μl of the mycobacterial suspension was added to each well of the test plates. Isoniazid was used as a reference drug. Positive (100% growth) and negative (0% growth) controls were included as well. Test plates were incubated at 37 °C for 7 days. After 7 days of exposure, extracellular mycobacterial replication was assessed by resazurin. To each test well, 20 μl of a 0.02% resazurin (Sigma-Aldrich) solution was added. Test plates were incubated at 37 °C until a color change from blue to pink occurred. Fluorescence was measured at $\lambda_{ex} = 550$ nm and $\lambda_{em} = 590$ nm using a spectrophotometer (Promega Discover). Results were presented as the mean of triplicate values.

5.6. Assessment of acute in vitro cytotoxicity

The 50% cytotoxic concentration towards the RAW264.7 murine macrophage cell line (ATCC® TIB-71™) was determined by a neutral red uptake (NRU) assay. The RAW264.7 cells were cultured in Dulbecco's modified Eagle's medium (DMEM; Thermo Fisher) supplemented with 10% (v/v) heat-inactivated fetal calf serum (iFCS; Thermo Fisher) in a 5% CO_2 atmosphere at 37 °C until a semi-confluent layer of cells was obtained. Next, the cells were harvested and seeded into transparent, flat-bottomed 96-well plates at a density of 40.000 cells per well and left for recovery at 37 °C and 5% CO_2. The following day, twofold serial dilutions of the tested compounds were made in DMEM +10% iFCS with a final starting concentration of 128 μM. As a positive control, tamoxifen (Sigma-Aldrich) was included. The RAW264.7 cells were washed with sterile phosphate-buffered saline (PBS; Thermo Fisher) and exposed to the compounds by adding volumes of 100 μl of the serial dilutions. Tamoxifen was used as a reference drug. Test plates were left for 24 h at 37 °C and 5% CO_2. After 24 h exposure to the compounds, the cells were washed two times with sterile PBS and 100 μl neutral red (Sigma-Aldrich) working solution was added per well. Subsequently, the test plates were incubated for 3 h at 37 °C and 5% CO_2. The cells were washed again with sterile PBS and 150 μl of a 1:1 ethanol/acetic acid (Merck) mixture was added in each well. The plates were left shaking until the color became homogenous purple, and the optical density was measured at 530 nm and 620 nm (reference wavelength) using a plate reader (Promega Discover). Results were presented as the mean of triplicate values.

5.7. Macrophage infection assay

The intracellular activity of the thiazolidinedione-hydroxamates was tested by infecting the murine RAW264.7 macrophage cell line with *Mtb* H37Ra^{lux}, a laboratory *Mtb* H37Ra strain transformed with a pSMT1 luciferase reporter plasmid. The RAW264.7 cells were cultured, harvested and seeded into transparent, flat-bottomed 96-well plates as described above. Upon recovery, the cells were washed with sterile PBS and infected with H37Ra^{lux} at a multiplicity of infection (MOI) of 10 for 2 h at 37 °C. RAW264.7 cells were washed two times with sterile PBS, incubated with 100 μg/ml gentamicin (Sigma-Aldrich) for 1 h to kill the residual extracellular bacteria and, again, washed with sterile PBS. Then, the infected RAW264.7 cells were treated with the thiazolidinedione-hydroxamates at a final test concentration of 10 and 100 μM. Isoniazid was included as a reference drug at 0.1 μM. Uninfected cells were used as control. At 24 h post-exposure, the infected RAW264.7 cells were washed and lysed with 200 μl of 1% Triton X-100 (Sigma-Aldrich). To assess the intracellular mycobacterial replication, 25 μl of 1% (v/v) n-decanal in ethanol was added to 100 μl of the lysate and luminescence was measured using a luminometer (Promega Discover). Results were presented the mean of triplicate values.

5.8. In silico molecular docking

All 3D structures of the designed library of ligands were obtained with Marvin 15.1.5, software which can be used for drawing, displaying and characterization of chemical structure, substructures and reactions. Polar hydrogens were added to all ligands and proteins with the AutoDock Tools program [45]. Docking of the library of the structures into *Mycobacterium tuberculosis* zinc metalloprotease Zmp1 (PDB ID: 3ZUK) was carried out using AutoDock Vina 1.1.2 [46]. A grid box with the edge of 21 Å was centred on the active site of Zmp1 in the crystal structure (grid x: 95.8, y: 93.2, z: 33.0). The exhaustiveness parameter was set to 80 (default: 8).

After docking, we compared the docked poses in bulk and that of the compound **2n** was further analyzed and interpreted.

Acknowledgements

This work was supported by grant no. JG_2019_002 from Palacký University in Olomouc.

Appendix A. Supplementary data

Supplementary data to this article can be found online at https://doi.org/10.1016/j.ejmech.2019.111812.

References

[1] M. Pai, M.A. Behr, M. Divangahi, D. Menzies, M. Pai, D. Dowdy, K. Dheda, C.C. Boehme, A. Ginsberg, S. Swaminathan, M. Spigelman, H. Getahun, M. Raviglione, Tuberculosis, Nat. Rev. Dis. Prim. 2 (2016) 16076.

[2] World Health Organization (WHO), Global Tuberculosis Report 2018, 2018 (Geneva).

[3] World Health Organization (WHO), WHO Consolidated Guidelines on Drug-Resistant Tuberculosis Treatment, 2019 (Geneva).

[4] World Health Organization (WHO), Implementing the End TB Strategy: the Essentials, 2015 (Geneva).

[5] K.C. Chang, C.C. Leung, E. Nuermberger, G. Sotgiu, New drugs and regimens for tuberculosis, Respirology 23 (2018) 978–990.

[6] R. Mehra, I.A. Khan, A. Nargotra, Anti-tubercular drug discovery: in silico implications and challenges, Eur. J. Pharm. Sci. 104 (2017) 1–15.

[7] D.M. Ferraris, D. Sbardella, A. Petrera, S. Marini, B. Amstutz, M. Coletta, P. Sander, M. Rizzi, Crystal structure of Mycobacterium tuberculosis zinc-dependent metalloprotease-1 (Zmp1), a metalloprotease involved in pathogenicity, J. Biol. Chem. 286 (2011) 32475–32482.

[8] S.S. Master, S.K. Rampini, A.S. Davis, C. Keller, S. Ehlers, B. Springer, G.S. Timmins, P. Sander, V. Deretic, *Mycobacterium tuberculosis* prevents inflammasome activation, Cell Host Microbe 3 (2008) 224–232.

[9] V. Lazarevic, F. Martinon, Linking inflammasome activation and phagosome maturation, Cell Host Microbe 3 (2008) 199–200.

[10] D.M. Ferraris, R. Miggiano, F. Rossi, M. Rizzi, *Mycobacterium tuberculosis* molecular determinants of infection, survival strategies, and vulnerable targets, Pathogens 7 (2018).

[11] D.M. Ferraris, M. Rizzi, Zinc-dependent Metalloprotease-1 (Zmp1), John Wiley & Sons Ltd., 2013, pp. 1–7.

[12] G. Hu, G. Lin, M. Wang, L. Dick, R.M. Xu, C. Nathan, H. Li, Structure of the *Mycobacterium tuberculosis* proteasome and mechanism of inhibition by a peptidyl boronate, Mol. Microbiol. 59 (2006) 1417–1428.

[13] A.F. Kisselev, Z. Songyang, A.L. Goldberg, Why does threonine, and not serine, function as the active site nucleophile in proteasomes? J. Biol. Chem. 275 (2000) 14831–14837.

[14] M. Mori, F. Moraca, D. Deodato, D.M. Ferraris, P. Selchow, P. Sander, M. Rizzi, M. Botta, Discovery of the first potent and selective *Mycobacterium tuberculosis* Zmp1 inhibitor, Bioorg. Med. Chem. Lett 24 (2014) 2508–2511.

[15] M. Mori, D. Deodato, M. Kasula, D.M. Ferraris, A. Sanna, A. De Logu, M. Rizzi, M. Botta, Design, synthesis, SAR and biological investigation of 3-(carboxymethyl)rhodanine and aminothiazole inhibitors of *Mycobacterium tuberculosis* Zmp1, Bioorg. Med. Chem. Lett 28 (2018) 637–641.

[16] M. Paolino, M. Brindisi, A. Vallone, S. Butini, G. Campiani, C. Nannicini, G. Giuliani, M. Anzini, S. Lamponi, G. Giorgi, D. Sbardella, D.M. Ferraris, S. Marini, M. Coletta, I. Palucci, M. Minerva, G. Delogu, I. Pepponi, D. Goletti, A. Cappelli, S. Gemma, S. Brogi, Development of potent inhibitors of the *Mycobacterium tuberculosis* virulence factor Zmp1 and evaluation of their effect on mycobacterial survival inside macrophages, ChemMedChem 13 (2018) 422–430.

[17] D.D. Subhedar, M.H. Shaikh, B.B. Shingate, L. Nawale, D. Sarkar, V.M. Khedkar, K.F. Kalam, J.N. Sangshetti, Quinolidene-rhodanine conjugates: facile synthesis and biological evaluation, Eur. J. Med. Chem. 125 (2017) 385–399.

[18] D.D. Subhedar, M.H. Shaikh, L. Nawale, A. Yeware, D. Sarkar, F.A. Kalam Khan, J.N. Sangshetti, B.B. Shingate, Novel tetrazoloquinoline-rhodanine conjugates: highly efficient synthesis and biological evaluation, Bioorg. Med. Chem. Lett 26 (2016) 2278–2283.

[19] S. Ponnuchamy, S. Kanchithalaivan, R. Ranjith Kumar, M. Ashraf Ali, T. Soo Choon, Antimycobacterial evaluation of novel hybrid arylidene thiazolidine-2,4-diones, Bioorg. Med. Chem. Lett 24 (2014) 1089–1093.

[20] N.B. Patel, I.H. Khan, Synthesis of newer 5-benzylidene-2,4-thiazolidinediones as potential antimicrobials, Indian J. Res. Pharm. Biotechnol. 2 (9) (2014) 993–1001.

[21] F.M. Shaikh, N.B. Patel, D. Rajani, Synthesis of new thiazolidine-2,4-dione derivatives and their antimicrobial and antitubercular activity, Indian J. Res. Pharm. Biotechnol. 1 (2013) 496–503.

[22] J.A. Jacobsen, J.L. Major Jourden, M.T. Miller, S.M. Cohen, To bind zinc or not to bind zinc: an examination of innovative approaches to improved metalloproteinase inhibition, Biochim. Biophys. Acta Mol. Cell Res. 1803 (2010) 72–94.

[23] M.W. Majewski, S. Cho, P.A. Miller, S.G. Franzblau, M.J. Miller, Syntheses and evaluation of substituted aromatic hydroxamates and hydroxamic acids that target *Mycobacterium tuberculosis*, Bioorg. Med. Chem. Lett 25 (2015) 4933–4936.

[24] M. Flipo, T. Beghyn, J. Charton, V.A. Leroux, B.P. Deprez, R.F. Deprez-Poulain, A library of novel hydroxamic acids targeting the metallo-protease family: design, parallel synthesis and screening, Bioorg. Med. Chem. 15 (2007) 63–76.

[25] Y.M. Lin, M.J. Miller, Practical synthesis of hydroxamate-derived siderophore components by an indirect oxidation method and syntheses of a DIG-siderophore conjugate and a biotin-siderophore conjugate, J. Org. Chem. 64 (1999) 7451–7458.

[26] K. Kar, U. Krithika, Mithuna, P. Basu, S. Santhosh Kumar, A. Reji, B.R. Prashantha Kumar, Design, synthesis and glucose uptake activity of some novel glitazones, Bioorg. Chem. 56 (2014) 27–33.

[27] S. Mohanty, A.K. Roy, V.K.P. Kumar, S.G. Reddy, A.C. Karmakar, Acetic anhydride-promoted one-pot condensation of 2,4-thiazolidinedione with bisulfite adducts of aldehydes, Tetrahedron Lett. 55 (2014) 4585–4589.

[28] U.R. Pratap, D.V. Jawale, R.A. Waghmare, D.L. Lingampalle, R.A. Mane, Synthesis of 5-arylidene-2,4-thiazolidinediones by Knoevenagel condensation catalyzed by Baker's yeast, New J. Chem. 35 (2011) 49–51.

[29] D. Lagorce, O. Sperandio, J.B. Baell, M.A. Miteva, B.O. Villoutreix, FAF-Drugs3: a web server for compound property calculation and chemical library design, Nucleic Acids Res. 43 (2015) W200–W207.

[30] F. Cheng, W. Li, Y. Zhou, J. Shen, Z. Wu, G. Liu, P.W. Lee, Y. Tang, admetSAR: a comprehensive source and free tool for assessment of chemical ADMET properties, J. Chem. Inf. Model. 52 (2012) 3099–3105.

[31] S. Chander, P. Ashok, D. Cappoen, P. Cos, S. Murugesan, Design, synthesis and biological evaluation of novel quinoline-based carboxylic hydrazides as anti-tubercular agents, Chem. Biol. Drug Des. 88 (2016) 585–591.

[32] S. Chander, P. Ashok, D. Cappoen, P. Cos, S. Murugesan, Design, synthesis and biological evaluation of novel quinoline-based carboxylic hydrazides as anti-tubercular agents, Chem. Biol. Drug Des. 88 (2016) 585–591.

[33] W.L. Jorgensen, E.M. Duffy, Prediction of drug solubility from Monte Carlo simulations, Bioorg. Med. Chem. Lett 10 (2000) 1155–1158.

[34] D.F. Veber, S.R. Johnson, H.Y. Cheng, B.R. Smith, K.W. Ward, K.D. Kopple, Molecular properties that influence the oral bioavailability of drug candidates, J. Med. Chem. 45 (2002) 2615–2623.

[35] J.A. Carson, T. Ansai, S. Awano, W. Yu, T. Takehara, A.J. Turner, Characterization of PgPepO, a bacterial homologue of endothelin-converting enzyme-1, Clin. Sci. (Lond.) 103 (Suppl 48) (2002) 90S–93S.

[36] M. Bucknall, K.Y.C. Fung, M.W. Duncan, Practical quantitative biomedical applications of MALDI-TOF mass spectrometry, J. Am. Soc. Mass Spectrom. 13 (2002) 1015–1027.

[37] N.V. Gogichaeva, T. Williams, M.A. Alterman, MALDI TOF/TOF tandem mass spectrometry as a new tool for amino acid analysis, J. Am. Soc. Mass Spectrom. 18 (2007) 279–284.

[38] Y. Zheng, X. Jiang, F. Gao, J. Song, J. Sun, L. Wang, X. Sun, Z. Lu, H. Zhang, Identification of plant-derived natural products as potential inhibitors of the *Mycobacterium tuberculosis* proteasome, BMC Complement Altern. Med. 14 (2014) 400–401, 400/7.

[39] E. Torfs, J. Vajs, M. Bidart de Macedo, F. Cools, B. Vanhoutte, Y. Gorbanev, A. Bogaerts, L. Verschaeve, G. Caljon, L. Maes, P. Delputte, P. Cos, J. Kosmrlj, D. Cappoen, Synthesis and in vitro investigation of halogenated 1,3-bis(4-nitrophenyl)triazenide salts as antitubercular compounds, Chem. Biol. Drug Des. 91 (2018) 631–640.

[40] R.J. Smets, E. Torfs, F. Lemiere, P. Cos, D. Cappoen, K. Abbaspour Tehrani, Synthesis and antitubercular activity of 1- and 3-substituted benzo[g]isoquinoline-5,10-diones, Org. Biomol. Chem. 17 (2019) 2923–2939.

[41] D. Cappoen, P. Claes, J. Jacobs, R. Anthonissen, V. Mathys, L. Verschaeve, K. Huygen, N.D. Kimpe, 1,2,3,4,8,9,10,11-Octahydrobenzo[j]phenanthridine-7,12-diones as New Leads against *Mycobacterium tuberculosis*, J. Med. Chem. 57 (2014) 2895–2907.

[42] R. Wang, X. Fang, Y. Lu, C.Y. Yang, S. Wang, The PDBbind database: methodologies and updates, J. Med. Chem. 48 (2005) 4111–4119.

[43] C. Oefner, A. D'Arcy, M. Hennig, F.K. Winkler, G.E. Dale, Structure of human neutral endopeptidase (neprilysin) complexed with phosphoramidon, J. Mol. Biol. 296 (2000) 341–349.

[44] A. Wisner, E. Dufour, M. Messaoudi, A. Nejdi, A. Marcel, M.N. Ungeeheuer, C. Rougeot, Human Opiorphin, a natural antinociceptive modulator of opioid-dependent pathways, Proc. Natl. Acad. Sci. U.S.A. 103 (2006) 17979–17984.

[45] G.M. Morris, R. Huey, W. Lindstrom, M.F. Sanner, R.K. Belew, D.S. Goodsell, A.J. Olson, AutoDock, AutoDockTools, Automated docking with selective receptor flexibility, J. Comput. Chem. 30 (2009) 2785–2791.

[46] O. Trott, A.J. Olson, AutoDock Vina, Improving the speed and accuracy of docking with a new scoring function, efficient optimization, and multithreading, J. Comput. Chem. 31 (2010) 455–461.

Appendix 4

Solid-phase synthetic approach towards new pyrimidines as potential antibacterial agents

Machníková. R.; Janovská L.; **Brulíková, L.***

J. Mol. Struct. **2020**, *1200*, 127101.

Journal of Molecular Structure 1200 (2020) 127101

Contents lists available at ScienceDirect

Journal of Molecular Structure

journal homepage: http://www.elsevier.com/locate/molstruc

Solid-phase synthetic approach towards new pyrimidines as potential antibacterial agents

Romana Machníková [a], Lucie Janovská [b, c], Lucie Brulíková [a, *]

[a] Department of Organic Chemistry, Faculty of Science, Palacký University, 17. Listopadu 12, Olomouc, 77146, Czech Republic
[b] Department of Chemical Biology and Genetics, Centre of the Region Haná for Biotechnological and Agricultural Research, Faculty of Science, Palacký University, Šlechtitelů 27, Olomouc, 783 71, Czech Republic
[c] Department of Microbiology, Faculty of Medicine and Dentistry, Palacký University, Hněvotínská 3, Olomouc, 775 15, Czech Republic

ARTICLE INFO

Article history:
Received 31 July 2019
Received in revised form
18 September 2019
Accepted 19 September 2019
Available online 24 September 2019

Keywords:
Pyrimidines
Solid-phase synthesis
Antimycobacterial
Antibacterial

ABSTRACT

Herein, we report the polymer-supported synthesis of new pyrimidine derivatives and their antimycobacterial and antimicrobial activity. Our methodology is based on the fast and efficient solid-phase synthesis having the ability to implement structural diversity from the readily available building blocks through minimum synthetic route and with high yields. Our method was validated in the synthesis of a model chemical library prepared via a combinatorial approach. All the prepared compounds were evaluated for their antimycobacterial activity against *Mycobacterium tuberculosis* H37Rv, antibacterial activity against *Staphylococcus aureus*, *Pseudomonas aeruginosa*, *Escherichia coli*, and *Enterococcus faecalis*, and activity against two fungal strains of *Candida albicans* and *Aspergillus niger*. Our results reveal that most of the tested compounds have modest antimycobacterial activity against *M. tuberculosis* H37Rv, with the most active being pyrimidine **2f** (MIC value 32 μg/mL). Moreover, compound **1b** showed considerable activity against *P. aeruginosa*. These results indicate the potential of our developed methodology that could lead to a pathway for the preparation of new drug candidates in the future.

1. Introduction

Recently, there has been a gradual increase in the number of multidrug-resistant (MDR) pathogens with a minimum response to the known antibacterial drugs [1]. In particular, *Mycobacterium tuberculosis* has an increasing prevalence of MDR and extensively drug-resistant strains; thus, tuberculosis (TB) remains a major health problem worldwide [2]. The current situation requires a search for novel antibacterial agents with new modes of an action directed as of yet unknown targets.

The pyrimidine scaffold plays an important role in several biologically active substances and possesses a range of diverse biological activities such as anti-cancer [3], anti-inflammatory [4], anti-hepatitis [5], anti-diabetic [6] etc. Moreover, variously modified pyrimidines were successfully studied as antibacterial agents [7–16]. Some of the representative examples are depicted in Fig. 1.

Given the biological significance of the pyrimidine heterocycle, we employed a fast and effective approach to prepare new pyrimidines based on solid-phase synthesis. Our method focuses on the ability to introduce structural diversity from abundant and readily available building blocks with a minimal synthetic route. Here, we have synthesized 30 new pyrimidines and presented their antibacterial activities.

2. Material and methods

Solvents and chemicals were purchased from Sigma-Aldrich (Milwaukee, US, www.sigmaaldrich.com) or Fluorochem (Derbyshire, UK, www.fluorochem.co.uk). The synthesis was carried out on Domino Blocks (www.torviq.com) in disposable polypropylene reaction vessels. All the reactions were carried out at room temperature of 21 °C unless stated otherwise. The volume of the wash solvent was 10 mL/g of the resin.

For LC-MS analysis, a sample of the resin (~5 mg) was treated with trifluoroacetic acid (TFA) in dichloromethane (DCM), the cleavage cocktail was evaporated by a stream of nitrogen, and cleaved compounds were extracted into 1 mL of MeOH.

The LC/MS analyses were carried out on the UHPLC-MS system consisting of UHPLC chromatograph Acquit with a photodiode array detector and single quadrupole mass spectrometer (Waters),

* Corresponding author.
E-mail address: lucie.brulikova@upol.cz (L. Brulíková).

https://doi.org/10.1016/j.molstruc.2019.127101
0022-2860/

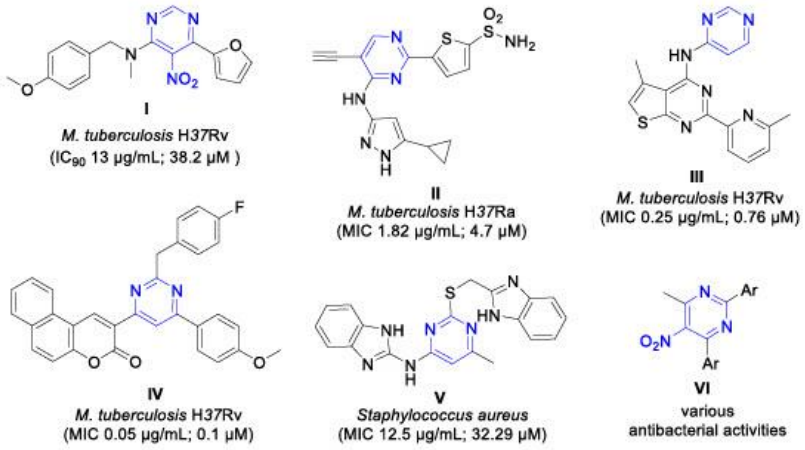

Fig. 1. Structures of known pyrimidines I [15], II [7], III [12], IV [16], V [11] and VI [13] with antimycobacterial or antibacterial properties.

using XSelect C18 column at 30 °C and a flow rate of 600 μL/min. The mobile phase was (A) 0.01 M ammonium acetate in H_2O, and (B) CH_3CN, linearly programmed from 10% A to 80% B over 2.5 min, kept for 1.5 min. The column was re-equilibrated with 10% of solution B for 1 min. The ESI source operated at a discharge current of 5 μA, vaporizer temperature of 350 °C and a capillary temperature of 200 °C.

Purification was carried out on the C18 reverse-phase column (YMC Pack ODS-A, 20 × 100 mm, 5 μm particles); gradient was formed from 10 mM aqueous ammonium acetate and CH_3CN, a flow rate of 15 mL/min. For the lyophilization of residual solvents at −110 °C, the ScanVac Coolsafe 110-4 was used.

NMR $^{1}H/^{13}C$ spectra were recorded on JEOL ECX-500SS (500 MHz) or JEOL ECA400II (400 MHz) spectrometer at a magnetic field strengths of 11.75 T (with operating frequencies 500.16 MHz for 1H and 125.77 MHz for 13C) and 9.39 T (with operating frequencies 399.78 MHz for 1H and 100.53 MHz for 13C) at room temperature (~21 °C). Chemical shifts (δ) are reported in parts per million (ppm), and coupling constants (J) are reported in Hertz (Hz). NMR spectra were recorded at 21 °C in DMSO-d_6 and referenced to the resonance signal of the solvent. Acetate salts exhibited a singlet at 1.7–1.9 ppm in the ^{1}H NMR spectrum and two resonances at 173 and 23 ppm in the ^{13}C spectrum.

HRMS analysis was performed using LC-MS an Orbitrap Elite high-resolution mass spectrometer (Dionex Ultimate 3000, Thermo Exactive plus, MA, US) operating at a positive full scan mode (120 000 FWMH) in the range of 100–1000 m/z. The settings for the electrospray ionization were at an oven temperature of 150 °C and a source voltage of 3.6 kV. The acquired data were internally calibrated with phthalate as a contaminant in CH_3OH (m/z 297.15909). Samples were diluted to a final concentration of 0.1 mg/mL in H_2O and CH_3OH (50:50, v/v). Before HPLC separation (column Phenomenex Gemini, 50 × 2.00 mm, 3 μm particles, C18), the samples were injected by direct infusion into the mass spectrometer using an autosampler. The mobile phase was isocratic CH_3CN/IPA/0.01 M ammonium acetate (40:5:55) and the flow rate was 0.3 mL/min.

2.1. Antimycobacterial and antimicrobial activity

Antimycobacterial activity of the pyrimidines against *M. tuberculosis* H37Rv (NCTC 7416) was evaluated using their minimum inhibitory concentration (MIC) by Resazurin microtiter assay [17,18] as we described earlier [19]. The antimicrobial activities of the final compounds against *Staphylococcus aureus* (CCM 3953), *Pseudomonas aeruginosa* (CCM 3955), *Escherichia coli* (CCM 3954), *Candida albicans* (ATCC 90028), *Aspergillus niger* (CCM 8189), and *Enterococcus faecalis* (CCM 4224) were determined from their MIC as described earlier [19,20].

3. Chemistry

3.1. Synthesis of resins 3 and 6

Wang resin (loading 1.0 mmol/g, ~1 g) was washed three times with DCM. A solution consisting of Fmoc-amino acid (2 mmol), *N*-hydroxybenzotriazole (HOBt, 2 mmol), 4-dimethylaminopyridine (DMAP, 0.5 mmol) and *N,N'*-diisopropylcarbodiimide (DIC, 2 mmol) in *N,N*-dimethylformamide (DMF)/DCM (1:1, *v/v*, 10 mL) was added to the resin. The resin slurry was shaken at rt for 16 h. After this time, the resin was washed three times with DMF and three times with DCM. The Fmoc protecting group was removed by exposure to 50% piperidine in DMF (*v/v* 10 mL) for 15 min, and then, the resin was washed three times with DMF and three times with DCM.

3.2. Reaction with 4,6-dichloro-5-nitropyrimidines (resins 4 and 7)

Resins 3 (~1 g) were washed three times with dry DMF and reacted with a solution consisting of 4,6-dichloro-5-nitropyrimidine (5 mmol) and *N,N*-diisopropylethylamine (DIEA, 5 mmol) in dry DMF (10 mL) at rt for 2 h. The resin was then washed five times with DMF and three times with DCM.

3.3. Reaction with amines (resins 5 and 8)

Resins 4 (~250 or 500 mg) were each washed three times with

dry DMF and reacted with a solution consisting of amine (1.25 mmol or 2.5 mmol) and DIEA (1.25 mmol or 2.5 mmol) in DMF (2.5 mL or 5 mL) at rt for 2 h. The resin was then washed three times with DMF and three times with DCM.

3.4. Reduction of the nitro group (resins 9)

Resin **5** (~250 mg) was washed three times with DCM. A solution of $Na_2S_2O_4$ (2.5 mmol), K_2CO_3 (3.0 mmol) and ethyl viologen diiodide (0.25 mmol) in water (2.5 mL) and DCM (2.5 mL) was added to the resin. The resin slurry was shaken at rt for 16 h. The resin was then washed three times with each solvent: DCM/water (1:1, *v/v*), DMF and DCM.

3.5. Acylation with carboxylic acids (resins 10)

Resins **6** (~250 mg) were washed three times with DCM. A solution of carboxylic acid (0.75 mmol), HOBt (0.75 mmol) and DIC (0.75 mmol) in DMF/DCM (1:1, *v/v*, 2.5 mL) was added to the resin. The resin slurry was shaken at rt for 16 h. The resin was then washed three times with DMF and three times with DCM.

3.6. Cleavage from resin with TFA (compounds 1 and 2)

Resins **5** and **6** (~250 mg) were each treated with 2 mL of a solution consisting of TFA/DCM (1:1, *v/v*) for 1 h. The cleavage cocktail was collected, and the resin was washed three times with 50% TFA in DCM. The combined extracts were evaporated by a stream of nitrogen, and the crude products were purified by reversed-phase HPLC.

3.7. Analytical data of individual compounds

3.7.1. 3-((5-Nitro-6-(propylamino)pyrimidin-4-yl)amino) propanoic acid 1a

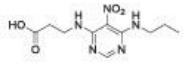

Yellow solid. Yield: 37.0 mg (80%). ^{1}H NMR (500 MHz, DMSO-d_6): δ 9.52 (t, J = 5.4 Hz, 1H), 9.43 (t, J = 5.7 Hz, 1H), 8.08 (s, 1H), 3.75 (q, J = 6.7 Hz, 2H), 3.50 (q, J = 6.2 Hz, 2H), 2.57 (t, J = 6.8 Hz, 2H), 1.59 (sxt, J = 7.3 Hz, 2H), 0.88 (t, J = 7.4 Hz, 3H).^{13}C NMR (101 MHz, DMSO-d_6): δ 175.96, 158.60, 157.03, 156.80, 112.75, 43.85, 37.23, 33.70, 22.52, 11.46. HRMS: *m/z*: calcd for $C_{10}H_{16}N_5O_4^+$: 270.1197 $[M+H]^+$; found: 270.1197.

3.7.2. 3-((6-(Cyclohexylamino)-5-nitropyrimidin-4-yl)amino) propanoic acid 1b

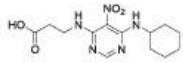

Yellow solid. Yield: 35.7 mg (78%). ^{1}H NMR (500 MHz, DMSO-d_6): δ 12.35 (s, 1H), 9.53 (t, J = 5.8 Hz, 1H), 9.19 (d, J = 7.7 Hz, 1H), 8.09 (s, 1H), 4.19–4.10 (m, 1H), 3.75 (q, J = 6.7 Hz, 2H), 2.57 (t, J = 6.7 Hz, 2H), 1.93–1.84 (m, 2H), 1.73–1.65 (m, 2H), 1.61–1.53 (m, 1H), 1.45–1.29 (m, 4H), 1.28–1.15 (m, 1H). ^{13}C NMR (126 MHz, DMSO-d_6): δ 173.04, 159.50, 156.69, 155.91, 111.88, 49.50, 36.84, 33.31, 31.76, 24.95, 24.24. HRMS: *m/z*: calcd for $C_{13}H_{20}N_5O_4^+$: 310.1510 $[M+H]^+$; found: 310.1509.

3.7.3. 3-((6-(Benzylamino)-5-nitropyrimidin-4-yl)amino) propanoic acid 1c

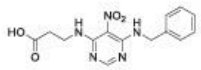

Yellow solid. Yield: 44.3 mg (80%). ^{1}H NMR (500 MHz, DMSO-d_6): δ 12.36 (s, 1H), 9.82 (t, J = 6.0 Hz, 1H), 9.52 (t, J = 5.8 Hz, 1H), 8.07 (s, 1H), 7.35–7.28 (m, 4H), 7.26–7.21 (m, 1H), 4.78 (d, J = 6.1 Hz, 2H), 3.76 (q, J = 6.6 Hz, 2H), 2.58 (t, J = 6.8 Hz, 2H). ^{13}C NMR (126 MHz, DMSO-d_6): δ 173.06, 159.38, 156.71, 156.65, 138.74, 128.30, 127.21, 126.85, 112.19, 44.15, 36.87, 33.33. HRMS: *m/z*: calcd for $C_{14}H_{16}N_5O_4^+$: 318.1197 $[M+H]^+$; found: 318.1194.

3.7.4. 3-((6-Morpholino-5-nitropyrimidin-4-yl)amino)propanoic acid 1d

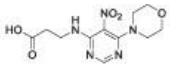

Yellow solid. Yield: 54.7 mg (62%). ^{1}H NMR (500 MHz, DMSO-d_6): δ 8.97 (t, J = 4.9 Hz, 1H), 8.05 (s, 1H), 3.67–3.63 (m, 6H), 3.50–3.41 (m, 4H), 2.36 (t, J = 6.5 Hz, 2H). ^{13}C NMR (126 MHz, DMSO-d_6): δ 173.19, 157.41, 157.33, 156.46, 112.81, 65.85, 47.58, 37.09, 33.64. HRMS: *m/z*: calcd for $C_{11}H_{16}N_5O_5^+$: 298.1146 $[M+H]^+$; found: 298.1145.

3.7.5. (5-Nitro-6-(propylamino)pyrimidin-4-yl)phenylalanine 1e

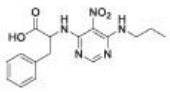

Yellow solid. Yield: 34.9 mg (70%). ^{1}H NMR (500 MHz, DMSO-d_6): δ 9.42 (t, J = 5.8 Hz, 1H), 9.37 (d, J = 7.1 Hz, 1H), 8.09 (s, 1H), 7.31–7.26 (m, 2H), 7.25–7.15 (m, 3H), 5.03 (dt, J = 6.9, 5.3 Hz, 1H), 3.50 (q, 6.2 Hz, 2H), 3.27 (dd, J = 13.9, 5.2 Hz, 1H), 3.20 (dd, J = 13.9, 6.8 Hz, 1H), 1.64–1.52 (m, 2H), 0.88 (t, J = 7.4 Hz, 3H). ^{13}C NMR (126 MHz, DMSO-d_6): δ 171.94, 159.31, 156.45, 156.19, 136.46, 129.26, 128.36, 126.81, 112.08, 55.00, 42.67, 36.52, 21.96, 11.18. HRMS: *m/z*: calcd for $C_{16}H_{20}N_5O_4^+$: 346.1510 $[M+H]^+$; found: 346.1510.

3.7.6. (6-(Cyclohexylamino)-5-nitropyrimidin-4-yl)phenylalanine 1f

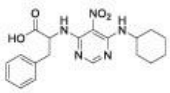

Yellow solid. Yield: 48.5 mg (75%). ^{1}H NMR (400 MHz, DMSO-d_6): δ 13.19 (br. s, 1H), 9.38 (d, J = 7.1 Hz, 1H), 9.13 (d, J = 7.8 Hz, 1H), 8.09 (s, 1H), 7.30–7.24 (m, 2H), 7.24–7.17 (m, 3H), 5.09–4.98 (m, 1H), 4.23–4.07 (m, 1H), 3.30–3.17 (m, 2H), 1.92–1.83 (m, 2H), 1.72–1.63 (m, 2H), 1.60–1.52 (m, 1H), 1.45–1.28 (m, 4H), 1.21–1.15 (m, 1H). ^{13}C NMR (126 MHz, DMSO-d_6): δ 171.89, 159.46, 156.19, 155.67, 136.45, 129.24, 128.36, 126.81, 111.97, 55.02, 49.65, 36.47, 31.70, 24.93, 24.25. HRMS: *m/z*: calcd for $C_{19}H_{24}N_5O_4^+$:

386.1823 [M+H]$^+$; found: 386.1825.

3.7.7. (6-(Benzylamino)-5-nitropyrimidin-4-yl)phenylalanine 1g

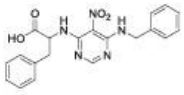

Yellow solid. Yield: 27.6 mg (50%). ^{1}H NMR (500 MHz, DMSO-d_6): δ 9.81 (t, J = 6.0 Hz, 2H), 9.52 (d, J = 6.8 Hz, 2H), 8.06 (s, 1H), 7.32–7.30 (m, 4H), 7.25–7.22 (m, 3H), 7.19–7.15 (m, 3H), 4.88 (q, J = 5.9 Hz, 1H), 4.77 (d, J = 6.0 Hz, 2H), 3.27 (dd, J = 13.7, 5.2 Hz, 1H), 3.19 (dd, J = 13.6, 6.1 Hz, 1H). ^{13}C NMR (126 MHz, DMSO-d_6): δ 171.82, 159.35, 156.59, 155.76, 138.68, 137.08, 129.36, 128.31, 128.11, 127.22, 126.86, 126.45, 112.11, 55.78, 44.17, 36.77. HRMS: m/z: calcd for $C_{20}H_{20}N_5O_4^+$: 394.1510 [M+H]$^+$; found: 394.1512.

3.7.8. (6-Morpholino-5-nitropyrimidin-4-yl)phenylalanine 1h

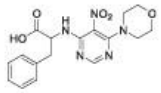

Yellow solid. Yield: 13.1 mg (25%). ^{1}H NMR (500 MHz, DMSO-d_6): δ 8.69 (d, J = 6.7 Hz, 1H), 8.05 (s, 1H), 7.23–7.12 (m, 3H), 7.10 (d, J = 7.0 Hz, 2H), 4.74–4.66 (m, 1H), 3.68–3.58 (m, 4H), 3.51 (dt, J = 13.0, 4.6 Hz, 2H), 3.38 (dt, J = 13.2, 4.6 Hz, 2H), 3.25 (dd, J = 13.5, 5.3 Hz, 1H), 3.15 (dd, J = 13.5, 5.6 Hz, 1H). ^{13}C NMR (126 MHz, DMSO-d_6): δ 171.95, 157.37, 157.21, 155.42, 137.63, 129.34, 127.91, 126.17, 112.84, 65.82, 56.23, 47.53, 36.91. HRMS: m/z: calcd for $C_{17}H_{20}N_5O_3^+$: 374.1459 [M+H]$^+$; found: 374.1459.

3.7.9. (5-Nitro-6-(propylamino)pyrimidin-4-yl)proline 1i

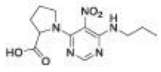

Yellow solid. Yield: 47.0 mg (90%). ^{1}H NMR (400 MHz, DMSO-d_6): δ 8.36 (t, J = 5.8 Hz, 1H), 8.01 (s, 1H), 4.62 (t, J = 7.1 Hz, 1H), 3.51–3.38 (m, 2H), 3.27–3.15 (m, 1H), 3.04 (br. s, 1H), 2.35–2.22 (m, 1H), 2.05–1.94 (m, 1H), 1.94–1.82 (m, 2H), 1.57 (sxt, J = 7.3 Hz, 2H), 0.87 (t, J = 7.4 Hz, 3H). ^{13}C NMR (126 MHz, DMSO-d_6): δ 172.71, 156.85, 155.61, 154.70, 113.54, 61.81, 50.12, 42.64, 28.40, 24.64, 22.13, 11.16. HRMS: m/z: calcd for $C_{12}H_{18}N_5O_4^+$: 296.1353 [M+H]$^+$; found: 296.1356.

3.7.10. (6-(Cyclohexylamino)-5-nitropyrimidin-4-yl)proline 1j

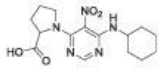

Yellow solid. Yield: 95 mg (86%). ^{1}H NMR (500 MHz, DMSO-d_6): δ 8.06–8.00 (m, 2H), 4.67–4.57 (m, 1H), 4.14–4.03 (m, 1H), 3.19 (br. s, 1H), 3.03 (br. s, 1H), 2.34–2.24 (m, 1H), 2.04–1.95 (m, 1H), 1.94–1.81 (m, 4H), 1.73–1.64 (m, 2H), 1.62–1.54 (m, 1H), 1.45–1.28 (m, 4H), 1.26–1.15 (m, 1H). ^{13}C NMR (126 MHz, DMSO-d_6): δ 172.64, 157.05, 154.88, 154.83, 113.31, 61.83, 50.24, 49.63, 31.92, 28.53, 24.98, 24.64, 24.40. HRMS: m/z: calcd for $C_{15}H_{22}N_5O_4^+$: 336.1666 [M+H]$^+$; found: 336.1666.

3.7.11. (6-(Benzylamino)-5-nitropyrimidin-4-yl)proline 1k

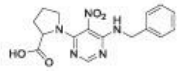

Yellow solid. Yield: 48.0 mg (85%). ^{1}H NMR (500 MHz, DMSO-d_6): δ 12.58 (br. s, 1H), 8.79 (t, J = 6.1 Hz, 1H), 8.00 (s, 1H), 7.31 (d, J = 4.4 Hz, 4H), 7.25–7.20 (m, 1H), 4.71 (d, J = 6.1 Hz, 2H), 4.62 (t, J = 7.0 Hz, 1H), 3.25–3.19 (m, 1H), 3.05 (br. s, 1H), 2.34–2.24 (m, 1H), 2.05–1.95 (m, 1H), 1.94–1.82 (m, 2H). ^{13}C NMR (126 MHz, DMSO-d_6): δ 172.53, 156.92, 155.61, 154.56, 139.16, 128.27, 127.14, 126.78, 113.74, 61.79, 50.08, 44.09, 28.55, 24.65. HRMS: m/z: calcd for $C_{16}H_{18}N_5O_4^+$: 344.1353 [M+H]$^+$; found: 344.1355.

3.7.12. (6-Morpholino-5-nitropyrimidin-4-yl)proline 1l

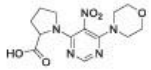

Yellow solid. Yield: 43.2 mg (80%). ^{1}H NMR (400 MHz, DMSO-d_6): δ 7.96 (s, 1H), 4.65 (t, J = 7.0 Hz, 1H), 3.78–3.64 (m, 6H), 3.61–3.46 (m, 3H), 3.44–3.34 (m, 1H), 2.38–2.27 (m, 1H), 2.05–1.83 (m, 3H). ^{13}C NMR (126 MHz, DMSO-d_6): δ 172.51, 158.27, 156.55, 155.89, 111.64, 66.18, 61.76, 51.00, 49.24, 28.88, 24.42. HRMS: m/z: calcd for $C_{13}H_{18}N_5O_5^+$: 324.1302 [M+H]$^+$; found: 324.1301.

3.7.13. (5-Nitro-6-(propylamino)pyrimidin-4-yl)methionine 1m

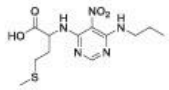

Yellow solid. Yield: 35.0 mg (50%). ^{1}H NMR (500 MHz, DMSO-d_6): δ 10.01 (d, J = 6.2 Hz, 1H), 9.44 (t, J = 5.8 Hz, 1H), 8.04 (s, 1H), 4.39 (q, J = 5.5 Hz, 1H), 3.55–3.43 (m, 2H), 2.47–2.35 (m, 2H), 2.17–2.01 (m, 2H), 1.99 (s, 3H), 1.59 (sxt, J = 7.3 Hz, 2H), 0.89 (t, J = 7.4 Hz, 3H). ^{13}C NMR (126 MHz, DMSO-d_6): δ 171.84, 159.36, 156.79, 155.25, 111.82, 55.55, 42.53, 31.89, 29.37, 22.00, 14.66, 11.22. HRMS: m/z: calcd for $C_{12}H_{20}N_5O_4S^+$: 330.1231 [M+H]$^+$; found: 330.1234.

3.7.14. (6-(Cyclohexylamino)-5-nitropyrimidin-4-yl)methionine 1n

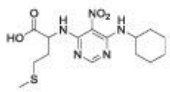

Yellow solid. Yield: 45.9 mg (68%). ^{1}H NMR (500 MHz, DMSO-d_6): δ 10.02 (d, J = 6.2 Hz, 1H), 9.22 (d, J = 7.7 Hz, 1H), 8.05 (s, 1H), 4.39 (q, J = 5.4 Hz, 1H), 4.20–4.09 (m, 1H), 3.02–2.94 (m, 1H), 2.48–2.34 (m, 2H), 2.15–2.00 (m, 2H), 1.99 (s, 3H), 1.90–1.88 (m, 1H), 1.72–1.63 (m, 2H), 1.58–1.53 (m, 1H), 1.45–1.30 (m, 4H), 1.28–1.19 (m, 1H). ^{13}C NMR (126 MHz, DMSO-d_6): δ 171.98, 159.49, 156.01, 155.24, 111.80, 55.59, 49.39, 43.38, 31.87, 29.36, 24.97, 24.25, 14.66. HRMS: m/z: calcd for $C_{15}H_{24}N_5O_4S^+$: 370.1544 [M+H]$^+$;

found: 370.1540.

3.7.15. (6-(Benzylamino)-5-nitropyrimidin-4-yl)methionine 1°

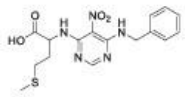

Yellow solid. Yield: 52.3 mg (66%). ^{1}H NMR (500 MHz, DMSO-d_6): δ 10.08 (d, J = 6.2 Hz, 1H), 9.82 (t, J = 6.1 Hz, 1H), 8.03 (s, 1H), 7.37–7.28 (m, 4H), 7.25–7.21 (m, 1H), 4.84–4.71 (m, 2H), 4.36–4.31 (m, 1H), 2.48–2.36 (m, 2H), 2.15–2.01 (m, 2H), 1.98 (s, 3H). ^{13}C NMR (126 MHz, DMSO-d_6): δ 172.08, 159.38, 156.84, 155.08, 138.80, 128.31, 127.25, 126.85, 112.07, 55.93, 44.10, 32.06, 29.37, 14.69. HRMS: m/z: calcd for $C_{16}H_{20}N_5O_4S^+$: 378.1231 $[M+H]^+$; found: 378.1232.

3.7.16. (6-Morpholino-5-nitropyrimidin-4-yl)methionine 1p

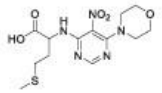

Yellow solid. Yield: 33.9 mg (45%). ^{1}H NMR (500 MHz, DMSO-d_6): δ 9.00 (d, J = 6.4 Hz, 1H), 8.05 (s, 1H), 4.47 (dd, J = 11.7, 5.7 Hz, 1H), 3.65 (t, J = 4.8 Hz, 4H), 3.51–3.42 (m, 4H), 2.47–2.43 (m, 2H), 2.12–2.02 (m, 2H), 2.00 (s, 3H). ^{13}C NMR (126 MHz, DMSO-d_6): δ 172.31, 157.37, 157.33, 155.48, 112.84, 65.83, 54.89, 47.55, 31.62, 29.38, 14.63. HRMS: m/z: calcd for $C_{13}H_{20}N_5O_5S^+$: 358.1180 $[M+H]^+$; found: 358.1176.

3.7.17. (5-Nitro-6-(propylamino)pyrimidin-4-yl)valine 1q

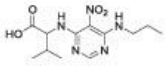

Yellow solid. Yield: 25.1 mg (57%). ^{1}H NMR (500 MHz, DMSO-d_6): δ 9.90 (d, J = 7.6 Hz, 1H), 9.46 (t, J = 5.8 Hz, 1H), 8.02 (s, 1H), 4.46 (dd, J = 7.7, 3.9 Hz, 1H), 3.56–3.44 (m, 2H), 2.25–2.15 (m, 1H), 1.59 (sxt, J = 7.4 Hz, 2H), 0.95 (d, J = 6.9 Hz, 3H), 0.88 (t, J = 7.4 Hz, 3H), 0.85 (d, J = 6.9 Hz, 3H). ^{13}C NMR (101 MHz, DMSO-d_6): δ 172.04, 159.43, 156.65, 156.54, 112.18, 58.76, 42.67, 30.24, 21.97, 18.70, 17.91, 11.19. HRMS: m/z: calcd for $C_{12}H_{20}N_5O_4^+$: 298.1510 $[M+H]^+$; found: 298.1508.

3.7.18. (6-(Cyclohexylamino)-5-nitropyrimidin-4-yl)valine 1r

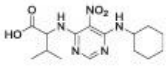

Yellow solid. Yield: 27.7 mg (57%). ^{1}H NMR (500 MHz, DMSO-d_6): δ 9.66 (d, J = 7.7 Hz, 1H), 9.21 (d, J = 7.8 Hz, 1H), 8.07 (s, 1H), 4.65 (dd, J = 7.8, 4.3 Hz, 1H), 4.21–4.12 (m, 1H), 2.30–2.21 (m, 1H), 1.93–1.85 (m, 2H), 1.70–1.67 (m, 2H), 1.61–1.53 (m, 1H), 1.46–1.30 (m, 4H), 1.28–1.18 (m, 1H), 0.97 (d, J = 6.9 Hz, 3H), 0.91 (d, J = 6.9 Hz, 3H). ^{13}C NMR (126 MHz, DMSO-d_6): δ 171.99, 159.48, 156.32, 155.85, 111.93, 59.39, 49.63, 49.47, 31.72, 30.42, 25.00, 24.28, 18.69, 18.08. HRMS: m/z: calcd for $C_{15}H_{24}N_5O_4^+$: 338.1823 $[M+H]^+$; found: 338.1821.

3.7.19. (6-(Benzylamino)-5-nitropyrimidin-4-yl)valine 1s

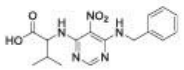

Yellow solid. Yield: 39.4 mg (79%). ^{1}H NMR (500 MHz, DMSO-d_6): δ 9.86 (t, J = 6.1 Hz, 1H), 9.60 (d, J = 7.8 Hz, 1H), 8.06 (s, 1H), 7.35–7.29 (m, 4H), 7.25–7.22 (m, 1H), 4.83–4.74 (m, 2H), 4.70 (dd, J = 7.8, 4.4 Hz, 1H), 2.31–2.22 (m, 1H), 0.98 (d, J = 6.9 Hz, 3H), 0.93 (d, J = 6.9 Hz, 3H). ^{13}C NMR (101 MHz, DMSO-d_6): δ 172.03, 159.43, 156.59, 156.53, 138.65, 128.30, 127.21, 126.86, 112.36, 58.90, 44.21, 30.30, 18.70, 17.95. HRMS: m/z: calcd for $C_{16}H_{20}N_5O_4^+$: 346.1510 $[M+H]^+$; found: 346.1513.

3.7.20. (6-Morpholino-5-nitropyrimidin-4-yl)valine 1t

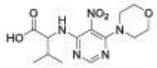

Yellow solid. Yield: 36.4 mg (77%). ^{1}H NMR (500 MHz, DMSO-d_6): δ 8.98 (d, J = 7.5 Hz, 1H), 8.02 (s, 1H), 4.39 (dd, J = 7.5, 3.9 Hz, 1H), 3.64 (t, J = 4.8 Hz, 4H), 3.50 (dt, J = 13.3, 4.7 Hz, 2H), 3.43 (dt, J = 13.4, 4.7 Hz. 2H), 2.25–2.13 (m, 1H), 0.94 (d, J = 6.9 Hz, 3H), 0.84 (d, J = 6.9 Hz, 3H). ^{13}C NMR (101 MHz, DMSO-d_6): δ 172.20, 157.44, 157.18, 156.48, 112.91, 65.86, 58.93, 47.70, 30.25, 18.72, 17.89. HRMS: m/z: calcd for $C_{13}H_{20}N_5O_5^+$: 326.1459 $[M+H]^+$; found: 326.1461.

3.7.21. (5-Nitro-6-(piperidin-1-yl)pyrimidin-4-yl)valine 1u

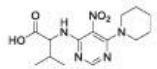

Yellow solid. Yield: 28.5 mg (60%). ^{1}H NMR (500 MHz, DMSO-d_6): δ 8.94 (d, J = 7.5 Hz, 1H), 7.97 (s, 1H), 4.39 (dd, J = 7.4, 3.8 Hz, 1H), 3.49–3.40 (m, 2H), 3.40–3.32 (m, 2H), 2.25–2.13 (m, 1H), 1.69–1.52 (m, 6H), 0.94 (d, J = 6.9 Hz, 3H), 0.84 (d, J = 6.8 Hz, 3H). ^{13}C NMR (101 MHz, DMSO-d_6): δ 172.23, 157.32, 157.26, 156.34, 112.53, 59.19, 48.33, 30.35, 25.42, 23.30, 18.75, 18.00. HRMS: m/z: calcd for $C_{14}H_{22}N_5O_4^+$: 324.1666 $[M+H]^+$; found: 324.1666.

3.7.22. (6-(Cyclooctylamino)-5-nitropyrimidin-4-yl)valine 1v

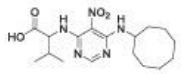

Yellow solid. Yield: 28.3 mg (54%). ^{1}H NMR (500 MHz, DMSO-d_6): δ 10.01 (d, J = 7.6 Hz, 1H), 9.34 (d, J = 7.9 Hz, 1H), 8.02 (s, 1H), 4.43–4.29 (m, 2H), 2.24–2.13 (m, 1H), 1.87–1.80 (m, 2H), 1.76–1.45 (m, 12H), 0.95 (d, J = 6.9 Hz, 3H), 0.83 (d, J = 6.9 Hz, 3H). ^{13}C NMR (126 MHz, DMSO-d_6): δ 171.83, 159.56, 155.77, 155.43, 111.63, 61.07, 50.54, 31.26, 31.22, 30.96, 26.70, 24.88, 23.11, 18.83, 18.76. HRMS: m/z: calcd for $C_{17}H_{28}N_5O_4^+$: 366.2136 $[M+H]^+$; found: 366.2135.

3.7.23. (6-(Hexylamino)-5-nitropyrimidin-4-yl)valine 1w

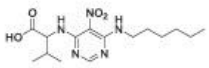

Yellow solid. Yield: 32.8 mg (67%). ^{1}H NMR (500 MHz, DMSO-d_6): δ 9.77 (d, J = 7.7 Hz, 1H), 9.45 (t, J = 5.8 Hz, 1H), 8.03 (s, 1H), 4.57 (dd, J = 7.8, 4.1 Hz, 1H), 3.53 (ddd, J = 13.1, 7.1, 1.5 Hz, 2H), 2.23 (dtd, J = 13.7, 6.9, 4.3 Hz, 1H), 1.64–1.52 (m, 2H), 1.34–1.23 (m, 6H), 0.96 (d, J = 6.9 Hz, 3H),0.88 (d, J = 3.8 Hz, 3H, overlapped with CH_3), 0.85 (t, J = 6.8 Hz, 3H, overlapped with CH_3). ^{13}C NMR (126 MHz, DMSO-d_6): δ 172.05, 159.42, 156.67, 156.02, 111.90, 59.93, 40.91, 30.91, 30.66, 28.63, 25.99, 21.98, 18.75, 18.33, 13.84. HRMS: m/z: calcd for $C_{15}H_{26}N_5O_4^-$: 340.1979 $[M+H]^+$; found: 340.1981.

3.7.24. (6-(Cyclohexylamino)-5-(2-(2,4-dioxothiazolidin-3-yl) acetamido)pyrimidin-4-yl)valine 2a

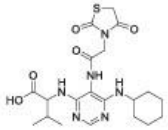

White solid. Yield: 23.6 mg (43%). ^{1}H NMR (500 MHz, DMSO-d_6): δ 9.20 (s, 1H), 7.91 (s, 1H), 5.62 (d, J = 8.0 Hz, 1H), 5.55 (d, J = 8.3 Hz, 1H), 4.51–4.47 (m, 1H), 4.36–4.25 (m, 4H), 3.86–3.76 (m, 1H), 2.13–2.03 (m, 1H), 1.87–1.79 (m, 2H), 1.76–1.66 (m, 2H), 1.63–1.55 (m, 1H), 1.35–1.08 (m, 5H),0.91 (d, J = 6.8 Hz, 3H, overlapped with CH_3), 0.90 (d, J = 6.8 Hz, 3H, overlapped with CH_3). ^{13}C NMR (126 MHz, DMSO-d_6): δ 173.74, 172.43, 171.87, 165.57, 157.27, 157.20, 155.35, 94.65, 58.58, 48.78, 44.04, 34.13, 32.85, 30.03, 25.37, 24.84, 19.12, 18.36. HRMS: m/z: calcd for $C_{20}H_{27}N_6O_5S^-$: 463.1769 [M-H]; found: 463.1769.

3.7.25. (6-(Cyclohexylamino)-5-(thiophene-2-carboxamido) pyrimidin-4-yl)valine 2b

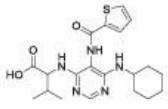

White solid. Yield: 9.1 mg (18%). ^{1}H NMR (500 MHz, DMSO-d_6): δ 9.31 (s, 1H), 8.03–7.94 (m, 2H), 7.83 (d, J = 4.8 Hz, 1H), 7.25–7.19 (m, 1H), 6.02 (br. s, 1H), 5.56 (br. s, 1H), 4.43 (dd, J = 8.3, 5.7 Hz, 1H), 3.87 (br. s, 1H), 2.09 (dq, J = 13.1, 6.6 Hz, 1H), 1.81 (br. s, 2H), 1.67 (br. s, 2H), 1.59–1.56 (m, 1H), 1.34–1.18 (m, 4H), 1.16–1.03 (m, 1H),0.88 (d, J = 7.1 Hz, 3H, overlapped with CH_3), 0.86 (d, J = 6.8 Hz, 3H, overlapped with CH_3). ^{13}C NMR (126 MHz, DMSO-d_6): δ 174.04, 161.05, 157.77, 155.49, 140.03, 131.76, 130.19, 128.46, 95.90, 58.73, 49.52, 33.26, 30.85, 25.88, 25.51, 19.40, 18.75. HRMS: m/z: calcd for $C_{20}H_{28}N_5O_3S^+$: 418.1907 $[M+H]^+$; found: 418.1909.

3.7.26. (6-(Cyclohexylamino)-5-(thiophene-3-carboxamido) pyrimidin-4-yl)valine 2c

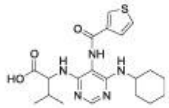

White solid. Yield: 7.2 mg (14%). ^{1}H NMR (500 MHz, DMSO-d_6): δ 9.12 (s, 1H), 8.34–8.31 (m, 1H), 7.96 (s, 1H), 7.66–7.61 (m, 2H), 5.86 (d, J = 8.1 Hz, 1H), 5.50 (d, J = 8.3 Hz, 1H), 4.41 (dd, J = 8.3, 5.6 Hz, 1H), 3.94–3.80 (m, 1H), 2.15–2.03 (m, 1H), 1.84–1.76 (m, 2H), 1.70–1.64 (m, 2H), 1.59–1.56 (m, 1H), 1.36–1.16 (m, 4H), 1.15–1.04 (m, 1H),0.87 (d, J = 6.6 Hz, 3H, overlapped with CH_3), 0.86 (d, J = 6.7 Hz, 3H, overlapped with CH_3). ^{13}C NMR (126 MHz, DMSO-d_6): δ 173.60, 161.32, 157.48, 157.20, 155.17, 137.43, 129.85, 127.62, 126.37, 95.67, 58.20, 48.84, 32.76, 30.35, 25.35, 24.96, 18.83, 18.26. HRMS: m/z: calcd for $C_{20}H_{28}N_5O_3S^+$: 481.1907 $[M+H]^+$; found: 418.1909.

3.7.27. (6-(Cyclohexylamino)-5-(2-oxo-2H-chromene-3-carboxamido)pyrimidin-4-yl)valine 2d

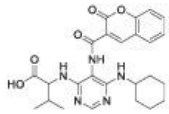

White solid. Yield: 15.9 mg (28%). ^{1}H NMR (500 MHz, DMSO-d_6): δ 9.41 (s, 1H), 8.85 (s, 1H), 8.03 (dd, J = 7.8, 1.5 Hz, 1H), 7.97 (s, 1H), 7.81–7.75 (m, 1H), 7.56 (d, J = 8.4 Hz, 1H), 7.47 (dt, J = 7.6, 1.0 Hz, 1H), 6.01 (t, J = 8.2 Hz, 2H), 4.41 (dd, J = 8.3, 6.5 Hz, 1H), 3.93–3.81 (m, 1H), 2.17–2.06 (m, 1H), 1.88–1.78 (m, 2H), 1.77–1.65 (m, 2H), 1.62–1.54 (m, 1H), 1.37–1.16 (m, 4H), 1.16–1.05 (m, 1H),0.93 (d, J = 6.7 Hz, 3H, overlapped with CH_3), 0.92 (d, J = 6.7 Hz, 3H, overlapped with CH_3). ^{13}C NMR (126 MHz, DMSO-d_6): δ 173.83, 161.48, 160.59, 157.15, 157.06, 155.44, 153.70, 145.99, 133.95, 130.13, 125.29, 121.17, 118.40, 116.16, 95.03, 58.64, 48.84, 32.87, 29.99, 25.39, 24.88, 19.15, 18.58. HRMS: m/z: calcd for $C_{25}H_{30}N_5O_5^+$: 480.2241 $[M+H]^+$; found: 480.2242.

3.7.28. (6-(Cyclohexylamino)-5-(4-fluoro-3-nitrobenzamido) pyrimidin-4-yl)valine 2e

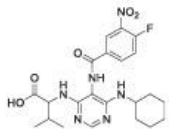

White solid. Yield: 14.3 mg (26%). ^{1}H NMR (500 MHz, DMSO-d_6): δ8.78 (dd, J = 7.3, 2.2 Hz, 1H), 8.43 (ddd, J = 8.7, 4.2, 2.3 Hz, 1H), 7.95 (s, 1H), 7.76 (dd, J = 11.0, 8.7 Hz, 1H), 6.02 (d, J = 8.1 Hz, 1H), 5.77 (d, J = 8.0 Hz, 1H), 4.31 (dd, J = 7.8, 5.8 Hz, 1H), 3.92–3.82 (m, 1H), 2.13–2.01 (m, 1H), 1.84–1.76 (m, 2H), 1.70–1.64 (m, 2H), 1.59–1.56 (m, 1H), 1.33–1.15 (m, 4H), 1.13–1.02 (m, 1H), 0.85 (d, J = 6.8 Hz, 3H, overlapped with CH_3), 0.86 (d, J = 6.8 Hz, 3H, overlapped with CH_3).^{13}C NMR (126 MHz, DMSO-d_6): δ 173.74, 162.75, 157.47, 157.30, 156.18 (d, J = 266 Hz), 155.39, 136.50 (d, J = 7.8 Hz), 136.04 (d, J = 9.7 Hz), 131.46 (d, J = 3.2 Hz), 126.12, 118.38 (d, J = 21.0 Hz), 95.19, 58.52. 48.94, 32.82, 30.18, 25.38, 25.06, 18.98, 18.57. HRMS: m/z: calcd for $C_{22}H_{28}FN_6O_5^+$: 475.2100 $[M+H]^+$; found: 475.2100.

3.7.29. (6-(Cyclohexylamino)-5-(isonicotinamido)pyrimidin-4-yl) valine 2f

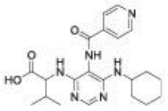

White solid. Yield: 22.5 mg (45%). ^{1}H NMR (500 MHz, DMSO-d_6): δ 9.54 (br. s, 1H), 8.79–9.74 (m, 2H), 7.96 (s, 1H), 7.95–7.92 (m, 2H), 5.98 (d, J = 8.1 Hz, 1H), 5.72 (d, J = 7.9 Hz, 1H), 4.31 (dd, J = 7.7, 5.6 Hz, 1H), 3.90–3.84 (m, 1H), 2.08 (dq, J = 13.6, 6.8 Hz, 1H), 1.84–1.76 (m, 2H), 1.70–1.64 (m, 2H), 1.59–1.56 (m, 1H), 1.34–1.16 (m, 4H), 1.15–1.02 (m, 1H), 0.86 (d, J = 6.8 Hz, 3H, overlapped with CH_3), 0.85 (d, J = 6.7 Hz, 3H, overlapped with CH_3). ^{13}C NMR (126 MHz, DMSO-d_6): δ 174.20, 164.72, 157.90, 157.75, 155.97, 150.53, 141.85, 122.57, 95.60, 59.21, 49.41, 33.36, 30.90, 25.93, 25.58, 19.43, 19.08. HRMS: m/z: calcd for $C_{21}H_{27}N_6O_3^-$: 411.2150 [M-H]; found: 411.2136.

3.7.30. (6-(Cyclohexylamino)-5-(picolinamido)pyrimidin-4-yl) valine 2g

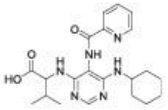

White solid. Yield: 23.4 mg (47%). ^{1}H NMR (500 MHz, DMSO-d_6): δ 9.63 (s, 1H), 8.75–8.73 (m, 1H), 8.11–8.07 (m, 1H), 8.03 (td, J = 7.6, 1.7 Hz, 1H), 7.97 (s, 1H), 7.68–7.64 (m, 1H), 5.82 (d, J = 8.0 Hz, 1H), 5.60 (d, J = 8.2 Hz, 1H), 4.40 (dd, J = 8.1, 5.8 Hz, 1H), 3.89–3.80 (m, 1H), 2.13–2.02 (m, 1H), 1.85–1.76 (m, 2H), 1.72–1.62 (m, 2H), 1.59–1.52 (m, 1H), 1.33–1.14 (m, 4H), 1.13–1.02 (m, 1H), 0.87 (d, J = 6.6 Hz, 3H, overlapped with CH_3), 0.85 (d, J = 6.6 Hz, 3H, overlapped with CH_3). ^{13}C NMR (126 MHz, DMSO-d_6): δ 173.58, 163.51, 157.30, 157.00, 155.13, 150.10, 148.34, 137.65, 126.57, 122.37, 95.63, 58.36, 48.88, 32.71, 30.30, 25.35, 24.93, 18.81, 18.42. HRMS: m/z: calcd for $C_{21}H_{27}N_6O_3^-$: 411.2150 [M-H]; found: 411.2137.

4. Results and discussion

Fig. 2 shows the two different types of scaffolds, consisting of the central pyrimidine heterocycle. The 5-nitropyrimidine central core was selected concerning the compounds depicted in Fig. 1 and which has a proven antibacterial activity. Moreover, the nitro group of scaffold **1** can open up a synthetic route for other modifications and can provide easy access to diverse pyrimidines **2** modified with other various pharmacophores (Fig. 2). Combining two pharmacophoric systems is a well-established approach for designing more potent drugs with a significant increase in the biological activity [2,21].

Structure **1** comprises the 5-nitropyrimidine scaffold and two positions on the pyrimidine central core that differ from the used amino acid and amine. Varying the substituents at these two positions allows the generation of a library with a diverse range of compounds. Amino acids were selected as one of the substituents as they are known for their ability to tune optimal pharmacokinetic and pharmacodynamic properties of the potential drugs [22–24]. Additionally, the impact of the amino acid moiety on antimycobacterial activity has also been reported for several purine derivatives [25,26]. We decided to modify the central pyrimidine core with five different amino acids. The amino acid side chain was selected considering its lipophilicity, as our new compounds were designed primarily as a potential antimycobacterial agent (more than 60% of the mycobacterial cell wall are lipids). The remaining second position of the pyrimidine scaffold was substituted with various amines that have also been found in the broad spectrum of antibacterial or antimycobacterial agents eg. Refs. [27,28]. For this study, we selected representative members of aliphatic, aromatic, alicyclic and heterocyclic amines.

The second moiety (Fig. 2, structures **2**) was introduced through the acylation of the amino group with various carboxylic acids. These moieties were selected considering their occurrence in various biologically active compounds (e.g. derivatives with antibacterial activities [7,12,14,29,30]) and ready availability. An overview of all the commercially available building blocks is presented in Fig. 3.

Target compounds **1** were synthesized from the resin-bound precursors **3** (Scheme 1). Firstly, Wang resin was acylated with five different Fmoc-protected amino acids (Fmoc-β-Ala-OH, Fmoc-Phe-OH, Fmoc-Pro-OH, Fmoc-Met-OH, and Fmoc-Val-OH). The Fmoc protecting group was then removed through exposure to 50% piperidine in DMF for 15 min to give resin **3**. Subsequent reaction of the free amino group of **3** with commercially available 4,6-dichloro-5-nitropyrimidine, followed by nucleophilic substitution of the resulting chloride **4** afforded resin-bound pyrimidines **5**. Standard cleavage with 50% TFA in DCM and subsequent high-performance liquid chromatography (HPLC) purification represents our first library of 5-nitropyrimidine compounds **1a-w** for biological testing.

[a]Reagents and conditions: (i) Fmoc-amino acid, HOBt, DMAP, DIC, DMF/DCM (1:1), rt, 16 h; (ii) 50% piperidine, DMF, rt, 15 min; (iii) 4,6-dichloro-5-nitropyrimidine, DIEA, dry DMF, rt, 2 h; (iv) amine, DIEA, DMF, rt, 16 h; (v) 50% TFA in DCM, rt, 1 h.

All final compounds **1a-w** depicted in Table 1 were obtained in excellent crude purity ranging from 74 to 92% as measured by LC-UV traces at 210–500 nm. Lower yields in the case of some compounds were probably caused by losses during HPLC purification.

Final compounds **1a-w** were screened for their *in vitro* antibacterial activity against *M. tuberculosis* H37Rv and several Gram-positive and Gram-negative strains such as *S. aureus*, *P. aeruginosa*, *E. coli*, and *E. faecalis* in the concentration range of 1024–0.0312 μg/mL. Additionally, their antifungal activity against

Fig. 2. Design of new pyrimidines.

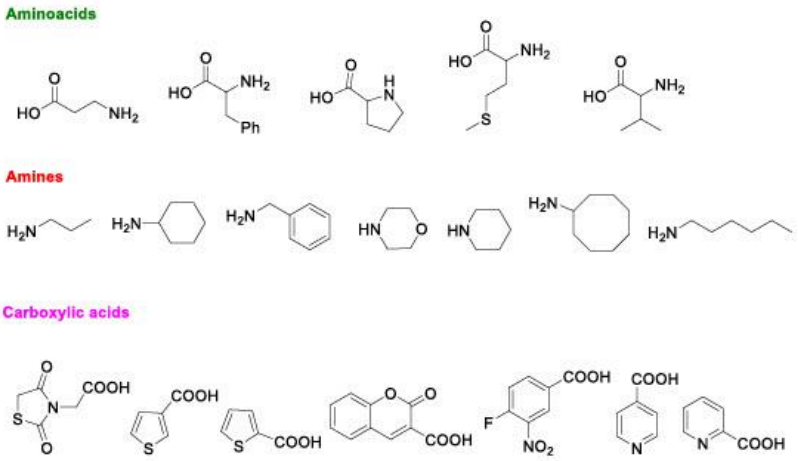

Fig. 3. Overview of the used building blocks.

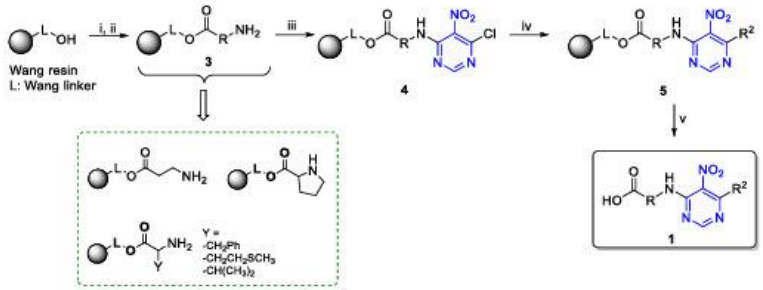

Scheme 1. Solid-phase synthesis of final compounds **1a-w**[a].

C. albicans and *A. niger* was also investigated. The antimicrobial activities were determined from their minimum inhibitory concentration (MIC) as described earlier [20]. Gentamicin was used as the drug control for bacteria, isoniazid (INH) for *M. tuberculosis* and amphotericin B for yeast and mold. Antimycobacterial activity of the pyrimidines **1a-w** against *M. tuberculosis* H37Rv (NCTC 7416) was evaluated by determining their MIC and Resazurin microtiter assay [17,18]. The results of the antibacterial activities for the first pyrimidine series **1a-w** are summarized in Table 2.

None of the tested compounds exhibited any activity against fungal strains and *E. coli*. On the other hand, compounds **1f** and **1n** displayed slight antibacterial activity against *S. aureus* and *E. faecalis*. Encouragingly, compound **1b** showed considerable activity against *P. aeruginosa* (the bactericidal activity was observed in the range of concentrations 2–8 μg/mL) and was found to be as active as the standard drug gentamicin. Additionally, many of the tested compounds displayed slight antimycobacterial activities ranging from 128 to 1024 μg/mL (see Table 2).

The results of the first series of pyrimidines **1a-w** indicate that the choice of amino acid has the least impact on antimycobacterial activity. Thus, we chose the amino acid valine, which exhibited the best properties during the synthesis route for the implementation of the second pyrimidine series **2**. On the other hand, it seems that the resulting activity differs concerning the selected amine. We initially tested the propylamine, cyclohexylamine, benzylamine, and morpholine containing adducts (**1a-t**) and found that the cyclohexylamine substitution exhibits the best activity. In light of this, we could find the possibility that the other amines could affect antimicrobial activity. Thus, we broadened the range of amines for the valine series by synthesizing three additional amines (piperidine **1u**, cyclooctylamine **1v**, and hexylamine **1w**). However, there was only a very slight improvement in the antimycobacterial activity for the cyclooctylamine containing moiety (compound **1v**). Nonetheless, we have chosen cyclohexylamine modification for implementation to the second pyrimidine series **2** considering other antibacterial activities of the cyclohexylamine modified pyrimidines **1f** and **1n**.

The synthesis route of the target compounds **2a-j** is depicted in Scheme 2. Valine (R^1) and cyclohexylamine (R^2) substitutions were chosen considering the initial antibacterial activity. After the

Table 1
An overview of synthesized products **1a-w**.

1

Entry	R^1	R^2	Yield [%]
1a			80
1b			78
1c			80
1d			62
1e			70
1f			75
1g			50
1h			25
1i			90
1j			86
1k			85
1l			80
1m			50
1n			68
1o			66
1p			45

Table 1 (*continued*)

Entry	R^1	R^2	Yield [%]
1q			57
1r			57
1s			79
1t			77
1u			60
1v			54
1w			67

immobilization of Fmoc-Val-OH on Wang resin and cleavage of the Fmoc protecting group by exposure to 50% piperidine in DMF for 15 min, the resulting intermediate **6** was reacted with 4,6-dichloro-5-nitropyrimidine. Nucleophilic substitution of chloride **7** with cyclohexylamine delivered 5-nitropyrimidine **8**.

Further, the reduction of the nitro group of **8** to corresponding amine **9** was essential. We explored several reaction conditions using two reducing agents, sodium dithionite and tin(II) chloride. The first strategy used sodium dithionite under phase-transfer catalysis conditions in a DCM—water system. For this, tetrabutylammonium hydrogen sulfate and ethyl viologen diiodide were used as phase-transfer catalysts. Here, the best results were observed for ethyl viologen diiodide. However, due to the incomplete conversion of starting material after an overnight reaction, the reduction was repeated twice for the satisfactory results. Thus, we decided to change the reducing agent and opted for the more common strategy using tin(II) chloride. Unfortunately, in this case, as well, the reaction had to be repeated twice for the full conversion of starting nitro derivative to amine **9**. Taking into account of the results obtained from our experiments and the risk in the removal of tin(II) salts (as we described earlier [31]), we decided to use the combination of sodium dithionite and ethyl viologen diiodide for further experiments.

The third and the remaining core was introduced to the resin-bound amine **9** via acylation for which ten different carboxylic acids were selected (Table 3). We used the standard HOBt/DIC protocol for this procedure but unfortunately struggled with poor solubility of some selected carboxylic acids in DMF (uracil-5-carboxylic acid, 6-fluoronicotinic acid or thiazolidine-4-carboxylic acid). As a result, the final products derived from these acids were obtained in a very low crude yield and were not isolated (Table 3). Finally, acid-mediated cleavage from the resin with TFA in DCM, and subsequent HPLC purification presented our second series of compounds **2a-g** for biological activity testing.

The final compounds **2a-g** were screened for their *in vitro* antibacterial activity against *M. tuberculosis* H37Rv, Gram-positive

Table 2
The *in vitro* antibacterial activity of compounds **1a-w** (MIC values in μg/mL).

Entry	*Mycobacterium tuberculosis* H37Rv	*Staphylococcus aureus* CCM 3953	*Enterococcus faecalis* CCM 4224	*Pseudomonas aeruginosa* CCM 3955
1a	*NA*[a]	*NA*	*NA*	*NA*
1b	512	*NA*	*NA*	**2**[b]
1c	512	*NA*	*NA*	*NA*
1d	*NA*	*NA*	*NA*	*NA*
1e	1024	*NA*	*NA*	*NA*
1f	256	512	512	*NA*
1g	1024	*NA*	*NA*	*NA*
1h	*NA*	*NA*	*NA*	*NA*
1i	1024	*NA*	*NA*	*NA*
1j	1024	*NA*	*NA*	*NA*
1k	1024	*NA*	*NA*	*NA*
1l	*NA*	*NA*	*NA*	*NA*
1m	*NA*	*NA*	*NA*	*NA*
1n	512	512	1024	*NA*
1o	*NA*	*NA*	*NA*	*NA*
1p	*NA*	*NA*	*NA*	*NA*
1q	1024	*NA*	*NA*	*NA*
1r	256	*NA*	*NA*	*NA*
1s	256	*NA*	*NA*	*NA*
1t	512	*NA*	*NA*	*NA*
1u	1024	*NA*	*NA*	*NA*
1v	128	*NA*	*NA*	*NA*
1w	1024	*NA*	*NA*	*NA*
INH	0.25	–	–	–
gentamicin	–	16	64	4

[a] *NA* – not active in the range of concentrations 1024–0.0312 μg/mL.
[b] The bactericidal activity was observed in the range of concentrations 2–8 μg/mL.

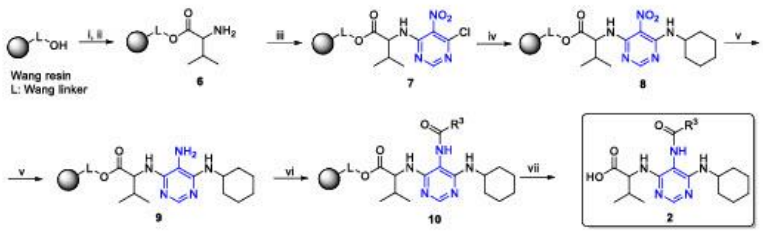

Scheme 2. Solid-phase synthesis of final compounds **2a-j**[a]. [a]Reagents and the conditions: (i) Fmoc-valine, *N*-hydroxybenzotriazole (HOBt), DMAP, DIC, DMF/DCM (1 : 1), rt, 16 h; (ii) 50% piperidine, DMF, rt, 15 min; (iii) 4,6-dichloro-5-nitropyrimidine, DIEA, dry DMF, rt, 2 h; (iv) amine, DIEA, DMF, rt, 16 h; (v) $Na_2S_2O_4$, K_2CO_3, ethyl viologen diiodide, H_2O/DCM, rt, 16 h; (vi) carboxylic acid, *N*-hydroxybenzotriazole (HOBt), DMAP, DIC, DMF/DCM (1 : 1) or DMF, rt, 16 h; (vii) 50% TFA in DCM, rt, 1 h.

and Gram-negative strains such as *S. aureus*, *P. aeruginosa*, *E. coli*, and *E. faecalis* and two fungal strains *C. albicans* and *A. niger*. None of the tested compounds **2a-g** exhibited any activity against *S. aureus*, *P. aeruginosa*, *E. coli* and *E. faecalis*, and fungal strains. On the contrary, the antimycobacterial activities of the synthesized pyrimidines **2a-g** were more promising (Table 4). Some of the tested compounds exhibited slight to moderate antimycobacterial activity against *M. tuberculosis* H37Rv. Encouragingly, among our new pyrimidines, compound **2f** with the 4-pyridinyl moiety exhibited moderate antimycobacterial activity with a MIC value of 32 μg/mL. Interestingly, the hetero-isomer, pyrimidine **2g** turned out to be inactive. Heteroatom position and its impact on antimycobacterial activity were also observed for thiophene derivatives **2b** and **2c**. Both of these examples suggest that the heteroatom position plays an important role in the bioactivity.

5. Conclusions

In summary, 30 new pyrimidines were synthesized and evaluated for their antimicrobial screening against *M. tuberculosis*, a selected panel of Gram-positive and Gram-negative bacteria, and two fungal strains. Compound **2f** exhibited moderate antimycobacterial activity with a MIC value of 32 μg/mL, whereas several other compounds were in the range of 128–1024 μg/mL. Additionally, some of the tested compounds displayed a slight antibacterial activity against *S. aureus* and *E. faecalis* (MIC value 512 μg/mL). Notably, the highest activity in the series was seen for compound **1b** against *P. aeruginosa*. This data indicates that there is a significant potential for this class of pyrimidines as they possess an entirely different molecular structure from the known *anti*-TB drugs and may even have a different mechanism of action. However, additional work is required to prove the potential of our

Table 3
Overview of synthesized products **2a-j**.

2(R^3)

Entry	R^3	Yield [%]
2a		43
2b		18
2c		14
2d		28
2e		26
2f		45
2g		47
2h		*NI*
2i		*NI*
2j		*NI*

NI – Not isolated.

Table 4
The *in vitro* antimycobacterial activity of compounds **2a-g** (MIC values in μg/mL).

Entry	*Mycobacterium tuberculosis* H37Rv
2a	1024
2b	128
2c	256
2d	*NA*
2e	*NA*
2f	32
2g	*NA*
INH	0.25

*NA – not active in the range of concentrations 1024–0.0312 μg/mL.

compounds and to discover novel *anti*-TB agents that could prevent the emergence of resistance.

Our methodology is based on the solid-phase synthetic approach that introduces structural diversity from the abundant and commercially available building blocks with minimal synthetic routes. This approach can aid in the rapid generation of a structure-activity relationship and for further improved drugs based on the promising pyrimidine scaffold.

Conflicts of interest

The authors declare no conflict of interest.

Acknowledgments

This work was supported by the Palacký University Olomouc (project JG_2019_002).

Appendix A. Supplementary data

Supplementary data to this article can be found online at https://doi.org/10.1016/j.molstruc.2019.127101.

References

[1] L. van Geelen, D. Meier, N. Rehberg, R. Kalscheuer, (Some) current concepts in antibacterial drug discovery, Appl. Microbiol. Biotechnol. 102 (2018) 2949–2963.
[2] A. Campanico, R. Moreira, F. Lopes, Drug discovery in tuberculosis. New drug targets and antimycobacterial agents, Eur. J. Med. Chem. 150 (2018) 525–545.
[3] S. Prachayasittikul, R. Pingaew, A. Worachartcheewan, N. Sinthupoom, V. Prachayasittikul, S. Ruchirawat, V. Prachayasittikul, Roles of pyridine and pyrimidine derivatives as privileged scaffolds in anticancer agents, Mini Rev. Med. Chem. 17 (2017) 869–901.
[4] A.P. Keche, G.D. Hatnapure, R.H. Tale, A.H. Rodge, S.S. Birajdar, V.M. Kamble, A novel pyrimidine derivatives with aryl urea, thiourea and sulfonamide moieties: synthesis, anti-inflammatory and antimicrobial evaluation, Bioorg. Med. Chem. Lett 22 (2012) 3445–3448.
[5] N. Shakya, S. Vedi, C. Liang, F. Yang, B. Agrawal, R. Kumar, 4'-Substituted pyrimidine nucleosides lacking 5'-hydroxyl function as potential anti-HCV agents, Bioorg. Med. Chem. Lett 24 (2014) 1407–1409.
[6] Z. Yang, Y. Fang, T.A. Pham, J. Lee, H. Park, Synthesis and biological evaluation of 5-nitropyrimidine analogs with azabicyclic substituents as GPR119 agonists, Bioorg. Med. Chem. Lett 23 (2013) 1519–1521.
[7] T. Wang, G. Bemis, B. Hanzelka, H. Zuccola, M. Wynn, C.S. Moody, J. Green, C. Locher, A. Liu, H. Gao, Y. Xu, S. Wang, J. Wang, Y.L. Bennani, J.A. Thomson, U. Muh, Mtb PKNA/PKNB dual inhibition provides selectivity advantages for inhibitor design to minimize host kinase interactions, ACS Med. Chem. Lett. 8 (2017) 1224–1229.
[8] N.H. Bhuva, P.K. Talpara, P.M. Singala, V.K. Gothaliya, V.H. Shah, Synthesis and biological evaluation of pyrimidinyl sulphonamide derivatives as promising class of antitubercular agents, J. Saudi Chem. Soc. 21 (2017) 517–527.
[9] C.R. Wilson, R.K. Gessner, A. Moosa, R. Seldon, D.F. Warner, V. Mizrahi, C. Soares de Melo, S.B. Simelane, A. Nchinda, E. Abay, D. Taylor, M. Njoroge, C. Brunschwig, N. Lawrence, H.I.M. Boshoff, C.E. Barry, F.A. Sirgel, P. van Helden, C.J. Harris, R. Gordon, S. Ghidelli-Disse, H. Pflaumer, M. Boesche, G. Drewes, O. Sanz, G. Santos, M.J. Rebollo-Lopez, B. Urones, C. Selenski, M.J. Lafuente-Monasterio, M. Axtman, J. Lelievre, L. Ballell, R. Mueller, L.J. Street, S.R. Ghorpade, K. Chibale, Novel antitubercular 6-dialkylaminopyrimidine carboxamides from phenotypic whole-cell high throughput screening of a SoftFocus library: structure-activity relationship and target identification studies, J. Med. Chem. 60 (2017) 10118–10134.
[10] E.V. Verbitskiy, S.A. Baskakova, M.A. Kravchenko, S.N. Skornyakov, G.L. Rusinov, O.N. Chupakhin, V.N. Charushin, Synthesis and evaluation of antitubercular activity of fluorinated 5-aryl-4-(hetero)aryl substituted pyrimidines, Bioorg. Med. Chem. 24 (2016) 3771–3780.
[11] D. Seenaiah, P.R. Reddy, G.M. Reddy, A. Padmaja, V. Padmavathi, N. Siva krishna, Synthesis, antimicrobial and cytotoxic activities of pyrimidinyl benzoxazole, benzothiazole and benzimidazole, Eur. J. Med. Chem. 77 (2014) 1–7.
[12] L. Ballell, R.H. Bates, R.J. Young, D. Alvarez-Gomez, E. Alvarez-Ruiz, V. Barroso, D. Blanco, B. Crespo, J. Escribano, R. Gonzalez, S. Lozano, S. Huss, A. Santos-Villarejo, J.J. Martin-Plaza, A. Mendoza, M.J. Rebollo-Lopez, M. Remuinan-Blanco, J.L. Lavandera, E. Perez-Herran, F.J. Gamo-Benito, J.F. Garcia-Bustos, D. Barros, J.P. Castro, N. Cammack, Fueling open-source drug discovery: 177 small-molecule leads against tuberculosis, ChemMedChem 8 (2013) 313–321.
[13] M.R. Sura, V.G.R. Peddiahgari, R.P.R. Bhoomireddy, R.K. Vadde, Synthesis of new 2,4-diaryl-6-methyl-5-nitropyrimidines as antibacterial and antioxidant agents, J. Heterocycl. Chem. 50 (2013) 1395–1399.
[14] C. Kishor, T. Arya, R. Reddi, X. Chen, V. Saddanapu, A.K. Marapaka, R. Gumpena, D. Ma, J.O. Liu, A. Addlagatta, Identification, biochemical and structural evaluation of species-specific inhibitors against type I methionine aminopeptidases, J. Med. Chem. 56 (2013) 5295–5305.

[15] M.L. Read, M. Braendvang, P.O. Miranda, L.L. Gundersen, Synthesis and biological evaluation of pyrimidine analogs of antimycobacterial purines, Bioorg. Med. Chem. 18 (2010) 3885–3897.
[16] D.S. Reddy, K.M. Hosamani, H.C. Devarajegowda, Design, synthesis of benzocoumarin-pyrimidine hybrids as novel class of antitubercular agents, their DNA cleavage and X-ray studies, Eur. J. Med. Chem. 101 (2015) 705–715.
[17] J.C. Palomino, A. Martin, M. Camacho, H. Guerra, J. Swings, F. Portaels, Resazurin microtiter assay plate: simple and inexpensive method for detection of drug resistance in Mycobacterium tuberculosis, Antimicrob. Agents Chemother. 46 (2002) 2720–2722.
[18] P.C. Nguyen, A. Madani, P. Santucci, B.P. Martin, R.R. Paudel, S. Delattre, J.L. Herrmann, C.D. Spilling, L. Kremer, S. Canaan, J.F. Cavalier, Cyclophostin and Cyclipostins analogues, new promising molecules to treat mycobacterial-related diseases, Int. J. Antimicrob. Agents 51 (2018) 651–654.
[19] V. Slachtova, L. Janovska, L. Brulikova, Solid phase synthesis of new thiazolidinedione-pyrimidine conjugates and their antibacterial properties, J. Mol. Struct. 1183 (2019) 182–189.
[20] Z. Ozdemir, U. Bildziukevich, D. Saman, L. Havlicek, L. Rarova, L. Navratilova, Z. Wimmer, Amphiphilic derivatives of (3+-,17+-)-3-hydroxyandrost-5-ene-17-carboxylic acid, Steroids 128 (2017) 58–67.
[21] C.H. Zhou, Y. Wang, Recent researches in triazole compounds as medicinal drugs, Curr. Med. Chem. 19 (2012) 239–280.
[22] S. Majumdar, S. Duvvuri, A.K. Mitra, Membrane transporter/receptor-targeted prodrug design: strategies for human and veterinary drug development, Adv. Drug Deliv. Rev. 56 (2004) 1437–1452.
[23] V.K. Singh, B.B. Subudhi, Development of reversible glutamine conjugate of methotrexate for enhanced brain delivery, Med. Chem. Res. 24 (2015) 624–635.
[24] I.S. Krylov, B.A. Kashemirov, J.M. Hilfinger, C.E. McKenna, Evolution of an amino acid based prodrug approach: stay tuned, Mol. Pharm. 10 (2013) 445–458.
[25] V.P. Krasnov, A.Y. Vigorov, V.V. Musiyak, I.A. Nizova, D.A. Gruzdev, T.V. Matveeva, G.L. Levit, M.A. Kravchenko, S.N. Skornyakov, O.B. Bekker, V.N. Danilenko, V.N. Charushin, Synthesis and antimycobacterial activity of N-(2-aminopurin-6-yl) and N-(purin-6-yl) amino acids and dipeptides, Bioorg. Med. Chem. Lett 26 (2016) 2645–2648.
[26] Y. Voynikov, V. Valcheva, G. Momekov, P. Peikov, G. Stavrakov, Theophylline-7-acetic acid derivatives with amino acids as anti-tuberculosis agents, Bioorg. Med. Chem. Lett 24 (2014) 3043–3045.
[27] D.S. Rawat Beena, Antituberculosis drug research: a critical overview, Med. Res. Rev. 33 (2013) 693–764.
[28] G. Poce, M. Cocozza, S. Consalvi, M. Biava, SAR analysis of new anti-TB drugs currently in pre-clinical and clinical development, Eur. J. Med. Chem. 86 (2014) 335–351.
[29] D.S. Reddy, K.M. Hosamani, H.C. Devarajegowda, Preparation of benzocoumarin-pyrimidine hybrids as antitubercular agents, Eur. J. Med. Chem. 101 (2015) 705–715.
[30] S. Tahlan Sucheta, P.K. Verma, Biological potential of thiazolidinedione derivatives of synthetic origin, Chem. Cent. J. 11 (2017) 130.
[31] L. Brulikova, S. Krupkova, M. Labora, K. Motyka, L. Hradilova, M. Mistrik, J. Bartek, J. Hlavac, Synthesis and study of novel pH-independent fluorescent mitochondrial labels based on Rhodamine B, RSC Adv. 6 (2016) 23242–23251.

Appendix 5

Synthesis of various 2-aminobenzoxazoles: the study of cyclization and Smiles rearrangement

Šlachtová, V.; Chasák, J.; **Brulíková, L.***

ACS Omega **2019**, *4*(21), 19314-19323.

ACS OMEGA

Article

Cite This: ACS Omega 2019, 4, 19314−19323

http://pubs.acs.org/journal/acsodf

Synthesis of Various 2-Aminobenzoxazoles: The Study of Cyclization and Smiles Rearrangement

Veronika Šlachtová, Jan Chasák, and Lucie Brulíková*

Department of Organic Chemistry, Faculty of Science, Palacky University Olomouc, 17. listopadu 12, 771 46 Olomouc, Czech Republic

Supporting Information

ABSTRACT: This study reports two synthetic approaches leading to 2-aminobenzoxazoles and their *N*-substituted analogues. Our first synthetic strategy involves a reaction between various *o*-aminophenols and *N*-cyano-*N*-phenyl-*p*-toluenesulfonamide as a nonhazardous electrophilic cyanating agent in the presence of Lewis acid. The second synthetic approach uses the Smiles rearrangement upon activation of benzoxazole-2-thiol with chloroacetyl chloride. Both developed synthetic protocols are widely applicable, afford the desired aminobenzoxazoles in good to excellent yields, and use nontoxic and inexpensive starting material.

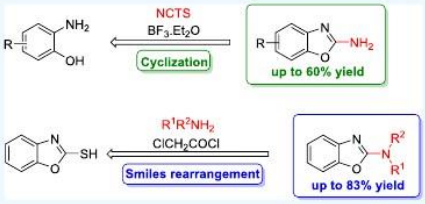

INTRODUCTION

2-Aminobenzoxazoles and their *N*-substituted analogues play an important role in medicinal chemistry and chemical biology.[1−7] They are described as potential therapeutic agents including various enzyme inhibitors (proteases, chymase, butyrylcholinesterase, topoisomerase II inhibitors, etc.).[4,7,8] They also have applications in materials chemistry.[9] In addition, aminobenzoxazoles serve as positron emission tomography probes.[2] Therefore, the development of effective methods leading to 2-aminobenzoxazoles and their analogues has attracted great attention.

Several methods for synthesis of 2-aminobenzoxazoles have been reported (Scheme 1).[8,10−20] However, most of these methods suffer from specific drawbacks. The most published protocol comprises the cyclization of 2-aminophenols using BrCN as a cyanating agent,[8,14−18,21] but this BrCN reagent is highly toxic. The next reported approach is the direct 2-C amination of benzoxazoles,[22−24] but its drawbacks include the use of transition metal catalysts, high temperatures, nitrogen atmosphere, or co-oxidants. In recent years, many efficient methods have been developed for the synthesis of *N*-substituted aminobenzoxazoles.[25−32] Most of these methods suffer from low yields and use toxic precursors or expensive reagents. *N*-substituted aminobenzoxazoles can be prepared from corresponding hydroxyl/thiol scaffolds through the aryl halides (Scheme 1).[30] Unfortunately, this method requires toxic and acidic halogenating agents. Amination using Rose Bengal as a photocatalyst has been recently reported.[28] Despite being efficient and the low cost of Rose Bengal catalyst, this protocol needs a strong organic base (DBU) and has long reaction time that downgrade its advantages. Microwave-enhanced on-water amination of 2-mercaptobenzoxazoles has also been recently introduced.[29] However, its drawbacks include an inert atmosphere or co-oxidants. In addition, transition metal catalysts used in this method may be expensive and higher temperatures are sometimes inevitable.

Given the shortcomings of the abovementioned methods, we attempted to develop a new, nontoxic, and efficient protocol relying on an inexpensive starting material. Thus, accordingly, we designed two independent protocols leading to 2-aminobenzoxazoles (Scheme 1, path a) and their *N*-mono or disubstituted analogues (Scheme 1, path b). The first protocol is based on the use of *N*-cyano-*N*-phenyl-*p*-toluenesulfonamide (NCTS) as a nonhazardous electrophilic cyanating agent. It combines operational simplicity, a nontoxic reagent, and wide substrate scope. The second approach is based on the Smiles rearrangement that enables the functionalization of heteroaromatic rings under economic conditions. Both the developed protocols are widely applicable and afford the desired compounds in good yields, thus indicating their efficacy.

RESULTS AND DISCUSSION

In 2015, Kasthuri et al. reported the synthesis of 2-aminobenzoxazoles using an efficient, air-stable, and nonhazardous electrophilic cyanating agent, i.e., NCTS.[13] NCTS can be easily synthesized from inexpensive and commercially available phenyl urea by dehydrative tosylation in pyridine in high yields.[33] The synthetic protocol described by Kasthuri et al.[13] required 1 equiv of LiHMDS to accomplish the reaction. Unfortunately, despite our efforts to acquire additional optimization, we found the reaction to be irreproducible in our hands as it yielded only up to 11% of the desired product **2a** (Table 1, entry 6).[34] Compound **3** was always detected as the major product according to liquid chromatography−mass spectrometry (LC−MS) traces.

Received: August 21, 2019
Accepted: October 18, 2019
Published: November 5, 2019

DOI: 10.1021/acsomega.9b02702
ACS Omega 2019, 4, 19314−19323

Scheme 1. Aminobenzoxazole Synthesis

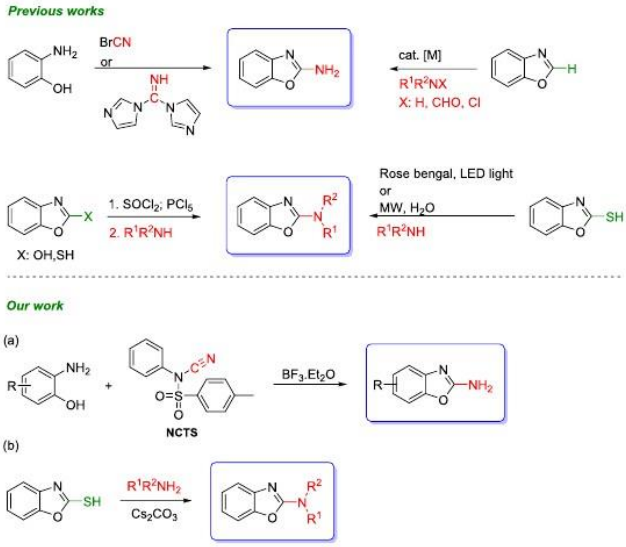

Table 1. Optimization of the Reaction Conditions[a]

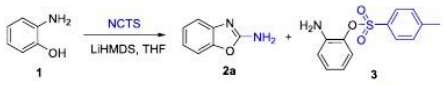

entry	NCTS (equiv)	LiHMDS (equiv)	T (°C)	results[b] (% of **2a**)
1	1	1	0 to rt	9
2	1	3	0 to rt	9
3	1.2	1	0 to rt	6
4	1.5	1	0 to rt	4
5	1.2	3	0 to rt	9
6	1	3	0 to 60	11

[a]Reaction conditions: *o*-aminophenol (0.18 mmol, 20 mg), NCTS, LiHMDS, tetrahydrofuran (THF; 1 mL), 2 h. [b]Conversion estimated from LC−MS traces at 210−500 nm.

Table 2. Optimization of the Reaction Conditions with Lewis Acids[a]

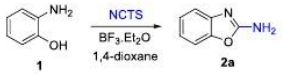

entry	BF_3·Et_2O (equiv)	NCTS (equiv)	T (°C)	results[c] (% of **2a**)
1	3	3	reflux	86
2	3	3	100[b]	39
3	3	2	reflux	75
4	3	1.5	reflux	87
5	3	1.2	reflux	54
6	2	1.5	reflux	90
7	1	1.5	reflux	71

[a]Reaction conditions: *o*-aminophenol (0.18 mmol, 20 mg), NCTS, BF_3·Et_2O, 1,4-dioxane (1 mL), 30 h. [b]External temperature of the bath. [c]Conversion estimated from LC−MS traces at 210−500 nm.

Following these results, we changed the reaction conditions keeping NCTS as a cyanating agent. Initial investigations were aimed at the direct use of NCTS without any activation. Unfortunately, NCTS was found to be ineffective in this case. Thus, we suggested that the use of a strong Lewis acid as BF_3·Et_2O in combination with NCTS could successfully activate the CN group toward a nucleophilic attack[33] and afford the desired product **2a**. Indeed, our expectations met with successful results, and after some optimization (Table 2), the desired product **2a** was obtained in good yield. Using these optimal conditions, the reaction can proceed even at a 5 mmol scale. This result suggested that the process might be scaled up with only a slightly lower yield.

With optimum reaction conditions, the substrate scope was explored (Table 3). We found out that the substitution pattern does not affect the reaction yields. Both EWG and EDG substituents yielded the desired products in moderate to good yields (45−60%). Considering the satisfactory LC−MS conversions, we estimated that the multistep isolation and purification procedure resulted in lowered isolated yields. Hence, different solvents were tried to improve the workup and isolated yield (Supporting Information, Table S1). Unfortunately, none of the used solvents led to a higher yield.

Based on the observations and prevalent literature,[35] the reaction mechanism was proposed (Scheme 2). The reaction is initiated through the Lewis acidic activation of NCTS via the coordination of its cyano group to BF_3·Et_2O. The activation facilitates the subsequent nucleophilic attack of the amino group and the elimination of the sulfonamide residue. The hydroxy group then attacks the electron-deficient carbon. Finally, the desired product **2** is formed during the workup. We confirmed the eliminated sulfonamide by mass m/z = 246 [M − H], providing the next experimental support for our mechanistic proposal.

DOI: 10.1021/acsomega.9b02702
ACS Omega 2019, 4, 19314−19323

Table 3. Substrate Scope of the Cyclization Reaction[a]

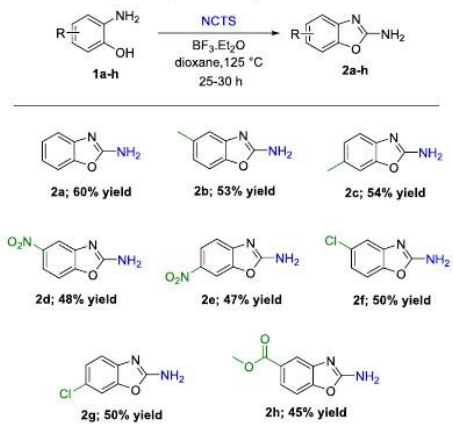

[a]Reaction conditions: *o*-aminophenol (0.9 mmol, 100 mg), NCTS (1.5 equiv), $BF_3{\cdot}Et_2O$ (2 equiv), 1,4-dioxane (5 mL), reflux, 25−30 h.

We were also interested in the catalyst-free synthesis of *N*-substituted benzoxazole analogues. Recently, the Smiles rearrangement, an intramolecular SN_{Ar} reaction, has received renewed attention.[36] It enables the functionalization of heteroaromatic rings via breaking a C−X single bond and forming a new C−X or C−C bond under economic conditions. In 2017, Wang et al. published an interesting synthesis of *N*-aryl-2-aminobenzoxazoles from substituted benzoxazole-2-thiol and 2-chloro-*N*-arylacetamides in a KOH−dimethylformamide (DMF) system.[37] However, this method is described only for aromatic substrates. By taking inspiration from the capabilities of the Smiles rearrangement and commercially available heterocyclic thiols, we suggested a synthetic approach to *N*-substituted aminobenzoxazoles.

First, we focused on the reaction of benzoxazole-2-thiol with various aliphatic bromoamines and expected the Smiles rearrangement to result in the desired thiol (Scheme 3). Interestingly, some of the investigated substrates reacted giving the mixture of thiol and disulfide or other unexpected products.

The reaction of benzoxazole-2-thiol **4** with 3-bromopropylamine HBr **5** according to the conditions listed by Abdelazeem et al.[3] gave a mixture of benzoxazole **6** and disulfide analogue **7** (Scheme 3). The reaction conditions were further optimized concerning the amine and base equivalents (Supporting Information, Table S2). If an excess of the base was used, disulfide was obtained as the main product of the reaction. However, 2 equiv of the amine together with 2 equiv of the base provided compound **6** selectively. Moreover, radical scavenger Et_3N strongly suppressed disulfide **7** formation. Therefore, disulfide **7** might be probably formed by a radical mechanism. On the other hand, there was no effect of oxidation (Supporting Information, Table S2, entry 8).

Subsequently, we explored the reaction of benzoxazole-2-thiol with 2-bromoethylamine HBr (Scheme 3). Surprisingly, we observed a different reactivity compared to bromopropylamine (Supporting Information, Table S3). The reaction of benzoxazole-2-thiol started with 4 equiv of the amine and 3 equiv of K_2CO_3, giving a mixture of products **9** and **10**. Disulfide **10** was formed selectively using just 2 equiv of the amine. The temperature was found to play a key role in the reaction. Heating at 70 °C resulted in a mixture of both compounds, and an increased temperature of 120 °C afforded disulfide **10** selectively. Changing the amount of K_2CO_3 did not provide the desired selectivity. Consequently, we tried Et_3N instead and realized that 2 equiv of the amine and 1 equiv of Et_3N are the most convenient conditions for the synthesis of compound **9**.

We also studied the reactivity of benzoxazole-2-thiol with 4-bromobutylamine HBr **11** (Scheme 3, Supporting Information, Table S4). The bromoamine **11** was synthesized from commercially available aminoalcohol according to the previously described procedure followed by ionex workup.[38] Surprisingly, the rapid 5-membered ring closure provided pyrrolidine **14** as the main product regardless of the reaction conditions. This ring-closing reaction is speeded up by negligible ring strain and insignificant entropy change. Lower temperature only slowed all of the conversion down. Finally, 2 equiv of the amine and 2 equiv of Et_3N in refluxing toluene provided compound **14** within 4 h.

The reactivity of 5-bromopentylamine HBr **15** was also explored (Scheme 3, Supporting Information, Table S5). Bromoamine **15** was synthesized from 5-aminopentan-1-ol according to the previously described procedure followed by ionex workup.[38] The substitution leading to product **16** proceeded smoothly after the careful optimizations using 2 equiv of Et_3N in refluxing toluene. Harsher reaction conditions were tried to obtain the rearranged compound **17**, but we

Scheme 2. Proposed Reaction Pathway

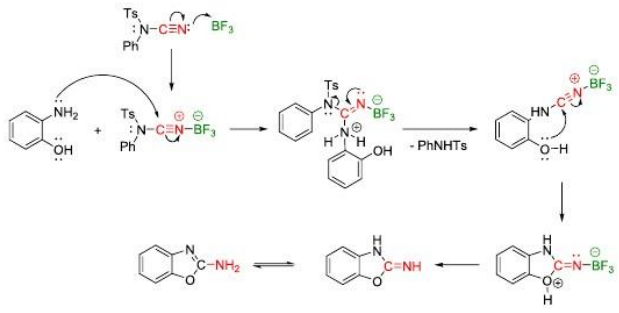

DOI: 10.1021/acsomega.9b02702
ACS Omega 2019, 4, 19314−19323

Scheme 3. Reaction of Benzoxazole-2-thiol with Various Aliphatic Bromoamines

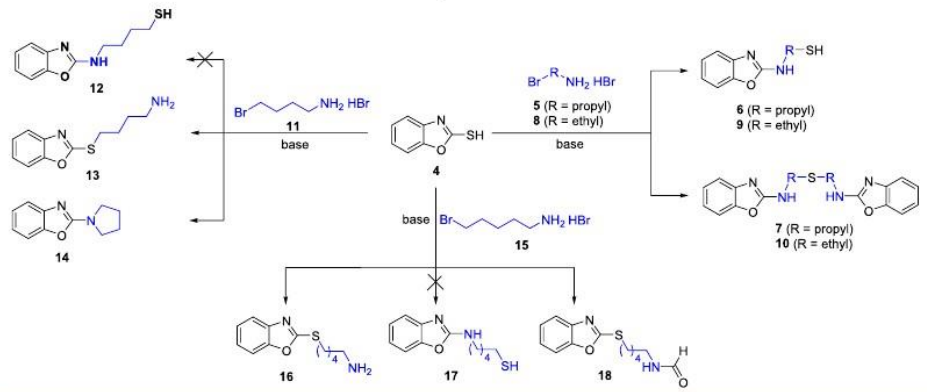

Scheme 4. Reaction of Benzoxazole-2-thiol with 4-Bromobenzylamine/2-Chloroacetamide/3-(Bromomethyl)aniline

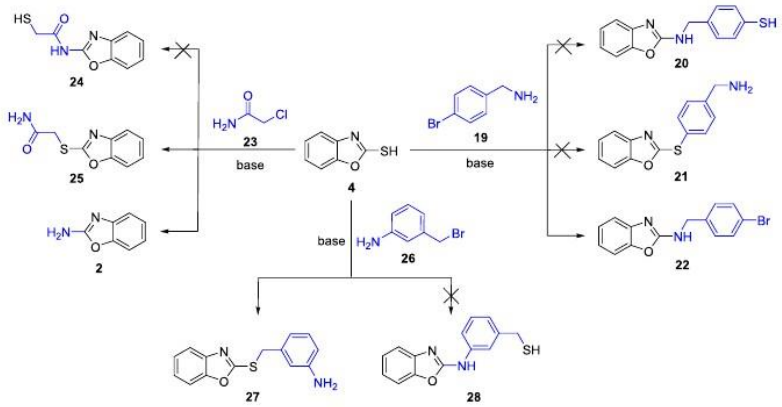

Table 4. Optimization of Reaction Conditions with Cyclohexylamine[a]

entry	chloride (equiv)	base (equiv)	T (°C)	time (h)	solvent	ratio of 30l:31l (%)[b]
1	1.2	Cs_2CO_3 (3.2)	160 (MW)	1/2	DMF	57:0
2	1.2	Cs_2CO_3 (3.2)	160	8	DMF	58:0
3	1.7	Cs_2CO_3 (3.2)	160 (MW)	1/2	DMF	31:0
4	1.2	Cs_2CO_3 (3.7)	160 (MW)	1/2	DMF	48:0
5	1.2	Cs_2CO_3 (3.2)	160 (MW)	1/2	*N*,*N*-DMA	25:0
6	1.2	Cs_2CO_3 (3.2)	160 (MW)	1/2	*N*,*N*-DMA	47:0
7	1.2	DBU (3.2)	reflux	2	MeCN	0:95
8	1.2	NaH (3.2)	150	2	*N*,*N*-DMA	0:42

[a]Reaction conditions: Benzoxazole-2-thiol (0.16 mmol, 25 mg), cyclohexylamine (0.16 mmol), base, $ClCH_2COCl$, solvent (1 mL). [b]Conversion estimated from LC−MS traces at 210−500 nm.

DOI: 10.1021/acsomega.9b02702
ACS Omega 2019, 4, 19314−19323

Table 5. Substrate Scope of the Rearrangement

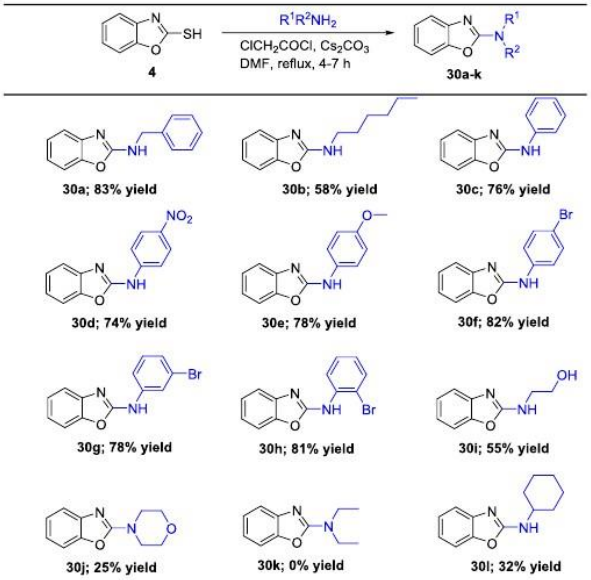

Scheme 5. Proposed Reaction Pathway

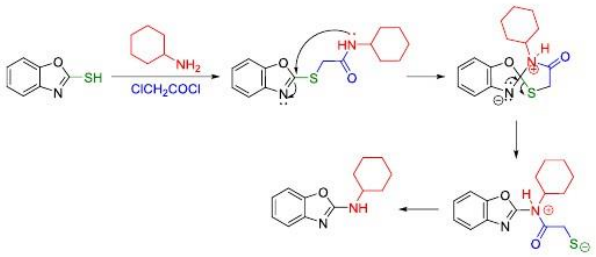

observed the formylation in DMF instead. As a result, compound **18** was isolated after the microwave irradiation.

We next investigated the behavior of chloroacetamide as well as aromatic substrates in the Smiles reaction (Scheme 4). For this, we studied the reactivity of aromatic 4-bromobenzylamine **19** (Scheme 4, Supporting Information, Table S6). Lower susceptibility to nucleophilic attack usually makes aromatic halides rather unreactive. However, the unexpected reaction occurred on using 2 equiv of Et_3N in refluxing toluene. Under these conditions, the amino group was found to be sufficiently nucleophilic to substitute the thiol, providing benzoxazolamine **22**.

The investigation of more challenging substrates such as amides and benzylic bromides gave only the expected substitution products. Their rearrangement was probably prevented by sterically and energetically demanding transition states. First, we examined the reactivity of 2-chloroacetamide **23** (Scheme 4, Supporting Information, Table S7). All of the optimizations gave mostly compound **25** probably due to lower acidic nitrogen nucleophilicity as well as an unfavorable transition state. Moreover, microwave irradiation afforded a mixture of **25** and 2-aminobenzoxazole **2**. We also explored the reactivity of 3-(bromomethyl)aniline (Scheme 4, Supporting Information, Table S8). There was no rearrangement regardless of the reaction conditions. We always obtained only the substitution product **27**. Finally, reactions with various aromatic bromoanilines were attempted, but no reaction occurred as expected.

Since we aimed at a wide substrate scope, a universal method was needed. Thus, a more challenging intramolecular variant of the Smiles rearrangement using chloroacetyl chloride was explored (Table 4). First, reaction conditions described by Tian et al.[39] applied on cyclohexylamine as a model substrate were attempted (Table 4, entry 1). This one-pot reaction was performed under microwave irradiation as well as under conventional heating in an oil bath at 160 °C. The second

DOI: 10.1021/acsomega.9b02702
ACS Omega 2019, 4, 19314−19323

reaction provided a slightly better result. Excess chloride or Cs_2CO_3, as well as changing the solvent, prolonged the reaction time, or the higher temperature gave worse conversion. On the other hand, no rearrangement occurred using different bases. Since bromoacetyl bromide showed better activating properties, milder reaction conditions were considered for aniline (Supporting Information, Table S9). The reaction proceeded even at 85 °C without compromising the isolated yield. Different bases provided only the substitution product **31c**. Unfortunately, these milder conditions failed with other amines giving the substitution product **31** only.

With the optimized reaction conditions, we studied the scope of the rearrangement (Table 5). Various types of amines, including aromatic, aliphatic, alicyclic (both primary and secondary), and bisnucleophilic ethanolamine, were tested. Regardless of the electron effects and substitution patterns, the aromatic and primary amines reacted smoothly, giving the desired products **30a−h** in good yields (58−83%). On the other hand, a steric hindrance on the amine lowered the yield significantly. The reaction resulted in a moderate isolated yield of benzoxazole **30l** (32%), while the reaction with morpholine gave low yield of **30j** (25%). The rearrangement of diethylamine completely failed. Finally, we upscaled the reaction of benzoxazole-2-thiol **4** with aniline to 3.5 mmol of **4**, which required a slightly prolonged reaction time (8 h), giving **30c** in a 71% isolated yield. This result suggested that the process also can be upscaled with only a slightly lower yield.

Based on the above observations and the existing literature, the reaction mechanism set out in Scheme 5 was suggested. First, *S*-alkylated thiol undergoes the Smiles rearrangement by the nucleophilic attack of the nitrogen at the benzoxazole ring carbon, forming a new C−N bond to give the spiro intermediate. Second, rearomatization and alkaline hydrolysis in the presence of Cs_2CO_3 afford the *N*-substituted benzoxazole **30**.

■ CONCLUSIONS

In conclusion, synthetic strategies affording various 2-aminobenzoxazoles and their *N*-substituted analogues from readily available starting materials have been developed. Our first approach to substituted 2-aminobenzoxazoles is based on the nonhazardous cyanating agent NCTS, activated with $BF_3{\cdot}Et_2O$. This newly developed synthetic protocol combines operational simplicity, a nontoxic and readily available reagent, and wide substrate scope. Moreover, an efficient one-pot amination of benzoxazole-2-thiol by various amines mediated with chloroacetyl chloride via the intramolecular Smiles rearrangement was developed. Our methodology stands out because of the wide amine scope, short reaction time, and a metal-free approach. The obtained results also indicated that the reactions can be scaled up, providing an alternative process for the chemical industry. Finally, we believe that our methodologies represent a straightforward way to various aminobenzoxazoles and their analogues as important building blocks in organic and medicinal chemistry.

■ EXPERIMENTAL SECTION

General Information. Solvents and chemicals were purchased from Sigma-Aldrich (www.sigmaaldrich.com) and Fluorochem (www.fluorochem.co.uk). All reactions were carried out at ambient temperature (21 °C) unless stated otherwise. Analytical thin-layer chromatography (TLC) was performed using aluminum plates precoated with silica gel (silica gel 60 F254).

The LC−MS analyses were carried out on an UHPLC−MS system consisting of UHPLC chromatograph Accela with a photodiode array detector and triple quadrupole mass spectrometer TSQ Quantum Access (Thermo Scientific, CA), using a Nucleodur Gravity C18 column (dimensions 1.8 μm, 2.1 × 50 mm^2 at 30 °C and a flow rate of 800 μL/min (Macherey-Nagel, Germany)). The mobile phase was (A) 0.1% ammonium acetate in water and (B) 0.1% ammonium acetate in acetonitrile, linearly programmed from 10 to 80% B over 2.5 min, kept for 1.5 min. The column was re-equilibrated with 10% of solution B for 1 min. The APCI source operated at a discharge current of 5 μA, vaporizer temperature of 400 °C, and a capillary temperature of 200 °C.

NMR 1H/13C spectra were recorded on a JEOL ECX-500SS (500 MHz) or JEOL ECA400II (400 MHz) spectrometer at magnetic field strengths of 11.75 T (with operating frequencies 500.16 MHz for 1H and 125.77 MHz for 13C) and 9.39 T (with operating frequencies 399.78 MHz for 1H and 100.53 MHz for 13C) at ambient temperature (~21 °C). Chemical shifts (δ) are reported in parts per million (ppm), and coupling constants (J) are reported in hertz (Hz). NMR spectra were recorded at ambient temperature (21 °C) in DMSO-d_6 and referenced to the resonance signal of the solvent.

HRMS analysis was performed with LC−MS and an Orbitrap high-resolution mass spectrometer (Dionex, Ultimate 3000, Thermo Exactive plus, MA) operating in positive full scan mode in the range of 80−1200 m/z. The settings for electrospray ionization were as follows: 150 °C oven temperature and 3.6 kV source voltage. The acquired data were internally calibrated with phthalate as a contaminant in methanol (m/z 297.15909). Samples were diluted to a final concentration of 0.1 mg/mL in a solution of water and acetonitrile (50:50, v/v). The samples were injected into the mass spectrometer following HPLC separation on a Kinetex C18 column (2.6 μm, 100 A, 50 × 3.0 mm^2) using an isocratic mobile phase of 0.01 M MeCN/ammonium acetate (80/20) at a flow rate of 0.3 mL/min.

All reactions carried out under microwave irradiation were performed with the CEM Discover SP microwave synthesizer, using the dynamic mode in the following settings: maximum amount of microwave power (150 W), premixing time (1 min), and stirring speed (high). A simultaneous cooling of the reaction vessel provided by compressed air (24 psi) was applied during the entire experiment (PowerMax option "ON"). All 0.5 mmol scale reactions were performed in a 10 mL borosilicate glass reaction vessel closed with a disposable silicon cap and equipped with a Teflon-coated egg-shaped magnetic stir bar. The temperature was monitored by an external infrared sensor.

General Procedures and Characterization of Individual Compounds. *Cyclization of Aminophenols with NCTS.* *O*-aminophenol **1** (0.9 mmol; 1 equiv) and NCTS (1.35 mmol; 1.5 equiv) were dissolved in 1,4-dioxane (4 mL). $BF_3{\cdot}Et_2O$ (1.8 mmol; 2 equiv) was added dropwise. The mixture was refluxed overnight (monitored by TLC, 24−30 h). After that, the cooled (rt) mixture was quenched with sat. $NaHCO_3$ (pH ~ 7), diluted with H_2O (30 mL), and extracted with EtOAc (3 × 30 mL). Combined organic layers were dried over anhydrous Na_2SO_4 and concentrated in vacuo. The residue was purified by column chromatography using Hex/EtOAc.

*Benzo[d]oxazol-2-amine (**2a**).* Brown solid. Yield: 60% (72 mg). ^{1}H NMR (400 MHz, DMSO-d_6): δ 7.35 (s, 2H), 7.30 (d, J = 7.8 Hz, 1H), 7.19 (d, J = 7.3 Hz, 1H), 7.08 (t, J = 7.2 Hz, 1H),

DOI: 10.1021/acsomega.9b02702
ACS Omega 2019, 4, 19314−19323

6.95 (t, J = 7.2 Hz, 1H). ^{13}C NMR (101 MHz, DMSO-d_6): δ 162.70, 147.92, 143.61, 123.45, 119.92, 115.25, 108.38. HRMS: m/z: calcd for $C_7H_6N_2O$: 135.0553 $[M + H]^+$; found: 135.0554.

*5-Methylbenzo[d]oxazol-2-amine (**2b**).* Brown solid. Yield: 53% (71 mg). ^{1}H NMR (400 MHz, DMSO-d_6): δ 7.29 (s, 2H), 7.16 (d, J = 8.0 Hz, 1H), 7.00 (s, 1H), 6.75 (d, J = 7.9 Hz, 1H), 2.30 (s, 3H). ^{13}C NMR (101 MHz, DMSO-d_6): δ 162.89, 146.09, 143.78, 132.47, 120.46, 115.69, 107.80, 21.10. HRMS: m/z: calcd for $C_8H_8N_2O$: 149.0709 $[M + H]^+$; found: 149.0709.

*6-Methylbenzo[d]oxazol-2-amine (**2c**).* Brown solid. Yield: 54% (72 mg). ^{1}H NMR (400 MHz, DMSO-d_6): δ 7.29 (s, 2H), 7.14 (s, 1H), 7.06 (d, J = 7.9 Hz, 1H), 6.90 (d, J = 7.6 Hz, 1H), 2.32 (s, 3H). ^{13}C NMR (101 MHz, DMSO-d_6): δ 162.30, 148.06, 140.89, 129.38, 124.09, 114.69, 108.9, 20.97. HRMS: m/z: calcd for $C_8H_8N_2O$: 149.0709 $[M + H]^+$; found: 149.0710.

*5-Nitrobenzo[d]oxazol-2-amine (**2d**).* Yellow solid. Yield: 48% (77 mg). ^{1}H NMR (400 MHz, DMSO-d_6): δ 7.98−7.96 (m, 1H), 7.95−7.90 (m, 3H), 7.55 (d, J = 8.7 Hz, 1H). ^{13}C NMR (101 MHz, DMSO-d_6): δ 164.80, 152.31, 144.65, 144.36, 116.65, 109.98, 108.64. HRMS: m/z: calcd for $C_7H_5N_3O_3$: 178.0258 $[M - H]^+$; found: 178.0242.

*6-Nitrobenzo[d]oxazol-2-amine (**2e**).* Yellow solid. Yield: 47% (75 mg). ^{1}H NMR (400 MHz, DMSO-d_6): δ 8.29−8.17 (m, 3H), 8.10 (dd, J = 8.7, 2.3 Hz, 1H), 7.32 (d, J = 8.7 Hz, 1H). ^{13}C NMR (101 MHz, DMSO-d_6): δ 166.35, 150.99, 147.19, 140.29, 121.09, 114.13, 104.65. HRMS: m/z: calcd for $C_7H_5N_3O_3$: 178.0258 $[M - H]^+$; found: 178.0241.

*5-Chlorobenzo[d]oxazol-2-amine (**2f**).* Brown solid. Yield: 50% (76 mg). ^{1}H NMR (400 MHz, DMSO-d_6): δ 7.58 (s, 2H), 7.32 (d, J = 8.4 Hz, 1H), 7.22 (d, J = 2.1 Hz, 1H), 6.97 (dd, J = 8.4, 2.2 Hz, 1H). ^{13}C NMR (101 MHz, DMSO-d_6): δ 163.86, 146.73, 145.30, 127.65, 119.43, 114.88, 109.39. HRMS: m/z: calcd for $C_7H_5ClN_2O$: 169.0163 $[M + H]^+$; found: 169.0165.

*6-Chlorobenzo[d]oxazol-2-amine (**2g**).* Red solid. Yield: 50% (75 mg). ^{1}H NMR (400 MHz, DMSO-d_6): δ 7.52 (s, 2H), 7.48 (d, J = 1.8 Hz, 1H), 7.17 (d, J = 8.3 Hz, 1H), 7.12 (dd, J = 8.3, 2.0 Hz, 1H). ^{13}C NMR (101 MHz, DMSO-d_6): δ 163.31, 148.27, 142.80, 123.69, 123.54, 115.85, 109.13. HRMS: m/z: calcd for $C_7H_5ClN_2O$: 169.0163 $[M + H]^+$; found: 169.0164.

*Methyl 2-Aminobenzo[d]oxazol-5-carboxylate (**2h**).* Yellow solid. Yield: 45% (49 mg). ^{1}H NMR (500 MHz, DMSO-d_6): δ 7.72 (d, J = 1.7 Hz, 1H), 7.65 (dd, J = 8.3, 1.7 Hz, 1H), 7.63 (s, 2H), 7.43 (d, J = 8.3 Hz, 1H), 3.84 (s, 3H). ^{13}C NMR (101 MHz, DMSO-d_6): δ 166.36, 163.71, 151.30, 144.02, 125.32, 122.17, 115.78, 108.47, 52.05. HRMS: m/z: calcd for $C_9H_8N_2O_3$: 193.0608 $[M + H]^+$; found: 193.0607.

Cyclization of Aminophenols with LiHMDS. *O*-Aminophenol **1** (1.61 mmol; 1 equiv) and NCTS were dissolved in THF (dry, 2.5 mL). The mixture was cooled down to 5 °C, and 1 M LiHMDS in hexane (1.61 mmol; 1 equiv) was added dropwise. It was stirred at 5 °C to rt for 1 h. Then, the reaction mixture was poured into ice water (50 mL) and stirred for 15 min. This was followed by an extraction with EtOAc (3 × 50 mL), and the organic layers were washed with brine (1×), dried over anhydrous Na_2SO_4, and concentrated in vacuo. The residue was purified by column chromatography using Hex/EtOAc.

*2-Aminophenyl-4-methylbenzenesulfonate (**3**).* Brown solid. Yield: 35% (148 mg). ^{1}H NMR (500 MHz, DMSO-d_6): δ 9.28 (s, 2H), 7.63 (d, J = 8.3 Hz, 2H), 7.30 (d, J = 8.2 Hz, 2H), 7.13 (dd, J = 8.0, 1.6 Hz, 1H), 6.91 (td, J = 7.9, 1.6 Hz, 1H), 6.72 (dd, J = 8.0, 1.1 Hz, 1H), 6.68 (td, J = 7.9, 1.4 Hz, 1H), 2.33 (s, 3H). ^{13}C NMR (101 MHz, DMSO-d_6): δ 150.19, 142.89, 137.82, 129.42, 126.86, 126.15, 124.40, 119.04, 115.59, 21.05. HRMS: m/z: calcd for $C_{13}H_{13}NO_3S$: 264.0689 $[M + H]^+$; found: 264.0689.

Smiles Rearrangement with 3-Bromopropylamine HBr. Benzoxazole-2-thiol **4** (1.61 mmol, 1 equiv), K_2CO_3 (3.2 mmol; 2 equiv/4.8 mmol; 3 equiv), and 3-bromopropylamine HBr **5** (3.2 mmol; 2 equiv/1.61 mmol; 1 equiv) were suspended in DMF (10 mL). The reaction mixture was stirred at 70 °C for 2 h. It was followed by dilution with H_2O (50 mL) and extraction with EtOAc (3 × 50 mL). Organic layers were washed with brine (1×), dried over anhydrous Na_2SO_4, and concentrated in vacuo. The residue was purified by column chromatography using Hex/EtOAc.

*3-(Benzo[d]oxazol-2-ylamino)propane-1-thiol (**6**).* White solid. Yield: 67% (222 mg). ^{1}H NMR (500 MHz, DMSO-d_6): δ 7.90 (t, J = 5.6 Hz, 1H), 7.32 (d, J = 7.8 Hz, 1H), 7.23 (d, J = 7.1 Hz, 1H), 7.10 (td, J = 7.6, 1.0 Hz, 1H), 6.96 (td, J = 7.7, 1.2 Hz, 1H), 3.39 (dd, J = 12.6, 6.7 Hz, 2H), 2.56 (dd, J = 13.8, 6.8 Hz, 2H), 2.40 (t, J = 7.3 Hz, 1H), 1.86 (p, J = 6.9 Hz, 2H). ^{13}C NMR (126 MHz, DMSO-d_6): δ 162.31, 147.98, 143.24, 123.51, 120.02, 115.36, 108.42, 40.74, 32.96, 21.11. HRMS: m/z: calcd for $C_{10}H_{12}N_2OS$: 209.0743 $[M + H]^+$; found: 209.0743.

*N,N′-(Disulfanediylbis(propane-3,1-diyl)bis(benzo[d]-oxazol-2-amine)) (**7**).* Yellow solid. Yield: 66% (219 mg). ^{1}H NMR (500 MHz, DMSO-d_6): δ 7.94 (t, J = 5.6 Hz, 2H), 7.31 (d, J = 7.8 Hz, 2H), 7.23 (d, J = 7.4 Hz, 2H), 7.09 (td, J = 7.7, 0.9 Hz, 2H), 6.96 (td, J = 7.8, 1.1 Hz, 2H), 3.39 (dd, J = 12.7, 6.6 Hz, 4H), 2.81 (t, J = 7.1 Hz, 4H), 2.03−1.90 (m, 4H). ^{13}C NMR (126 MHz, DMSO-d_6): δ 162.25, 147.99, 143.23, 123.51, 120.04, 115.39, 108.43, 40.89, 35.02, 28.38. HRMS: m/z: calcd for $C_{20}H_{22}N_4O_2S_2$: 415.1257 $[M + H]^+$; found: 415.1258

Smiles Rearrangement with 2-Bromoethylamine HBr. Benzoxazole-2-thiol **4** (1.61 mmol, 1 equiv), K_2CO_3 (4.8 mmol; 3 equiv), and 2-bromoethylamine HBr **8** (3.2 mmol; 2 equiv) were suspended in DMF (10 mL). The reaction mixture was stirred at 120 °C for 2 h. This was followed by dilution with H_2O (50 mL) and extraction with EtOAc (3 × 50 mL). Organic layers were washed with brine (1×), dried over anhydrous Na_2SO_4, and concentrated in vacuo. The residue was purified by column chromatography using Hex/EtOAc.

*N,N′-(Disulfanediylbis(ethane-2,1-diyl)bis(benzo[d]-oxazol-2-amine)) (**10**).* White solid. Yield: 71% (220 mg). ^{1}H NMR (400 MHz, DMSO-d_6): δ 8.14 (t, J = 5.7 Hz, 2H), 7.33 (d, J = 7.8 Hz, 2H), 7.25 (d, J = 7.6 Hz, 2H), 7.10 (td, J = 7.5, 0.9 Hz, 2H), 6.97 (td, J = 7.7, 1.1 Hz, 2H), 3.61 (dd, J = 12.9, 6.4 Hz, 4H), 3.01 (t, J = 6.7 Hz, 4H). ^{13}C NMR (101 MHz, DMSO-d_6): δ 162.03, 148.02, 143.08, 123.62 120.24, 115.56, 108.58, 41.45, 36.86. HRMS: m/z: calcd for $C_{18}H_{18}N_4O_2S_2$: 387.0944 $[M + H]^+$; found: 387.0944.

Smiles Rearrangement with 4-Bromobutylamine HBr. Benzoxazole-2-thiol **4** (0.6 mmol, 1 equiv) and Et_3N (1.2 mmol, 2 equiv) were dissolved in toluene (5 mL) and premixed at rt for 10 min. Subsequently, 4-bromobutylamine HBr **11** (1.2 mmol, 2 equiv) was added. The reaction mixture was refluxed for 4 h. It was cooled to room temperature, diluted with H_2O (20 mL), and extracted with EtOAc (3 × 20 mL). Organic layers were dried over anhydrous Na_2SO_4 and concentrated in vacuo. The residue was purified by column chromatography using Hex/EtOAc.

*2-(Pyrrolidin-1-yl)benzo[d]oxazole (**14**).* White solid. Yield: 54% (60 mg). ^{1}H NMR (400 MHz, DMSO-d_6): δ 7.37 (dd, J = 7.9, 0.5 Hz, 1H), 7.25 (dd, J = 7.8, 0.8 Hz, 1H), 7.12 (td, J = 7.7, 1.1 Hz, 1H), 6.97 (td, J = 7.7, 1.3 Hz, 1H), 3.54 (ddd, J = 6.7, 4.3, 2.6 Hz, 4H), 2.00−1.93 (m, 4H). ^{13}C NMR (101 MHz, DMSO-

DOI: 10.1021/acsomega.9b02702
ACS Omega 2019, 4, 19314−19323

d_6): δ 160.51, 148.54, 143.59, 123.72, 119.77, 115.36, 108.63, 47.16, 25.03. HRMS: m/z: calcd for $C_{11}H_{12}N_2O$: 189.1022 [M + H]$^+$; found: 189.1022.

Smiles Rearrangement with 5-Bromopentylamine HBr. Benzoxazole-2-thiol **4** (0.6 mmol, 1 equiv) and Et_3N (1.2 mmol, 2 equiv) were dissolved in toluene (5 mL) and premixed at rt for 10 min. Subsequently, 5-bromopentylamine HBr **15** (1.2 mmol, 2 equiv) was added. The reaction mixture was refluxed for 4 h. It was cooled to room temperature, diluted with H_2O (20 mL), and extracted with EtOAc (3 × 20 mL). Organic layers were dried over anhydrous Na_2SO_4 and concentrated in vacuo.

*5-(Benzo[d]oxazol-2-ylthio)pentan-1-amine HBr (**16**).* White solid. Yield: 95% (134 mg). ^{1}H NMR (400 MHz, DMSO-d_6): δ 7.68−7.59 (m, 2H), 7.37−7.28 (m, 2H), 3.54 (br s, 3H), 3.37−3.28 (m, 2H), 2.60 (t, J = 6.5 Hz, 2H), 1.85−1.71 (m, 2H), 1.53−1.35 (m, 4H). ^{13}C NMR (101 MHz, DMSO-d_6): δ 164.47, 151.18, 141.31, 124.52, 124.12, 118.15, 110.09, 41.04, 31.77, 31.68, 28.75, 25.30. HRMS: m/z: calcd for $C_{12}H_{16}N_2OS$: 237.1056 [M + H]$^+$; found: 237.1056.

*Smiles Rearrangement with **16**.* Compound **16** (0.42 mmol, 1 equiv) and Et_3N (0.84 mmol, 2 equiv) were dissolved in DMF (4 mL). The reaction mixture was stirred under microwave irradiation at 120 °C for 2 h. After that, it was cooled to room temperature, diluted with H_2O (20 mL), and extracted with EtOAc (3 × 20 mL). Organic layers were dried over anhydrous Na_2SO_4 and concentrated in vacuo. The residue was purified by column chromatography using Hex/EtOAc.

*N-(5-(Benzo[d]oxazol-2-ylthio)pentyl)formamide (**18**).* Brown oil. Yield: 58% (64 mg). ^{1}H NMR (400 MHz, DMSO-d_6): δ 7.99 (s, 1H), 7.97 (br s, 1H), 7.68−7.59 (m, 2H), 7.36−7.28 (m, 3H), 3.35−3.28 (m, 2H, overlapped with H_2O), 3.09 (q, J = 6.3 Hz, 2H), 1.84−1.73 (m, 2H), 1.50−1.38 (m, 4H). ^{13}C NMR (101 MHz, DMSO-d_6): δ 164.43, 160.87, 151.18, 141.31, 124.52, 124.12, 118.16, 110.10, 36.83, 31.59, 28.51, 28.39, 25.30. HRMS: m/z: calcd for $C_{13}H_{16}N_2O_2S$: 265.1005 [M + H]$^+$; found: 265.1006.

Smiles Rearrangement with 4-Bromobenzylamine. Benzoxazole-2-thiol **4** (0.6 mmol, 1 equiv) and Et_3N (1.2 mmol, 2 equiv) were dissolved in toluene (5 mL) and premixed at rt for 10 min. Subsequently, 4-bromobenzylamine **19** (1.2 mmol, 2 equiv) was added. The reaction mixture was refluxed overnight (monitored by TLC, 18 h). It was cooled to room temperature, diluted with H_2O (20 mL), and extracted with EtOAc (3 × 20 mL). Organic layers were dried over anhydrous Na_2SO_4 and concentrated in vacuo. The residue was purified by column chromatography using Hex/EtOAc.

*N-(4-Bromobenzyl)benzo[d]oxazol-2-amine (**22**).* Brown solid. Yield: 69% (125 mg). ^{1}H NMR (400 MHz, DMSO-d_6): δ 8.48 (t, J = 6.1 Hz, 1H), 7.56−7.49 (m, 2H), 7.34 (d, J = 8.6 Hz, 3H), 7.24 (dd, J = 7.8, 0.6 Hz, 1H), 7.10 (td, J = 7.6, 1.0 Hz, 1H), 6.98 (td, J = 7.7, 1.2 Hz, 1H), 4.50 (d, J = 6.0 Hz, 2H). ^{13}C NMR (101 MHz, DMSO-d_6): δ 162.29, 148.11, 143.01, 138.54, 131.21, 129.39, 123.61, 120.28, 120.02, 115.58, 108.58, 45.02. HRMS: m/z: calcd for $C_{14}H_{11}BrN_2O$: 303.0128 [M + H]$^+$; found: 303.0126.

Smiles Rearrangement with 2-Chloroacetamide. Benzoxazole-2-thiol **4** (1.61 mmol, 1 equiv), K_2CO_3 (4.8 mmol; 3 equiv), and 2-chloroacetamide **23** (3.2 mmol; 2 equiv) were suspended in DMF (10 mL). The reaction mixture was stirred at 70 °C for 4 h. It was cooled to room temperature, diluted with H_2O (50 mL), and extracted with EtOAc (3 × 50 mL). Organic layers were washed with brine (1×), dried over anhydrous Na_2SO_4, and concentrated in vacuo. The residue was purified by column chromatography using Hex/EtOAc.

*2-(Benzo[d]oxazol-2-ylthio)acetamide (**25**).* Yellow solid. Yield: 46% (152 mg). ^{1}H NMR (400 MHz, DMSO-d_6): δ 7.75 (s, 1H), 7.63 (ddd, J = 7.0, 3.1, 1.2 Hz, 2H), 7.39−7.27 (m, 3H), 4.12 (s, 2H). ^{13}C NMR (101 MHz, DMSO-d_6): δ 168.00, 164.10, 151.28, 141.27, 124.63, 124.25, 118.19, 110.19, 35.82. HRMS: m/z: calcd for $C_9H_8N_2O_2S$: 209.0379 [M + H]$^+$; found: 209.0378.

Smiles Rearrangement with 3-(Bromomethyl)aniline. Benzoxazole-2-thiol **4** (0.6 mmol, 1 equiv), 3-(bromomethyl)-aniline **26** (1.2 mmol, 2 equiv), and K_2CO_3 (1.2 mmol, 2 equiv) were suspended in DMF (5 mL). The reaction mixture was stirred at 70 °C for 2 h. It was cooled to room temperature, diluted with H_2O (20 mL), and extracted with EtOAc (3 × 20 mL). Organic layers were dried over anhydrous Na_2SO_4 and concentrated in vacuo. The residue was purified by column chromatography using Hex/EtOAc.

*3-((Benzo[d]oxazol-2-ylthio)methyl)aniline (**27**).* White solid. Yield: 80% (123 mg). ^{1}H NMR (400 MHz, DMSO-d_6): δ 7.65 (m, 2H), 7.37−7.29 (m, 2H), 6.97 (t, J = 7.7 Hz, 1H), 6.66 (t, J = 1.9 Hz, 1H), 6.59 (d, J = 7.5 Hz, 1H), 6.47 (m, 1H), 5.13 (br s, 2H), 4.47 (s, 2H). ^{13}C NMR (101 MHz, DMSO-d_6): δ 164.04, 151.22, 148.92, 141.28, 136.52, 129.10, 124.60, 124.27, 118.27, 116.19, 114.01, 113.35, 110.18, 36.00. HRMS: m/z: calcd for $C_{14}H_{12}N_2OS$: 257.0743 [M + H]$^+$; found: 257.0742.

Smiles Rearrangement with Amines. To a stirred solution of amine **29** (0.48 mmol, 1 equiv) and Cs_2CO_3 (1.54 mmol, 3.2 equiv) in DMF (3 mL) cooled to −5 °C were added chloroacetyl chloride (0.58 mmol, 1.2 equiv) and benzoxazole-2-thiol **4** (0.48 mmol, 1 equiv). The reaction mixture was refluxed (monitored by TLC, 4−7 h). After that, the cooled (rt) mixture was diluted by H_2O (20 mL), extracted with CH_2Cl_2 (3 × 30 mL), and washed with brine (50 mL). Combined organic layers were dried over Na_2SO_4 and concentrated in vacuo. The residue was purified by column chromatography using Hex/EtOAc and Tol/MeCN.

*N-Benzylbenzo[d]oxazol-2-amine (**30a**).* Yellow solid. Yield: 83% (89 mg). ^{1}H NMR (500 MHz, DMSO-d_6): δ 8.45 (t, J = 6.1 Hz, 1H), 7.41−7.30 (m, 5H), 7.25 (dd, J = 15.1, 7.8 Hz, 2H), 7.10 (td, J = 7.7, 1.0 Hz, 1H), 6.98 (td, J = 7.8, 1.2 Hz, 1H), 4.52 (d, J = 6.2 Hz, 2H). ^{13}C NMR (101 MHz, DMSO-d_6): δ 162.46, 148.13, 143.15, 139.06, 128.39, 127.19, 127.06, 123.64, 120.24, 115.54, 108.60, 45.69. HRMS: m/z: calcd for $C_9H_{12}N_2O_4S$: 225.1022 [M + H]$^+$; found: 225.1023.

*N-Hexylbenzo[d]oxazol-2-amine (**30b**).* Orange solid. Yield: 58% (60 mg). ^{1}H NMR (400 MHz, DMSO-d_6): δ 7.89 (t, J = 5.6 Hz, 1H), 7.31 (d, J = 7.8 Hz, 1H), 7.22 (d, J = 7.6 Hz, 1H), 7.09 (t, J = 7.6 Hz, 1H), 6.95 (td, J = 7.8, 0.9 Hz, 1H), 3.28 (dd, J = 13.0, 6.8 Hz, 2H), 1.62−1.51 (m, 2H), 1.35−1.25 (m, 6H), 0.86 (t, J = 6.7 Hz, 3H). ^{13}C NMR (101 MHz, DMSO-d_6): δ 162.40, 147.99, 143.40, 123.52, 119.94, 115.32, 108.42, 42.29, 30.98, 28.88, 25.96, 22.10, 13.93. HRMS: m/z: calcd for $C_{13}H_{18}N_2O$: 219.1492 [M + H]$^+$; found: 219.1491

*N-Phenylbenzo[d]oxazol-2-amine (**30c**).* Yellow solid. Yield: 76% (76 mg). ^{1}H NMR (400 MHz, DMSO-d_6): δ 10.61 (s, 1H), 7.76 (d, J = 7.8 Hz, 2H), 7.47 (dd, J = 13.3, 7.7 Hz, 2H), 7.37 (t, J = 7.9 Hz, 2H), 7.22 (td, J = 7.7, 0.9 Hz, 1H), 7.13 (td, J = 7.8, 1.2 Hz, 1H), 7.03 (t, J = 7.4 Hz, 1H). ^{13}C NMR (101 MHz, DMSO-d_6): δ 157.97, 146.99, 142.43, 138.73, 129.00, 124.01, 122.12, 121.68, 117.55, 116.62, 108.97. HRMS: m/z: calcd for $C_{13}H_{10}N_2O$: 211.0866 [M + H]$^+$; found: 211.0864

DOI: 10.1021/acsomega.9b02702
ACS Omega 2019, 4, 19314−19323

*N-(4-Nitrophenyl)benzo[d]oxazol-2-amine (**30d**).* Yellow solid. Yield: 74% (90 mg). ^{1}H NMR (400 MHz, DMSO-d_6): δ 11.45 (s, 1H), 8.30 (d, J = 9.1 Hz, 2H), 7.98 (d, J = 8.8 Hz, 2H), 7.60−7.54 (m, 2H), 7.29 (t, J = 7.6 Hz, 1H), 7.22 (t, J = 7.7 Hz, 1H). ^{13}C NMR (101 MHz, DMSO-d_6): δ 156.87, 147.00, 144.93, 141.67, 141.27, 125.37, 124.38, 122.68, 117.30, 117.15, 109.41. HRMS: m/z: calcd for $C_{13}H_9N_3O_3$: 256.0717 [M + H]$^+$; found: 256.0719.

*N-(4-Methoxyphenyl)benzo[d]oxazol-2-amine (**30e**).* Orange solid. Yield: 78% (90 mg). ^{1}H NMR (500 MHz, DMSO-d_6): δ 10.36 (s, 1H), 7.65 (d, J = 9.1 Hz, 2H), 7.45 (d, J = 7.8 Hz, 1H), 7.41 (d, J = 7.1 Hz, 1H), 7.19 (td, J = 7.6, 1.1 Hz, 1H), 7.09 (td, J = 7.7, 1.2 Hz, 1H), 6.96 (d, J = 9.1 Hz, 2H), 3.74 (s, 3H). ^{13}C NMR (101 MHz, DMSO-d_6): δ 158.36, 154.65, 147.08, 142.64, 131.92, 123.91, 121.34, 119.15, 116.34, 114.23, 108.82, 55.25. HRMS: m/z: calcd for $C_{14}H_{12}N_2O_2$: 241.0972 [M + H]$^+$; found: 241.0970.

*N-(4-Bromophenyl)benzo[d]oxazol-2-amine (**30f**).* Yellow solid. Yield: 82% (113 mg). ^{1}H NMR (500 MHz, DMSO-d_6): δ 10.77 (s, 1H), 7.74 (d, J = 8.9 Hz, 2H), 7.55 (d, J = 8.9 Hz, 2H), 7.48 (dd, J = 14.3, 7.7 Hz, 2H), 7.23 (td, J = 7.7, 1.0 Hz, 1H), 7.15 (td, J = 7.8, 1.2 Hz, 1H). ^{13}C NMR (101 MHz, DMSO-d_6): δ 157.63, 146.97, 142.19, 138.14, 131.77, 124.11, 121.94, 119.46, 116.77, 113.58, 109.09. HRMS: m/z: calcd for $C_{13}H_9BrN_2O$: 288.9971 [M + H]$^+$; found: 288.9969.

*N-(3-Bromophenyl)benzo[d]oxazol-2-amine (**30g**).* Yellow solid. Yield: 78% (108 mg). ^{1}H NMR (400 MHz, DMSO-d_6) δ 10.82 (s, 1H), 8.11 (t, J = 1.9 Hz, 1H), 7.67 (dd, J = 8.2, 1.2 Hz, 1H), 7.51 (d, J = 8.9 Hz, 2H), 7.33 (t, J = 8.1 Hz, 1H), 7.23 (m, 2H), 7.16 (td, J = 7.6, 1.1 Hz, 1H). ^{13}C NMR (101 MHz, DMSO-d_6): δ 157.44, 146.94, 142.07, 140.34, 130.97, 124.66, 124.16, 122.08, 121.93, 119.62, 116.94, 116.46, 109.14. HRMS: m/z: calcd for $C_{13}H_9BrN_2O$: 288.9971 [M + H]$^+$; found: 288.9971.

*N-(2-Bromophenyl)benzo[d]oxazol-2-amine (**30h**).* White solid. Yield: 81% (112 mg). ^{1}H NMR (400 MHz, DMSO-d_6): δ 9.87 (s, 1H), 7.93 (s, 1H), 7.70 (d, J = 8.0 Hz, 1H), 7.45 (t, J = 7.2 Hz, 2H), 7.37 (d, J = 7.6 Hz, 1H), 7.25−7.08 (m, 3H). ^{13}C NMR (101 MHz, DMSO-d_6): δ 133.00, 128.48, 126.53, 125.46, 124.07, 121.55, 117.20, 109.10. HRMS: m/z: calcd for $C_{13}H_9BrN_2O$: 288.9971 [M + H]$^+$; found: 288.9969.

*2-(Benzo[d]oxazol-2-ylamino)ethan-1-ol (**30i**).* White solid. Yield: 55% (47 mg). ^{1}H NMR (400 MHz, DMSO-d_6): δ 7.92 (t, J = 5.7 Hz, 1H), 7.32 (d, J = 7.8 Hz, 1H), 7.22 (d, J = 7.4 Hz, 1H), 7.09 (td, J = 7.7, 0.8 Hz, 1H), 6.96 (td, J = 7.7, 1.1 Hz, 1H), 4.80 (t, J = 5.5 Hz, 1H), 3.56 (q, J = 5.9 Hz, 2H), 3.35 (q, J = 5.8 Hz, 2H overlapped with H_2O). ^{13}C NMR (101 MHz, DMSO-d_6): δ 162.49, 148.03, 143.31, 123.56, 120.01, 115.34, 108.47, 59.44, 44.99. HRMS: m/z: calcd for $C_9H_{10}N_2O_2$: 179.0815 [M + H]$^+$; found: 179.0814.

*2-Morpholinobenzo[d]oxazole (**30j**).* White solid. Yield: 31% (30 mg). ^{1}H NMR (400 MHz, DMSO-d_6) δ 7.42−7.40 (m, 1H), 7.33−7.28 (m, 1H), 7.16 (td, J = 7.6, 1.1 Hz, 1H), 7.03 (td, J = 7.7, 1.3 Hz, 1H), 3.76−3.69 (m, 4H), 3.62−3.55 (m, 4H).^{13}C NMR (101 MHz, DMSO-d_6): δ 161.85, 148.30, 142.79, 124.02, 120.69, 115.98, 108.98, 65.41, 45.37. HRMS: m/z: calcd for $C_{11}H_{12}N_2O_2$: 205.0972 [M + H]$^+$; found: 205.0972.

*N-Cyclohexylbenzo[d]oxazol-2-amine (**30l**).* Orange solid. Yield: 33% (34 mg). ^{1}H NMR (400 MHz, DMSO-d_6): δ 7.84 (d, J = 7.7 Hz, 1H), 7.31 (d, J = 7.8 Hz, 1H), 7.22 (d, J = 7.7 Hz, 1H), 7.08 (t, J = 7.6 Hz, 1H), 6.95 (t, J = 7.7 Hz, 1H), 3.54 (brs, 1H), 1.96 (m, 2H), 1.73 (m, 2H), 1.59 (m, 1H), 1.36−1.23 (m, 4H), 1.21−1.10 (m, 1H). ^{13}C NMR (101 MHz, DMSO-d_6): δ 161.65, 147.85, 143.41, 123.50, 119.90, 115.27, 108.37, 51.56, 32.42, 25.20, 24.55. HRMS: m/z: calcd for $C_{13}H_{16}N_2O$: 217.1335 [M + H]$^+$; found: 217.1337.

Substitution with Cyclohexylamine. To a stirred solution of amine **29** (0.48 mmol, 1 equiv) and DBU (1.54 mmol, 3.2 equiv) in MeCN (3 mL) cooled to −5 °C were added chloroacetyl chloride (0.58 mmol, 1.2 equiv) and benzoxazole-2-thiol **4** (0.48 mmol, 1 equiv). The reaction mixture was refluxed (monitored by TLC, 3 h). After that, the cooled (rt) mixture was diluted by H_2O (20 mL), extracted with CH_2Cl_2 (3 × 30 mL), and washed with brine (50 mL). Combined organic layers were dried over Na_2SO_4 and concentrated in vacuo. The residue was purified by column chromatography using Hex/EtOAc.

*2-(Benzo[d]oxazol-2-ylthio)-N-cyclohexylacetamide (**31l**).* White solid. Yield: 62% (86 mg). ^{1}H NMR (400 MHz, DMSO-d_6): δ 8.19 (d, J = 7.7 Hz, 1H), 7.66−7.58 (m, 2H), 7.38−7.29 (m, 2H), 4.11 (s, 2H), 3.62−3.48 (m, 1H), 1.79−1.63 (m, 4H), 1.53 (m, 1H), 1.32−1.11 (m, 5H). ^{13}C NMR (101 MHz, DMSO-d_6): δ 164.96, 163.94, 151.22, 141.24, 124.61, 124.24, 118.14, 110.12, 48.02, 35.83, 32.14, 25.11, 24.31. HRMS: m/z: calcd for $C_{15}H_{18}N_2O_2S$: 291.1162 [M + H]$^+$; found: 291.1161.

■ ASSOCIATED CONTENT

Supporting Information

The Supporting Information is available free of charge on the ACS Publications website at DOI: 10.1021/acsomega.9b02702.

Optimization of the reaction conditions with Lewis acids, 3-bromopropylamine HBr, 2-bromoethylamine HBr, 4-bromobutylamine HBr, 5-bromopentylamine HBr, 4-bromobenzylamine, 2-chloroacetamide, 3-(bromomethyl)aniline, and aniline; copies of ^{1}H and ^{13}C NMR spectra (Tables S1−S9) (PDF)

■ AUTHOR INFORMATION

Corresponding Author

*E-mail: lucie.brulikova@upol.cz.

ORCID

Lucie Brulíková: 0000-0001-8380-073X

Notes

The authors declare no competing financial interest.

■ ACKNOWLEDGMENTS

This work was supported by the Ministry of Education, Youth and Sport of the Czech Republic (project IGA_PrF_2019_027) and by grant no. JG_2019_002 from Palacký University in Olomouc.

■ REFERENCES

(1) Šlachtová, V.; Brulikova, L. Benzoxazole Derivatives as Promising Antitubercular Agents. *ChemistrySelect* **2018**, *3*, 4653−4662.

(2) Cui, M.; Ono, M.; Kimura, H.; Ueda, M.; Nakamoto, Y.; Togashi, K.; Okamoto, Y.; Ihara, M.; Takahashi, R.; Liu, B.; Saji, H. Novel 18F-Labeled Benzoxazole Derivatives as Potential Positron Emission Tomography Probes for Imaging of Cerebral +–Amyloid Plaques in Alzheimer's Disease. *J. Med. Chem.* **2012**, *55*, 9136−9145.

(3) Abdelazeem, A. H.; Khan, S. I.; White, S. W.; Sufka, K. J.; McCurdy, C. R. Design, synthesis and biological evaluation of bivalent benzoxazolone and benzothiazolone ligands as potential anti-inflammatory/analgesic agents. *Bioorg. Med. Chem.* **2015**, *23*, 3248−3259.

(4) Harmange, J. C.; Weiss, M. M.; Germain, J.; Polverino, A. J.; Borg, G.; Bready, J.; Chen, D.; Choquette, D.; Coxon, A.; DeMelfi, T.;

DiPietro, L.; Doerr, N.; Estrada, J.; Flynn, J.; Graceffa, R. F.; Harriman, S. P.; Kaufman, S.; La, D. S.; Long, A.; Martin, M. W.; Neervannan, S.; Patel, V. F.; Potashman, M.; Regal, K.; Roveto, P. M.; Schrag, M. L.; Starnes, C.; Tasker, A.; Teffera, Y.; Wang, L.; White, R. D.; Whittington, D. A.; Zanon, R. Naphthamides as Novel and Potent Vascular Endothelial Growth Factor Receptor Tyrosine Kinase Inhibitors: Design, Synthesis, and Evaluation. *J. Med. Chem.* **2008**, *51*, 1649−1667.

(5) Khajondetchairit, P.; Phuangsawai, O.; Suphakun, P.; Rattanabunyong, S.; Choowongkomon, K.; Gleeson, M. P. Design, synthesis, and evaluation of the anticancer activity of 2-amino-aryl-7-aryl-benzoxazole compounds. *Chem. Biol. Drug Des.* **2017**, *90*, 987−994.

(6) Sweis, R. F.; Hunt, J. A.; Sinclair, P. J.; Chen, Y.; Eveland, S. S.; Guo, Q.; Hyland, S. A.; Milot, D. P.; Cumiskey, A. M.; Latham, M.; Rosa, R.; Peterson, L.; Sparrow, C. P.; Anderson, M. S. 2-(4-Carbonylphenyl)benzoxazole inhibitors of CETP: Attenuation of hERG binding and improved HDLc-raising efficacy. *Bioorg. Med. Chem. Lett.* **2011**, *21*, 2597−2600.

(7) Potashman, M. H.; Bready, J.; Coxon, A.; DeMelfi, T. M., Jr; DiPietro, L.; Doerr, N.; Elbaum, D.; Estrada, J.; Gallant, P.; Germain, J.; Gu, Y.; Harmange, J. C.; Kaufman, S. A.; Kendall, R.; Kim, J. L.; Kumar, G. N.; Long, A. M.; Neervannan, S.; Patel, V. F.; Polverino, A.; Rose, P.; Van der Plas, S.; Whittington, D.; Zanon, R.; Zhao, H. Design, Synthesis, and Evaluation of Orally Active Benzimidazoles and Benzoxazoles as Vascular Endothelial Growth Factor-2 Receptor Tyrosine Kinase Inhibitors. *J. Med. Chem.* **2007**, *50*, 4351−4373.

(8) Chikhale, R.; Thorat, S.; Choudhary, R. K.; Gadewal, N.; Khedekar, P. Design, synthesis and anticancer studies of novel aminobenzazolyl pyrimidines as tyrosine kinase inhibitors. *Bioorg. Chem.* **2018**, *77*, 84−100.

(9) Ko, C. W.; Tao, Y. T.; Danel, A.; Krzeminska, L.; Tomasik, P. Organic Light-Emitting Diodes Based on 2-(Stilbene-4-yl)benzoxazole Derivatives: An Implication on the Emission Mechanism. *Chem. Mater.* **2001**, *13*, 2441−2446.

(10) Grytsai, O.; Druzhenko, T.; Demange, L.; Ronco, C.; Benhida, R. Cyanoguanidine as a versatile, eco-friendly and inexpensive reagent for the synthesis of 2-aminobenzoxazoles and 2-guanidinobenzoxazoles. *Tetrahedron Lett.* **2018**, *59*, 1642−1645.

(11) Nagano, T.; Itoh, M.; Matsumura, K. Preparation of certain derivatives of benzoxazole. *J. Am. Chem. Soc.* **1953**, *75*, 2770−2771.

(12) Wu, Y. Q.; Limburg, D. C.; Wilkinson, D. E.; Hamilton, G. S. Formation of nitrogen-containing heterocycles using di(imidazole-1-yl)methanimine. *J. Heterocycl. Chem.* **2003**, *40*, 191−193.

(13) Kasthuri, M.; Babu, H. S.; Kumar, K. S.; Sudhakar, C.; Kumar, P. V. N. A Facile Synthesis of 2-Aminobenzoxazoles and 2-Aminobenzimidazoles Using N-Cyano-N-phenyl-p-toluenesulfonamide (NCTS) as an Efficient Electrophilic Cyanating Agent. *Synlett* **2015**, *26*, 897−900.

(14) Glotz, G.; Lebl, R.; Dallinger, D.; Kappe, C. O. Integration of Bromine and Cyanogen Bromide Generators for the Continuous-Flow Synthesis of Cyclic Guanidines. *Angew. Chem., Int. Ed.* **2017**, *56*, 13786−13789.

(15) Reddy, L. M.; Prakash, T. B.; Padmaja, A.; Padmavathi, V. Synthesis and antimicrobial activity of pyrazolyl benzoxazoles, benzothiazoles and benzimidazoles. *Med. Chem. Res.* **2015**, *24*, 970−979.

(16) Gudipati, R.; Anreddy, R. N. R.; Manda, S. Synthesis, anticancer and antioxidant activities of some novel N-(benzo[d]oxazol-2-yl)-2-(7- or 5-substituted-2-oxoindolin-3-ylidene) hydrazinecarboxamide derivatives. *J. Enzyme Inhib. Med. Chem.* **2011**, *26*, 813−818.

(17) Kaupp, G.; Schmeyers, J.; Boy, J. Quantitative gas-solid reactions with ClCN and BrCN: synthesis of cyanamides, cyanates, thiocyanates, and their derivatives. *Chem. - Eur. J.* **1998**, *4*, 2467−2474.

(18) Schuart, J.; Mueller, H. K. Reactions with 2-aminobenzoxazoles. 8. 2-Aminooxazole and 2-iminooxazoline. *Pharmazie* **1975**, *30*, 155−157.

(19) Liu, J.; Hoover, J. M. Cobalt-Catalyzed Aerobic Oxidative Cyclization of 2-Aminophenols with Isonitriles: 2-Aminophenol Enabled O2 Activation by Cobalt(II). *Org. Lett.* **2019**, *21*, 4510−4514.

(20) Lee, S.; Lee, Y. Copper-Catalyzed Electrophilic Amination of Benzoxazoles via Magnesation. *Eur. J. Org. Chem.* **2019**, *2019*, 3045−3050.

(21) Wu, Y. Q.; Limburg, D. C.; Wilkinson, D. E.; Hamilton, G. S. Formation of nitrogen-containing heterocycles using di(imidazole-1-yl)methanimine. *J. Heterocycl. Chem.* **2003**, *40*, 191−193.

(22) Kim, J. Y.; Cho, S. H.; Joseph, J.; Chang, S. Cobalt- and Manganese-Catalyzed Direct Amination of Azoles under Mild Reaction Conditions and the Mechanistic Details. *Angew. Chem., Int. Ed.* **2010**, *49*, 9899−9903.

(23) Cho, S. H.; Kim, J. Y.; Lee, S. Y.; Chang, S. Silver-mediated direct amination of benzoxazoles: tuning the amino group source from formamides to parent amines. *Angew. Chem., Int. Ed.* **2009**, *48*, 9127−9130.

(24) Wang, J.; Hou, J. T.; Wen, J.; Zhang, J.; Yu, X. Q. Iron-catalyzed direct amination of azoles using formamides or amines as nitrogen sources in air. *Chem. Commun.* **2011**, *47*, 3652−3654.

(25) Cioffi, C. L.; Lansing, J. J.; Yuksel, H. Synthesis of 2-Aminobenzoxazoles Using Tetramethyl Orthocarbonate or 1,1-Dichlorodiphenoxymethane. *J. Org. Chem.* **2010**, *75*, 7942−7945.

(26) Liu, B.; Yin, M.; Gao, H.; Wu, W.; Jiang, H. Synthesis of 2-Aminobenzoxazoles and 3-Aminobenzoxazines via Palladium-Catalyzed Aerobic Oxidation of o-Aminophenols with Isocyanides. *J. Org. Chem.* **2013**, *78*, 3009−3020.

(27) Liu, M.; Zeng, M. T.; Xu, W.; Wu, L.; Dong, Z. B. Selective synthesis of 2-aminobenzoxazoles and 2-mercaptobenzoxazoles by using o-aminophenols as starting material. *Tetrahedron Lett.* **2017**, *58*, 4352−4356.

(28) Rattanangkool, E.; Sukwattanasinitt, M.; Wacharasindhu, S. Organocatalytic Visible Light Enabled SNAr of Heterocyclic Thiols: A Metal-Free Approach to 2-Aminobenzoxazoles and 4-Aminoquinazolines. *J. Org. Chem.* **2017**, *82*, 13256−13262.

(29) Tankam, T.; Srisa, J.; Sukwattanasinitt, M.; Wacharasindhu, S. Microwave-Enhanced On-Water Amination of 2-Mercaptobenzoxazoles To Prepare 2-Aminobenzoxazoles. *J. Org. Chem.* **2018**, *83*, 11936−11943.

(30) Wang, G.; Peng, Z.; Wang, J.; Li, J.; Li, X. Synthesis, biological evaluation and molecular docking study of N-arylbenzo[d]oxazol-2-amines as potential +-glucosidase inhibitors. *Bioorg. Med. Chem.* **2016**, *24*, 5374−5379.

(31) Zhang, X.; Jia, X.; Wang, J.; Fan, X. An economically and environmentally sustainable synthesis of 2-aminobenzothiazoles and 2-aminobenzoxazoles promoted by water. *Green Chem.* **2011**, *13*, 413−418.

(32) Zhou, Y.; Liu, Z.; Yuan, T.; Huang, J.; Liu, C. The synthesis of 2-aminobenzoxazoles using reusable ionic liquid as a green catalyst under mild conditions. *Molecules* **2017**, *22*, 576/1−576/9.

(33) Mo, S. N-Cyano-N-phenyl-p-toluenesulfonamide. *Synlett* **2014**, *25*, 1337−1338.

(34) Yang, Y.; Zhang, Y.; Wang, J. B. Lewis Acid Catalyzed Direct Cyanation of Indoles and Pyrroles with N-Cyano-N-phenyl-p-toluenesulfonamide (NCTS). *Org. Lett.* **2011**, *13*, 5608−5611.

(35) Nagata, T.; Matsubara, H.; Kiyokawa, K.; Minakata, S. Catalytic Activation of 1-Cyano-3,3-dimethyl-3-(1H)-1,2-benziodoxole with B(C6F5)3 Enabling the Electrophilic Cyanation of Silyl Enol Ethers. *Org. Lett.* **2017**, *19*, 4672−4675.

(36) Holden, C. M.; Greaney, M. F. Modern Aspects of the Smiles Rearrangement. *Chem. - Eur. J.* **2017**, *23*, 8992−9008.

(37) Wang, G.; Wang, J.; Li, L.; Chen, S.; Peng, Y.; Xie, Z.; Chen, M.; Deng, B.; Li, W. Synthesis of N-aryl-2-aminobenzoxazoles from substituted benzoxazole-2-thiol and 2-chloro-N-arylacetamides in KOH-DMF system. *Heterocycles* **2017**, *94*, 1257−1268.

(38) Minin, P. L.; Walton, J. C. Radical Ring Closures of 4-Isocyanato Carbon-Centered Radicals. *J. Org. Chem.* **2003**, *68*, 2960−2963.

(39) Tian, X.; Wu, R. M.; Liu, G.; Li, Z. B.; Wei, H. L.; Yang, H.; Shin, D. S.; Wang, L. Y.; Zuo, H. Smiles rearrangement for the synthesis of diarylamines. *ARKIVOC* **2011**, 118−126.

DOI: 10.1021/acsomega.9b02702
ACS Omega 2019, 4, 19314−19323

Appendix 6

Solid phase synthesis of new thiazolidinedione-pyrimidine conjugates and their antibacterial properties

Šlachtová, V.; Janovská, L.; **Brulíková, L.***

J. Mol. Struct. **2019**, *1183*, 182-189.

Journal of Molecular Structure 1183 (2019) 182–189

Contents lists available at ScienceDirect

Journal of Molecular Structure

journal homepage: http://www.elsevier.com/locate/molstruc

Solid phase synthesis of new thiazolidinedione-pyrimidine conjugates and their antibacterial properties

Veronika Šlachtová [a], Lucie Janovská [b, c], Lucie Brulíková [d, *]

[a] Department of Organic Chemistry, Faculty of Science, Palacký University, 17. Listopadu 12, Olomouc, 77146, Czech Republic
[b] Department of Chemical Biology and Genetics, Centre of the Region Haná for Biotechnological and Agricultural Research, Faculty of Science, Palacký University, Šlechtitelů 27, Olomouc, 783 71, Czech Republic
[c] Department of Microbiology, Faculty of Medicine and Dentistry, Palacký University, Hněvotínská 3, Olomouc, 775 15, Czech Republic
[d] Department of Medicinal Chemistry, Institute of Molecular and Translational Medicine, Hněvotínská 5, Olomouc, 77900, Czech Republic

ARTICLE INFO

Article history:
Received 18 December 2018
Received in revised form
23 January 2019
Accepted 24 January 2019
Available online 29 January 2019

Keywords:
Solid-phase synthesis
Pyrimidine
Thiazolidinedione
Conjugates
Antimycobacterial
Antibacterial

ABSTRACT

The polymer-supported synthetic protocol for preparation of thiazolidinedione-pyrimidine hybrids was developed and applied for rapid and effective synthesis of a library of variously substituted conjugates. Reported synthetic methodology is based on easy accessible building blocks and very simple chemical operations enabling effective development of potent experimental therapeutics of this type *via* a combinatorial manner. Synthesized model compounds were tested for their antitubercular activity against *Mycobacterium tuberculosis* H37Rv, antimicrobial activity against several Gram-positive and Gram-negative strains such as *Staphylococcus aureus*, *Pseudomonas aeruginosa*, *Escherichia coli* and *Enterococcus faecalis and two fungal strains* (*Candida albicans and Aspergillus niger*). Slight activity was found for some of them.

1. Introduction

The thiazolidine-2,4-diones (glitazones) are well-known pharmacophores introduced in the late 1990's for the treatment of type 2 diabetes mellitus [1]. Thiazolidinediones are found to exhibit a broad spectrum of biological activities [2] that can be antidiabetic [2,3], antimicrobial [2,4–15], *anti*-HIV [11,16] or anti-inflammatory [17–20]. Several thiazolidinediones have been synthesized and screened for their antitubercular activity against *M. tuberculosis* H37Rv that showed promising results indicating the potential of this scaffold in the development of novel *anti*-TB agents [2,3,10–15,21–24]. For example, several hybrid arylidene thiazolidinediones synthesized by Kumar et al. in 2014 [23] exhibited moderate to good activity with MIC value < 50 μM. To date, the best result in this field has been described by Khan et al. [25] Screening of 700 compounds, known to be active against the whole cell of *M. tuberculosis* led to the selection of one thiazolidinedione showing excellent *anti*-TB activity with MIC value 1.4 μM. Subsequently, they validated mycobacterial ATP synthase as the target for the selected thiazolidinedione.

Pyrimidine pharmacophore plays an important role in several biological active substances and was found to possess a range of diverse biological activities such as anticancer [26], anti-inflammatory [27], anti-hepatitis [28], anti-diabetic [29] and many others. Moreover, variously modified pyrimidines were successfully studied as antibacterial agents [30–39].

Since the combination of two pharmacophores is a well-established approach for designing more potent drugs with a significant increase in biological activity [40,41], we decided to combine two known pharmacophores - thiazolidinedione scaffold and 5-nitropyrimidine (Fig. 1) primarily as novel potent antitubercular agents.

Herein, we introduce the solid-phase synthesis protocol for the preparation of thiazolidinediones conjugated with 5-nitropyrimidine that does not require isolation/purification of intermediates and uses relatively inexpensive starting materials. Our methodology is based on easy access to structural diversity from abundant and easily available building blocks with minimal synthetic operations. Very few papers have described the solid-phase synthetic approach using Merrifield resin for the construction of

* Corresponding author.
E-mail address: lucie.brulikova@upol.cz (L. Brulíková).

https://doi.org/10.1016/j.molstruc.2019.01.073
0022-2860/

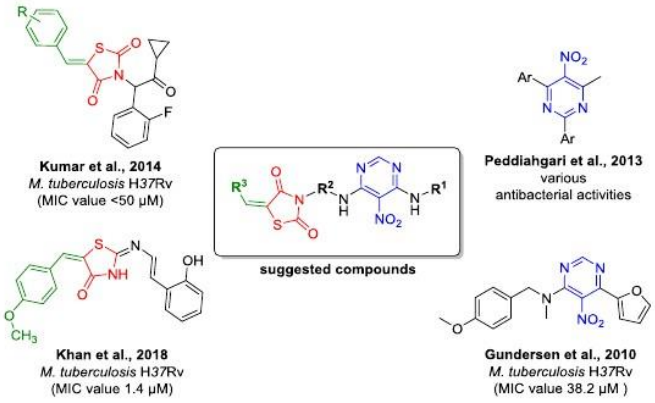

Fig. 1. Design of novel thiazolidinediones.

novel thiazolidinediones [42–44]. To the best of our knowledge, none of the reported solid-phase synthetic approaches have been used for rapid and effective preparation of the chemical library of thiazolidinediones-pyrimidine conjugates.

2. Materials and methods

Solvents, chemicals and the polystyrene resins were purchased from Sigma-Aldrich (St. Louis, Missouri, USA). Synthesis was carried out on Domino Blocks in disposable polypropylene reaction vessels (Torviq, Niles, MI).

All reactions were carried out at ambient temperature (21 °C) unless stated otherwise. The volume of wash solvent was 10 mL per 1 g of resin. For washing, resin slurry was shaken with the fresh solvent for 1 min before changing the solvent. After adding the individual reagents, the resin slurry was shaken vigorously to break any potential resin clumps. Resin-bound intermediates were dried by a stream of nitrogen for prolonged storage and/or quantitative analysis.

For LC-MS analysis, a sample of the resin (~5 mg) was treated with trifluoracetic acid (TFA) in dichloromethane (DCM), the cleavage cocktail was evaporated by a stream of nitrogen, and cleaved compounds extracted into 1 mL of MeOH. The LC-MS analyses were carried out on UHPLC-MS system consisting of UHPLC chromatograph Accela with photodiode array detector and triple quadrupole mass spectrometer TSQ Quantum Access (Thermo Scientific, CA, USA), using Nucleodur Gravity C18 column (dimensions 1.8 μm, 2.1 × 50 mm) at 30 °C and flow rate of 800 μL/min (Macherey-Nagel, Germany). Mobile phase was (A) 0.1% ammonium acetate in water, and (B) 0.1% ammonium acetate in acetonitrile, linearly programmed from 10% to 80% B over 2.5 min, kept for 1.5 min. The column was re-equilibrated with 10% of solution B for 1 min. The APCI source operated at a discharge current of 5 μA, vaporizer temperature of 400 °C and a capillary temperature of 200 °C.

Purification was carried out on C18 column 19 × 100 mm for 5 μm particles; gradient was formed from 10 mM aqueous ammonium acetate and acetonitrile with a flow rate 15 mL/min. For lyophilization of residual solvents at −110 °C the ScanVac Coolsafe 110–4 was used.

NMR $^{1}H/^{13}C$ spectra were recorded on JEOL ECX500 spectrometer at magnetic field strengths of 11.75 T (with operating frequencies 500.16 MHz for 1H and 125.77 MHz for 13C). Chemical shifts (δ) are reported in parts per million (ppm), and coupling constants (J) are reported in Hertz (Hz). NMR spectra were recorded at ambient temperature (21 °C) in DMSO-d_6, or CD_3OD solutions and referenced to the resonance signal of the solvent. Acetate salts exhibited singlet at 1.7–1.9 ppm in the ^{1}H NMR spectrum and two resonances at 173 and 23 ppm in ^{13}C spectrum. In some cases, residual signal for DMF appeared at 2.54 ppm; 1 carbon from diamine linker is overlapped with DMSO.

HRMS analysis was performed with LC-MS and an Orbitrap high-resolution mass spectrometer (Dionex Ultimate 3000, Thermo Exactive plus, MA, USA) operating in positive full scan mode in the range of 80–1200 m/z. The settings for electrospray ionization were as follows: 150 °C oven temperature and 3.6 kV source voltage. The acquired data were internally calibrated with phthalate as a contaminant in methanol (m/z 297.15909). Samples were diluted to a final concentration of 0.1 mg/mL in a solution of water and acetonitrile (50:50, v/v). The samples were injected into the mass spectrometer following HPLC separation on a Kinetex C18 column (2.6 μm, 100 A, 50 × 3.0 mm) using an isocratic mobile phase of 0.01 M MeCN/ammonium acetate (80/20) at a flow rate of 0.3 mL/min.

2.1. General synthetic methods

2.1.1. Synthesis of resins 1

Wang resin (loading 1.0 mmol/g, ~1 g) was washed three times with DCM. A solution consisting of Fmoc-amino acid (2 mmol), HOBt (2 mmol), DMAP (0.5 mmol) and DIC (2 mmol) in DMF/DCM (1:1, v/v, 10 mL) was added to the resin. The resin slurry was shaken at rt for 16 h. The resin was washed three times with DMF and three times with DCM.

2.1.2. Reaction with 4,6-dichloro-5-nitropyrimidines (resins 2)

Firstly, Fmoc protecting group of resins **1** (~1 g) was removed by exposure to 50% piperidine in DMF (v/v 10 mL) for 15 min, and then, the resin was washed three times with DMF and three times with DCM. Further, resins were washed three times with dry DMF and reacted with a solution consisting of 4,6-dichloro-5-nitropyrimidine (5 mmol) and DIEA (5 mmol) in dry DMF (10 mL) at rt for 2 h. The resin was washed five times with DMF and three times with DCM.

2.1.3. Reaction with amino alcohols (resins 3)

Resins **2** (~500 mg) were each washed three times with dry DMF and reacted with a solution consisting of amino alcohol (2.5 mmol) and DIEA (2.5 mmol) in dry DMF (5 mL) at rt for 2 h. The resin was washed three times with DMF and three times with DCM.

2.1.4. Fukuyama-Mitsunobu reaction with thiazolidinedione (resins 4)

Resins **3** (~500 mg) were each washed three times with anhydrous THF. A solution consisting of thiazolidine-2,4-dione (1.25 mmol) and PPh_3 (1.25 mmol) in anhydrous THF (5 mL) was added. The resin was stored in a freezer for 30 min followed by reaction with DIAD (1.25 mmol) at rt for 1 h. The resin was washed three times with THF and five times with DCM.

2.1.5. Knoevenagel condensation with aldehydes (resins 5)

Resins **4** (~250 mg) were each washed three times with DMF and reacted with a solution consisting of aldehyde (0.62 mmol) and piperidine (0.25 mmol) in DMF (2.5 mL) at 70 °C for 20 h. The resin was washed three times with DMF and three times with DCM.

2.1.6. Cleavage from resin with TFA (compounds 6 and 7)

Resins **4** and **5** (~250 mg) were each treated with 2 mL of a solution consisting of TFA/DCM (1:1, *v/v*) for 1 h. The cleavage cocktail was collected, and the resin was washed three times with 50% TFA in DCM. The combined extracts were evaporated by a stream of nitrogen, and the crude products were purified by reversed-phase HPLC.

2.2. Analytical data of individual compounds

2.2.1. (6-((2-(2,4-Dioxothiazolidin-3-yl)ethyl)amino)-5-nitropyrimidin-4-yl)valine 6a

Orange solid. Yield: 27%. ^{1}H NMR (500 MHz, DMSO-d_6): δ 9.64 (d, J = 7.7 Hz, 1H), 9.52 (t, J = 4.9 Hz, 1H), 8.06 (s, 1H), 4.63 (dd, J = 7.8, 4.3 Hz, 1H), 4.08 (s, 2H), 3.75 (s, 4H), 2.28–2.22 (m, 1H), 0.97 (d, J = 6.9 Hz, 3H), 0.90 (d, J = 6.9 Hz, 3H). ^{13}C NMR (126 MHz, DMSO-d_6): δ 172.44, 172.01, 159.23, 157.11, 156.14, 112.10, 59.45, 40.73, 38.80, 33.77, 30.52, 18.75, 18.16. HRMS: *m/z*: calcd for $C_{14}H_{18}N_6O_6S$: 399.1081 $[M+H]^+$; found: 399.1085.

2.2.2. (6-((3-(2,4-Dioxothiazolidin-3-yl)propyl)amino)-5-nitropyrimidin-4-yl)valine 6b

Orange solid. Yield: 58%. ^{1}H NMR (500 MHz, DMSO-d_6): δ 9.97 (d, J = 7.6 Hz, 1H), 9.51 (t, J = 6.0 Hz, 1H), 8.01 (s, 1H), 4.40 (dd, J = 7.6, 3.8 Hz, 1H), 4.17 (s, 2H), 3.57–3.50 (m, 4H), 2.19 (qd, J = 10.8, 6.8 Hz, 1H), 1.81 (p, J = 6.8 Hz, 2H), 0.95 (d, J = 6.9 Hz, 3H), 0.83 (d, J = 6.9 Hz, 3H). ^{13}C NMR (126 MHz, DMSO-d_6): δ 172.58, 172.23, 159.40, 156.63, 156.44, 112.29, 59.03, 38.26, 30.33, 26.82, 18.71, 18.00. HRMS: *m/z*: calcd for $C_{15}H_{20}N_6O_6S$: 413.1238 $[M+H]^+$; found: 413.1241.

2.2.3. (6-((2-(2,4-Dioxothiazolidin-3-yl)ethyl)amino)-5-nitropyrimidin-4-yl)phenylalanine 6c

Orange solid. Yield: 51%. ^{1}H NMR (500 MHz, DMSO-d_6): δ 9.59 (d, J = 6.7 Hz, 1H), 9.47 (t, J = 5.1 Hz, 1H), 8.07 (s, 1H), 7.21 (t, J = 7.2 Hz, 2H), 7.15 (t, J = 7.2 Hz, 1H), 7.10 (d, J = 6.9 Hz, 2H), 4.75 (dd, J = 11.9, 5.5 Hz, 1H), 4.07 (s, 2H), 3.75 (s, 4H), 3.28 (dd, J = 13.5, 5.4 Hz, 1H), 3.18 (dd, J = 13.5, 5.4 Hz, 1H). ^{13}C NMR (126 MHz, DMSO-d_6): δ 172.42, 172.08, 171.88, 159.15, 157.15, 155.42, 137.49, 129.41, 127.96, 126.23, 111.93, 56.28, 40.78, 38.71, 36.86, 33.77. HRMS: *m/z*: calcd for $C_{18}H_{18}N_6O_6S$: 447.1081 $[M+H]^+$; found: 447.1085.

2.2.4. (6-((3-(2,4-Dioxothiazolidin-3-yl)propyl)amino)-5-nitropyrimidin-4-yl)phenyl-alanine 6d

Brown solid. Yield: 74%. ^{1}H NMR (500 MHz, DMSO-d_6): δ 9.48 (dd, J = 14.1, 6.6 Hz, 2H), 8.08 (s, 1H), 7.24 (t, J = 7.2 Hz, 2H), 7.17 (dd, J = 17.5, 7.1 Hz, 3H), 4.91 (dd, J = 12.3, 6.0 Hz, 1H), 4.17 (s, 2H), 3.53 (dt, J = 11.1, 6.7 Hz, 4H), 3.27 (dd, J = 13.7, 5.2 Hz, 1H), 3.19 (dd, J = 13.7, 6.2 Hz, 1H), 1.81 (p, J = 6.8 Hz, 2H). ^{13}C NMR (126 MHz, DMSO-d_6): δ 172.57, 172.22, 171.94, 159.32, 156.60, 155.81, 136.99, 129.33, 128.14, 126.49, 112.12, 55.67, 38.84, 38.25, 36.73, 33.96, 26.82. HRMS: *m/z*: calcd for $C_{19}H_{20}N_6O_6S$: 461.1238 $[M+H]^+$; found: 461.1239.

2.2.5. (6-((2-(2,4-Dioxothiazolidin-3-yl)ethyl)amino)-5-nitropyrimidin-4-yl)proline 6e

Yellow solid. Yield: 50%. ^{1}H NMR (500 MHz, DMSO-d_6): δ 8.38 (t, J = 5.6 Hz, 1H), 7.98 (s, 1H), 4.56 (s, 1H), 4.06 (s, 2H), 3.71 (s, 4H), 3.07 (d, J = 59.0 Hz, 2H), 2.26–2.18 (m, 1H), 2.01–1.93 (m, 1H), 1.88–1.79 (m, 2H). ^{13}C NMR (126 MHz, DMSO-d_6): δ 172.95, 172.37, 172.06, 156.59, 156.03, 154.42, 113.78, 62.90, 49.97, 40.95, 38.63, 33.75, 24.46, 21.25. HRMS: *m/z*: calcd for $C_{14}H_{16}N_6O_6S$: 397.0925 $[M+H]^+$; found: 397.0928.

2.2.6. (6-((3-(2,4-Dioxothiazolidin-3-yl)propyl)amino)-5-nitropyrimidin-4-yl)proline 6f

Yellow solid. Yield: 84%. ^{1}H NMR (500 MHz, DMSO-d_6): δ 8.40 (t, J = 6.0 Hz, 1H), 7.98 (s, 1H), 4.57 (s, 1H), 4.18 (s, 2H), 3.53 (t, J = 6.8 Hz, 2H), 3.46 (dt, J = 9.3, 6.8 Hz, 2H), 3.15 (s, 1H), 3.03 (s, 1H), 2.28–2.18 (m, 1H), 2.02–1.92 (m, 1H), 1.91–1.83 (m, 2H), 1.82–1.75 (m, 2H). ^{13}C NMR (126 MHz, DMSO-d_6): δ 172.91, 172.56, 172.21, 156.80, 155.78, 154.65, 113.62, 62.96, 50.17, 38.90, 38.20, 33.95, 27.05. HRMS: *m/z*: calcd for $C_{15}H_{18}N_6O_6S$: 411.1081 $[M+H]^+$; found: 411.1084.

2.2.7. (Z)-(6-((2-(2,4-dioxo-5-(4-(trifluoromethyl)benzylidene) thiazolidin-3-yl)ethyl)amino)-5-nitropyrimidin-4-yl)valine 7a

Brown solid. Yield: 36%. ^{1}H NMR (500 MHz, DMSO-d_6): δ 9.66 (d, J = 7.8 Hz, 1H), 9.60 (t, J = 6.1 Hz, 1H), 7.98 (s, 1H), 7.95 (s, 1H), 7.88 (d, J = 8.4 Hz, 2H), 7.81 (d, J = 8.3 Hz, 2H), 4.57 (dd, J = 7.8, 4.2 Hz, 1H), 3.94 (ddd, J = 13.7, 6.4, 3.3 Hz, 2H), 3.87–3.78 (m, 2H), 2.22–2.15 (m, 1H), 0.91 (d, J = 6.9 Hz, 3H), 0.84 (d, J = 6.9 Hz, 3H). ^{13}C NMR (126 MHz, DMSO-d_6): δ 171.98, 167.15, 165.60, 159.12, 157.16, 156.02, 136.97, 130.53, 130.48, 129.86 (q, J = 28.75 Hz), 126.11, 126.09, 124.56, 123.81 (q, J = 271.25 Hz), 112.05, 59.52, 41.27, 30.58, 18.68, 18.14. HRMS: *m/z*: calcd for $C_{22}H_{21}F_3N_6O_6S$: 555.1268 $[M+H]^+$; found: 555.1272.

2.2.8. (Z)-(6-((2-(5-(4-fluorobenzylidene)-2,4-dioxothiazolidin-3-yl)ethyl)amino)-5-nitropyrimidin-4-yl)valine 7b

Brown solid. Yield: 42%. ^{1}H NMR (500 MHz, DMSO-d_6): δ 9.60 (t, J = 7.7 Hz, 2H), 7.99 (s, 1H), 7.88 (s, 1H), 7.67 (dd, J = 8.8, 5.4 Hz, 2H), 7.38 (t, J = 8.8 Hz, 2H), 4.62 (dd, J = 7.8, 4.3 Hz, 1H), 3.92 (ddd, J = 13.3, 6.4, 3.2 Hz, 2H), 3.83 (ddd, J = 16.4, 8.4, 4.7 Hz, 2H), 2.23–2.16 (m, 1H), 0.92 (d, J = 6.9 Hz, 3H), 0.85 (d, J = 6.9 Hz, 3H). ^{13}C NMR (126 MHz, DMSO-d_6): δ 171.98, 167.39, 165.79, 163.90, 161.91, 159.12), 157.12, 156.16, 132.53, 131.35, 129.69, 121.23, 116.60, 116.42, 112.11, 59.25, 41.14, 30.51, 18.68, 18.05. HRMS: *m/z*: calcd for $C_{21}H_{21}FN_6O_6S$: 505.1300 $[M+H]^+$; found: 505.1302.

2.2.9. (Z)-(6-((2-(5-benzylidene-2,4-dioxothiazolidin-3-yl)ethyl) amino)-5-nitropyrimidin-4-yl)valine 7c

White solid. Yield: 49%. ^{1}H NMR (500 MHz, DMSO-d_6): δ 9.60 (t, J = 7.5 Hz, 2H), 7.99 (s, 1H), 7.87 (s, 1H), 7.60 (d, J = 7.2 Hz, 2H), 7.53 (t, J = 7.4 Hz, 2H), 7.49 (t, J = 7.2 Hz, 1H), 4.63 (dd, J = 7.8, 4.3 Hz, 1H), 3.95–3.90 (m, 1H), 3.83 (ddd, J = 15.9, 8.3, 4.7 Hz, 2H), 2.24–2.17 (m, 1H), 0.93 (d, J = 6.9 Hz, 3H), 0.86 (d, J = 6.9 Hz, 3H). ^{13}C NMR

(126 MHz, DMSO-d_6): δ 171.94, 167.51, 165.83, 159.12, 157.11, 156.20, 133.00, 132.42, 130.50, 130.01, 129.33, 121.52, 112.13, 59.16, 41.10, 30.47, 18.67, 18.04. HRMS: *m/z*: calcd for $C_{21}H_{22}N_6O_6S$: 487.1394 $[M+H]^+$; found: 487.1399.

2.2.10. (Z)-(6-((2-(5-(4-methoxybenzylidene)-2,4-dioxothiazolidin-3-yl)ethyl)amino)-5-nitropyrimidin-4-yl)valine 7d

White solid. Yield: 39%. ^{1}H NMR (500 MHz, DMSO-d_6): δ 9.59 (dd, *J* = 10.7, 5.0 Hz, 2H), 7.99 (s, 1H), 7.82 (s, 1H), 7.56 (d, *J* = 8.8 Hz, 2H), 7.10 (d, *J* = 8.9 Hz, 2H), 4.64 (dd, *J* = 7.8, 4.3 Hz, 1H), 3.94–3.88 (m, 2H), 3.88–3.79 (m, 5H), 2.24–2.18 (m, 1H), 0.93 (d, *J* = 6.9 Hz, 3H), 0.87 (d, *J* = 6.9 Hz, 3H). ^{13}C NMR (126 MHz, DMSO-d_6): δ 171.98, 167.59, 165.95, 161.07, 159.11, 157.10, 156.23, 132.46, 132.13, 125.48, 118.24, 114.94, 112.15, 59.11, 55.48, 41.00, 30.47, 18.67, 18.02. HRMS: *m/z*: calcd for $C_{22}H_{24}N_6O_7S$: 517.1500 $[M+H]^+$; found: 517.1500.

2.2.11. (Z)-(6-((2-(2,4-dioxo-5-(pyridin-4-ylmethylene)thiazolidin-3-yl)ethyl)amino)-5-nitropyrimidin-4-yl)valine 7e

Orange solid. Yield: 39%. ^{1}H NMR (500 MHz, DMSO-d_6): δ 9.60 (dd, *J* = 12.3, 6.9 Hz, 2H), 8.72 (d, *J* = 6.1 Hz, 2H), 7.99 (s, 1H), 7.84 (s, 1H), 7.53 (d, *J* = 6.1 Hz, 2H), 4.61 (dd, *J* = 7.8, 4.3 Hz, 1H), 3.99–3.90 (m, 2H), 3.87–3.77 (m, 2H), 2.25–2.17 (m, 1H), 0.92 (d, *J* = 6.9 Hz, 3H), 0.85 (d, *J* = 6.9 Hz, 3H). ^{13}C NMR (126 MHz, DMSO-d_6): δ 172.05, 166.94, 165.47, 159.15, 157.13, 156.15, 150.63, 140.04, 129.42, 126.62, 123.32, 112.11, 59.32, 41.31, 30.54, 18.71, 18.07. HRMS: *m/z*: calcd for $C_{20}H_{21}N_7O_6S$: 488.1347 $[M+H]^+$; found: 488.1350.

2.2.12. (6-((2-((Z)-2,4-dioxo-5-((E)-3-phenylallylidene)thiazolidin-3-yl)ethyl)amino)-5-nitropyrimidin-4-yl)valine 7f

Yellow solid. Yield: 31%. ^{1}H NMR (500 MHz, DMSO-d_6): δ 9.59 (t, *J* = 7.0 Hz, 2H), 8.01 (s, 1H), 7.66 (d, *J* = 7.0 Hz, 2H), 7.56 (d, *J* = 11.2 Hz, 1H), 7.45–7.36 (m, 3H), 7.30 (d, *J* = 15.2 Hz, 1H), 6.96 (dd, *J* = 15.2, 11.4 Hz, 1H), 4.66 (dd, *J* = 7.8, 4.3 Hz, 1H), 3.91–3.86 (m, 2H), 3.85–3.76 (m, 2H), 2.26–2.20 (m, 1H), 0.94 (d, *J* = 6.8 Hz, 3H), 0.89 (d, *J* = 6.8 Hz, 3H). ^{13}C NMR (126 MHz, DMSO-d_6): δ 171.97, 167.33, 165.31, 159.13, 157.09, 156.27, 143.82, 135.53, 132.81, 129.76, 128.90, 127.84, 123.20, 122.70, 112.16, 59.08, 40.93, 30.45, 18.69, 18.02. HRMS: *m/z*: calcd for $C_{23}H_{24}N_6O_6S$: 513.1551 $[M+H]^+$; found: 513.1555.

2.2.13. (Z)-(6-((2-(2,4-dioxo-5-pentylidenethiazolidin-3-yl)ethyl)amino)-5-nitropyrimidin-4-yl)valine 7g

White solid. Yield: 29%. ^{1}H NMR (500 MHz, DMSO-d_6): δ 9.57 (t, *J* = 5.9 Hz, 1H), 9.51 (d, *J* = 7.8 Hz, 1H), 7.99 (s, 1H), 6.96 (t, *J* = 7.7 Hz, 1H), 4.72 (dd, *J* = 7.8, 4.4 Hz, 1H), 3.85 (d, *J* = 5.0 Hz, 2H), 3.82–3.76 (m, 2H), 2.29–2.24 (m, 1H), 2.17 (q, *J* = 7.4 Hz, 2H), 1.49–1.42 (m, 2H), 1.30 (dt, *J* = 14.7, 7.3 Hz, 2H), 0.97 (d, *J* = 6.9 Hz, 3H), 0.93 (d, *J* = 6.8 Hz, 3H), 0.87 (t, *J* = 7.3 Hz, 3H). ^{13}C NMR (126 MHz, DMSO-d_6): δ 171.97, 167.36, 164.53, 159.11, 157.04, 156.44, 138.03, 124.77, 112.18, 58.76, 40.87, 30.82, 30.35, 29.31, 21.71, 18.68, 17.91, 13.56. HRMS: *m/z*: calcd for $C_{19}H_{26}N_6O_6S$: 467.1707 $[M+H]^+$; found: 467.1706.

2.2.14. (Z)-(6-((3-(2,4-Dioxo-5-(4-(trifluoromethyl)benzylidene) thiazolidin-3-yl)propyl)amino)-5-nitropyrimidin-4-yl)valine 7h

Yellow solid. Yield: 55%. ^{1}H NMR (500 MHz, DMSO-d_6): δ 9.85 (d, *J* = 7.7 Hz, 1H), 9.54 (t, *J* = 6.0 Hz, 1H), 8.00 (d, *J* = 9.7 Hz, 2H), 7.89 (d, *J* = 8.4 Hz, 2H), 7.83 (d, *J* = 8.4 Hz, 2H), 4.49 (dd, *J* = 7.7, 4.0 Hz, 1H), 3.72 (t, *J* = 6.7 Hz, 2H), 3.58 (dt, *J* = 16.2, 6.8 Hz, 2H), 2.23–2.17 (m, 1H), 1.93 (t, *J* = 6.8 Hz, 2H), 0.94 (d, *J* = 6.9 Hz, 3H), 0.84 (d, *J* = 6.9 Hz, 3H). ^{13}C NMR (126 MHz, DMSO-d_6): δ 172.06, 167.20, 165.63, 159.36, 156.85, 155.75, 136.97, 130.88, 130.54, 129.81 (q, *J* = 32.50 Hz), 126.13, 126.10, 124.49, 123.81 (q, *J* = 271.25 Hz), 112.02, 60.38, 38.25, 30.80, 26.78, 18.77, 18.50. HRMS: *m/z*: calcd for $C_{23}H_{23}F_3N_6O_6S$: 569.1425 $[M+H]^+$; found: 569.1440.

2.2.15. (Z)-(6-((3-(5-(4-Fluorobenzylidene)-2,4-dioxothiazolidin-3-yl)propyl)amino)-5-nitropyrimidin-4-yl)valine 7i

Yellow solid. Yield: 55%. ^{1}H NMR (500 MHz, DMSO-d_6): δ 9.90 (d, *J* = 7.7 Hz, 1H), 9.54 (t, *J* = 6.0 Hz, 1H), 8.00 (s, 1H), 7.93 (s, 1H), 7.69 (dd, *J* = 8.8, 5.4 Hz, 2H), 7.38 (t, *J* = 8.8 Hz, 2H), 4.44 (dd, *J* = 7.7, 3.9 Hz, 1H), 3.71 (t, *J* = 6.6 Hz, 2H), 3.56 (ddt, *J* = 19.7, 13.3, 6.5 Hz, 2H), 2.24–2.15 (m, 1H), 1.95–1.89 (m, 2H), 0.94 (d, *J* = 6.9 Hz, 3H), 0.84 (d, *J* = 6.9 Hz, 3H). ^{13}C NMR (126 MHz, DMSO-d_6): δ 172.00, 167.42, 165.81, 163.94, 161.95, 159.35, 156.88, 155.60, 132.59, 131.74, 129.67, 121.14, 116.62, 116.44, 111.96, 60.66, 38.22, 30.88, 26.86, 18.78, 18.64. HRMS: *m/z*: calcd for $C_{22}H_{23}FN_6O_6S$: 519.1457 $[M+H]^+$; found: 519.1457.

2.2.16. (Z)-(6-((3-(5-Benzylidene-2,4-dioxothiazolidin-3-yl)propyl) amino)-5-nitropyrimidin-4-yl)valine 7j

White solid. Yield: 40%. ^{1}H NMR (500 MHz, DMSO-d_6): δ 9.67 (d, *J* = 7.8 Hz, 1H), 9.54 (t, *J* = 6.0 Hz, 1H), 8.04 (s, 1H), 7.92 (s, 1H), 7.62 (d, *J* = 7.2 Hz, 2H), 7.54 (t, *J* = 7.4 Hz, 2H), 7.49 (t, *J* = 7.2 Hz, 1H), 4.63 (dd, *J* = 7.8, 4.3 Hz, 1H), 3.72 (t, *J* = 6.7 Hz, 2H), 3.58 (dt, *J* = 13.0, 6.7 Hz, 2H), 2.28–2.21 (m, 1H), 1.96–1.89 (m, 2H), 0.95 (d, *J* = 6.9 Hz, 3H), 0.89 (d, *J* = 6.9 Hz, 3H). ^{13}C NMR (126 MHz, DMSO-d_6): δ 171.99, 167.55, 165.85, 159.36, 156.70, 156.22, 132.98, 132.82, 130.58, 130.06, 129.35, 121.41, 112.21, 59.44, 38.32, 30.49, 26.83, 18.73, 18.14. HRMS: *m/z*: calcd for $C_{22}H_{24}N_6O_6S$: 501.1551 $[M+H]^+$; found: 501.1553.

2.2.17. (Z)-(6-((3-(5-(4-Methoxybenzylidene)-2,4-dioxothiazolidin-3-yl)propyl)amino)-5-nitropyrimidin-4-yl)valine 7k

Yellow solid. Yield: 63%. ^{1}H NMR (500 MHz, DMSO-d_6): δ 9.63 (d, *J* = 7.8 Hz, 1H), 9.54 (t, *J* = 6.0 Hz, 1H), 8.04 (s, 1H), 7.87 (s, 1H), 7.58 (d, *J* = 8.9 Hz, 2H), 7.10 (d, *J* = 8.9 Hz, 2H), 4.65 (dd, *J* = 7.8, 4.3 Hz, 1H), 3.83 (s, 3H), 3.70 (t, *J* = 6.6 Hz, 2H), 3.61–3.53 (m, 2H), 2.27–2.21 (m, 1H), 1.91 (p, *J* = 6.8 Hz, 2H), 0.96 (d, *J* = 6.9 Hz, 3H), 0.90 (d, *J* = 6.9 Hz, 3H). ^{13}C NMR (126 MHz, DMSO-d_6): δ 172.03, 167.60, 165.96, 161.14, 159.36, 156.67, 156.29, 132.90, 132.20, 125.44, 118.06, 114.95, 112.24, 59.29, 55.48, 38.33, 30.45, 26.88, 18.72, 18.08. HRMS: *m/z*: calcd for $C_{23}H_{26}N_6O_7S$: 531.1656 $[M+H]^+$; found: 531.1656.

2.2.18. (Z)-(6-((3-(2,4-Dioxo-5-(pyridin-4-ylmethylene) thiazolidin-3-yl)propyl)amino)-5-nitropyrimidin-4-yl)valine 7l

Brown solid. Yield: 50%. ^{1}H NMR (500 MHz, DMSO-d_6): δ 9.54 (dd, *J* = 14.1, 7.0 Hz, 2H), 8.73 (d, *J* = 6.1 Hz, 2H), 8.06 (s, 1H), 7.87 (s, 1H), 7.55 (d, *J* = 6.1 Hz, 2H), 4.69 (dd, *J* = 7.8, 4.4 Hz, 1H), 3.72 (t, *J* = 6.6 Hz, 2H), 3.59 (dd, *J* = 13.6, 6.8 Hz, 2H), 2.30–2.22 (m, 1H), 1.93 (dt, *J* = 12.0, 5.9 Hz, 2H), 0.96 (d, *J* = 6.9 Hz, 3H), 0.91 (d, *J* = 6.9 Hz, 3H). ^{13}C NMR (126 MHz, DMSO-d_6): δ 172.01, 167.00, 165.50, 159.39, 156.63, 156.49, 150.64, 140.04, 129.75, 126.53, 123.34, 112.34, 58.95, 38.37, 30.32, 26.71, 18.70, 17.96. HRMS: *m/z*: calcd for $C_{21}H_{23}N_7O_6S$: 502.1503 $[M+H]^+$; found: 502.1503.

2.2.19. (6-((3-((Z)-2,4-dioxo-5-((E)-3-phenylallylidene)thiazolidin-3-yl)propyl)amino)-5-nitropyrimidin-4-yl)valine 7m

Yellow solid. Yield: 41%. ^{1}H NMR (500 MHz, DMSO-d_6): δ 9.54 (d, *J* = 7.2 Hz, 2H), 8.06 (s, 1H), 7.67 (d, *J* = 7.1 Hz, 2H), 7.61 (d, *J* = 11.4 Hz, 1H), 7.46–7.36 (m, 3H), 7.33 (d, *J* = 15.2 Hz, 1H), 6.99 (dd, *J* = 15.2, 11.4 Hz, 1H), 4.72 (dd, *J* = 7.7, 4.5 Hz, 1H), 3.68 (t, *J* = 6.5 Hz, 2H), 3.57 (dt, *J* = 9.9, 6.8 Hz, 2H, overlapped with water), 2.26 (dd, *J* = 11.4, 6.8 Hz, 1H), 1.90 (t, *J* = 6.6 Hz, 2H), 0.96 (d, *J* = 6.9 Hz, 3H), 0.93 (d, *J* = 6.8 Hz, 3H). ^{13}C NMR (126 MHz, DMSo-d_6): δ 172.01, 167.35, 165.32, 159.37, 156.60, 156.56, 144.02, 135.52, 133.21, 129.81, 128.90, 127.87, 123.24, 122.52, 112.35, 58.83, 38.40, 30.27, 26.87, 18.70, 17.92. HRMS: *m/z*: calcd for $C_{24}H_{26}N_6O_6S$: 527.1707 $[M+H]^+$; found: 527.1706.

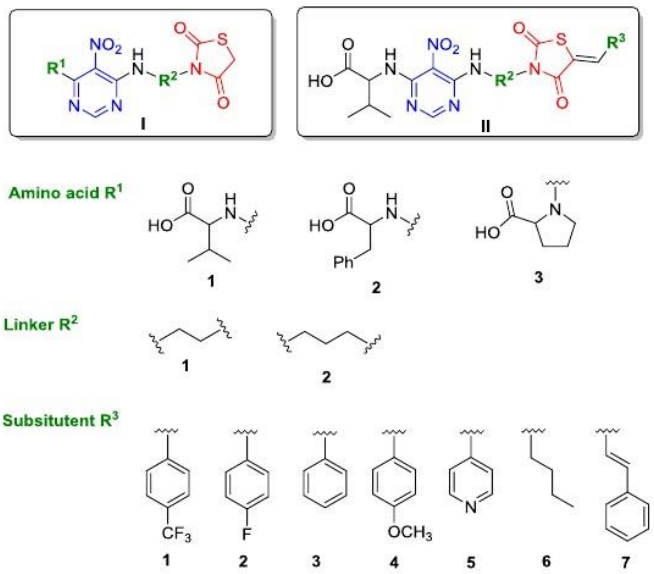

Fig. 2. Structures selected for this study.

2.2.20. (Z)-(6-((3-(2,4-Dioxo-5-pentylidenethiazolidin-3-yl)propyl) amino)-5-nitropyrimidin-4-yl)valine 7n

Yellow solid. Yield: 47%. ^{1}H NMR (500 MHz, DMSO-d_6): δ 9.62 (d, J = 7.8 Hz, 1H), 9.51 (t, J = 6.0 Hz, 1H), 8.04 (s, 1H), 7.02 (t, J = 7.7 Hz, 1H), 4.68 (dd, J = 7.8, 4.3 Hz, 1H), 3.64 (t, J = 6.7 Hz, 2H), 3.54 (dt, J = 10.5, 6.7 Hz, 2H), 2.29–2.23 (m, 1H), 2.21 (dd, J = 14.8, 7.4 Hz, 2H), 1.87 (p, J = 6.7 Hz, 2H), 1.48 (dt, J = 14.9, 7.4 Hz, 2H), 1.31 (dq, J = 14.4, 7.3 Hz, 2H), 0.97 (d, J = 6.9 Hz, 3H), 0.92 (d, J = 6.9 Hz, 3H), 0.88 (t, J = 7.3 Hz, 3H). ^{13}C NMR (126 MHz, DMSO-d_6): δ 172.00, 167.34, 164.55, 159.35, 156.64, 156.35, 138.50, 124.62, 112.25, 59.17, 38.37, 30.91, 30.42, 29.33, 26.79, 21.74, 18.72, 18.04, 13.57. HRMS: m/z: calcd for $C_{20}H_{28}N_6O_6S$: 481.1864 $[M+H]^+$; found: 481.1867.

2.3. Antimycobacterial activity

Antimycobacterial activity of the pyrimidines against *M. tuberculosis* H37Rv (NCTC 7416) was evaluated in duplicates by determining their minimum inhibitory concentration (MIC) in 96-well microtitre plates. Stock solutions of the drugs and their subsequent 2-fold serial dilutions were prepared in 5% DMSO. Isoniazid was used as the drug control. *M. tuberculosis* H37Rv was cultured in Middlebrook 7H9 broth (Himedia, Mumbai) supplemented with 10% OADC (Himedia, Mumbai). The inoculums were prepared by diluting the mycobacterial culture in 7H9 broth. The controls consisted of drug-free media for sterility check and the media inoculated with *M. tuberculosis* H37Rv for the growth patterns in drug-inoculated tubes. The tubes were incubated for 1–2 weeks at 37 °C. The MICs were defined as the lowest concentration of the compound at which no visible bacterial growth was observed and evaluated by Resazurin microtiter assay [45,46].

2.4. Antimicrobial activity

The antimicrobial activities of the final compounds against *Staphylococcus aureus* (CCM 3953), *Pseudomonas aeruginosa* (CCM 3955), *Escherichia coli* (CCM 3954), *Candida albicans* (ATCC 90028), *Aspergillus niger* (CCM 8189), and *Enterococcus faecalis* (CCM 4224) were determined by their MIC as described earlier [47]. Gentamicin was used as the drug control for bacteria, and amphotericin B for yeast and mould.

Antimicrobial activities of the synthesized compounds were assessed using the standard dilution micromethod in duplicates. Disposable microtitration plates were used for the tests. The stock solution of compounds in 5% DMSO (1024 μg/mL) were diluted 2–16 times with an additional Breath heart infusion broth (50 μL) inoculated with the tested bacteria/yeast at a concentration of 10^5–10^6 CFU mL^{-1}. Tested concentrations of compounds were 512–0.015 μg/mL.

The minimum inhibitory concentration (MIC) of aerobic bacteria was read after 24 h of incubation at 37 °C as the minimum inhibitory concentration (MIC) of the tested substance that inhibited the growth of the bacterial strain. The MIC of anaerobic bacteria, yeast and mould was read after 48 h of incubation at 30 °C.

The minimum bactericidal concentration (MBC) or minimum fungicidal concentration (MFC) may be characterized as the minimum concentration of the sample required to achieve irreversible inhibition, i.e., killing the bacteria/yeast after a defined period of incubation. The MBC was examined by a modified imprint method. With an applicator, ~5 μL of the tested samples with defined concentrations were transferred from the microplate wells and imprinted on the surface of blood agar for bacteria or Sabouraud agar without antimicrobial agents for yeast. The MBC was determined as the lowest concentration that inhibited the visible growth of the used bacterium.

The minimum bacteriostatic concentration (MBS) may be characterized as the minimum concentration of the sample required to achieve reversible inhibition, i.e., the bacteria growth after removing the effects of the antimicrobial compound.

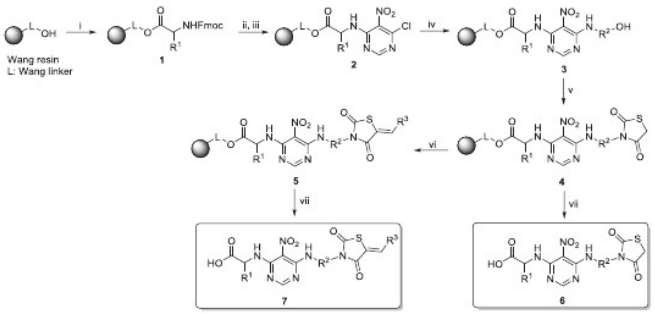

Scheme 1. Solid-phase synthesis of model compounds 6 and 7[a].

3. Results and discussion

In view of the biological significance of thiazolidinedione and 5-nitropyrimidine scaffolds, we designed and synthesized a library of novel hybrids depicted in Fig. 2.

The two scaffolds (thiazolidinedione and 5-nitropyrimidine) are connected *via* an appropriate linker. For primary screening and the development of synthetic protocol, we selected ethylenediamine and propylenediamine linkers. The whole system was built on the Wang resin *via* the immobilization of various amino acids that are known for their ability to tune optimal pharmacokinetic and pharmacodynamics properties of potential drugs [48–50]. Since all novel compounds were designed primarily as promising antitubercular agents (more than 60% of the mycobacterial cell wall are lipids), the central part of amino acid linker was selected considering its lipophilicity. For the first group of novel thiazolidinediones (structures I) three different amino acids were selected (with respect to their lipophilicity) to test the impact of amino acid on resulting biological activity. For the second group of compounds (structures II) only valine linker containing lipophilic central part was chosen. Furthermore, thiazolidinedione scaffold was modified with variously substituted benzylidenes or alkylidenes. Some benzylidenes have already been found to be involved in the construction of biologically active structures (see Fig. 1) [23,25].

3.1. Solid-phase synthesis of the model compounds

Solid-phase synthesis of the desired compounds commenced with the immobilization of amino acids on Wang resin to give corresponding resin **1** (Scheme 1). Subsequent deprotection of amino group and substitution with 4,6-dichloro-5-nitropyrimidine afforded resin **2**. The chlorine atoms of resin **2** are very reactive and can be easily hydrolyzed as we had described earlier [51]. For this reason, resin **2** was immediately modified with aminoethanol or aminopropanol giving resin **3**. Desired precursor **4** was obtained after Fukuyama-Mitsunobu reaction where thiazolidinedione was easily prepared from thiourea and chloroacetic acid according to previously described procedure [10]. Here, thiazolidinedione was allowed to react with resin **3** for 16 h; however, subsequent optimization studies showed that 99% conversion was possible in 1 h.

[a] Reagents and conditions: (i) Fmoc-amino acid, *N*-hydroxybenzotriazole (HOBt), DMAP, DIC, DMF/DCM (1:1), 16 h; (ii) 50% piperidine, DMF, 15 min; (iii) 4,6-dichloro-5-nitro-pyrimidine, DIEA, dry DMF, 2 h; (iv) amino alcohol, DIEA, dry DMF, rt, 2 h; (v) thiazolidine-2,4-dione, PPh_3, DIAD, dry THF, rt, 1 h; (vi) aldehyde, piperidine, DMF, 60 °C, 20 h; (vii) 50% TFA in DCM, rt, 1 h.

Further, Knoevenagel condensation of resin 4 with variously substituted aldehydes afforded polymer-bound intermediate 5. When thiazolidinedione-resin 4 reacted with aldehyde in the presence of *N*,*N*-diisopropylethylamine (DIEA) as a base in DCM at room temperature, conversion of 4 to resin 5 was only about 30% according to LC-MS traces at 210–500 nm. Then, trials with various bases, solvents and reaction temperature were carried out; the optimal reaction conditions were aldehyde, piperidine, DMF, 70 °C, 20 h. The reaction occurred smoothly with aromatic aldehydes bearing electron-withdrawing or electron-donating groups as well as aliphatic aldehydes in crude purity between 58 and 91%. Finally, the resulting derivatives 6 and 7 were isolated by standard cleavage and HPLC purification (Tables 1 and 2). Overall yields ranged from 29 to 63% and the lower yields were caused with some losses during HPLC purification procedure.

After Knoevenagel condensation, formation of two geometrical isomers *E* or *Z* is possible. These two isomers can be easily distinguished by the ^{1}H NMR spectral characteristics. It is well known

Table 1
Overview of synthesized products 6.

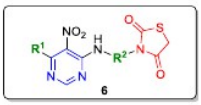

Entry	R^1	R^2	Yield [%]
6a			27
6b			58
6c			51
6d			74
6e			50
6f			84

Table 2
Overview of synthesized products 7.

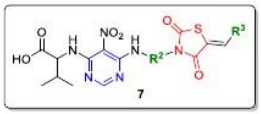

Entry	R^2	R^3	Yield [%]
7a			36
7b			42
7c			49
7d			39
7e			39
7f			31
7g			29
7h			55
7i			55
7j			40
7k			63
7l			50
7m			41
7n			47

that benzylidine proton appears above 7.90 ppm in *Z* isomer and below 7.42 ppm in *E* isomer [52,53]. The NMR elucidation confirmed the formation of *Z* isomers for all our products.

3.2. In vitro evaluation of antitubercular activity against *M. tuberculosis H37Rv* and antimicrobial activity against other strains

The final compounds 6 and 7 were tested for their antimicrobial activity against reference Gram-positive and Gram-negative bacterial strains (*Staphylococcus aureus* CCM 3953, *Pseudomonas aeruginosa* CCM 3955, *Escherichia coli* CCM 3954, *Enterococcus faecalis* CCM 4224), against two fungal strains (*Candida albicans* ATCC 90028, *Aspergillus niger* CCM 8189) and against *Mycobacterium tuberculosis* H37Rv.

Thiazolidinediones 6 exhibited no significant activities and none of the derivatives showed activity against *E. Coli*, *P. aeruginosa*, *C. albicans* and *A. niger*. On the contrary, compounds 7 showed more interesting results. Thiazolidinedione 7h (see Table 3) showed the highest antimicrobial activity against *S. aureus* CCM 3953 (MIC = 128 μg/mL) and antitubercular activity against *M. tuberculosis* H37Rv (MIC = 256 μg/mL). *Mycobacterium* has a similar cell wall construction as Gram-positive bacteria. The compounds that had an antimicrobial effect on Gram-positive bacteria (like 7f or 7h) may have a bacteriostatic or inhibitory effect on the strain *Mycobacterium tuberculosis* H37Rv.

Table 3
Minimum inhibition concentrations (MIC; μg/mL), minimum bacteriostatic concentrations (MBS) or minimum bactericidal concentrations (MBC) of synthesized compounds 7.

Entry	*Mycobacterium tuberculosis*	*Staphylococcus aureus*		*Enterococcus faecalis*	
	MIC	MIC	MBS/MBC	MIC	MBS/MBC
7a	–	256	256/-	1024	1024/-
7b	–	1024	1024/-	–	–
7c	–	1024	1024/-	–	–
7f	1024	256	256/-	256	256/-
7g	–	–	–	1024	1024/-
7h	256	128	128/1024	256	256/-
7i	–	1024	1024/-	–	–
7j	–	1024	-/1024	–	–
7k	–	512	512/-	–	–
7l	–	1024	1024/-	1024	1024/-
isoniazid	0.125	×	×	×	×
gentamicine	×	16	-/16	64	-/64

Moreover, we observed certain structure-activity dependence for compounds 7. While derivative 7h with propylenediamine linker between two pharmacophores exhibited the most interesting activities, compounds 7a with ethylenediamine linker showed only slight antimicrobial activity against *S. aureus* and *P. aeruginosa*.

4. Conclusion

In summary, we have developed a rapid and effective approach to the synthesis of novel thiazolidinedione-pyrimidine conjugates by employing an efficient solid-phase synthetic protocol. Our methodology is based on easy access to structural diversity from abundant and easily available building blocks with minimal synthetic operations and was validated in synthesis of model chemical library prepared *via* a combinatorial manner. Although the design of our library was motivated by testing the reactivity of various building blocks, some of the prepared derivatives exhibited slight antimicrobial and antitubercular activity mainly against *S. aureus* CCM 3953 (MIC = 128 μg/mL) and moderate activity against *M. tuberculosis* H37Rv (MIC = 256 μg/mL). The developed synthetic protocol can be used for fast and efficient synthesis of a chemical library designed with use of sophisticated methods in the future.

Acknowledgement

This work was supported by the Ministry of Education, Youth and Sport of the Czech Republic (projects IGA_PrF_2018_029, IGA_LF_2018_032) and the National Program of Sustainability (project LO1304).

Appendix A. Supplementary data

Supplementary data to this article can be found online at https://doi.org/10.1016/j.molstruc.2019.01.073.

References

[1] M.J. Nanjan, M. Mohammed, B.R. Prashantha Kumar, M.J.N. Chandrasekar, Thiazolidinediones as antidiabetic agents: a critical review, Bioorg. Chem. 77 (2018) 548–567.
[2] S. Sucheta, P. Tahlan, K. Verma, Biological potential of thiazolidinedione derivatives of synthetic origin, Chem. Cent. J. 11 (2017) 130.
[3] S. Pattan, M. Kedar, J. Pattan, S. Dengale, M. Sanap, U. Gharate, et al., Synthesis and evaluation of some novel 2,4-thiazolidinedione derivatives for

antibacterial, antitubercular and antidiabetic activities, Indian J. Chem. Sect. B Org. Chem. Incl. Med. Chem. 51B (2012) 1421–1425.
[4] S. Bondock, W. Khalifa, A.A. Fadda, Synthesis and antimicrobial evaluation of some new thiazole, thiazolidinone and thiazoline derivatives starting from 1-chloro-3,4-dihydronaphthalene-2-carboxaldehyde, Eur. J. Med. Chem. 42 (2007) 948–954.
[5] N.C. Desai, A.M. Dodiya, A.H. Makwana, Antimicrobial screening of novel synthesized benzimidazole nucleus containing 4-oxo-thiazolidine derivatives, Med. Chem. Res. 21 (2012) 2320–2328.
[6] N.C. Desai, A.M. Dodiya, P.N. Shihora, A clubbed quinazolinone and 4-thiazolidinone as potential antimicrobial agents, Med. Chem. Res. 21 (2012) 1577–1586.
[7] N.K. Fuloria, V. Singh, M.S. Yar, M. Ali, Synthesis, characterization and antimicrobial evaluation of novel imines and thiazolidinone derivatives, Acta Pol. Pharm. 66 (2009) 141–146.
[8] S. Ozkirimli, F. Kazan, Y. Tunali, Synthesis, antibacterial and antifungal activities of 3-(1,2,4-triazol-3-yl)-4-thiazolidinones, J. Enzym. Inhib. Med. Chem. 24 (2009) 447–452.
[9] N.B. Patel, S.D. Patel, Synthesis and antimicrobial study of fluoroquinolone-based 4-thiazolidinones, Med. Chem. Res. 19 (2010) 757–770.
[10] N.M. Parekh, K.V. Juddhawala, B.M. Rawal, Antimicrobial activity of thiazolyl benzenesulfonamide-condensed 2,4-thiazolidinediones derivatives, Med. Chem. Res. 22 (2013) 2737–2745.
[11] F.M. Shaikh, N.B. Patel, G. Sanna, B. Busonera, P. La Colla, D.P. Rajani, Synthesis of some new 2-amino-6-thiocyanato benzothiazole derivatives bearing 2,4-thiazolidinediones and screening of their in vitro antimicrobial, antitubercular and antiviral activities, Med. Chem. Res. 24 (2015) 3129–3142.
[12] S.S. Purohit, A. Alman, J. Shewale, Synthesis and antimicrobial activity of a new series of 3,5-disubstituted thiazolidine-2,4-diones, Int. J. Pharm. Pharmaceut. Sci. 4 (2012) 273–276.
[13] N.B. Patel, A.C. Purohit, D. Rajani, Design and synthesis of newer thiazolidinediones incorporated with pyridine and 1,3,4-oxadiazole moieties as antimicrobial agents, Int. J. Drug Des. Discovery 5 (2014) 1342–1351.
[14] N.B. Patel, I.H. Khan, Synthesis of newer 5-benzylidene-2,4-thiazolidinediones as potential antimicrobials, Indian J. Res. Pharm. Biotechnol. 2 (9) (2014) 993–1001.
[15] F.M. Shaikh, N.B. Patel, D. Rajani, Synthesis of new thiazolidine-2,4-dione derivatives and their antimicrobial and antitubercular activity, Indian J. Res. Pharm. Biotechnol. 1 (2013) 496–503.
[16] M.L. Barreca, A. Chimirri, L. De Luca, A.M. Monforte, P. Monforte, A. Rao, et al., Discovery of 2,3-diaryl-1,3-thiazolidin-4-ones as potent anti-HIV-1 agents, Bioorg. Med. Chem. Lett 11 (2001) 1793–1796.
[17] A. Deep, S. Jain, P.C. Sharma, P. Phogat, M. Malhotra, Synthesis of 2-(aryl)-5-(arylidene)-4-thiazolidinone derivatives with potential analgesic and anti-inflammatory activity, Med. Chem. Res. 21 (2012) 1652–1659.
[18] A.A. Geronikaki, A.A. Lagunin, D.I. Hadjipavlou-Litina, P.T. Eleftheriou, D.A. Filimonov, V.V. Poroikov, et al., Computer-aided discovery of anti-inflammatory thiazolidinones with dual cyclooxygenase/lipoxygenase inhibition, J. Med. Chem. 51 (2008) 1601–1609.
[19] A. Kumar, C.S. Rajput, Synthesis and anti-inflammatory activity of newer quinazolin-4-one derivatives, Eur. J. Med. Chem. 44 (2009) 83–90.
[20] R. Ottana, R. Maccari, M.L. Barreca, G. Bruno, A. Rotondo, A. Rossi, et al., 5-Arylidene-2-imino-4-thiazolidinones: design and synthesis of novel anti-inflammatory agents, Bioorg. Med. Chem. 13 (2005) 4243–4252.
[21] S.G. Kucukguzel, E.E. Oruc, S. Rollas, F. Sahin, A. Ozbek, Synthesis, characterization and biological activity of novel 4-thiazolidinones, 1,3,4-oxadiazoles and some related compounds, Eur. J. Med. Chem. 37 (2002) 197–206.
[22] G. Kuecuekguezel, A. Kocatepe, E. De Clercq, F. Sahin, M. Guelluece, Synthesis and biological activity of 4-thiazolidinones, thiosemicarbazides derived from diflunisal hydrazide, Eur. J. Med. Chem. 41 (2006) 353–359.
[23] S. Ponnuchamy, S. Kanchithalaivan, R. Ranjith Kumar, M. Ashraf Ali, T. Soo Choon, Antimycobacterial evaluation of novel hybrid arylidene thiazolidine-2,4-diones, Bioorg. Med. Chem. Lett 24 (2014) 1089–1093.
[24] N. Babu, K.K. Rajasekhar, T. Singirisetty, VS, Synthesis, Characterisation and Anti-tubercular Activity of Some New 3,5-Disubstituted-2,4-Thiazolidinediones, 6 ed, 2013.
[25] S. Kumar, R. Mehra, S. Sharma, N.P. Bokolia, D. Raina, A. Nargotra, et al., Screening of antitubercular compound library identifies novel ATP synthase inhibitors of Mycobacterium tuberculosis, Tuberculosis 108 (2018) 56–63.
[26] S. Prachayasittikul, R. Pingaew, A. Worachartcheewan, N. Sinthupoom, V. Prachayasittikul, S. Ruchirawat, et al., Roles of pyridine and pyrimidine derivatives as privileged scaffolds in anticancer agents, Mini Rev. Med. Chem. 17 (2017) 869–901.
[27] A.P. Keche, G.D. Hatnapure, R.H. Tale, A.H. Rodge, S.S. Birajdar, V.M. Kamble, A novel pyrimidine derivatives with aryl urea, thiourea and sulfonamide moieties: synthesis, anti-inflammatory and antimicrobial evaluation, Bioorg. Med. Chem. Lett 22 (2012) 3445–3448.
[28] N. Shakya, S. Vedi, C. Liang, F. Yang, B. Agrawal, R. Kumar, 4'-Substituted pyrimidine nucleosides lacking 5'-hydroxyl function as potential anti-HCV agents, Bioorg. Med. Chem. Lett 24 (2014) 1407–1409.
[29] Z. Yang, Y. Fang, T.A. Pham, J. Lee, H. Park, Synthesis and biological evaluation of 5-nitropyrimidine analogs with azabicyclic substituents as GPR119 agonists, Bioorg. Med. Chem. Lett 23 (2013) 1519–1521.
[30] T. Wang, G. Bemis, B. Hanzelka, H. Zuccola, M. Wynn, C.S. Moody, et al., Mtb PKNA/PKNB dual inhibition provides selectivity advantages for inhibitor design to minimize host kinase interactions, ACS Med. Chem. Lett. 8 (2017) 1224–1229.
[31] N.H. Bhuva, P.K. Talpara, P.M. Singala, V.K. Gothaliya, V.H. Shah, Synthesis and biological evaluation of pyrimidinyl sulphonamide derivatives as promising class of antitubercular agents, J. Saudi Chem. Soc. 21 (2017) 517–527.
[32] C.R. Wilson, R.K. Gessner, A. Moosa, R. Seldon, D.F. Warner, V. Mizrahi, et al., Novel antitubercular 6-dialkylaminopyrimidine carboxamides from phenotypic whole-cell high throughput screening of a SoftFocus library: structure-activity relationship and target identification studies, J. Med. Chem. 60 (2017) 10118–10134.
[33] E.V. Verbitskiy, S.A. Baskakova, M.A. Kravchenko, S.N. Skornyakov, G.L. Rusinov, O.N. Chupakhin, et al., Synthesis and evaluation of antitubercular activity of fluorinated 5-aryl-4-(hetero)aryl substituted pyrimidines, Bioorg. Med. Chem. 24 (2016) 3771–3780.
[34] D. Seenaiah, P.R. Reddy, G.M. Reddy, A. Padmaja, V. Padmavathi, N. Siva krishna, Synthesis, antimicrobial and cytotoxic activities of pyrimidinyl benzoxazole, benzothiazole and benzimidazole, Eur. J. Med. Chem. 77 (2014) 1–7.
[35] L. Ballell, R.H. Bates, R.J. Young, D. Alvarez-Gomez, E. Alvarez-Ruiz, V. Barroso, et al., Fueling open-source drug discovery: 177 small-molecule leads against tuberculosis, ChemMedChem 8 (2013) 313–321.
[36] M.R. Sura, V.G.R. Peddiahgari, R.P.R. Bhoomireddy, R.K. Vadde, Synthesis of new 2,4-diaryl-6-methyl-5-nitropyrimidines as antibacterial and antioxidant agents, J. Heterocycl. Chem. 50 (2013) 1395–1399.
[37] C. Kishor, T. Arya, R. Reddi, X. Chen, V. Saddanapu, A.K. Marapaka, et al., Identification, biochemical and structural evaluation of species-specific inhibitors against type I methionine aminopeptidases, J. Med. Chem. 56 (2013) 5295–5305.
[38] M.L. Read, M. Braendvang, P.O. Miranda, L.L. Gundersen, Synthesis and biological evaluation of pyrimidine analogs of antimycobacterial purines, Bioorg. Med. Chem. 18 (2010) 3885–3897.
[39] D.S. Reddy, K.M. Hosamani, H.C. Devarajegowda, Design, synthesis of benzocoumarin-pyrimidine hybrids as novel class of antitubercular agents, their DNA cleavage and X-ray studies, Eur. J. Med. Chem. 101 (2015) 705–715.
[40] C.H. Zhou, Y. Wang, Recent researches in triazole compounds as medicinal drugs, Curr. Med. Chem. 19 (2012) 239–280.
[41] A. Campanico, R. Moreira, F. Lopes, Drug discovery in tuberculosis. New drug targets and antimycobacterial agents, Eur. J. Med. Chem. 150 (2018) 525–545.
[42] K.M. Brummond, J. Lu, Solid-phase synthesis of BRL 49653, J. Org. Chem. 64 (1999) 1723–1726.
[43] N.C.O. Tomkinson, A.M. Sefler, K.D. Plunket, S.G. Blanchard, D.J. Parks, T.M. Willson, Solid-phase synthesis of hybrid thiazolidinedione-fatty acid PPAR+- ligands, Bioorg. Med. Chem. Lett 7 (1997) 2491–2496.
[44] D.L. Mohler, G. Shen, A.K. Dotse, Solution- and solid-phase synthesis of peptide-substituted thiazolidinediones as potential PPAR ligands, Bioorg. Med. Chem. Lett 10 (2000) 2239–2242.
[45] J.C. Palomino, A. Martin, M. Camacho, H. Guerra, J. Swings, F. Portaels, Resazurin microtiter assay plate: simple and inexpensive method for detection of drug resistance in Mycobacterium tuberculosis, Antimicrob. Agents Chemother. 46 (2002) 2720–2722.
[46] P.C. Nguyen, A. Madani, P. Santucci, B.P. Martin, R.R. Paudel, S. Delattre, et al., Cyclophostin and Cyclipostins analogues, new promising molecules to treat mycobacterial-related diseases, Int. J. Antimicrob. Agents 51 (2018) 651–654.
[47] Z. Ozdemir, U. Bildziukevich, D. Saman, L. Havlicek, L. Rarova, L. Navratilova, et al., Amphiphilic derivatives of (3β,17β)-3-hydroxyandrost-5-ene-17-carboxylic acid, Steroids 128 (2017) 58–67.
[48] S. Majumdar, S. Duvvuri, A.K. Mitra, Membrane transporter/receptor-targeted prodrug design: strategies for human and veterinary drug development, Adv. Drug Deliv. Rev. 56 (2004) 1437–1452.
[49] V.K. Singh, B.B. Subudhi, Development of reversible glutamine conjugate of methotrexate for enhanced brain delivery, Med. Chem. Res. 24 (2015) 624–635.
[50] I.S. Krylov, B.A. Kashemirov, J.M. Hilfinger, C.E. McKenna, Evolution of an amino acid based prodrug approach: stay tuned, Mol. Pharm. 10 (2013) 445–458.
[51] L. Brulikova, S. Krupkova, M. Labora, K. Motyka, L. Hradilova, M. Mistrik, et al., Synthesis and study of novel pH-independent fluorescent mitochondrial labels based on Rhodamine B, RSC Adv. 6 (2016) 23242–23251.
[52] S. Mohanty, A.K. Roy, V.K.P. Kumar, S.G. Reddy, A.C. Karmakar, Acetic anhydride-promoted one-pot condensation of 2,4-thiazolidinedione with bisulfite adducts of aldehydes, Tetrahedron Lett. 55 (2014) 4585–4589.
[53] U.R. Pratap, D.V. Jawale, R.A. Waghmare, D.L. Lingampalle, R.A. Mane, Synthesis of 5-arylidene-2,4-thiazolidinediones by Knoevenagel condensation catalyzed by Baker's yeast, New J. Chem. 35 (2011) 49–51.

Appendix 7

Benzoxazole Derivatives as Promising Antitubercular Agents

Šlachtová, V.; **Brulíková, L.***

ChemistrySelect **2018**, *3*(17), 4653-4662.

ChemPubSoc Europe

DOI: 10.1002/slct.201800631

Chemistry SELECT Reviews

Medicinal Chemistry & Drug Discovery

Benzoxazole Derivatives as Promising Antitubercular Agents

Veronika Šlachtová[b] and Lucie Brulíková*[a]

Tuberculosis (TB) is an infectious disease caused predominantly by bacillus *Mycobacterium tuberculosis (MTB)*. The increasing prevalence of multidrug-resistant *MTB* necessitates the discovery and development of alternative drugs against tuberculosis with a new mechanism of action. Over the past years, several benzoxazole derivatives have been synthesized and screened for their biological activity. Interestingly, some of them had promising antitubercular activity. Despite that, none of the benzoxazole derivatives has entered the phase of the preclinical hit-to-lead optimization step in anti-TB research. In this review, we are summarizing recently published articles that evaluate the potency of benzoxazole heterocycle in the development of novel anti-TB agents and outlined the future aspects of this promising heterocycle.

1. Introduction

TB is a bacterial infection caused by *Mycobacterium tuberculosis* (*MTB*) which belongs to *Mycobacterium tuberculosis complex* (MTC). *MTB* is a very slow-growing, intracellular organism known for its lipid-rich cell wall. Consequently, the treatment of infected patients requires the use of multiple-drug therapy for several months. Moreover, an increasing number of the *MTB* strains are becoming resistant to one or more of the standard anti-TB drugs, which complicate treatment and the rise of the number of people affected by drug-resistant TB and latent TB is alarming. Multidrug-resistant (MDR) tuberculosis is defined by its *in vitro* resistance to at least isoniazid (INH) and rifampicin; while extensively drug-resistant (XDR) TB is resistant to at least one fluoroquinolone and one second-line anti-TB drug in addition to INH and rifampicin.[1–6] The occurrence of MDR and XDR *MTB* infections intensified the efforts to discover novel anti-TB agents with a new mode of action and directed at yet unknown targets of *MTB*.

The current situation and effort to effectively control TB requires development of new antitubercular agents acting on new targets. Overall, new antitubercular drug should meet at least some of these criteria: (1) be more potent than the existing drugs; (2) should have a good safety profile; (3) should be able to reduce the duration of therapy; (4) should be effective to treat multidrug-resistant and extensively drug-resistant tuberculosis; (5) should be compatible with concomitant ART since many patients are co-infected with HIV, and (6) should have no antagonistic activity against other tuberculosis drugs in the treatment regimen. With no doubt, the discovery of entirely new compounds with an alternative mechanism of action to the existing therapeutics remains challenging.

Over the past years, the benzoxazole skeleton was found to have a wide range of biological activities and it is currently one the most important scaffolds found in pharmacologically active compounds. As a consequence of this enormous interest, benzoxazole heterocycles and their biological properties have been reviewed many times.[7–10] Furthermore, variously substituted benzoxazoles have been found in many natural products such as Boxazomycin A, Calcimycin or Nakijinol B (Figure 1).[11–13]

Figure 1. Benzoxazoles as component of natural products.

Inspired by the nature, researches synthesized a variety of benzoxazole derivatives and screened for their biological activity[7–9] which resulted in several marketed drugs (Figure 2).[14–18]

Two different synthetic approaches were applied to prepare different benzoxazoles: (a) solution-phase synthetic approach and (b) solid-phase synthetic approach. Both of this approaches have been clearly summarized in 2017.[19] A conventional solution-phase synthetic approach (Figure 3) comprises the condensation of *o*-aminophenols with aldehydes[20–22] or carboxylic acids.[23–25] Benzoxazoles can also be synthesized *via* the condensation of *o*-aminophenols with ortho-esters[26] or 1,1-dihaloalkenes.[27,28]

Solid-phase synthetic approach covers the efficient methods leading to benzoxazole libraries formed by combinatorial

[a] *Dr. L. Brulíková*
Department of Medicinal Chemistry, Institute of Molecular and Translational Medicine, Hněvotínská 5, Olomouc, Czech Republic, 77900
E-mail: lucie.brulikova@upol.cz
[b] *V. Šlachtová*
Department of Organic Chemistry, Faculty of Science, 17. listopadu 12, Olomouc, Czech Republic, 77146

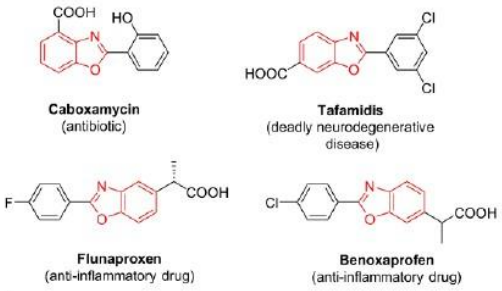

Figure 2. Marketed drugs based on the benzoxazole structure.

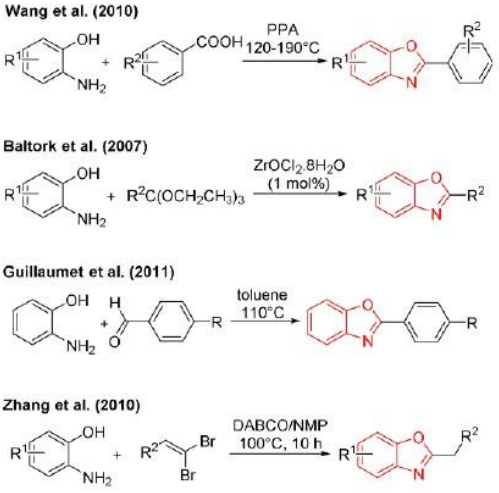

Figure 3. Solution-phase methods leading to benzoxazoles.

assembly (Figure 4). Wang et al. reported the synthesis of benzoxazole using Wang resin,[29] Beebe et al. used polystyrene-based linker and 3-nitrotyrosins,[30] Chen with coworkers established a strategy on PEG-5000 soluble support.[31] Gong

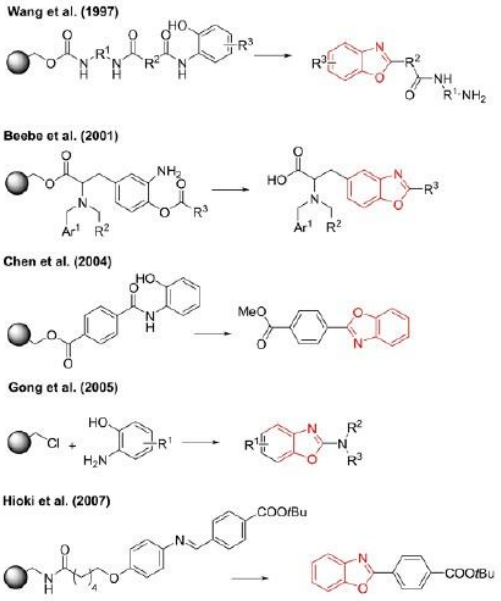

Figure 4. Solid-phase methods leading to benzoxazoles.

and his coworkers described the solid-supported synthesis using Merrifield resin[32] and Hioki with his group reported solid-phase synthesis with use of a traceless aniline linker.[33]

Both above mentioned approaches produced a number of interesting compounds. The unflagging effort resulted in several above mentioned marketed drugs. Despite that, none of the benzoxazole derivatives has entered the phase of the preclinical hit-to-lead optimization step in anti-TB research.

For this reason, benzoxazole-based compounds remain promising heterocyclic scaffold and the detailed SAR studies might reveal entirely new approach to help with the struggles to find a new treatment against tuberculosis. In this review, we will focus on benzoxazole derivatives as promising antitubercular agents considering the type and position of substitution and also the future aspects in anti-TB research.

Lucie Brulíková received her Ph.D. in Organic Chemistry at Charles University in Prague under supervising of prof. Antonín Holý. After that, she joined prof. Hlaváč group at Department of Organic chemistry, Palacky University in Olomouc, where she is currently working as assistant professor. In 2017 she set up junior research group focused on the design and development of new antituberculotics.

Veronika Šlachtová studied at Faculty of Pharmacy in Brno, where she also received her M.Sc degree in 2017. Afterwards, she joined the group of Lucie Brulíková as a doctoral student. Her research interest is solution-phase as well as solid-phase synthesis of biologically active compounds.

2. Benzoxazoles as anti-TB agents

Benzoxazole skeleton has been studied as antitubercular agent since 1949.[34] However, this structure has attracted the considerable attention mostly during the last two decades. Different substituents can be incorporated onto the benzene ring to improve the biological activity; especially the substitution at the position 2 and 5 is influential.

2.1. Benzoxazole-pyrazoline derivatives

Pyrazoline heterocycle has been found to have an interesting antitubercular activity.[35–37] Considering this fact, Soni group designed and synthesized a series of novel pyrazoline based benzoxazole derivatives **1** and **2** (Table 1) and screened for their activity against *MTB* $H_{37}Rv$, MDR-TB and XDR-TB strains.[38] Two compounds of these series had interesting activity, even better than all of the standard drugs (Streptomycin (6.25 μg/mL), Pyrazinamide (3.12 μg/mL) and Ciprofloxacin (3.12 μg/mL)) with value 0.8 μg/mL (**1h**) and 1.6 μg/mL (**2i**) against *MTB* $H_{37}Rv$ strain.

Table 1. *In vitro* antitubercular activity of pyrazoline-benzoxazoles **1** and **2** against *MTB* $H_{37}Rv$ strain.

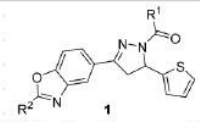

1

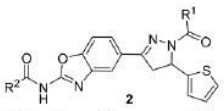

2

Entry	R^1	R^2	MIC (μg/mL)	Entry	R^1	R^2	MIC (μg/mL)
1a	CH_3	SH	6.25	**1m**	CH_3	4-pyridyl	25
1b	CH_3	NH_2	6.25	**1n**	NH_2	NH_2	6.25
1c	CH_3	C_6H_5	25	**1o**	NH_2	SH	12.5
1d	CH_3	2-ClC_6H_4	25	**2a**	CH_3	CH_3	25
1e	CH_3	2-$OMeC_6H_4$	25	**2b**	CH_3	$CH(CH_3)_2$	25
1f	CH_3	3-$OMeC_6H_4$	25	**2c**	CH_3	$CH_2CH_2CH_3$	12.5
1g	CH_3	4-$OMeC_6H_4$	12.5	**2d**	CH_3	CH_2Cl	6.25
1h	CH_3	4-OHC_6H_4	0.8	**2e**	CH_3	C_6H_5	6.25
1i	CH_3	3,4,5-$(OMe)_3C_6H_2$	25	**2f**	CH_3	2-ClC_6H_4	25
1j	CH_3	$CH_2C_6H_5$	50	**2g**	CH_3	2-$OMeC_6H_4$	25
1k	CH_3	2-pyridyl	25	**2h**	CH_3	3-ClC_6H_4	12.5
1l	CH_3	3-pyridyl	25	**2i**	CH_3	3-$OMeC_6H_4$	1.6

In 2014 Brahmkshatriya group reported two papers focused on combining of the pyrazoline and benzoxazole pharmacophores.[39,40] *In vitro* antitubercular activity evaluation of the first group of compounds against *MTB* $H_{37}Rv$, MDR-TB and XDR-TB revealed significant potency of target compounds **3** (Table 2). Most of the prepared compounds had potent activity (MIC value 1.25 - 25 μg/mL) against $H_{37}Rv$ strain. More interestingly, a few compounds showed better antitubercular activity than INH against MDR-TB and XDR-TB strains.[39]

The second group of conjugates (Table 3) revealed a few analogues with an activity comparable with INH against $H_{37}Rv$ strain (**4a**) and against MDR-TB strain (**4a**, **4k** and **4n**).[40]

In 2016, Devi group reported QSAR (Monte Carlo method) and docking studies of benzoxazole-pyrazoline based structures **4**.[41] Their computational results indicate that the presence of F or Cl substitution is preferred to Br and I, thiol group is preferred to amino group and OH or CH_3 group are more preferable then OCH_3. These results might be valuable for the design of further benzoxazole-pyrazoline compounds with potent antitubercular activity.

2.2. Benzoxazoles with 2-phenyl/benzyl substitution

Recently, Temiz-Arpaci group published two articles describing a series of 2-phenyl/benzyl substituted benzoxazoles with potent antimicrobial activity.[42,43] Firstly, they described the synthesis of series of benzyl substituted benzoxazoles **5** and their antitubercular activity against *MTB* and its *isolate* (Table 4).[42] Further, authors suggested that a [4-(*p*-chloro/fluoro-phenyl)piperazin-1-yl]acetamido moiety in position 5 might permit an easier penetration through the lipophilic mycobacterial cell wall. The series of ten tested compounds revealed certain structure-activity relationships reflected the presence of halogen (F or Cl). On the other hand, all of the tested compounds were less active then the reference drugs (INH and ethambutol).

Three years later, Temiz-Arpaci et al. modified the structure **5** with *p-tert*-butylphenyl moiety giving compounds **6** (Table 5).[43] Again, they expected that a lipophilic *p-tert*-butylphenyl moiety in the position 2 of the benzoxazole part might improve the penetration through the lipophilic mycobacterial cell wall. Unfortunately, neither this substitution of benzoxazole skeleton brought better results than those from the previous report. The best MIC values were 8 μg/mL.

In 2016, Ertan-Bolelli et al. reported the synthesis and biological evaluation of 5-amino-2-(4-substitutedphenyl)-benzoxazoles **7** and **8** (Table 6).[44] Few of the tested compounds had interesting antitubercular activity with MIC value of 8 μg/mL. Moreover, molecular docking of the most active compounds from this series into the active site of InhA revealed interaction with Tyr158 and/or co-factor NAD^+. For this reason, compounds **7a**, **7c** and **7f** might be considered as promising scaffolds for new potent anti-TB drugs.

2.3. Benzylsulfanyl benzoxazoles

Benzylsulfanyl modification of the benzoxazole skeleton revealed promising results in the field of anti-TB research. In 2002 and subsequently in 2009, Klimešová et al. reported synthesis and biological evaluation of 2-benzylsulfanyl benzoxazole derivatives **9** (Table 7).[45,46] Moreover, compounds **9e** and **9i** were tested against MDR *M. tuberculosis* (*MTB* 7357/98, 4166/04, 4977/03 and 550/04). Compound **9e** exhibited significant activity against both sensitive and resistant strains of MTB (MIC value 2–4 μmol/L). In contrast, derivative **9i** had activity with MIC value 8–32 μmol/L. Furthermore, benzoxazole **9e**

Table 2. *In vitro* antitubercular activity and cytotoxicity of pyrazoline-benzoxazoles **3**.

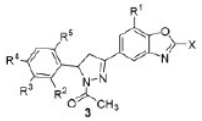

Entry	X	R^1	R^2	R^3	R^4	R^5	MIC (μg/mL) $H_{37}Rv$	MIC (μg/mL) MDR-TB	XDR-TB	Cytotoxicity IC50 (μg/mL)
3a	SH	H	H	OCH_3	OCH_3	H	12.5	12.5	>100	ND
3b	SH	H	H	H	OCH_3	H	6.25	6.25	50	ND
3c	SH	H	Cl	H	H	H	6.25	12.5	>100	ND
3d	SH	H	H	Cl	H	H	3.25	12.5	50	>62.5
3e	SH	H	H	H	Cl	H	3.25	25	50	32.5
3f	SH	OCH_3	H	OCH_3	OCH_3	H	6.25	12.5	50	ND
3g	SH	OCH_3	H	H	OCH_3	H	12.5	12.5	25	ND
3h	SH	OCH_3	Cl	H	H	H	6.25	50	25	ND
3i	SH	OCH_3	H	Cl	H	H	25	6.25	50	ND
3j	SH	OCH_3	H	H	Cl	H	3.25	25	50	>62.5
3k	SH	OCH_3	OCH_3	H	H	OCH_3	12.5	50	12.5	>62.5
3l	SH	OCH_3	H	Br	H	H	1.25	3.25	12.5	>62.5
3m	SH	OCH_3	H	H	Br	H	3.25	25	25	32.5
3n	NH_2	H	H	OCH_3	OCH_3	H	6.25	6.25	>100	ND
3o	NH_2	H	H	H	OCH_3	H	12.5	25	50	ND
3p	NH_2	H	Cl	H	H	H	25	25	50	ND
3q	NH_2	H	H	Cl	H	H	25	50	>100	ND
3r	NH_2	H	H	H	Cl	H	6.25	3.25	>100	ND
3s	NH_2	OCH_3	Cl	H	H	H	12.5	12.5	>100	ND
3t	NH_2	OCH_3	H	H	Br	H	25	3.25	50	ND
INH	-	-	-	-	-	-	0.5	6.25	50	ND

Table 3. *In vitro* antitubercular activity of pyrazoline-benzoxazoles **4**.

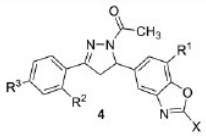

Entry	X	R^1	R^2	R^3	MIC (μg/mL) $H_{37}Rv$	MIC (μg/mL) MDR-TB
4a	NH_2	OCH_3	H	H	0.625	6.25
4b	NH_2	OCH_3	Cl	Cl	12.5	12.5
4c	NH_2	OCH_3	H	F	6.25	25
4d	NH_2	OCH_3	Br	H	12.5	25
4e	NH_2	H	H	H	25	25
4f	NH_2	H	Br	H	25	12.5
4g	NH_2	Cl	H	H	25	25
4h	NH_2	Cl	Br	H	3.25	25
4i	SH	OCH_3	H	H	6.25	12.5
4j	SH	OCH_3	Cl	Cl	6.25	12.5
4k	SH	OCH_3	H	F	12.5	6.25
4l	SH	OCH_3	Br	H	12.5	25
4m	SH	H	H	H	25	25
4n	SH	H	Br	H	12.5	6.25
4o	SH	Cl	H	H	1.25	25
4p	SH	Cl	Br	H	6.25	12.5
INH	-	-	-	-	0.625	6.25

Table 4. *In vitro* antitubercular activity of benzoxazoles **5**.

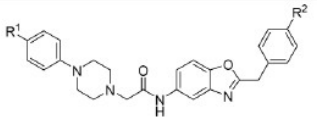

Entry	R^1	R^2	MIC (μg/mL) $H_{37}Rv$	MIC (μg/mL) *MTB isolate*
5a	Cl	Cl	32	8
5b	F	Cl	16	8
5c	Cl	CH_3	64	32
5d	F	CH_3	32	16
5e	Cl	H	64	16
5f	F	H	16	64
5g	Cl	F	8	8
5h	F	F	8	32
5i	Cl	Br	64	8
5j	F	Br	16	8
INH	-	-	<0.25	<0.25
ethambutol	-	-	2	2

showed the lowest lipophilicity (log $P = 3.779$) and enlarged molar refractivity (MR = 84.365 Å^3). All these results indicate that the introduction of benzyl moiety and two nitro groups increase the anti-TB activity compared to other substituent.

2.4. Benzoxazole alkaloids

In 1999, Rodriguez et al. screened marine natural products from the West Indian gorgonian coral *Pseudopterogorgia elisabethae* with anti-TB properties.[47] Their effort resulted in the isolation of two active alkaloids – pseudopteroxazol **10** and its biogenetic precursor seco-pseudopteroxazole **11** (Figure 5). Pseudopteroxazol **10** exhibited potent growth inhibition (97%)

Table 5. *In vitro* antitubercular activity of benzoxazoles **6**.

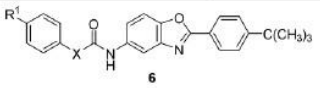

6

Entry	R^1	X	MIC (μg/mL) $H_{37}Rv$	MIC (μg/mL) MTB isolate
6a	H	-	8	8
6b	F	CH_2	8	8
6c	F	-	16	32
6d	Br	-	128	128
6e	C_2H_5	-	32	32
6f	NO_2	-	32	16
6g	H	CH_2	8	32
6h	CH_3	-	16	8
6i	Cl	-	64	16
6j	CH_3	CH_2	8	8
6k	C_4H_9	-	32	16
6l	CN	-	64	32
6m	OCH_3	CH_2	64	16
6n	NO_2	CH_2	32	32
6o	Br	CH_2	16	8
INH	-	-	<0.25	<0.25
ethambutol	-	-	2	2

of *MTB* $H_{37}Rv$ with MIC value 12.5 μg/mL. On the other hand, seco-pseudopteroxazole **11** inhibited only 66% of mycobacterial growth.

Several years later, the same group reported biological evaluation of ileabethoxazole **12** (Figure 5), perhydroacenaphthene-type diterpene alkaloid from *Pseudopterogorgia elisabethae*.[48] This novel benzoxazole alkaloid showed interesting activity against *MTB* $H_{37}Rv$ at the concentration range of 128-64 μg/mL.

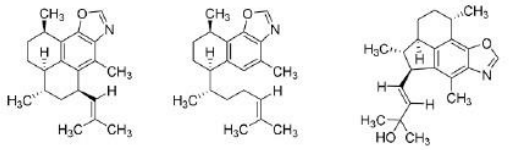

10 **11** **12**

Figure 5. Structure of the benzoxazole alkaloids **10**–**12**.

2.5. 2-Amino benzoxazoles and related structures

Between 1966–1973 Sycheva and others reported several papers describing various benzoxazoles amino-(or hydrazino)-modified at the position 2 (Figure 6).[49–53]

First attempts of Sycheva group at benzoxazole derivatization at the position 2 in order to reach active anti-TB compound led to the synthesis compounds **13** (Figure 6).[51] Investigation of anti-TB activity ($H_{37}Rv$ strain) of the synthesized compounds revealed that the most interesting activity possessed the thioamide of 6-ethoxy-2-benzoxazole carboxylic acid, 6-ethoxy-2-hydrazinobenzoxazole and 6-ethoxy-2-(thiazolyl-2′-amino)benzoxazole with MIC value 0.5 μg/mL, 4 μg/mL and 8 μg/mL, respectively (in the absence of serum). The presence of serum led to the dramatic decreasing in tuberculostatic activity.

The consecutive *in vitro* tests of derivatives **14** (Figure 6) revealed interesting activity against $H_{37}Rv$ strain of thiazoyl compound **14b** with MIC value 0.5 μg/mL in absence of serum and 2 μg/mL in serum.[49] On the other hand, 2-pyridyl derivative **14a** showed lower activity (with MIC value 4 μg/mL in absence of serum and 15 μg/mL in serum). Moreover, the

Table 6. *In vitro* antitubercular activity of benzoxazole compounds **7** and **8**.

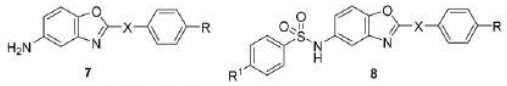

7 **8**

Entry	X	R	R^1	MIC (μg/mL) $H_{37}Rv$	MIC (μg/mL) *MTB isolate*	Entry	X	R	R^1	MIC (μg/mL) $H_{37}Rv$	MIC (μg/mL) *MTB isolate*
7a	-	H	-	8	8	**8g**	-	OCH_3	NO_2	64	16
7b	-	Cl	-	16	8	**8h**	CH_2	H	NO_2	32	16
7c	-	F	-	8	8	**8i**	CH_2	Cl	NO_2	32	16
7d	-	Br	-	8	32	**8j**	CH_2	F	NO_2	32	16
7e	-	C_2H_5	-	16	8	**8k**	CH_2	Br	NO_2	32	16
7f	-	CH_3	-	8	8	**8l**	CH_2	CH_3	NO_2	32	16
7g	-	OCH_3	-	64	8	**8m**	-	H	NH_2	64	32
7h	CH_2	H	-	32	32	**8n**	-	Cl	NH_2	64	64
7i	CH_2	Cl	-	16	8	**8o**	-	F	NH_2	64	64
7j	CH_2	F	-	16	32	**8p**	-	Br	NH_2	64	64
7k	CH_2	Br	-	16	16	**8q**	-	C_2H_5	NH_2	64	16
7l	CH_2	CH_3	-	32	64	**8r**	-	CH_3	NH_2	64	64
8a	-	H	NO_2	64	32	**8s**	-	OCH_3	NH_2	64	64
8b	-	Cl	NO_2	64	32	**8t**	CH_2	H	NH_2	32	16
8c	-	F	NO_2	64	64	**8u**	CH_2	Cl	NH_2	16	16
8d	-	Br	NO_2	64	32	**8v**	CH_2	F	NH_2	32	16
8e	-	C_2H_5	NO_2	64	16	**8w**	CH_2	Br	NH_2	16	16
8f	-	CH_3	NO_2	64	64	**8x**	CH_2	CH_3	NH_2	16	16

Table 7. *In vitro* antitubercular activity of benzoxazoles **9a-j**[46] and **9k-a**.[45]

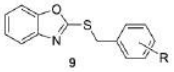

9

Entry	R	*MTB My 331/88* 14 days	21 days
9a	H	250	500
9b	4-NO_2	>62	>125
9c	3-NO_2	>62	125
9d	2-NO_2	>250	>250
9e	3,5-NO_2	8	8
9f	2,4-NO_2	8	8
9g	4-CN	>62	>62
9h	3-CN	125	125
9i	4-$CSNH_2$	8	16
9j	3-$CSNH_2$	8	16
9k	4-Cl	250	>500
9l	3-Cl	62	125
9m	2-Cl	>250	>250
9n	4-F	250	500
9o	3-F	62	125
9p	4-CH_3	>500	>500
9q	3-CH_3	250	500
9r	4-OCH_3	62	125
9s	3-OCH_3	125	250
9t	2-F	125	250
9u	4-Br	>62	>125
9v	3-Br	125	250
9w	2-F, 6-Cl	62	125
9x	3,4-Cl	>125	>250
9y	3,4-F	125	125
9z	2-F, 6-NO_2	>62	>62
9aa	4-CF_3	125	125
9ab	3-CF_3	62	125
9ac	3,5-CF_3	62	125
INH	-	0.5	1

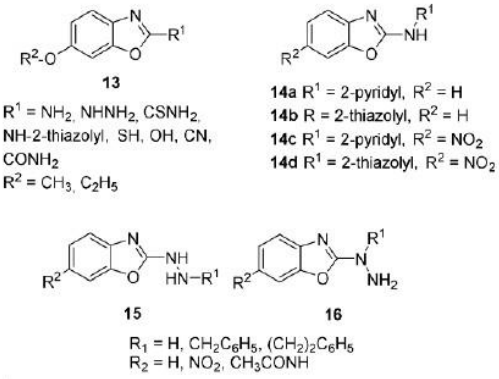

Figure 6. Structures of the 2-amino modified benzoxazoles **13–16**.

introduction of nitro group to the position 6 afforded compounds with decreased activity.

In 1967, Sycheva et al. broaden the series of their benzoxazole derivatives with (benzoxazol-2-yl) hydrazines **15** and **16** (Figure 6).[52] *In vitro* tuberculostatic activity testing showed 1-phenyl-2-(benzoxazolyl-2′)hydrazine and (6-nitrobenzoxazolyl-2) hydrazine as the most active compounds from this series (MIC = 4 μg/mL, without serum).

Based on the previous promising result showing the potency of 2-(2′-thiazolylamino)-benzoxazole, Sycheva and coworkers reported the synthesis and biological evaluation of 2-(2′-thiazolylamino)benzoxazole analogues **17** (Figure 7).[53]

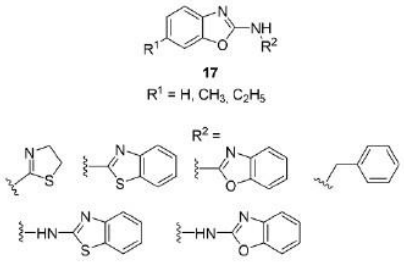

Figure 7. Structures of the 2-amino modified benzoxazoles **17**.

Results obtained from anti-TB testing against $H_{37}Rv$ strain indicated that the di(benzoxazolyl-2-)amine and *N*-benzothiazolyl-2-benzoxazolyl-2)amine are the most interesting compounds from this study with MIC value 2 and 8 μg/mL without serum, respectively. The presence of an alkoxy group in the position 6 decreases the activity.

Sycheva et al. also described a number of *N*-(benzoxazol-2-yl)-*N*′-phenylthioureas **18** (Figure 8).[50] Biological evaluation of

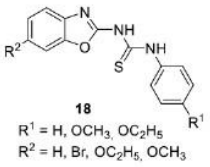

Figure 8. Structures of the benzoxazoles **18**.

18 revealed, that the most active compound from this series, *N*-(2-benzoxazolyl)-*N*′-*p*-ethoxyphenyl)thiourea, inhibited the growth of *MTB* (strain $H_{37}Rv$) at concentration of 2 μg/mL in the absence of serum (15 μg/mL in the presence of serum). In contrast, benzoxazole without *p*-ethoxy substitution had lower activity (8 μg/mL in the absence of serum, 250 μg/mL in serum), that indicates the importance of an alkoxy group in the *p*-position of the benzene ring. Furthermore, introduction of an alkyl group into the position 6 of the benzoxazole skeleton did not result in an increase in anti-TB activity.

The group of Khazi reported the synthesis and biological evaluation of benzoxazole derivatives of 1,3,4-thiadiazoles and

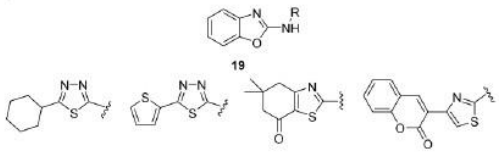

Figure 9. Structures of the benzoxazoles **19**.

thiazoles **19** (Figure 9).[54] All prepared compounds were tested against *M. tuberculosis*; however, none of the tested compounds had interesting antitubercular activity.

Thiadiazole compounds represent other heterocyclic scaffold having very interesting pharmacological and biological profile. Based on this knowledge, Hegde et al. combined benzoxazole with thiadiazole heterocycle and obtained compounds **20** evaluated for their antitubercular properties against *MTB* $H_{37}Rv$ using the BACTEC 460 radiometric system (Figure 10). Both derivatives had a very good inhibitory activity against *MTB* $H_{37}Rv$ at < 6.25 μg/mL.[55]

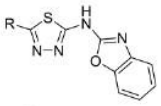

20a R = benzyl
20b R = 3-pyridiyl

Figure 10. Structure of the thiadiazole-based benzoxazoles **20**.

2.6. 2-Substituted 5,7-di-*tert*-butylbenzoxazoles

Vinsova et al. paid their attention to the synthesis of lipophilic benzoxazoles, since lipophilic part in molecules may permit their easier penetration through the mycobacterial cell wall. Firstly, they reported the synthesis and biological evaluation of 2-substituted 5,7-di-*tert*-butylbenzoxazoles.[56,57] By the reaction of substituted benzoquinone with amino acids and dipeptides a series of several 5,7-di-*tert*-butylbenzoxazoles **21** was obtained (Figure 11). Unfortunately, none of the tested compounds had any promising anti-TB activity.[56]

After that, Vinsova and coworkers pursued the synthesis and biological evaluation of 2-substituted 5,7-di-*tert*-butylbenzoxazoles **22** and **23** (Figure 12).[57] All of the prepared benzoxazoles were screened for their antitubercular activity against *M. tuberculosis* $H_{37}Rv$ strain. Interestingly, 5,7-di-*tert*-butyl-2-(pyridin-4-yl)benzoxazole and 5,7-di-*tert*-butyl-2-styryl-benzoxazole exhibited the highest activity in vitro with MIC

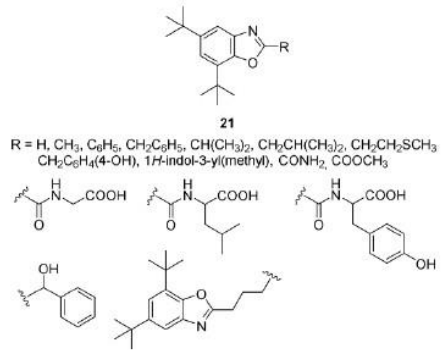

21

R = H, CH_3, C_6H_5, $CH_2C_6H_5$, $CH(CH_3)_2$, $CH_2CH(CH_3)_2$, $CH_2CH_2SCH_3$, $CH_2C_6H_4$(4-OH), 1*H*-indol-3-yl(methyl), $CONH_2$, $COOCH_3$

Figure 11. Structure of the tri-substituted benzoxazoles **21**.

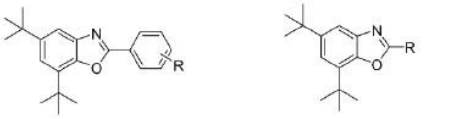

22

R = H, CH_3, Cl, Br, CF_3, OH, NO_2, $N(CH_3)_2$, SCH_3, 4-F-3-OC_6H_4

23

R = CH_2OH, styryl, 5-, 6-membered heterocycle, substituted heterocycle

Figure 12. Structure of the tri-substituted benzoxazoles **22** and **23**.

value 6.25 and 3.13 μg/mL, respectively (INH as standard – MIC value 0.02 μg/mL).

2.7. Others

Imramovsky et al. reported synthesis and biological evaluation of 2-[(*E*)-2-substituted-ethenyl]-1,3-benzoxazoles **24** (Figure 13).[58] In spite of the relatively large series of synthesized

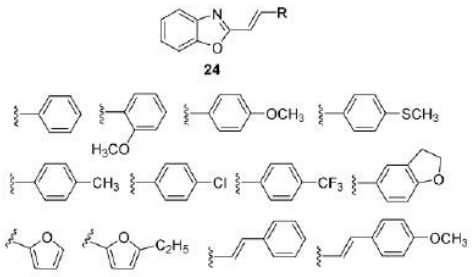

24

Figure 13. Structure of benzoxazoles **24**.

compounds, none of them had any potential based on the anti-TB activity shown. However, derivatives modified with 4-

OMePh, 4-SMePh and 2,3-dihydro-1-benzofuran-5-yl moiety were active against *M. avium* 330/88 (MIC = 32-62.5; 62.5 and 32 μmol/L, respectively). SAR observations also indicate that electron-donor groups (4-OMe) are favorable substituent.

Another promising scaffold was reported by Sycheva et al.[59] They designed and synthesized *S*-heterylmercaptoacetic acids comprising also the benzoxazoles **25** (Figure 14) and

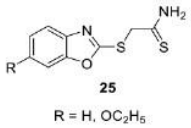

25

R = H, OC_2H_5

Figure 14. Structure of benzoxazoles **25**.

evaluated their biological activity. Compounds **25** substituted with ethoxy group was active against *MTB* $H_{37}Rv$ (MIC = 1 μg/mL, without serum). However, studied benzoxazole **25** did not have appropriate pharmacological properties.

Sankar et al. reported *in silico* design, synthesis and biological evaluation of 1,3-benzoxazole-5-carbohydrazide **26** (Figure 15) that had *in vitro* activity against *MTB* $H_{37}Rv$ strain.[60] A small substitution in the position 2 enhances biological activity.

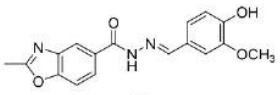

26

Figure 15. Structure of benzoxazoles **26**.

The group of Westwell published the synthesis and biological evaluation of several 4-hydroxycyclohexa-2,5-dienones.[61] Benzoxazole **27** (Figure 16) had potency against *MTB*

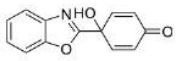

27

Figure 16. Structure of benzoxazoles **27**.

$H_{37}Rv$ with MIC value 1.56 μg/mL. Moreover, benzoxazole **27** showed inhibition of *MTB* Thioredoxin C/Thioredoxin reductase signaling (IC_{50} = 50 μM).

One of the best result to date emerged from a library of more than 60 novel quinolone analogues.[62] Compound **28** (Figure 17) showed a MIC value of 5.5 μM and no measurable cytotoxicity. Moreover, this benzoxazole was found to have good blood stability and no hERG affinity.

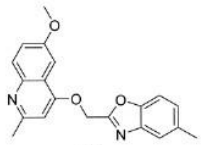

28

Figure 17. Structure of benzoxazole **28**.

3. Potential targets of benzoxazole-based compounds

The most promising approach against tuberculosis is targeting specific mycobacterial enzymes with small molecules. As a consequence of this external intervention, the disruption of some important cellular processes may occur. However, the discovery of novel anti-TB agents with a new mode of action and directed towards unknown targets of *MTB* remains also challenging.

The benzoxazole skeleton offers a number of interactions with the host protein. The planar aromatic heterocycle can act through the π-π stacking, nitrogen and oxygen atoms can mediate the hydrogen bonding and lipophilic character may enable the hydrophobic interactions.

Mycobacterium tuberculosis enoyl acyl carrier protein reductase (*Mt*InhA) is one of the most attractive enzymes to design and develop novel drugs for tuberculosis therapy[63–66] and might be a promising target for novel inhibitors active against MDR and XDR *MTB*.[67] Several benzoxazoles have been studied in respect to the *Mt*InhA inhibition.[40] The synthesized benzoxazole-pyrazoline compounds **4** (Table 3) were docked into the enoyl-acyl carrier protein (ACP) reductase, a known molecular target of INH. Reported experiments showed a successful docking into the active site of enoyl-ACP reductase with significant contribution of benzoxazole core over the other two ring nucleus (pyrazoline, aryl). These results might indicate the potential target of benzoxazole-based compounds.

Further, Pauli et al. reported *in silico* approach that might reveal new InhA inhibitors.[66] Among others, benzoxazole **29** (Figure 18) was selected for *in vitro* evaluation. Pauli group

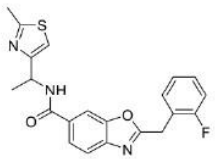

29

Figure 18. Structure of benzoxazole **29** as potent InhA inhibitor.

reported that benzoxazole **29** interacts via hydrogen bond to NADH and several hydrophobic interactions with the protein, including Ala198 (important to tight binding).

One of the other potential target of tuberculosis is *Mycobacterium protein tyrosine phosphatase B* (mPTPB). Zhang with co-workers applied the Diversity-Oriented Synthesis (DOS) strategy in order to find novel and selective drug-like inhibitors of this enzyme and synthesized a range of novel bicyclic salicylic acids as mPTPB inhibitors.[68] However, benzoxazoles comprised in this study did not show any interesting specificity to the studied enzyme. Nevertheless, other substitution might be worthy.

4. Conclusion

In this review, we have summarized the available information regarding to benzoxazole scaffold and its antitubercular properties. Benzoxazole moiety has been frequently studied and successfully combined with another promising heterocycle such is pyrazoline. However, none of the reviewed benzoxazole derivatives reached nanomolar concentrations and has entered the phase of the preclinical hit-to-lead optimization in anti-TB research.

Despite this, the search for new benzoxazole-based compounds active against TB remains a challenge. In particular, since the occurrence of MDR and XDR *MTB* infections is alarming and the molecular mechanism involved in the resistance and its possible targets is still not completely understood.

In this review, benzoxazoles several possible targets have been also outlined; however, additional efforts must be made in order to discover novel anti-TB agents with a new mode of action and directed at unknown targets of *MTB*. This review should serve the researchers working in the area of the development of new antituberculotics as a guide through both the successful and less successful research that has been done during the recent past years in order to find new antituberculotics based on benzoxazole scaffold and help them to focus their future research towards the most promising structures.

5. Future perspectives

TB is one of the top 10 causes of deaths worldwide and the first among the mortality caused by bacterial infections. It is estimated that until 2020 nearly 1 billion additional people will be infected with TB, 200 million will become sick, and 35 million will die of this disease. Many *M. tuberculosis* strains are resistant to one or more of the standard TB drugs, which complicates treatment and the rise in number of people affected by drug-resistant TB and latent TB is alarming. The current situation and effort to effectively control TB requires development of new antitubercular agents acting on new targets. With no doubt, the discovery of entirely new compounds with an alternative mechanism of action to the existing therapeutics remains challenging.

The question is, can any benzoxazole serve as a lead for the discovery of new antitubercular agents acting on new targets? The above literature findings reveal benzoxazoles as a promising scaffold that is in the most cases substituted with other heterocycle contributing to the antitubercular activity. From this point of view, the pyrazoline modification of benzoxazole remains the most promising from all studied substitutions. Several compounds of these series had interesting activity, even better than all of the standard drugs against *MTB* $H_{37}Rv$ strain.

All biological studies reported in this review make benzoxazole nucleus highly suitable for discovery of new antitubercular agents. However, detailed SAR studies and additional efforts must be made in order to discover novel anti-TB agents with a new mode of action and directed at unknown targets of *MTB*.

Acknowledgement

This work was supported by the Ministry of Education, Youth and Sport of the Czech Republic (projects IGA_PrF_2018_029, IGA_LF_2018_032) and the National Program of Sustainability (project LO1304).

Conflict of Interest

The authors declare no conflict of interest.

Keywords: antitubercular · benzoxazole · biological activity · *Mycobacterium tuberculosis* · tuberculosis

[1] G. B. Migliori, M. Dara, C. P. de, H. Kluge, M. C. Raviglione, *Eur. Respir. J.* **2012**, *39*, 1290–1291.
[2] A. Skrahina, H. Hurevich, A. Zalutskaya, E. Sahalchyk, A. Astrauko, G. W. van, S. Hoffner, V. Rusovich, M. Zignol, *Eur. Respir. J.* **2012**, *39*, 1425–1431.
[3] D. Falzon, N. Gandhi, G. B. Migliori, G. Sotgiu, H. S. Cox, T. H. Holtz, M. G. Hollm-Delgado, S. Keshavjee, K. DeRiemer, R. Centis, L. D'Ambrosio, C. G. Lange, M. Bauer, D. Menzies, *Eur. Respir. J.* **2013**, *42*, 156–168.
[4] G. B. Migliori, G. Sotgiu, N. R. Gandhi, D. Falzon, K. DeRiemer, R. Centis, M. G. Hollm-Delgado, D. Palmero, C. Perez-Guzman, M. H. Vargas, L. D'Ambrosio, A. Spanevello, M. Bauer, E. D. Chan, H. S. Schaaf, S. Keshavjee, T. H. Holtz, D. Menzies, *Eur. Respir. J.* **2013**, *42*, 169–179.
[5] M. Zignol, M. Dara, A. Dadu, K. Kremer, A. S. Dean, D. Falzon, K. Floyd, H. Hoffmann, S. Hoffner, *Drug Resist Updat* **2013**, *16*, 108–115.
[6] N. R. Gandhi, P. Nunn, K. Dheda, H. S. Schaaf, M. Zignol, S. D. van, P. Jensen, J. Bayona, *Lancet* **2010**, *375*, 1830–1843.
[7] C. S. Demmer, L. Bunch, *Eur. J. Med. Chem.* **2015**, *97*, 778–785.
[8] M. K. Gautam, Sonal, N. K. Sharma, Priyanka, K. K. Jha, *Int. J. ChemTech Res.* **2012**, *4*, 640–650.
[9] Maruthamuthu, S. Rajam, P. C. R. Stella, A. G. B. Dileepan, R. Ranjith, *J. Chem. Pharm. Res.* **2016**, *8*, 505–526.
[10] S. Singh, G. Veeraswamy, D. Bhattarai, J. I. Goo, K. Lee, Y. Choi, *Asian J. Org. Chem.* **2015**, *4*, 1338–1361.
[11] I. Oren, I. Yalcin, *Ankara Univ. Eczacilik Fak. Derg.* **1993**, *21*, 53–65.
[12] S. P. B. Ovenden, J. L. Nielson, C. H. Liptrot, R. H. Willis, D. M. Tapiolas, A. D. Wright, C. A. Motti, *J. Nat. Prod.* **2011**, *74*, 65–68.
[13] T. Kusumi, T. Ooi, M. R. Walchli, H. Kakisawa, *J. Am. Chem. Soc.* **1988**, *110*, 2954–2958.
[14] C. Hohmann, K. Schneider, C. Bruntner, E. Irran, G. Nicholson, A. T. Bull, A. L. Jones, R. Brown, J. E. M. Stach, M. Goodfellow, W. Beil, M. Kraemer, J. F. Imhoff, R. D. Suessmuth, H. P. Fiedler, *J. Antibiot.* **2009**, *62*, 99–104.
[15] L. J. Scott, *Drugs* **2014**, *74*, 1371–1378.

[16] C. Hohmann, K. Schneider, C. Bruntner, E. Irran, G. Nicholson, A. T. Bull, A. L. Jones, R. Brown, J. E. M. Stach, M. Goodfellow, W. Beil, M. Kraemer, J. F. Imhoff, R. D. Suessmuth, H. P. Fiedler, *J. Antibiot.* **2009**, *62*, 99–104.
[17] D. W. Dunwell, D. Evans, T. A. Hicks, *J. Med. Chem.* **1975**, *18*, 1158–1159.
[18] E. Marmo, R. Acampora, M. Angrisani, L. Berrino, M. Cazzola, D. De Santis, A. Filippelli, W. Filippelli, V. Guarino, a. et, *Riforma Med.* **1986**, *101*, 253–282.
[19] S. Rajasekhar, B. Maiti, K. Chanda, *Synlett* **2017**, *28*, 521–541.
[20] A. Kumar, R. A. Maurya, P. Ahmad, *J. Comb. Chem.* **2009**, *11*, 198–201.
[21] M. B. Madhusudana Reddy, A. Nizam, M. A. Pasha, *Synth. Commun.* **2011**, *41*, 1838–1842.
[22] Y. Riadi, R. Mamouni, R. Azzalou, M. El Haddad, S. Routier, G. Guillaumet, S. Lazar, *Tetrahedron Lett.* **2011**, *52*, 3492–3495.
[23] S. Kaul, A. Kumar, B. Sain, A. K. Bhatnagar, *Synth. Commun.* **2007**, *37*, 2457–2460.
[24] B. Wang, Y. Zhang, P. Li, L. Wang, *Chin. J. Chem.* **2010**, *28*, 1697–1703.
[25] D. R. Chancellor, K. E. Davies, O. De Moor, C. R. Dorgan, P. D. Johnson, A. G. Lambert, D. Lawrence, C. Lecci, C. Maillol, P. J. Middleton, G. Nugent, S. D. Poignant, A. C. Potter, P. D. Price, R. J. Pye, R. Storer, J. M. Tinsley, R. van Well, R. Vickers, J. Vile, F. J. Wilkes, F. X. Wilson, S. P. Wren, G. M. Wynne, *J. Med. Chem.* **2011**, *54*, 3241–3250.
[26] I. Mohammadpoor-Baltork, A. R. Khosropour, S. F. Hojati, *Catal. Commun.* **2007**, *8*, 1865–1870.
[27] K. Tao, J. Zheng, Z. Liu, W. Shen, J. Zhang, *Tetrahedron Lett.* **2010**, *51*, 3246–3249.
[28] X. Fan, Y. He, X. Zhang, S. Guo, Y. Wang, *Tetrahedron* **2011**, *67*, 6369–6374.
[29] F. Wang, J. R. Hauske, *Tetrahedron Lett.* **1997**, *38*, 6529–6532.
[30] X. Beebe, D. Wodka, T. J. Sowin, *J. Comb. Chem.* **2001**, *3*, 360–366.
[31] C. Chen, Y. J. Chen, *Tetrahedron Lett.* **2004**, *45*, 113–115.
[32] J. Y. Hwang, Y. D. Gong, *J. Comb. Chem.* **2006**, *8*, 297–303.
[33] H. Hioki, K. Matsushita, M. Kubo, K. Harada, M. Kodama, Y. Fukuyama, *Tetrahedron* **2007**, *63*, 11315–11324.
[34] W. H. Wagner, H. Vonderbank, *Z. Gesamte Exp. Med.* **1949**, *115*, 66–81.
[35] K. Manna, Y. K. Agrawal, *Eur. J. Med. Chem.* **2010**, *45*, 3831–3839.
[36] M. S. Yar, A. A. Siddiqui, M. A. Ali, *Bioorg. Med. Chem. Lett.* **2006**, *16*, 4571–4574.
[37] S. Sharma, P. K. Sharma, N. Kumar, R. Dudhe, *Biomed. Pharmacother.* **2011**, *65*, 244–251.
[38] H. M. Soni, P. K. Patel, M. T. Chhabria, A. K. Patel, D. N. Rana, P. S. Brahmkshatriya, *Int. J. Org. Chem.* **2016**, *6*, 157–176.
[39] D. N. Rana, M. T. Chhabria, N. K. Shah, P. S. Brahmkshatriya, *Med. Chem. Res.* **2014**, *23*, 370–381.
[40] D. N. Rana, M. T. Chhabria, N. K. Shah, P. S. Brahmkshatriya, *Med. Chem. Res.* **2014**, *23*, 2218–2228.
[41] K. Devi, M. Kachroo, L. Pathak, *J. Comput. Methods Mol. Des.* **2016**, *6*, 8–19.
[42] M. Arisoy, O. Temiz-Arpaci, F. Kaynak-Onurdag, *Ankara Univ. Eczacilik Fak. Derg.* **2010**, *39*, 155–162.
[43] M. Arisoy, O. Temiz-Arpaci, F. Kaynak-Onurdag, S. Ozgen, *Z. Naturforsch., C: J. Biosci.* **2013**, *68*, 453–460.
[44] T. Ertan-Bolelli, I. Yildiz, S. Ozgen-Ozgacar, *Med. Chem. Res.* **2016**, *25*, 553–567.
[45] V. Klimesova, J. Koci, K. Waisser, J. Kaustova, U. Moellmann, *Eur. J. Med. Chem.* **2009**, *44*, 2286–2293.
[46] J. Koci, V. Klimesova, K. Waisser, J. Kaustova, H. M. Dahse, U. Moellmann, *Bioorg. Med. Chem. Lett.* **2002**, *12*, 3275–3278.
[47] A. D. Rodriguez, C. Ramirez, I. I. Rodriguez, E. Gonzalez, *Org Lett* **1999**, *1*, 527–530.
[48] I. I. Rodriguez, A. D. Rodriguez, Y. Wang, S. G. Franzblau, *Tetrahedron Lett.* **2006**, *47*, 3229–3232.
[49] T. P. Sycheva, I. D. Kiseleva, M. N. Shchukina, *Khim. Geterotsikl. Soedin.* **1966**, 205–211.
[50] T. P. Sycheva, I. D. Kiseleva, M. N. Shchukina, *Khim. Geterotsikl. Soedin.* **1966**, 687–689.
[51] T. P. Sycheva, Z. A. Pankina, I. D. Kiseleva, M. N. Shchukina, *Khim. Geterotsikl. Soedin.* **1966**, *4*, 506–510.
[52] T. P. Sycheva, I. D. Kiseleva, M. N. Shchukina, *Khim. Geterotsikl. Soedin.* **1967**, 43–47.
[53] T. P. Sycheva, T. N. Pavlova, T. N. Zykova, M. N. Shchukina, *Khim. Farm. Zh.* **1973**, *7*, 3–5.
[54] G. Kolavi, V. Hegde, I. Ahmedkhazi, *J. Sulfur Chem.* **2006**, *27*, 225–231.
[55] V. S. Hegde, G. D. Kolavi, R. S. Lamani, I. A. Khazi, *Phosphorus, Sulfur Silicon Relat. Elem.* **2007**, *182*, 911–920.
[56] J. Vinsova, V. Horak, V. Buchta, J. Kaustova, *Molecules* **2005**, *10*, 783–793.
[57] J. Vinsova, K. Cermakova, A. Tomeckova, M. Ceckova, J. Jampilek, P. Cermak, J. Kunes, M. Dolezal, F. Staud, *Bioorg. Med. Chem.* **2006**, *14*, 5850–5865.
[58] A. Imramovsky, J. Kozic, M. Pesko, J. Stolarikova, J. Vinsova, K. Kralova, J. Jampilek, *Sci. World J.* **2014**, 705973–1-705973/12.
[59] T. P. Sycheva, T. N. Pavlova, T. N. Zykova, M. N. Shchukina, *Khim. Farm. Zh.* **1969**, *3*, 18–21.
[60] S. P. Sankar, A. Mathew, T. Jayakumar, S. Chand, C. Mathew, *Asian J. Pharm. Health Sci.* **2013**, *3*, 661–676.
[61] M. Shah, G. Wells, T. D. Bradshaw, C. A. Laughton, M. F. G. Stevens, A. D. Westwell, *Lett. Drug Des. Discovery* **2006**, *3*, 419–423.
[62] E. Pitta, M. K. Rogacki, O. Balabon, S. Huss, F. Cunningham, E. M. Lopez-Roman, J. Joossens, K. Augustyns, L. Ballell, R. H. Bates, P. Van der Veken, *J. Med. Chem.* **2016**, *59*, 6709–6728.
[63] L. Encinas, H. O'Keefe, M. Neu, M. J. Remuinan, A. M. Patel, A. Guardia, C. P. Davie, N. Perez-Macias, H. Yang, M. A. Convery, J. A. Messer, E. Perez-Herran, P. A. Centrella, D. Alvarez-Gomez, M. A. Clark, S. Huss, G. K. O'Donovan, F. Ortega-Muro, W. McDowell, P. Castaneda, C. C. Arico-Muendel, S. Pajk, J. Rullas, I. Angulo-Barturen, E. Alvarez-Ruiz, A. Mendoza-Losana, L. Ballell Pages, J. Castro-Pichel, G. Evindar, *J. Med. Chem.* **2014**, *57*, 1276–1288.
[64] O. Holas, P. Ondrejcek, M. Dolezal, *J. Enzyme Inhib. Med. Chem.* **2015**, *30*, 629–648.
[65] B. Inturi, G. V. Pujar, M. N. Purohit, *Arch. Pharm.* **2016**, *349*, 817–826.
[66] I. Pauli, R. N. dos Santos, D. C. Rostirolla, L. K. Martinelli, R. G. Ducati, L. F. S. M. Timmers, L. A. Basso, D. S. Santos, R. V. C. Guido, A. D. Andricopulo, O. Norberto de Souza, *J. Chem. Inf. Model.* **2013**, *53*, 2390–2401.
[67] P. Pan, P. J. Tonge, *Curr. Top. Med. Chem.* **2012**, *12*, 672–693.
[68] R. He, Y. Bai, Z. H. Yu, L. Wu, A. M. Gunawan, Z. Y. Zhang, *MedChemComm* **2014**, *5*, 1496–1499.

Submitted: March 3, 2018
Revised: April 12, 2018
Accepted: April 16, 2018